UNIVERSITAT DE BARCELONA

Genetic and biochemical approaches to decipher the molecular basis of the pathology in LCA12 and RP10 retinal dystrophies

Anna Maria Plana Bonamaisó

Doctoral Program in Biomedicine

Genetic and biochemical approaches to decipher the molecular basis of the pathology in LCA12 and RP10 retinal dystrophies

Department of Physiological Sciences
Faculty of Medicine and Health Sciences, Campus Bellvitge
Universitat de Barcelona

Thesis Director	Thesis Tutor	Doctoral Candidate
Dr. Ana Méndez Zunzunegui	Dr. Jordi Llorens Baucells	Anna Plana Bonamaisó

A l'Andreu,

TABLE OF CONTENTS

ABBREVIATION LIST *9*

GENE LIST *13*

ABSTRACT *15*

1. INTRODUCTION *17*

1.1 The first steps in visual transduction. **19**
1.1.1 The retina: organization and function 20
1.1.2 Photoreceptor cells: structure and function 21

1.2 The light response: roles of cGMP and Ca^{2+} **23**
1.2.1 The dark current 24
1.2.2 The dark-steady state 25
1.2.3 Activation phase of the light response 25
1.2.4 Inactivation phase and light adaptation 27

1.3 Retinal inherited diseases **28**

1.4 The protein complex responsible for cGMP synthesis in rods and cones **31**
1.4.1 cGMP production by Retinal guanylate cyclase 31
1.4.2 RetGCs regulation by GCAP calcium sensors 31
1.4.3 Trafficking of RetGCs to the outer segment: the role of RD3 33
1.4.4 *GUCY2D* blindness associated mutations. Mouse models to study RetGC function. 34
1.4.5 *GUCA1A* and *GUCA1B* blindness-associated mutations. Mouse models to study GCAP1 and GCAP2 function. 35
1.4.6 *RD3* blindness mutations. The *rd3* mice. 37

1.5 Photoreceptor cell death mediated by alterations in cGMP levels **38**
1.5.1 Cell death mediated by ER stress 42

1.6 IMPDH1 in the retina **44**
1.6.1 Purine nucleotide control in photoreceptors 44
1.6.2 IMPDH structure and catalytic cycle 45
1.6.3 IMPDH1 in photoreceptor cells 46
1.6.4 IMPDH negative allosteric regulation by nucleotides 48
1.6.5 IMPDH capacity to reversibly polymerize into filaments 50

2. AIMS *53*

2.1 AIMS OF THE STUDY **55**
2.1.1 SPECIFIC AIMS 55

3. RESULTS *57*

3.1 RESULTS CHAPTER 1. ANTIBODY GENERATION AGAINST THE PROTEINS OF STUDY: RETGC1, RD3 AND IMPDH1 ..... **59**
3.1.1 Contributions 61
3.1.2 Antibody against murine RetGC1 63
3.1.3 Antibody against murine RD3 65
3.1.4 Antibody against bovine IMPDH1 67

3.2 RESULTS CHAPTER 2. EXPLORING THE PUTATIVE ROLE OF GCAPS AS DAMAGE MEDIATORS IN THE *RD3* MOUSE MODEL OF LCA12 ..... **69**
3.2.1 Contributions 71
3.2.2 Rationale 73

3.2.3 Retinal degeneration due to RD3 deficiency is substantially rescued by GCAPs ablation. 75
3.2.4 Morphological rescue of *rd3* retinas by GCAPs ablation does not correlate with an amelioration of visual function 80
3.2.5 Subcellular localization of RD3 in retinal sections 81
3.2.6 GCAP2 in *rd3* mice is mostly in its phosphorylated Ca2+-free form, a target for 14-3-3 binding 83
3.2.7 Endoplasmic reticulum stress and mitochondrial swelling are prominent early signs of retinal degeneration in the *rd3* mice that are substantially rescued by GCAPs ablation..... 86
3.2.8 Discussion 91

3.3 RESULTS CHAPTER 3. CHARACTERIZING THE IN VIVO MODULATION OF IMPDH1 IN DARK/LIGHT AND ITS EFFECT ON THE LIGHT RESPONSE 95
3.3.1 Contributions 97
3.3.2 Rationale 99
3.3.3 Dark/light-dependent phosphorylation of retinal IMPDH1. 101
3.3.4 IMPDH1 is phosphorylated *in vivo* at a high extent in both dark and light conditions 105
3.3.5 *In vitro* effects of phosphorylation on IMPDH1 catalytic activity 107
3.3.6 T159 and S160 phosphorylation impairs GDP/GTP regulation of IMPDH1..... 109
3.3.7 Photoreceptor cells present roughly equimolar levels of GTP and ATP in the dark and light steady-states 111
3.3.8 Prolonged bright light exposure of living mice causes the accumulation of IMPDH1 aggregates at the rod outer segment layer of the retina..... 114
3.3.9 Constant bright light exposure substantially increases the flux towards *de novo* GTP and ATP synthesis 118
3.3.10 Inhibition of IMPDH catalytic activity delays mass rod recovery in electroretinogram responses. 121
3.3.11 T159 and S160 sites are phosphorylated by PKC *in vitro* 123
3.3.12 Discussion..... 127

4. GLOBAL DISCUSSION AND FUTURE PERSPECTIVES 135

4.1 Role of GCAPs as damage mediators in the *rd3* mouse model of LCA12 137

4.2 *In Vivo* regulation of IMPDH1 in the retina, and effect of adRP10 IMPDH1 mutations on retinal physiology 140

5. CONCLUSIONS 143

6. MATERIALS AND METHODS 147

6.1. Materials and methods for Chapter 1 149
6.1.1. Ethics statement 149
6.1.2 Generation and affinity purification of antibodies against RetGC1 and RD3..... 149
6.1.3 Generation and affinity purification of antibody against bIMPDH1 canonical protein ... 149
6.1.4 Antibodies preservation..... 150
6.1.5 Testing of antibodies by Western Blot..... 150
6.1.6 Testing of antibodies in indirect immunofluorescence localization assays 151
6.1.7 Titration of bIMPDH1 antibody in Immunoprecipitation..... 152

6.2 Materials and methods for Chapter 2 154
6.2.1 Mice 154
6.2.2 Antibodies..... 155
6.2.3 Specimen preparation for light and electron microscopy 156
6.2.4 Retinal morphometry analysis 156
6.2.5 Ultrathin sectioning and image acquisition at the transmission electron microscope.... 157
6.2.6 Immunofluorescence analysis in fixed tissue..... 157
6.2.7 Confocal microscopy and data analysis 158
6.2.8 Western blot 158
6.2.9 Isoelectric focusing separation of murine retinal homogenates 159

6.2.10 Expression, purification, and in vitro phosphorylation of myristoylated GCAP2 for pull-down assays 160
6.2.11 LC-MS/MS 160
6.2.12 Characterizing differential protein interactions of GCAP2-P and GCAP2 161
6.2.13 Electroretinography 162
6.2.14 Generation of pRho-mRd3.V5-dsRed expression vector and in vivo DNA electroporation 162

6.3 Materials and methods for chapter 3 164
6.3.1 Label-free quantitative proteomic analysis of enriched phosphopeptides from dark- and light-adapted bovine retinas. 164
6.3.2 Data Analysis 165
6.3.3 *In situ* metabolic labeling 165
6.3.4 Isolectrofocusing separation of IMPDH1 166
6.3.5 Cloning of HsIMPDH1 different spliced forms into pETEV and site-directed mutagenesis. 167
6.3.6 Purification of IMPDH1 enzymes. 169
6.3.7 Enzymatic assays 169
6.3.8 *In vitro* phosphorylation with PKC 169
6.3.9 Nucleotide determination in retinal extracts by HPLC 170
6.3.10 *In vivo* metabolic flux analysis by injection of a stable isotope of Gly 171
6.3.11 Electroretinogram analysis 171
6.3.12 IMPDH1 immunofluorescence localization in retinal sections 172

7. BIBLIOGRAPHY 175

8. APPENDIX 199

8.1 Cover 201

9. ACKNOWLEDGEMENTS- AGRAÏMENTS 203

10. PUBLICATION 207

ABBREVIATION LIST

$[Ca^{2+}]_i$	intracellular concentration of calcium
$[Mg^{2+}]_i$	intracellular concentration of magnesium
Ab	antibody
AC	amacrine cell
ACHM	achromatopsia
ad	autosomal dominant
ADP	adenosine diphosphate
AMD	age-related macular degeneration
AMP	adenosine monophosphate
AMPK	AMP-activated protein kinase
ar	autosomal recessive
Arr	arrestin
Asp	aspartic acid
ATF6	activating transcription factor-6
ATP	adenosine triphosphate
BB	basal body
BC	bipolar cell
BCL-2	B-cell lymphoma 2
BIP	binding-immunoglobulin-protein
BL	bright light
BM	bisindolylmaleimide I
BSA	bovine serum albumin
BZM	benzamide
Ca^{2+}	calcium ion
CamKII	calmodulin kinase II
cAMP	cyclic adenosine monophosphate
CASP3	caspase 3
CBS	cystathione beta-synthase
CC	conecting cilium
CD	cone dystrophy
cG-PDE	cGMP phosphodiesterase
cGMP	cyclic guanosine monophosphate
CHOP	C/EBP homologous protein
CKII	casein kinase II
CNG-channel	cyclic nucleotide gated-channel
CNGA3	cyclic nucleotide gated-channel alpha 3
CNGB3	cyclic nucleotide gated-channel beta 3
CNSB	congenital stationary night blindness
CORD	cone-rod dystrophy
Cys	cysteine
D	dark
DMEM	dulbecco's Modified Eagle Medium
DMSO	dimethyl sulfoxide
EIF2-α	eukaryotic inhitiation factor-2 alpha
Ellip.	ellipsoid
ER	endoplasmatic reticulum
ERG	electroretinography/ electroretinogram
GC	guanylate cyclase
GCAP	guanylyl cyclase activating protein
GCAP1	guanylate cyclase-activating protein isoform 1
GCAP2	guanylate cyclase-activating protein isoform 2
GCAP2-P	phosphorylated GCAP2
GCAPs-/-	knock-out in GCAP1 and GCAP2 isoforms
GCL	ganglion cell layer
GDP	guanosine diphosphate
GK	guanylate kinase
Glu	glutamic acid
Gly	glycine
GMP	guanosine monophosphate
GPCR	G protein-coupled receptor
GRK1	rhodopsin kinase
GRP78	glucose regulated protein-78
GTP	guanosine triphosphate
Gtα,β,γ	transducin α, β and γ subunits
HC	horizontal cell

HPLC	high performance liquid chromatography
HPRT	hypoxanthine phosphoribosyltransferase
HSP90	heat shock protein 90
HspB8	heat shock protein beta-8
IEF	isoelectric focusing
IMP	inosine monophosphate
IMPDH	inosine monophosphate dehydrogenase
IMPDH1	inosine monophosphate dehydrogenase isoform 1
IMPDH2	inosine monophosphate dehydrogenase isoform 2
INL	inner nuclear layer
IP	isoelectric point
IPL	inner plexiform layer
iPSCs	induced pluripotent stem cells
IRE1	inositol-requiring enzyme 1
IS	inner segment
IST	interestimulus time
KLH	keyhole limpet hemocyanin
KO	knock-out
L	light
LC-MS/MS	liquid chromatography and mass spectrometry
LCA	leber congenital amaurosis
M	microvilli
MD	macular degeneration
Mg2+	magnesium ion
MMF	mycophenolate mofetil
MPA	mycophenolic acid
MS	mass spectrometry
N	nucleus
NAD	adenine dinucleotide
NCKX	Na+/Ca+/K+ exchanger
NdelI	nuclear distribution protein nude-like1
NDK	nucleoside diphosphate kinase
NDUFS5	NADH dehydrogenase[ubiquinone] iron-sulfur protein 5
NSAF	normalized spectral abundance factor
OLM	outer limitting membrane
ONL	outer nuclear layer
OPL	outer plexiform layer
OS	outer segment
PARP	poly (ADP-ribose) polymerase
PBS	phosphate buffered saline
PDE	phosphodiesterase
PERK	protein kinase R-like ER protein kinase
PhR	photoreceptor cell
PKA	protein kinase A
PKB-Akt	protein kinase B
PKC	protein kinase C
PKG	protein kinase G
PMA	phorbol 12-myristate 13-acetate
PMSF	phenylmethylsulfonyl fluoride
PNA	peanut agglutinin
PRDX6	peroxiredoxin 6
PRS	ribose phosphate pyrophosphokinase
R	ribbon synapse
R	inactivated rhodopsin
R*	activated rhodopsin
RD3	retinal degeneration 3
rd3* or *rd3/rd3	indistinctly, mice deficient in RD3 protein
Rec	recoverin
RetGC	retinal guanylate cyclase
RetGC1	retinal guanylate cyclase isoform 1
RetGC1/ RetGC2 dKO	Knock-out in RetGC1 and RetGC2 isoforms
RetGC2	retinal guanylate cyclase isoform 2
RGC	retinal ganglion cell
ROS	rod outer segment
RP	retinitis pigmentosa
RPE	retinal pigmented epithelium
RPL31	60S ribosomal protein L31
SD	standard deviation
SDS	sodium dodecyl sulfate

SEM	standard error of the mean
Ser	serine
SNP	single-nucleotide polymorphism
SOD1	superoxide dismutase-1
ST	synaptic terminal
STDEV	standard deviation
TEM	transmission electron microscopy
Thr	threonine
TMD	transmembrane domain
UPR	unfolded protein response
WT	wild-type

GENE LIST

AIPL1	aryl hydrocarbon receptor interacting protein like 1
ALMS1	centrosome and basal body associated protein 1
CABP4	calcium binding protein 4
CEP290	centrosomal protein 290
CLUAP1	clusterin associated protein 1
CNGA1	cyclic nucleotide gated channel subunit alpha 1
CNGA3	cyclic nucleotide gated channel subunit alpha 3
CNGB1	cyclic nucleotide gated channel subunit beta 1
CNGB3	cyclic nucleotide gated channel subunit beta 3
CRB1	crumbs cell polarity complex component 1
CRX	cone-rod homeobox
DTHD1	death domain containing 1
GDF6	growth differentiation factor 6
GNAT1	G protein subunit alpha transducin 1
GNAT2	G protein subunit alpha transducin 2
GRK1	rhodopsin kinase
GUCA1A	guanylate cyclase activator 1A
GUCA1B	guanylate cyclase activator 1B
GUCY2D	guanylate cyclase 2D, retinal
IFT140	intraflagellar transport 140
IMPDH1	inosine monophosphate dehydrogenase 1
IQCB1	IQ motif containing B1
KCNJ13	potassium inwardly rectifying channel subfamily J member 13
LCA5	lebercilin LCA5
LRAT	lecithin retinol acyltransferase
NMNAT1	nicotinamide nucleotide adenylyltransferase 1
OTX2	orthodenticle homeobox 2
PDE6A	phosphodiesterase 6A
PDE6B	phosphodiesterase 6B
PDE6C	phosphodiesterase 6C
PDE6G	phosphodiesterase 6G
PDE6H	phosphodiesterase 6H
PRPH2	peripherin 2
RD3	retinal degeneration 3
RDH12	retinol dehydrogenase 12
REEP6	receptor accessory protein 6
RHO	rhodopsin
RPE65	retinoid isomerohydrolase RPE65
RPGRIP1	RPGR interacting protein 1
SAG	S-antigen visual arrestin
SPATA7	spermatogenesis associated 7
TULP1	tubby-like protein 1

ABSTRACT

The main aim of this work was to characterize the molecular mechanisms that underlie the physiopathology of LCA12 and RP10, that are inherited retinal dystrophies caused by alterations in guanine nucleotide metabolism.

First, LCA12 is caused by loss-of-function mutations in the retinal degeneration 3 (*RD3*) gene, that impair rod and cone function and cause a fast retinal degeneration in patients. This disease is reproduced in the natural strain of *rd3* mice. The underlying physiopathology mechanisms of LCA12 are not well understood. We previously proposed that Guanylate Cyclase Activating Proteins (GCAPs) might be key Ca^{2+}-sensors mediating the physiopathology of this disorder, based on the demonstrated toxicity of GCAP2 when blocked in its Ca^{2+}-free form at photoreceptor inner segments. We here show that the retinal degeneration in *rd3* mice is substantially delayed by GCAPs ablation. While the number of retinal photoreceptor cells is halved in six weeks in *rd3* mice, it takes eight months to halve in *rd3*/*rd3* GCAPs-/- mice. Although this substantial morphological rescue does not correlate with recovery of visual function due to very diminished guanylate cyclase activity in *rd3* mice, it is very informative of the mechanisms underlying photoreceptor cell death. By showing that GCAP2 is mostly in its Ca^{2+}-free phosphorylated state in *rd3* mice, we infer that the $[Ca^{2+}]_i$ at rod inner segments is permanently low. GCAPs are therefore retained at the inner segments in their Ca^{2+}-free, guanylate-cyclase-activator state. We show that in this conformational state GCAPs induce endoplasmic reticulum stress, mitochondrial swelling and cell death. ER stress and mitochondrial swelling are early hallmarks of *rd3* retinas preceding photoreceptor cell death, that are substantially rescued by GCAPs ablation. By revealing the involvement of GCAPs-induced ER stress in the physiopathology of LCA12 this work will aid to guide novel therapies to preserve retinal integrity in LCA12 patients to expand the window for gene therapy intervention to restore vision.

Second, RP10 is caused by gain-of-function mutations in *IMPDH1* gene. Inosine-5´-monophosphate dehydrogenase 1 (IMPDH1) catalyzes the rate-limiting step in the *de novo* synthesis of guanine nucleotides, impacting the cellular pools of GMP, GDP and GTP. Guanine nucleotide homeostasis is central to photoreceptor cells of the retina, where cGMP is the signal transducing molecule in the light response. Mutations in *IMPDH1* lead to inherited blindness, but the physiological relevance of IMPDH1 in the retina or its *in vivo* regulation remain largely unknown. We here investigate the *in vivo* regulation and physiological relevance of IMPDH1 in the retina, to gain insight into how *IMPDH1* mutations lead to retinal dystrophies. We here report that retinal IMPDH1 *in vivo* is regulated by light-dependent phosphorylation at Thr^{159}/Ser^{160} in the Bateman domain by protein kinase C, that desensitizes the enzyme to allosteric inhibition by GDP/GTP. The projected enhancement in guanine

nucleotide synthesis would contribute to sustain the GTP levels during illumination. Accordingly, we show that living mice accumulate IMPDH1 aggregates at rod outer segments upon prolonged bright light exposure; and that inhibiting IMPDH1 activity in living mice by intravitreal injection of IMPDH1 inhibitors delays rod mass response recovery. Based on these results we propose a novel mechanism of *in vivo* regulation of IMPDH1 that when disrupted leads to blindness.

1. INTRODUCTION

INTRODUCTION

1.1 The first steps in visual transduction.

The sense of sight permits to extract information about the natural world, like color, shape, distance, texture and movement of objects in the visual field and thus, allows organisms an efficient interaction with its environment. Almost 30% of the human cerebral cortex is largely or exclusively dedicated to visual processing, evidencing the importance of vision in high mammals (Van Essen 1997).

At the visual system, light enters the eye through the cornea (refracts the light), pupil (controls the amount of light that enters) and lens (focuses the light) and is projected to the retina at the back of the eye (**Fig 1**).

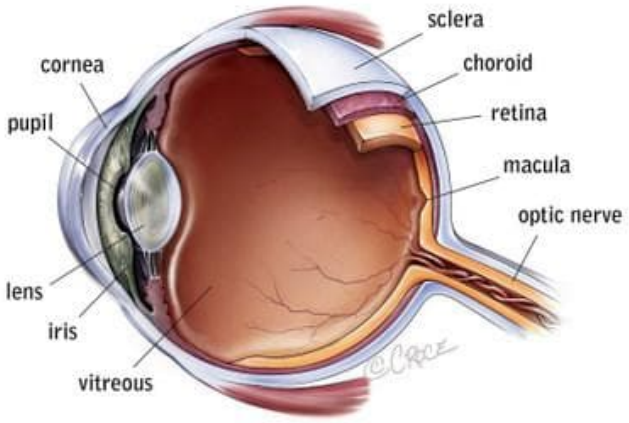

Figure 1. Structure of the eye. From Bionic Vision Australia, accessed 10 December 2019 <http://bionicvision.org.au/eye/healthy_vision>

At the retina, rod and cone photoreceptors absorb photons and convert them into electrochemical signals that are relayed along a subset of retinal cells to ganglion cells. This pathway from photoreceptor cells to ganglion cells is a highly convergent pathway that incorporates lateral inhibition, ultimately emphasizing luminance contrast. Photoreceptor cells measure the light intensity at the different points of the visual field, but ganglion cells ultimately inform the brain about those points in the visual field that present spatial or temporal changes in luminosity. In this way the retina initiates the coding of the shape and movement of objects in any luminosity environment of the natural world. The axons of ganglion cells converge into the optic nerve, that sends the electrical signals to a thalamus relay station and ultimately to the visual cortex, thus allowing the brain to create and perceive an image.

1.1.1 The retina: organization and function

The retina presents a laminar structure and is made up of five classes of neurons arranged in three nuclear layers: the outermost layer (outer nuclear layer, ONL) accommodates photoreceptors, a middle layer (inner nuclear layer, INL) contains bipolar, amacrine and horizontal cells and the innermost layer (ganglion cell layer, GCL) contains the ganglion cells (**Fig 2**). These neurons are interconnected at two synaptic levels: the outer and inner plexiform layers (OPL, IPL) (Wässle 2004). The architecture of the retina is sustained by non-neural cells: the retinal pigmented epithelial (RPE) cells and Müller cells, that provide trophic support and contribute to prevent oxidative stress in photoreceptors.

Visual processing begins with light entering through the pupil, traversing the transparent interior of the eye and reaching the retina, where it passes through the different retinal layers until reaching the photoreceptor cells. Beyond the photoreceptor cells, the adjacent retinal pigmented epithelium captures the excess of photons, thus preventing light reflection that would otherwise blur the image. The outer segment of the photoreceptor cells contains photopigments named opsins that are specialized in the capture of photons. When photopigments are photoexcited they trigger a complex enzymatic amplification cascade that ultimately changes the membrane potential and the rate of neurotransmitter release, in a process known as phototransduction (the conversion of photons into a change in membrane potential).

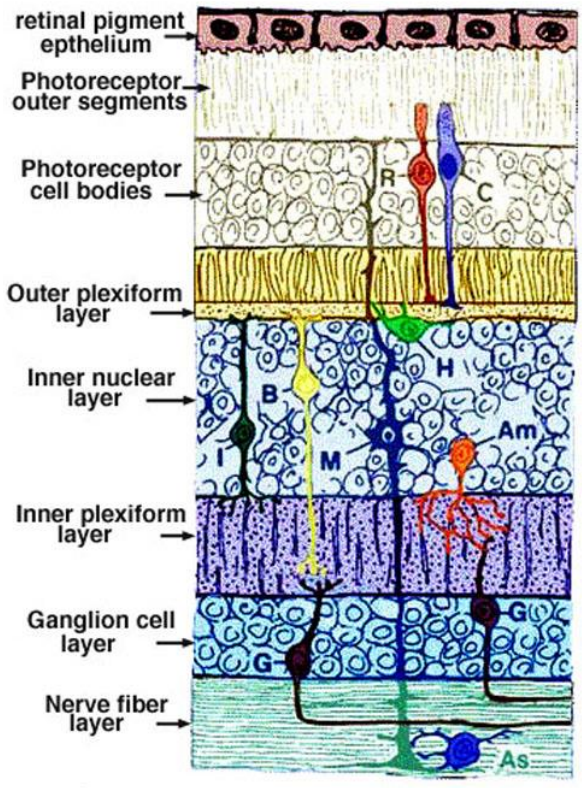

Figure 2. Retinal layer organization. In response to light, photoreceptors (PhRs) hyperpolarize and reduce the rate of glutamate release at their synapses. PhRs synapse with horizontal cells (HCs) and bipolar cells (BCs) at the OPL. BCs in turn synapse with retinal ganglion cells (RGCs). The PhR-BC-RGC connection constitutes the direct pathway of information flow in the retina, while HCs and amacrine cells (ACs) are inhibitory interneurons that provide lateral connections to emphasize contrast. HCs mediate lateral interactions between PhRs and BCs providing feedback inhibition as a function of background illumination (Boycott 1988). PhRs-HCs-BPs synapses set the basis for the coding of brightness and color contrast. BCs release glutamate onto ACs and RGCs. ACs are interneurons mainly inhibitory that interconnect neurons both laterally and vertically within the IPL. BCs-ACs-RGCs synapses set the basis for movement detection. Finally, RGCs integrate information typically across many BCs and ACs, and generate action potentials along well-defined axons that converge forming the optic nerve, transmitting the information to the brain. Illustration from (Odgen 1989).

Photoreceptor cells (PhR) use glutamate as a neurotransmitter and synapse onto second order glutamatergic bipolar cells (BCs) at the OPL level. Synaptic transmissions in the convergent connections between PhR and BCs in the direct pathway are modulated by horizontal cells (HCs) that confer lateral inhibition. BCs stablish synapses with retinal ganglion cells (RGCs) at the IPL level, that are modulated by amacrine cells (ACs). Finally, the axons of RGCs converge across the optic nerve and transmit visual information to the brain.

1.1.2 Photoreceptor cells: structure and function

Photoreceptor cells are the most abundant cell type in the retina, constituting approximately 70% of total cells (Curcio et al. 1990). There are two types of photoreceptor cells in the vertebrate retina: rods and cones. Rods are much more abundant than cones, and rod/cone distribution and relative proportion varies among species. In the human retina there are 120 million rods and 6 million cones. Rods localize all along the peripheral retina with rod cell density increasing in the central retina and fovea surrounding regions, but are absent from the fovea. Cones, on the other hand, are sparsed in the peripheral retina and their concentration increases in a linear gradient towards the macula lutea and fovea, where their density is maximal.

Rods are extremely sensitive to light. They are so sensitive that they can detect even a single photon (Rieke, 2000; Sampath and Rieke, 2004). As a result of their extreme sensitivity rods reach electrical saturation at relatively low background illumination. Rods are thus responsible for dim-light vision.

Cones are 100 times less sensitive than rods, but they exhibit much faster responses to variations in light intensity and never reach electrical saturation, being able to operate at the brightest light intensities in the natural world. Furthermore, in humans there are three types of cones: S, M and L – sensitive to Short (blue), Medium (green) and Long (red) light wavelengths, respectively. Thus, cones are responsible for bright-light, high acuity and color-coding vision.

Rods and cones are extremely specialized neurons, and are highly compartmentalized (**Fig 3**). They consist of an outer segment (OS), separated by a connecting cilium (CC) from an inner segment (IS) and cell nucleus (cell soma); and an axonic terminal.

The OS derives from a primary non-motile cilium and constitutes the "sensory antenna" of the cell, that captures light and converts it into electrochemical signals in the phototransduction process. Rods and cones can be easily distinguished by their OS architecture. Rod OS are large (25 μm in mice) (Mustafi, Engel, and Palczewski 2009) and contain a stack of membranous discs, physically separated from the plasma membrane. Cone outer segments are shorter (13 μm in mice) and consist of folds of

the plasma membrane, which are in direct contact with the extracellular plasma. These membranous structures at the OS compartment are where the phototransduction proteins are organized. Physiologically, cones and rods differ in their photopigments or opsins. Rods only express one photopigment, rhodopsin; whereas cones express one of three opsins depending on their spectral sensitivity.

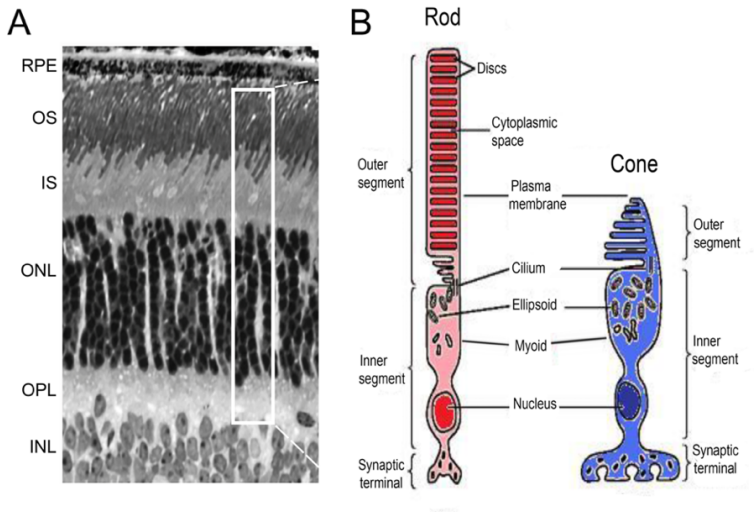

Figure 3. Rod and cone cellular structure. A) Vertical section of a murine retina stained with Richardson´s stain showing the photoreceptor cell layer. **B)** Scheme of vertebrate rod and cone photoreceptors. The light-sensitive outer segment (OS) is connected through a thin connecting cilium (CC) to the cell soma that comprises the inner segment (IS) and the nucleus. Morphological section from the lab. Rod and cone illustration from (O'Brien 1982).

The OS is separated from the cell soma by a thin connecting cilium, reminiscent of a primary cilium (**Fig 4E**). At the cell soma, the IS contains the metabolic and biosynthetic machinery of the cell. Photoreceptor cells present a high energetic demand, as they must sustain the electrochemical gradients that keep these cells partially depolarized in darkness and a huge rate of neurotransmitter release and vesicle recycling at the axonic terminal; and the phototransduction cascade and opsin chromophore recycling under light conditions. Furthermore, photoreceptor OS compartments are constantly renewed. Their tips are constantly phagocytosed by the adjacent RPE cells, so new discs have to be incorporated at the OS base on a daily basis (**Fig 4A**). This OS renewal requires a massive protein and lipid synthesis, as well as a massive vectorial vesicular trafficking from the IS to the OS across the connecting cilium. The IS contains the biosynthetic machinery to sustain this energetic and anabolic demands. The distal zone of the IS accommodates the ellipsoid region (**Fig 4C**) which is rich in mitochondria for aerobic respiration. At the proximal zone of the IS, adjacent to the nucleus, the myoid region contains the endoplasmatic reticulum and golgi apparatus, where protein synthesis and maturation takes place. Contiguous to the inner segment there is the nucleus of the cell. Collectively, the nucleus of rods and cones constitute the outer nuclear layer of the retina (**Fig 4D**).

Finally, the axonic terminals of rods and cones (rod spherules, cone pedicles) contain one (rods) or various (cones) synaptic ribbons that organize the synaptic vesicles for their massive tonic release in darkness, and tight regulation as a function of light intensity (**Fig 4F**).

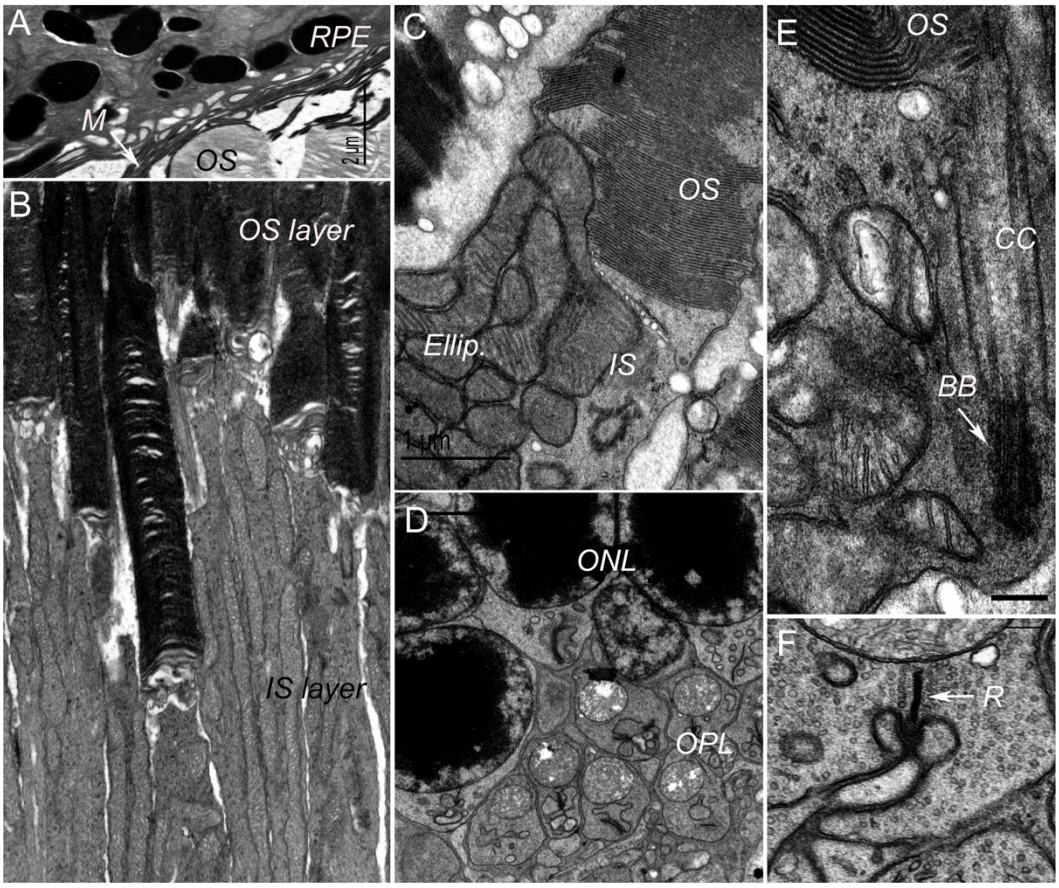

Figure 4. Photoreceptor cell compartments observed by transmission electron microscopy. A. Photoreceptor outer segment (OS) in contact with adjacent retinal pigmented epithelium cells (RPE). Note microvilli (M) from RPE cells intercalating with photoreceptor OS. **B.** Stacks of membrane discs at OS compartments, in contact with the ellipsoid region of the IS. **C.** Magnified inner segment/outer segment region of a bovine rod. Ellip., ellipsoid. **D.** Photoreceptor nuclei at the ONL and adjacent axonic terminals showing a "gigantic" mitochondria each, in the proximity of the synaptic ribbon at synaptic contacts with BCs and HCs. **E.** Connecting cilium (CC) and its basal body (BB) from a bovine rod. **F.** Magnified rod synaptic ribbon at a characteristic triad (two HCs and a BC). TEM images from our lab.

1.2 The light response: roles of cGMP and Ca^{2+}

Phototransduction is initiated by photoexcitation of the visual pigments at the OS disc membranes. This triggers a series of enzymatic steps that ultimately convey a change in the cell transmembrane potential. Communication between the membrane discs -where photopigment locates- and the plasma membrane -where conductance is altered- is facilitated by a second messenger, a small soluble signaling molecule, the cyclic-GMP (cGMP). Thus, cGMP acts as the second messenger in the light response.

Free levels of cGMP set the opening probability of the cGMP-gated channels (CNG-channels) at the plasma membrane. That is, the **free levels of cGMP set the transmembrane potential at any illumination condition**. The balance between cGMP synthesis by retinal guanylate cyclase (RetGC) and cGMP consumption by cGMP phosphodiesterase (cG-PDE) determines the response to light at any illumination condition (see below).

Calcium (Ca^{2+}) is another key molecule as it plays a critical role in light adaptation, a regulatory process required to maintain responsiveness of the visual system to light over a wide range of illumination conditions.

1.2.1 The dark current

In contrast to a typical neuron at rest, that has a membrane potential of about -65mV close to the equilibrium potential for K^+, the membrane potential of the rod outer segment in complete darkness is about -40mV. That is, photoreceptor cells are partially depolarized in the dark. This depolarization is caused by the steady influx of Na^+ through special channels in the outer segment membrane (the cGMP-gated channels, CNG-channels), that are gated by cGMP. The levels of cGMP are high in the dark, keeping the channels open. The movement of inward positive charge across the outer segment membrane in the dark is called the dark current (**Fig 5**) (Hagins, Penn, and Yoshikami 1970). Light reduces cGMP, causing the CNG-channels to close, and the membrane potential to become more negative. That is, light causes the hyperpolarization of photoreceptor cells (**Fig 5**).

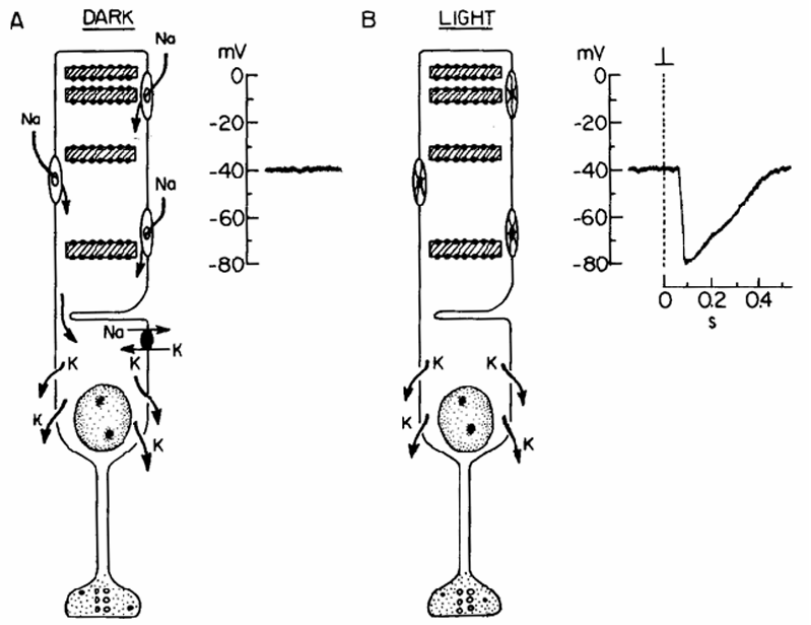

Figure 5. Dark current. In dark adapted conditions the CNG-channels at the outer segments are open because cGMP levels are high. Hence, positively charged ions (mainly Na^+) enter the photoreceptor, keeping these cells depolarized at about -40mV. This depolarizing current is known as the dark current. From University of Minnesota Medical School Duluth, accessed 14 December 2019 <https://www.d.umn.edu/~jfitzake/Lectures/DMED/Vision/Retina/ReceptorPotential.html)>

1.2.2 The dark-steady state

In the dark, the visual pigment and other signaling proteins involved in the light response are in their inactive or basal states (**Fig 6**). Opsins (rhodopsin and cone opsins) are composed of the apoprotein opsin and a chromophore molecule derived from vitamin A: *11-cis*-retinal. Opsins are seven transmembrane GTP-binding protein-coupled receptors (GPCRs). In the dark steady-state, the covalently bound *11-cis*-retinal blocks the receptors in their inactive state (R, in the case of rhodopsin). Because cGMP levels are high in the dark equilibrium, CNG-channels are kept open, allowing a constant influx of Na^+ into the outer segments. This current results in a relatively depolarized state of photoreceptor cells, characterized by the continuous release of glutamate neurotransmitter at the axonic terminals of rods and cones.

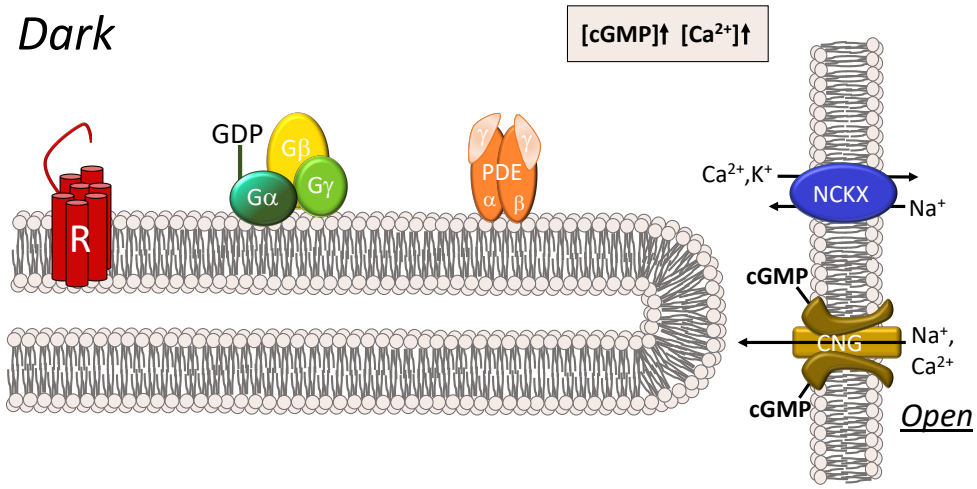

Figure 6. Illustration showing a rod disc in dark-adapted conditions. Rhodopsin (R) is bound to *11-cis*-retinal and blocked in its inactive state. The heterotrimeric complex transducin (GTα,β,γ) is assembled and inactive. The enzyme responsible for cGMP hydrolysis, cGMP-phosphodiesterase (cG-PDE), is kept at its basal state with the catalytic activity of the α/β subunits inhibited by the γ–subunits. CNG–channels at the plasma membrane are kept open, sustaining the dark current. Image modified from (Burns and Arshavsky 2005).

1.2.3 Activation phase of the light response

The absorption of a photon initiates the phototransduction enzymatic cascade by causing the *cis to trans*-isomerization of the chromophore, which induces a rapid conformational change in rhodopsin. Photoisomerization of the chromophore confers rhodopsin its active state, metarhodopsin II or R* (Wald, Durell, and St. George 1950).

R* activates the heterotrimeric G-protein transducin ($G_t\alpha$, β and γ) by promoting the GDP/GTP exchange on transducin α subunit, $G_t\alpha$, that dissociates it from $G_t\beta\gamma$ (**Fig 7**) (Arshavsky, Lamb, and Pugh 2002). $G_t\alpha$-GTP activation constitutes the first amplification step in the phototransduction cascade. Activated $G_t\alpha$ molecules bind to the γ-subunit of its effector, cGMP-phosphodiesterase (cG-PDE), relieving PDEγ inhibition of PDEαβ catalytic subunits (Hurley and Stryer 1982). This reaction results in activated PDEαβ molecules that hydrolyze hundreds of cGMP molecules per second, constituting the second amplification step in the phototransduction cascade.

The drop in cytoplasmic cGMP leads to the closure of the CNG-channels preventing the influx of Na^+ and Ca^{2+} into the outer segment, while $Na^+/Ca^{2+}/K^+$ exchanger (NCKX) continues extruding Ca^{2+}. **In this way, the light response causes a drop in the intracellular levels of cGMP and Ca^{2+}.** This is a graded effect. A slight lowering of the cGMP levels leads to the closure of some channels, whereas a large decrease in the cGMP levels will eventually lead to a complete closure of the channels (photoreceptor electrical saturation). Hyperpolarized photoreceptors reduce the rate of glutamate release at the ribbon synapse, transmitting visual information to second-order neurons.

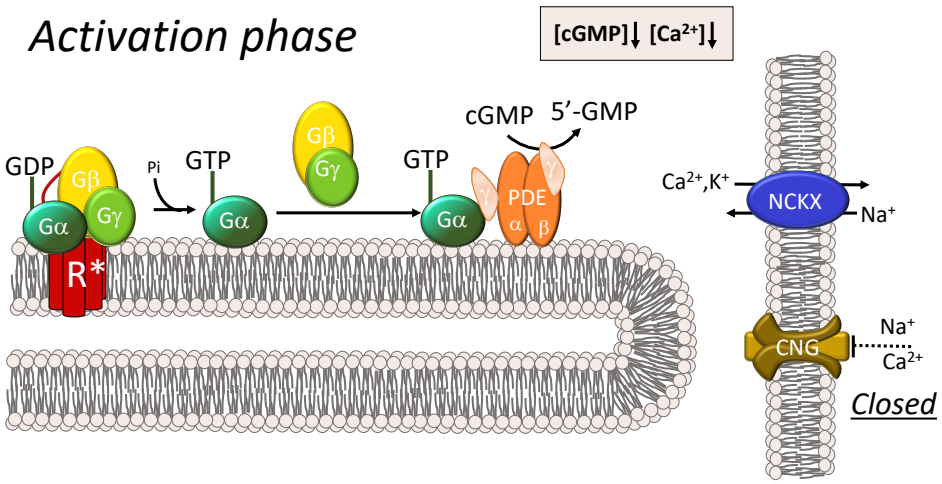

Figure 7. Phototransduction cascade. Photoisomerized rhodopsin (R*) causes transducin α ($G_t\alpha$) dissociation from $G_t\beta\gamma$. $G_t\alpha$.GTP activates cGMP phosphodiesterase (cG-PDE) which dramatically increases the rate of cGMP hydrolysis, reducing the intracellular concentration of free cGMP. CNG-channels close while the $Na^+/Ca^{2+}/K^+$ exchanger (NCKX) continues extruding Ca^{2+} ions from the outer segment cytosol, causing a drop in the intracellular Ca^{2+} levels. The reduction in the dark current causes a transient hyperpolarization. Image modified from (Burns and Arshavsky 2005).

1.2.4 Inactivation phase and light adaptation

Once the photoreceptor has responded to light, when the light ceases the phototransduction cascade is inactivated to restore the darkness equilibrium. If the light persists (e.g. under exposure to a steady light), the photoreceptor cell adapts to the light condition in order to avoid saturation. Photoreceptor cells employ many mechanisms to avoid saturation by bright light and to adjust the amplitude and time course of their photoresponses to changing ambient illumination in a process known as light adaptation. The $[Ca^{2+}]_i$ drop that accompanies the light response plays a key role both in termination of the light response and in light adaptation.

Termination of the light response involves: i) that all components of the phototransduction cascade that have been activated are deactivated to cease signaling; and ii) that cGMP levels are restored to the dark-state levels by new synthesis. Deactivation of R* involves rhodopsin phosphorylation by rhodopsin kinase (GRK1) and arrestin binding, that effectively uncouples rhodopsin from transducin (**Fig 8**). Deactivation of the effector $G_t\alpha$.PDE$\alpha\beta$ involves the protein complex responsible for catalyzing the GTPase activity in $G_t\alpha$: comprising RGS9-1, Gβ5-L and R9AP proteins. By promoting GTP/GDP exchange in $G_t\alpha$, this protein complex sequesters $G_t\alpha$ from PDE to promote its eventual re-assembly to $G_t\beta\gamma$ to re-establish the heterotrimetic inactive complex, **Fig 8**.

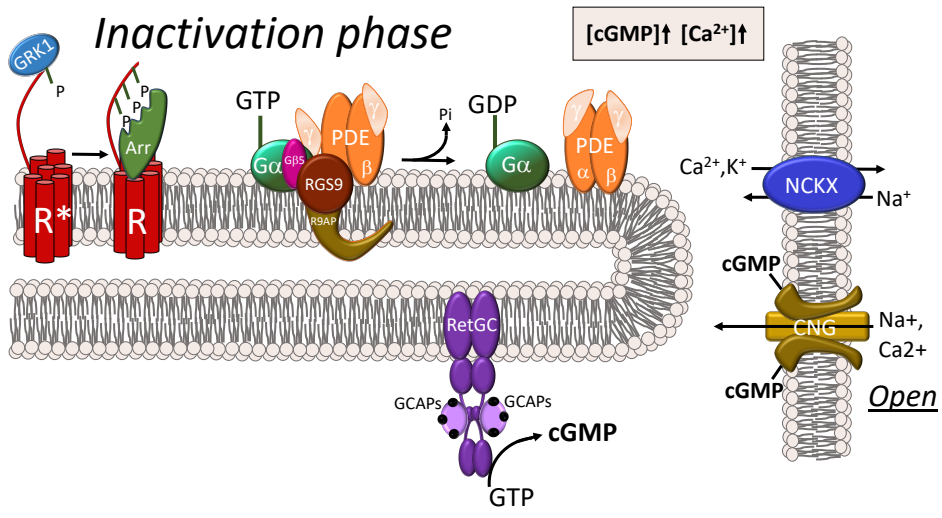

Figure 8. Termination of the light response/light-adaptation. The steps involved in termination of the light response or light-adaptation consist on 1) R* inactivation to R by rhodopsin kinase (GRK1) phosphorylation and arrestin (Arr) binding, an step that is promoted by the drop in $[Ca^{2+}]_i$; 2) effector inactivation by RGS9-1.Gβ5.R9AP catalysis of transducin alpha intrinsic GTPase activity; 3) RetGC activation by GCAP proteins promoted by the drop in $[Ca^{2+}]_i$ and 4) the gain of CNG-channels affinity for cGMP due to calmodulin detachment upon the drop in $[Ca^{2+}]_i$. Image modified from (Burns and Arshavsky 2005).

The drop in $[Ca^{2+}]_i$ exerts a negative feedback signal to the enzymatic cascade with the overall effect of counteracting the effect of light and restoring dark current. Ca^{2+} acts at three different levels in the light response, by acting on different molecular targets. First, the drop in $[Ca^{2+}]_i$ is sensed by the calcium sensor protein recoverin (Rec), which stops recruiting rhodopsin kinase (GRK1) (Kawamura 1993; C. K. Chen et al. 1995). Increased free GRK1 phosphorylates rhodopsin at multiple C-terminal sites, allowing arrestin binding that caps rhodopsin to prevent further activation of transducin (Gurevich and Benovic 1993). Rhodopsin phosphorylation and arrestin binding results in fewer $G_t\alpha$-GTP and consequently in less PDE activated molecules. As a consequence the rate of cGMP hydrolysis is reduced.

Second, the drop in $[Ca^{2+}]_i$ acts at activating guanylate cyclase activating proteins (GCAPs) and promoting cGMP synthesis. GCAPs are calcium sensor proteins that regulate retinal guanylate cyclase (RetGC) activity (depicted in **Fig 8** at the inferior part of rod's disc). As the Ca^{2+} drops in the light response, Ca^{2+} dissociates from GCAPs and in their Ca^{2+}-free state GCAPs stimulate RetGC activity, promoting cGMP synthesis. Synthesis of cGMP restores sensitivity (Dizhoor, Olshevskaya, and Peshenko 2010; Peshenko, Olshevskaya, Savchenko, et al. 2011a; Makino et al. 2012; A Mendez et al. 2001; Burns et al. 2002a).

A third Ca^{2+} dependent adaptation mechanism is the regulation of the affinity of CNG-channels for its ligand cGMP by the calcium sensor protein calmodulin (T. Y. Chen et al. 1994). Under dark-adapted conditions calmodulin or calmodulin-like proteins are bound to CNG-channels reducing their affinity for cGMP. As the $[Ca^{2+}]_i$ falls during the light response, calmodulin dissociates from the channel, increasing CNG-channel affinity for cGMP. This allows the channel in a light-adapted cell to operate at a lower range of cGMP concentrations than in a dark-adapted photoreceptor.

1.3 Retinal inherited diseases

Blindness and visual impairment has a direct impact on individual's quality of life and has also public health consequences. In a twenty year's retrospective study, the Global Burden of Disease (GBD) alerted that 285 million people are visually impaired worldwide with 39 million classified as blind (Bourne et al. 2013). Huge efforts are currently made in research to fight the most prevalent visual diseases such as age-related macular degeneration, glaucoma, diabetic retinopathy and cataracts. However, there are retinal inherited diseases that for its minoritary-nature have been more poorly studied and are less understood.

Retinal inherited diseases are a group of clinically and genetically heterogenous disorders that account for the main cause of vision loss in persons between 14 and 45 years of age, with 1:2000 individuals affected (Rattner, Sun, and Nathans 1999). They are linked to mutations in genes encoding proteins that are critical for photoreceptor development, function or survival. Nowadays more than 200 genes have been linked to inherited retinal diseases. The currently known genes are related to vital processes for photoreceptor cells, such as phototransduction, outer segment structure and morphogenesis, protein trafficking, protein folding, post-translational modifications, nucleotide homeostasis, carbohydrate and lipid metabolism, RNA splicing and transcription, ion transport, synaptic neurotransmission, extracellular matrix structure, development, etc.

The principal types of inherited retinal degenerative disease are progressive: retinitis pigmentosa (RP) and macular degeneration (MD). Retinitis pigmentosa (RP) affects rods primarily, causing night blindness. In advanced phases of RP, as a consequence of the loss of rods, cones start to die as well. This results in a loss of cone-mediated central vision that often leads to total blindness. RP affects approximately 1:3500 people, with mutations in the *RHO* gene (encoding rhodopsin) being the most prevalent by accounting for 20-30% of all cases (Parmeggiani et al. 2011). Macular degeneration affects the macular region of the retina where most cones are concentrated, causing a loss in central vision and visual acuity. Although some mutations have been linked to early MD, more frequently it is life-style and genetic predisposition that result in age-related macular degeneration (AMD).

Other progressive retinal disorders are cone dystrophies (CD) characterized by compromised cone function; and cone-rod dystrophies (CORD) in which both rod and cone function are affected.

Leber congenital amaurosis (LCA) is an early-onset retinal inherited disease affecting both cones and rods and is characterized by a severe loss of vision at birth or within the first years of life (den Hollander et al. 2008). The extent of vision loss varies from patient to patient, but can be quite severe with little or no light perception. LCA is one of the most common causes of blindness in children. The prevalence of LCA is 2 to 3 per 100000 newborns; and it accounts for 5% of total retinal dystrophies (Weleber et al. 1993). The most prevalent LCA mutations map at *CEP290*, *CRB1*, *GUCY2D* and *RPE65* genes, and are inherited in an autosomal recessive pattern. However, LCA has also been associated with autosomal dominant inheritance caused by mutations in *CRX* and *IMPDH1* genes. **Table 1** shows the frequency of LCA-associated genes (in blue, genes under study in the present work).

Table 1: Frequency of LCA-associated mutations

Gene	Protein	Frequency	References
ALMS1	Alstrom Syndrome Protein 1	?	
AIPL1	Aryl-hydrocarbon interacting protein-like 1	<5%	(Aboshiha et al. 2015)
CABP4	Calcium binding protein 4	?	(Aldahmesh et al. 2010)
CEP290	Centrosomal protein 290	15%-20%	
CLUAP1	Clusterin-associated protein 1	?	(Soens et al. 2016)
CRB1	Crumbs homolog 1	10%	
CRX	Cone rod homebox	1%	(S G Jacobson et al. 1998)
DTHD1	Death domain containing 1	?	(Abu-Safieh et al. 2013)
GDF6	Growth differentiation factor 6	?	
GUCY2D	Retinal guanylate cyclase 1	10%-20%	(Samuel G. Jacobson et al. 2013)
IFT140	Intraflagellar transport 140	?	(M. Xu et al. 2015)
IMPDH1	Inosine monophosphate dehydrogenase 1	5%	
IQCB1	IQ-Motif containing protein	?	(Estrada-Cuzcano et al. 2011)
KCNJ13	Inward rectifier potassium channel 13	?	
LCA5	Lebercilin	1%-2%	
LRAT	Lecithin retinol acyltransferase	<1%	
NMNAT1	Nicotinamide/nicotinic acid mononuclease adenylyltransferase 1	?	(Kumaran, Robson, and Michaelides 2018)
OTX2	Homebox 2 protein	?	(Henderson et al. 2009)
RD3	Retinal degeneration 3	<1%	
RDH12	Retinal dehydrogenase 12	10%	(Mackay et al. 2011)
RPE65	Retinal pigmented epithelium-specific 65 kDa	5%-10%	(Kumaran et al. 2018)
RPGRIP1	X-linked retinitis pigmentosa GTPase regulator-interacting protein 1	5%	
PRPH2	Peripherin-2	?	
SPATA7	Spermatogenesis-associated protein 7	3%	
TULP1	Tubby-related protein 1	<1%	

From (Kumaran et al. 2017).

There are also non-progressive disorders such as congenital stationary night blindness (CSNB) which affect rods and are characterized by impaired night vision but preservation of retinal morphology (therefore "stationary", that does not involve retinal degeneration); and achromatopsia (ACHM) is a stationary cone disorder associated with loss of color vision.

1.4 The protein complex responsible for cGMP synthesis in rods and cones

1.4.1 cGMP production by Retinal guanylate cyclase

In photoreceptor cells, RetGCs (retinal guanylate cyclases) are the enzymes responsible for cGMP synthesis. These enzymes belong to the membrane-bound GC (guanylate cyclase) family. Membrane-bound GCs display similar topologies and are type I transmembrane proteins that have an extracellular domain linked by a single transmembrane domain to an intracellular catalytic domain (**Fig 9**). Most of particulate GCs are stimulated by the binding of a ligand to its extracellular domain. In contrast, RetGCs are stimulated intracellularly by guanylate cyclase-activating proteins (GCAPs).

In the human retina there are two RetGC isoforms: RetGC1 (encoded by *GUCY2D* gene) that is present in both rods and cones and RetGC2 (encoded by *GUCY2F* gene) that is exclusive of rods. RetGC1 is the isoform that has been linked to human blindness, and therefore is the most relevant isoform.

1.4.2 RetGCs regulation by GCAP calcium sensors

Guanylyl cyclase-activating proteins (GCAPs) are EF-hand Ca^{2+}-binding proteins that regulate RetGC activity. They present four EF-hand domains, of which EF2, EF3 and EF4 are functional to bind Ca^{2+} and EF1 is not. Apparently EF1 has evolved in GCAP proteins to be a critical region in the contact surface with RetGC (Peshenko, Olshevskaya, and Dizhoor 2008).

GCAPs are thought to form stable complexes with RetGCs at photoreceptor outer segments, where they exert their function. At RetGC/GCAP complexes, GCAPs bind or dissociate Ca^{2+} according to the $[Ca^{2+}]_i$ set by illumination.

In the dark, Ca^{2+}-bound GCAPs are in an "inhibitory conformational state" in which they inhibit guanylate cyclase activity. Upon Ca^{2+} dissociation upon light exposure GCAPs acquire an "activator state" and stimulate RetGC activity, causing a boost of cGMP synthesis that serves to reopen CNG-channels and restore sensitivity (A Mendez et al. 2001; Burns et al. 2002a; Dizhoor, Olshevskaya, and Peshenko 2010; Peshenko, Olshevskaya, Savchenko, et al. 2011b).

It has been recently specified that GCAPs are Ca^{2+}/Mg^{2+} sensors (Peshenko and Dizhoor 2004), that bind Mg^{2+} in their Ca^{2+}-free state. Because $[Ca^{2+}]_i$ levels drop drastically in response to light, while the $[Mg^{2+}]_i$ remains unchanged (C. Chen, Nakatani, and Koutalos 2003), it is the $[Ca^{2+}]_i$ that determines the "inhibitor" or "activator" state of GCAPs and sets the proper dynamic regulation of RetGC (**Fig 9**).

In humans there are two different isoforms of GCAPs: GCAP1 (encoded by *GUCA1A* gene) and GCAP2 (encoded by *GUCA1B* gene). While RetGC1 is regulated by both GCAP1 and GCAP2 in both rods and cones; RetGC2 is only regulated by GCAP2 almost exclusively in rods (Peshenko, Olshevskaya, and Dizhoor 2015).

The mechanisms by which GCAPs regulate RetGCs have been extensively characterized by biochemical, structural, genetic and electrophysiological studies. Based on the *in vitro* determined individual Ca^{2+} sensitivities of GCAP1 and GCAP2, and the electrophysiological phenotype of double and individual knockout mice, a model was proposed of GCAPs sequential action in the light response. GCAP1, that has a slightly lower sensitivity for Ca^{2+}, acquires its active state first as the $[Ca^{2+}]_i$ drops during the light response. GCAP2, with a slightly higher sensitivity for Ca^{2+}, would only acquire its active state later in the light response, as the $[Ca^{2+}]_i$ approaches its lower limit (Makino et al. 2012). This so-called "Ca^{2+}-relay model" would secure a fine tune of RetGC activity to subtle changes in $[Ca^{2+}]_i$ across the wide range of physiological calcium concentrations.

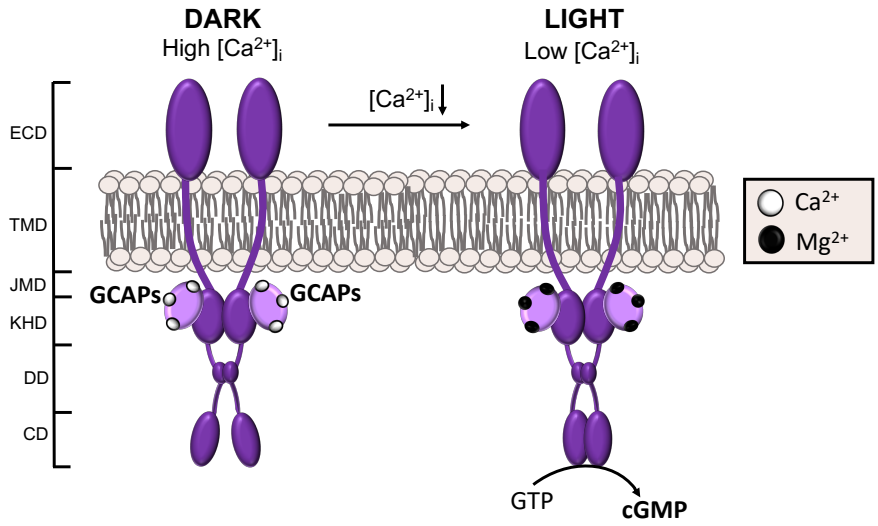

Figure 9. Model of RetGCs regulation by GCAPs. RetGCs are transmembrane polypeptides that consist of an extracellular domain (ECD); a transmembrane domain (TMD) that anchors the enzyme at the disc membrane; a juxtamembrane domain (JMD); a kinase homology domain (KHD); a dimerization domain (DD) that mediates cyclase activation; and a catalytic domain (CD) that converts GTP to cGMP. RetGC polypeptides are active as dimers. They are thought to be permanently bound to the GCAP proteins, that confer Ca^{2+} sensitivity to their catalytic activity. In the dark, the $[Ca^{2+}]_i$ is high and GCAPs are in their "inhibitory" Ca^{2+}-bound state, maintaining the catalytic domain of RetGC dimers at a distance and therefore inactive. In response to light, as the $[Ca^{2+}]_i$ drops, GCAPs switch to their Mg^{2+}-bound conformation that prompts the dimerization of the cyclase catalytic domains, stimulating cGMP synthesis. GCAP1 and GCAP2 activate RetGC sequentially, according to the $[Ca^{2+}]_i$ set by illumination. GCAP1 and GCAP2 bind to RetGC at overlapping residues situated in the KHD domain (Peshenko, Olshevskaya, and Dizhoor 2015).

1.4.3 Trafficking of RetGCs to the outer segment: the role of RD3

While the mechanisms of RetGC modulation by GCAPs have been extensively studied and are becoming clear, the mechanisms underlying RetGC/GCAPs complex assembly and transport to the outer segment in living rods and cones have been less explored. As integral membrane polypeptides, RetGCs are synthesized at the endoplasmic reticulum and subjected to posttranslational maturation at the Golgi.

RetGCs therefore rely on the secretory pathway (vectorial vesicular trafficking) for their distribution to the cilium. Whether RetGCs contain an intrinsic ciliary targeting sequence that confer them ciliary destination has remained elusive. Deletion and mutational analysis in transgenic *Xenopus laevis* have failed to identify a RetGC ciliary targeting sequence (Karan et al. 2011).

More recently RetGCs were found to depend on the 23 kDa blindness-associated protein RD3 (from the natural strain of blind mice "retinal degeneration 3" with the rd3 locus mutated) for their extraction from the endoplasmic reticulum, protein stability and ciliary trafficking (Seifollah Azadi, Molday, and Molday 2010). The *rd3* mice, lacking functional RD3, have dramatically reduced levels of RetGCs and are characterized by fast retinal degeneration. This phenotype is reverted by heterologous expression of RD3 (L. L. Molday et al. 2013). The 23 kDa RD3 was therefore established as a protein required for RetGCs stability and ciliary trafficking. However, the mechanism by which RD3 confers stability to RetGCs and facilitate their distribution to the cilium are not yet known.

On the other hand, GCAP1 and GCAP2 are known to depend on RetGCs for their own stability and transport to the outer segment. In the absence of RetGC1 and RetGC2 (RetGC1/RetGC2 double knock out) GCAPs fail to distribute to the outer segment compartment of rods and cones, and their stability is compromised (Baehr et al. 2007). The same is observed in the *rd3* mice due to the dramatically decreased levels of RetGCs (Seifollah Azadi, Molday, and Molday 2010). Actually, direct binding of GCAP1 to the cyclase is required for GCAP1 distribution to rod outer segments, which suggests that RetGC and GCAP assemble at the inner segment and are transported as a complex (López-Begines et al. 2018).

Interestingly, while investigating the effect of RD3 on *in vitro* RetGC catalytic activity, Peshenko et al. found that RD3 was a high-affinity inhibitor of RetGC. In addition to inhibiting RetGC basal activity, RD3 also competed with GCAP1, precluding GCAP1 activation of the cyclase. Based on this *in vitro* data Peshenko et al. proposed that one physiological role of RD3 could be preventing cGMP synthesis at the cell soma while RetGC was being transported to the cilium (Peshenko, Olshevskaya, Azadi, et al. 2011).

This predicted function of RD3 required that RD3 was localized at the inner segment and was excluded from the outer segment. This model appeared to be at odds with RD3 immunolocalization results reported in the original study, that localized RD3 at the outer segment (Seifollah Azadi, Molday, and Molday 2010). This discrepancy created the urge to determine the *in vivo* localization of RD3 in photoreceptor cells by rigorous, unbiased methods.

Furthermore, the mutually exclusive binding of RD3 and GCAPs to the cyclase raised key questions about the trafficking of this protein complex, by implying the need of a series of sequential regulated steps that account for the facts that RetGCs depended on RD3 for their trafficking to the cilium; at the same time that GCAPs depend on RetGCs for their outer segment distribution.

1.4.4 *GUCY2D* blindness associated mutations. Mouse models to study RetGC function.

GUCY2D (encoding RetGC1) was the first gene associated with Leber congenital amaurosis (LCA) and was thus assigned to the LCA1 locus (I. Perrault et al. 1996). Since then, over 100 mutations have been identified in the *GUCY2D* gene causing different forms of retinal dystrophies (Wimberg et al. 2018). Autosomal recessive mutations in *GUCY2D* result in loss-of-function of RetGC1 by compromising protein stability, impairing catalytic activity or dimerization capacity. Mutations ultimately reduce the cGMP content at the outer segment, causing the permanent closure of CNG-channels. Closure of the channels precludes rod and cone visual function and presumably results in a permanent hyperpolarization state that is deleterious for the cell.

Heterozygous mutations in *GUCY2D* have been associated to autosomal dominant cone dystrophies (adCD) and cone-rod dystrophies (adCORD, namely CORD6) (Gregory-Evans et al. 2000). These are gain-of-function mutations that lead to constitutive activity of the cyclase *in vitro* (S E Wilkie et al. 2000). Based on the *in vitro* phenotype of the mutations, the underlying mechanism of the pathology in adCD and adCORD is thought to be the unabated synthesis of cGMP *in vivo*, which would lead to abnormally high levels of cGMP. Abnormally high cGMP would keep a higher-than-normal fraction of CNG-channels open, increasing the influx of calcium. Elevated intracellular cGMP and calcium are both established as causes of toxicity in photoreceptor cells (Power et al. 2019; Krizaj and Copenhagen 2002).

Several loss-of-function models of RetGC have been generated and characterized. The individual targeted depletion of the *Gucy2d* and *Gucy2f* genes allowed the characterization of RetGC1 and RetGC2 roles in murine retinas (Yang et al. 1999; Baehr et al. 2007b). Subsequently the RetGC1/RetGC2 double KO was also generated (RetGC1/RetGC2 dKO) (Baehr et al. 2007).

The mouse system differs from the human system in that both RetGC1 and RetGC2 play a physiological role in the light response. RetGC1 KO showed cone degeneration but largely retained rod function; while RetGC2 KO retained largely normal retinas, which pointed to some RetGC1/RetGC2 functional redundancy. The RetGC1/RetGC2 dKO, though, presented a rapid retinal degeneration that reduced the number of photoreceptor cells to 50% in six months, resembling the human LCA1 phenotype. This loss-of-function model of RetGC activity lacked rod and cone visual function and showed reduced levels of GCAP1 and GCAP2 that were abnormally retained at the inner segment compartment (Baehr et al. 2007).

1.4.5 *GUCA1A* and *GUCA1B* blindness-associated mutations. Mouse models to study GCAP1 and GCAP2 function.

To date, fourteen mutations have been identified in the *GUCA1A* gene encoding GCAP1 that lead to inherited retinal dystrophies (Listed in **Table 2**).

Mutations in *GUCA1A* mainly affect cones and cause autosomal dominant cone-dysthrophies (adCD), cone-rod dystrophies (adCORD) and macular degeneration (Kamenarova et al. 2013). Most of the mutations in *GUCA1A* map at one of the functional EF-hands, with the effect of diminishing Ca^{2+} binding affinity. This decrease in Ca^{2+} binding affinity of GCAP1 alters the calcium sensitivity of RetGC activity in *in vitro* assays, displacing the sensitivity curve to higher values of $[Ca^{2+}]_i$ (Susan E. Wilkie et al. 2001; Nishiguchi et al. 2004; Bowne et al. 2002; Peshenko et al. 2019). The *in vivo* effect of a displacement of RetGC activity towards higher $[Ca^{2+}]_i$ would be the constitutive activity of the cyclase in the physiological range of $[Ca^{2+}]_i$, independently on the light conditions. That GCAP1 mutations that decrease Ca^{2+} binding affinity lead to unabated cGMP synthesis in photoreceptors *in vivo* has by now been demonstrated (Olshevskaya et al. 2004; Woodruff et al. 2007).

One mutation in the *GUCA1B* gene (encoding GCAP2) that impairs Ca^{2+} binding has been linked to retinitis pigmentosa, as GCAP2 is mainly expressed in rods (Sato et al. 2005).

Table 2: Mutations in *GUCA1A* and *GUCA1B* genes leading to retinal dystrophies

GCAP	Mutation	Domain	Dystrophy	Activity GC	References
GCAP1	P50L		AdCD, AdCORD	Like WT	(Sokal et al. 2000)
GCAP1	G86R		AdCORD	Constitutive activation	(Peshenko et al. 2019)
GCAP1	L84F	EF3	AdCD, AdCORD, Macular	Constitutive activation	(Marino et al. 2015)
GCAP1	E89K	EF3	AdCD	Constitutive activation	(Kitiratschky et al. 2009)
GCAP1	Y99C	EF3	AdC, AdCORD, Macular	Constitutive activation	(Michaelides et al. 2005)
GCAP1	D100E	EF3	AdCD	Constitutive activation	(Kitiratschky et al. 2009)
GCAP1	N104K	EF3	AdCD	Constitutive activation	(Jiang et al. 2008)
GCAP1	I107T	EF3	AdCD, AdCORD, Macular	Constitutive activation	(Marino et al. 2015)
GCAP1	E111V	EF3	AdCORD	Constitutive activation	(Marino et al. 2018)
GCAP1	T114I	EF3	atypical RP		
GCAP1	I143NT	EF4	AdCD	Constitutive activation	(Nishiguchi et al. 2004)
GCAP1	L151F	EF4	AdCORD	Constitutive activation	(Jiang et al. 2005)
GCAP1	E155GD	EF4	AdCD	Constitutive activation	(Susan E. Wilkie et al. 2001)
GCAP1	G159V	EF4	AdCD	Constitutive activation	(Kitiratschky et al. 2009)
GCAP2	G157R	EF4	AdRP		(Sato et al. 2005)

Compiled from (Jiang et al. 2014, Kamenarova et al. 2013, Dell'orco et al. 2014, Palczewski et al. 2004, Nishiguchi et al. 2004; Sato et al. 2005; Peshenko et al. 2019).

Loss-of-function models of the GCAP proteins were also generated and characterized. The analysis of the GCAP1/GCAP2 dKO preceded the analysis of the individual KOs, given that *GUCA1A* and *GUCA1B* are contiguous in the genome (A Mendez et al. 2001). GCAP1/GCAP2 dKO (GCAPs-/- mice) presented largely normal retinas with unaltered **basal** RetGC activity (A Mendez et al. 2001).

However, the ablation of GCAPs eliminated the Ca^{2+}-feedback loop to RetGC activity during dark-adapted light responses and during light adaptation. These mice elicited abnormally large responses and reached saturation at lower background light intensities. The analysis of GCAPs-/- revealed the important individual contribution of the Ca^{2+} feedback loop to RetGC to single photon response sensitivity and kinetics. In terms of photoreceptor viability, GCAPs depletion did not have a noticeable effect on retinal morphology. GCAPs-/- mice retained largely normal retinas for up to a

year of age (A Mendez et al. 2001); consistent with blindness-associated GCAP mutations being autosomal dominant, of gain-of-function nature.

Transgenic mice expressing GCAP1 mutants linked to adCORD, such as Y99C-GCAP1 with a Tyr99Cys substitution at EF-hand 3, and E155G-GCAP1 with a Glu155Gly substitution at EF-hand 4 (Woodruff et al. 2007), were developed to demonstrate how the lowered GCAP1 affinity for Ca^{2+} shifted the Ca^{2+} sensitivity of RetGC *in vivo*. The enhanced activity of the cyclase *in vivo* at any light condition increased CNG-channel activity, causing an elevation of $[Ca^{2+}]_i$ which in turn caused cell death (Olshevskaya et al. 2004).

To study the *in vivo* effect of impaired Ca^{2+} binding to GCAP2 (as a generic approach to GCAP2 mutations associated to RP), a transgenic mouse model was established that expressed a form of GCAP2 impaired to bind calcium at the three functional EF-hand domains (EF$^-$GCAP2 mice). EF$^-$GCAP2 mice showed a rapid retinal degeneration by a mechanism independent of cGMP at the OS (Hoyo et al. 2014). The mechanism underlying GCAP2 toxicity in this context was GCAP2 retention at rod inner segments (Hoyo et al. 2014). **Based on these results it was proposed that GCAPs could act as damage mediators in the genetic contexts expected to result in GCAPs retention at the cell soma in a context of chronic low $[Ca^{2+}]_i$, such as in LCA1 or LCA12.**

1.4.6 *RD3* blindness mutations. The *rd3* mice.

In 1969 four wild-type mice captured in Valle di Poschiavo, Switzerland, were imported to the Jakson Laboratories because they were known to have Robertsonian chromosomes. These mice were crossed with Swiss mice to obtain the RBF/DnJ strain (Festing 1979) and subsequently inbred in different black and albino mouse strains. These animals were characterized for retinopathies (Heckenlively et al. 1993) and were found to show a rapid retinal degeneration whose progression varied among the genetic backgrounds. Black strains developed nearly normal retinas that retained electroretinogram (ERG) responses up to p32, showing initial signs of degeneration at three weeks; while albino strains degenerated much faster showing extinguished ERG responses earlier. These animals were renamed as rd3 (retinal degeneration 3) mice.

Later, Friedman et al. characterized the rd3 mice more deeply (Friedman et al. 2006), and identified a c.319→t transition in the third exon of the *C1orf36* gene. This mutation caused a premature truncation in the *C1orf36* gene product, a protein of 195 aa, that led to a 106 aa unstable protein that was rapidly degraded. Thus *C1orf36* gene was renamed as *Rd3*. It was predicted that similar mutations in the *RD3* human locus would lead to early-onset retinal dystrophies in humans (Friedman et al. 2006).

A screening for mutations in the *RD3* locus in patients with different retinal dystrophies including LCA revealed that two siblings affected by LCA presented a homozygous G→A transition (c.296+1G→A) in a donor splice site in the *RD3* gene. This mutation was predicted to result in the premature truncation of the RD3 protein; and LCA patients affected by loss-of-function mutations in the *RD3* gene were assigned the LCA12 form of this disease (Friedman et al. 2006).

To date four extra mutations in *RD3* have been linked to human LCA12 (Listed in **Table 3**). These mutations lead to premature truncation of the protein, or to deletion of the intracellular coiled-coil domain. Intriguingly, a lysine to glutamic acid substitution in residue 87 has been identified in a family affected by retinitis pigmentosa (RP) rather than LCA (De Castro-Miró et al. 2014).

Table 3: Mutations identified in *RD3* leading to retinal dystrophies

Mutation	Dystrophy	Effect on protein	References
R38X	LCA12	Lacking residues 38-99	(Perrault et al. 2013)
c.296+1G→A	LCA12	Truncated protein	(Friedman et al. 2006)
E46X	LCA12	Lacking residues 46-99	(Perrault et al. 2013)
E46A2bp deletion 83X	LCA12	Truncated protein	(Perrault et al. 2013)
Y60X	LCA12	Truncated protein	(Preising et al. 2012)
K87E	RP	Unknown	(De Castro-Miró et al. 2014)

Compilled from (Friedman et al. 2006; Perrault et al. 2013; De Castro-Miró et al. 2014).

1.5 Photoreceptor cell death mediated by alterations in cGMP levels

Mutations in many apparently unrelated genes linked to different forms of inherited retinal dystrophies converge at altering cGMP levels in rods and/or cones as the insult that ultimately causes photoreceptor cell death.

Free cGMP levels determine the transmembrane potential of photoreceptor cells at any illumination condition. cGMP turn-over rates are very high in rods and cones so that even small changes in illumination are reproducibly transduced to changes in membrane potential with fast kinetics. The cGMP turn-over rate is determined by the rate of cGMP synthesis by RetGCs and the rate of cGMP hydrolysis by cG-PDE. These enzymatic activities change with the illumination levels, but a balance between synthesis and hydrolysis must be established for each steady-state, so that cGMP levels are always kept within a physiological range of concentrations.

The cGMP turn-over rate in photoreceptor cells is at least 10-fold higher than in any other cell type (Pugh and Lamb 1990; Granovsky and Artemyev 2001), with the rate of cGMP synthesis estimated at 100-600 μM cGMP/s in the recovery phase that follows photoexcitation (Burns et al. 2002a). This high cGMP turn-over helps to explain why mutations in any of the genes that affect cGMP synthesis or cGMP hydrolysis create an unbalance of forces that produces large alterations in cGMP levels. Disruption of cGMP homeostasis has profound effects on cell physiology and compromise viability, causing photoreceptor cell death (Power et al. 2019).

Several mutations have been shown to disrupt cGMP homeostasis in photoreceptor cells. Loss-of-function mutations in the different subunits of rod and cone cGMP-phosphodiesterases (cG-PDEs) responsible for cGMP hydrolysis, lead to **abnormally high cGMP levels** that are associated to different forms of blindness, both in humans (Dryja et al. 1999; McLaughlin et al. 1993; Tsang et al. 1996; Grau et al. 2011; Kohl et al. 2012) and in naturally occurring animal models (Bowes et al. 1990; D B Farber, Danciger, and Aguirre 1992; McLaughlin et al. 1993). In these models the cGMP levels rise dramatically as soon as the animals open their eyes and lack cGMP hydrolysis, due to light-activated RetGC activity. The resulting abnormally high cGMP levels cause the opening of an abnormally high fraction of CNG-channels, increasing the influx of Na^+ and Ca^{2+}. It is presumably the increase in $[Ca^{2+}]_i$ that leads to apoptosis (Olshevskaya et al. 2004; Woodruff et al. 2007; Paquet-Durand et al. 2009; Trifunović et al. 2010; Sothilingam et al. 2015).

Loss-of-function mutations in transducin subunits that prevent cG-PDE activation are also associated with abnormally high cGMP levels (Dryja et al. 1996; Kohl et al. 2002); and null mutations in the CNG-channel subunits, *CNGA3* and *CNGB3*, lead to a cGMP accumulation in cones that underlies the physiopathology of achromatopsia (Ma et al. 2015b). As mentioned above, gain-of-function mutations in *GUCY2D* or in *GUCA1A* associated to cone or cone/rod dystrophies are also detrimental for photoreceptor cells by affecting the Ca^{2+} sensitivity of RetGC activity and causing an excessive production of cGMP (Kelsell et al. 1998; Sato et al. 2005; Kamenarova et al. 2013; Wimberg et al. 2018).

On the other hand there are mutations on several genes that lead to the opposite situation: **abnormally low cGMP**. Representative mutations leading to abnormally low cGMP levels are the already mentioned null mutations in *GUCY2D* encoding RetGC1 and the *RD3* gene, linked to LCA1 and LCA12 respectively (Seifollah Azadi, Molday, and Molday 2010; Agrawal et al. 2017). Loss-of-function mutations in genes that encode proteins involved in termination of the light response such as rhodopsin kinase and arrestin (Fuchs et al. 1995; Nahazawa, Wada, and Tamai 1998; Cideciyan et al. 1998), or gain-of-function mutations in transducin alpha (Szabo et al. 2007) that lead to unabated

signaling in response to light, also result in an abnormal decrease of cGMP. These contexts are generally referred to as **"light equivalent" genetic contexts**, in the sense that prolonged bright light exposure that results in prolonged low cGMP can also result in photoreceptor cell death and retinal degeneration (Fain 2006). In this scenario, which is the opposite to the one leading to abnormally high cGMP, chronic hyperpolarization would lead to chronic low Ca^{2+}, that could be the basis of the pathology.

Examples of mutations in genes expected to alter cGMP regulation are listed in **Table 4** (in blue genes under study in the present work).

Table 4.

Genes that when mutated may cause inherited retinal dystrophies by altering cGMP levels in photoreceptor cells

Gene	Mutation effect	cGMP	Phenotype	References
AIPL1	Blocks the functional assembly of PDE	High	LCA	(Ramamurthy et al. 2004)
CNGA1	Disrupts the cGMP-Ca^{2+} negative feedback loop	High	RP	(Dryja et al. 1995)
CNGB1	Disrupts the cGMP-Ca^{2+} negative feedback loop	High	RP	(Hartong, Berson, and Dryja 2006)
CNGA3	Disrupts the cGMP-Ca^{2+} negative feedback loop	High	ACHM	(Johnson et al. 2004)
CNGB3	Disrupts the cGMP-Ca^{2+} negative feedback loop	High	ACHM	(Kohl et al. 2005)
REEP6	Decreases the RetGC1/2 isozymes	Low	RP	(Agrawal et al. 2017)
GNAT1	Loss-of-function prevents PDE activation Gain-of-function accelerates PDE activity	High/Low	CSNB RP	(Dryja et al. 1996) (Szabo et al. 2007) (Carrigan et al. 2016)
GNAT2	Prevents PDE activation	High	ACHM	(Rosenberg et al. 2004)
GRK1	Fails to inactivate Rhodopsin	Low	CSNB	(Cideciyan et al. 1998)
GUCA1A	Disrupts the cGMP-Ca^{2+} negative feedback loop	High	CD, CORD, MD	(Kamenarova et al. 2013)
GUCA1B	Disrupts the cGMP-Ca^{2+} negative feedback loop	High	RP	(Sato et al. 2005)
GUCY2D	Gain-of-function leads to constitutive cGMP production Loss-of-function impairs cGMP production	High/Low	LCA, CD, CORD	(Wimberg et al. 2018)
IMPDH1?	Autosomal dominant mutations predicted to be gain-of-function mutations that would elevate GTP pool, that would in turn elevate cGMP levels	High	LCA, RP	(Kennan et al. 2002) (den Hollander et al. 2008)
PDE6A	Impairs cGMP consumption	High	RP, CSNB	(Dryja et al. 1999)
PDE6B	Impairs cGMP consumption	High	RP	(McLaughlin et al. 1993)
PDE6C	Impairs cGMP consumption	High	ACHM	(Grau et al. 2011)
PDE6G	Impairs cGMP consumption	High	RP	(Tsang et al. 1996)
PDE6H	Impairs cGMP consumption	High	ACHM	(Kohl et al. 2012)
RHO	Inactivates the phototransduction cascade Impairs cGMP consumption	High	RP	(Hartong, Berson, and Dryja 2006)
RD3	Decreases the RetGC1/2 isozymes	Low	LCA	(Friedman et al. 2006)
SAG	Fail to inactivate Rhodopsin	Low	CSNB RP	(Fuchs et al. 1995) (Nahazawa, Wada, and Tamai 1998)

Modified from (Power et al. 2019). Gene nomenclature is found in gene list section.

Besides gating CNG-channels and therefore controlling ionic flux at the outer segment, cGMP has other effects in photoreceptor cells. An effect of cGMP that has more recently been revealed is its activation of protein kinase G (PKG). Excessive activation of PKG was found to be the cause of cell death in mouse models of achromatopsia caused by mutations in the alpha and beta subunits of cone CNG-channels (Ma et al. 2015).

1.5.1 Cell death mediated by ER stress

The endoplasmic reticulum (ER) is a complex, dynamic organelle whose functions include protein folding, Ca^{2+} storage, and lipid and carbohydrate metabolism (Senft and Ronai 2015). Various cellular stresses such as protein folding defects, perturbations in Ca^{2+} homeostasis, altered protein glycosylation or redox imbalance disrupt ER functions and lead to unfolded or misfolded proteins to accumulate in the ER lumen in a process known as ER stress (Hetz and Mollereau 2014). To alleviate ER stress, cells respond with an integrated signaling system by activating the unfolded protein response (UPR), ER-associated degradation (ERAD), autophagy, hypoxic signaling and mitochondrial biogenesis (Walter and Ron 2011). The combined activity of these mechanisms determines the magnitude of ER stress and thus governs whether cells will recover homeostasis or activate cell death programs (Ferri and Kroemer 2001).

ER-stress and the UPR are intricately connected and are transduced by three ER resident proteins: 1) the inositol-requiring enzyme 1 (IRE1); 2) the activating transcription factor-6 (ATF6) and 3) the protein kinase R-like ER protein kinase (PERK) (Hetz 2012). The three ER stress branches act at different levels to reestablish cell homeostasis: 1) by regulating the expression of chaperones such as glucose regulated protein-78 or binding-immunoglobulin-protein (GRP78/BIP); 2) by reducing protein synthesis through phosphorylation of eukaryotic initiation factor-2α (eIF2α); or 3) ultimately by activating apoptotic responses by expression of several genes such as CHOP/GADD153 encoding a transcription factor that negatively regulates the anti-apoptotic factor BCL-2 (**Fig 10**).

The BCL-2 family (from "B cell lymphoma") is essential to mediate the crosstalk between the ER and mitochondria to trigger apoptosis under conditions of chronic ER stress by controlling the release of cytochrome C and apoptosome assembly (Rodriguez, Rojas-Rivera, and Hetz 2011).

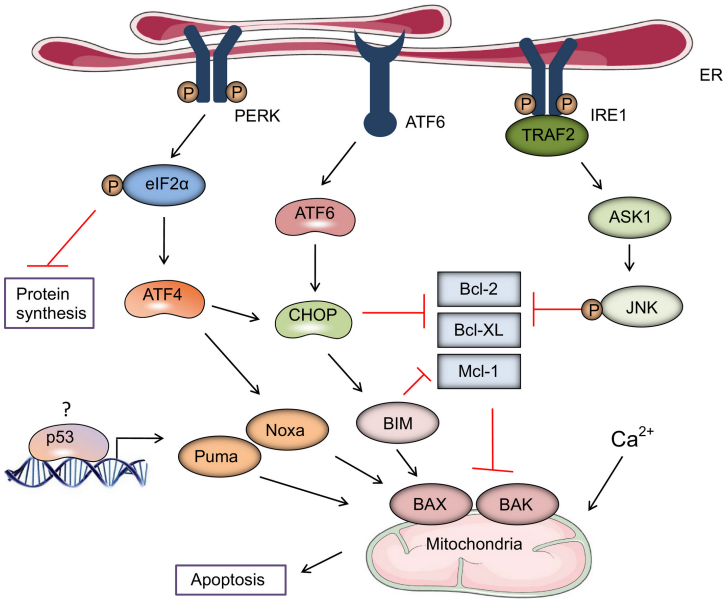

Figure 10. The unfolded protein response. Image obtained from (Iurlaro and Muñoz-Pinedo 2016)

In photoreceptor cells, abnormally high cGMP levels have shown to result in ER stress either by causing an elevation of Ca^{2+} influx by increasing the fraction of CNG-channels open (Butler et al. 2017); or through PKG activation (Ma et al. 2015); whereas abnormally low cGMP levels, that ultimately cause a drop in the $[Ca^{2+}]_i$ may also ultimately result in ER stress (Agrawal et al. 2017).

1.6 IMPDH1 in the retina

Mutations in the housekeeping gene *IMPDH1* have been associated to severe forms of blindness: autosomal dominant retinitis pigmentosa 10 (adRP10) and Leber's Congenital Amaurosis 11 (LCA11). Inosine monophosphate dehydrogenase 1 (IMPDH1) is the enzyme responsible for the first committed step in the *de novo* synthesis of GTP. Despite the ubiquitous nature of this enzyme, mutations in *IMPDH1* are restricted to the retina for reasons that are not yet understood. The levels of IMPDH1 in photoreceptors cells are higher than in any other cell type, and there are retinal specific spliced-forms of the enzyme. Despite its relevance in human blindness little is known about the physiological role of this enzyme in photoreceptor cells of the retina, or its *in vivo* regulation.

1.6.1 Purine nucleotide control in photoreceptors

Cells use different pathways to synthesize purine nucleotides and balance the guanine and adenine pools (**Fig 11**). In the *salvage* pathways, nucleotides are produced from recycled purine bases (blue arrows in **Fig 11**). In *de novo* biosynthesis, a purine ring is assembled over ribose 5´-phosphate by sequential enzymatic steps that use precursors of the carbohydrate and amino acid metabolism (Zhao et al. 2013; Pedley and Benkovic 2017) (black arrows in **Fig 11**). In this pathway, inosine monophosphate (IMP) is the first molecule with a complete purine ring and is the common precursor for GTP and ATP synthesis. Inosine monophosphate dehydrogenase 1 (IMPDH1) is the enzyme catalyzing the rate limiting step in the *de novo* synthesis of GTP (red in **Fig 11**).

In the phototransduction cascade, guanine nucleotides play a central role, as cGMP is a key signaling molecule in the light response. The balance between cGMP consumption by PDE and re-synthesis by RetGC dictates the polarized/depolarized state of the cell, and its synaptic communication with second-order neurons. It is not clear how RetGC obtains its substrate GTP to replenish cGMP. It has been proposed that after phosphodiesterase consumption of cGMP, the resulting 5'-GMP diffuses to the inner segments for its recycling to GTP (Ridge et al. 2003). Guanylate kinase (GK) and nucleoside diphosphokinases (NDK) at the inner segment would sequentially convert GMP to GDP and GTP. Both GK and NDK have been immunolocalized to inner segments, perinuclear regions and synaptic terminals of photoreceptor cells (Wimberg, Janssen-Bienhold, and Koch 2018b) and (Rueda et al. 2016), respectively.

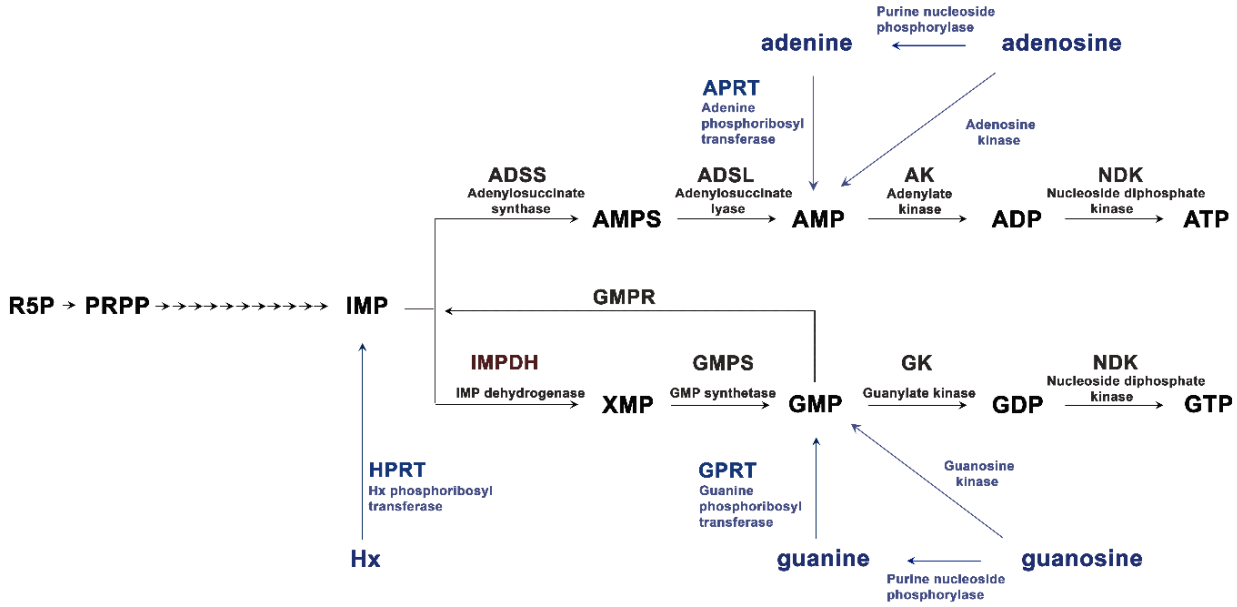

Figure 11. *De novo* and *salvage* pathways of purine synthesis in eukaryotic cells. Modified from (Zhao et al. 2013).

The contribution of the *de novo* pathway to GTP supply in photoreceptor cells has not been thoroughly addressed, despite the fact that mutations in *IMPDH1* have been associated with severe forms of blindness (see below), and that hypoxanthine phosphoribosyl transferase (HRPT), the key enzyme in the *salvage* pathway, presents a very low expression in photoreceptor cells (Kennan et al. 2003). This apparent oblivion of IMPDH1 role in photoreceptor cells is probably due in part to the observation that a mouse model of IMPDH1 deficiency presents only a mild retinopathy (Aherne et al. 2004).

1.6.2 IMPDH structure and catalytic cycle

Inosine monophosphate dehydrogenase (IMPDH) is the enzyme catalyzing the rate-limiting step in the *de novo* synthesis of GTP. Eukaryotic IMPDH monomers consist of two domains: a catalytic domain consisting in a $(\beta/\alpha)_8$ barrel, and a regulatory domain containing two nucleotide-binding CBS domains (named after their homology to "cystathionine beta synthase" domains), also known as Bateman domain (**Fig 12**). IMPDH is a tetrameric enzyme that adopts a square planar geometry with CBS domains protruding from the corners of the tetramer.

IMPDH catalyzes the conversion of inosine monophosphate (IMP) to xanthosine monophosphate (XMP) in two different chemical transformations: the first being a dehydrogenase reaction that results in NADH and the E-XMP* intermediate; and the second a hydrolysis step that converts E-XMP* to

XMP (Hedstrom 2009). Both reactions take place in the active site of the enzyme and involve a profound rearrangement of the enzyme.

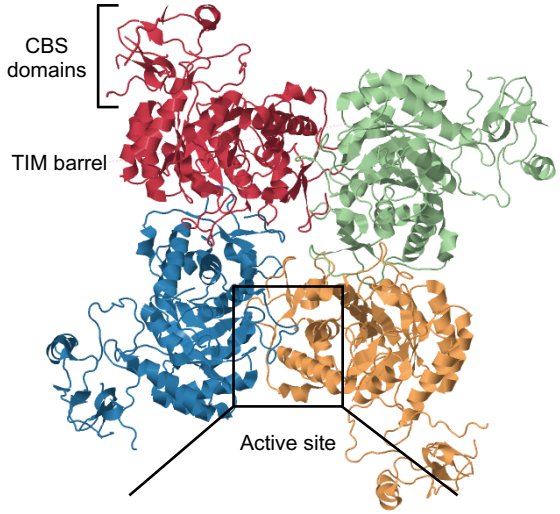

Figure 12. Human type-I ionosine 5'-monophosphate dehydrogenase crystal structure (514 aa). Each monomer appears in a different color. Each monomer consists of two CBS domains, in the extremes of the tetramer; and in a catalytic domain with a TIM barrel structure. Image obtained from PDB: 1jcn.

Three mobile structural elements allow these two distinct reactions to occur at the same active site: a mobile flap [residues 412-432], a catalytic loop [residues 313-328] and the C-terminal segment [residues 481-503]. The rearrangement of these mobile structures allows an open conformation for the enzyme during the initial redox reaction and a closed conformation during the E-XMP* hydrolysis.

The Bateman domain is not required for enzymatic activity since its deletion does not affect catalytic activity *in vitro* (Nimmesgern et al. 1999; Gan, Petsko, and Hedstrom 2002). However, this domain acts as an ATP and GTP sensor for allosteric modulation of the enzyme (Anthony et al., 2017; Buey et al., 2015; Fernández-Justel et al., 2019; Labesse et al., 2013).

1.6.3 IMPDH1 in photoreceptor cells

There are two IMPDH isozymes, IMPDH1 and IMPDH2, that are 84% identical in humans. While most human tissues show only basal IMPDH1 and high IMPDH2 expression, the retina is one of a few exceptions where IMPDH1 predominates (Hedstrom 2009). In the retina, IMPDH1 shows very high levels of expression specifically in photoreceptor cells, as demonstrated with specific antibodies against unique IMPDH1 regions (Bowne, Liu, et al. 2006).

In the retina, major unique IMPDH1 spliced forms outweigh the canonical 514 aa protein (Bowne, Liu, et al. 2006). The number of splicing isoforms and their relative abundance differ in the different species analyzed. Four isoforms have been characterized in humans, where isoform α predominates;

while seven isoforms have been characterized in the murine system, in which isoforms γ and δ predominate (**Fig 13**).

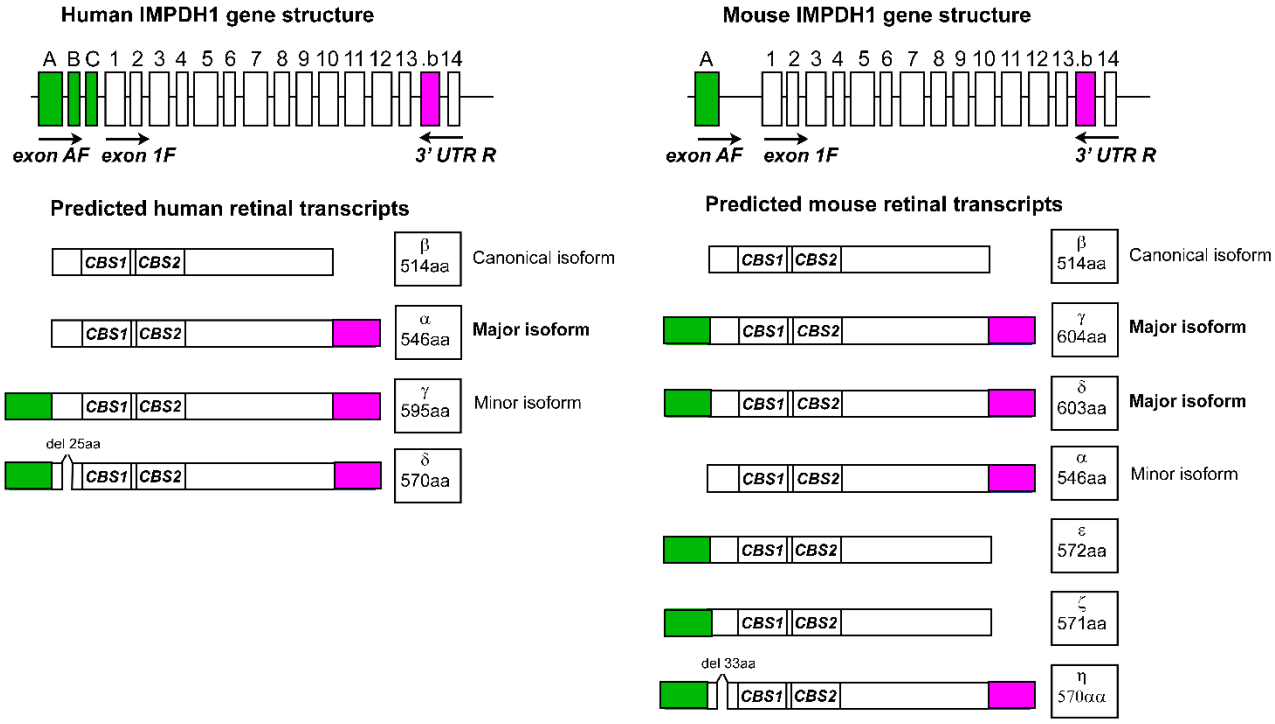

Figure 13. Gene structure and predicted retinal transcripts of IMPDH1 in human and mouse. Four different retinal transcripts have been identified for the human IMPDH1. Human β corresponds to the 514 aa canonical transcript. The major isoform α presents 32 extra aa from exon 13b. Minor isoforms γ and δ are from AF to 3'UTR R (49 extra amino acids from AF and 32 extra amino acids from intron 13b) but δ lacks exon 4. In mouse seven different retinal transcripts have been identified. Murine β corresponds to the canonical transcript. Major isoforms γ and δ are from AF to 3'UTR R and use exon 13b, with the only difference between these transcripts being the inclusion of 3bp at the 5'-end of exon 1 in transcript γ resulting in one additional amino acid. Minor isoforms present extra amino acids from exon AF or exon 13b. From (Bowne, Liu, et al. 2006).

Mutations in *IMPDH1* are associated to severe forms of inherited blindness. At least nine mutations have been associated to the RP10 form of autosomal dominant retinitis pigmentosa, that primarily manifests as night blindness and gradually progresses to loss of central vision (**Table 5**). Together they account for about 1% of adRP cases (Sullivan et al. 2013). *IMPDH1* mutations have also been associated to rare autosomal dominant Leber Congenital Amaurosis, LCA11. Despite the ubiquitous nature of guanine nucleotide synthesis, clinical manifestations of *IMPDH1* mutations are limited to the retina, for reasons that are not yet understood.

RP10 mutations are "gain-of-function" mutations, given that IMPDH1 knock-out mice present only a mild retinopathy (Aherne et al. 2004). Mutations do not directly affect IMPDH1 catalytic activity *in vitro* (Mortimer and Hedstrom 2005; D. Xu et al. 2008; Aherne et al. 2004). IMPDH1 capacity to bind

single-stranded nucleic acids (Mortimer et al. 2008; Hedstrom 2008) as well as IMPDH1 tendency to aggregate (Tam et al. 2008; Aherne et al. 2004) have been suggested to contribute to the pathophysiology based on results *in vitro*; but have not been demonstrated *in vivo*.

Table 5: Mutations in *IMPDH1* gene leading to retinal dystrophies

Mutation	Mapping	Phenotype	Reference
R105W		adLCA	(Bowne, Sullivan, et al. 2006)
T116M	CBS domain	adRP10	(Bowne, Sullivan, et al. 2006)
N198K	CBS domain	adLCA	(Bowne, Sullivan, et al. 2006)
R224P	CBS domain	adRP10	(Kennan et al. 2002b)
D226N	CBS domain	adRP10	(Bowne et al. 2002)
R231P	CBS domain	adRP10	(Grover, Fishman, and Stone 2004)
K238E		adRP10	(Wada et al. 2005)
K238R		adRP10	(Wada et al. 2005)
V268I		adRP10	(Bowne, Sullivan, et al. 2006)
G324D	Catalytic domain	adRP10	(Bowne, Sullivan, et al. 2006)
H372P	Catalytic domain	adRP10	(Bowne, Sullivan, et al. 2006)

Compiled from (Kennan et al. 2002, Bowne et al. 2006)

1.6.4 IMPDH negative allosteric regulation by nucleotides

Cells use different strategies to regulate the nucleotide levels. On the *de novo* biosynthesis pathway of purines three major feedback mechanisms cooperate to regulate the overall rate of purine synthesis and the relative rates of formation of AMP and GMP (**Fig 14**). The **first control mechanism** is exerted on the first reaction in purine synthesis: the transfer of an amino group to PRPP to form 5-phosphoribosylamine. This reaction is catalyzed by the allosteric enzyme glutamine-PRPP amidotransferase (GPA), which is inhibited by the end products IMP, AMP, and GMP. These same nucleotides act synergistically to inhibit the synthesis of PRPP from ribose phosphate by ribose phosphate pyrophosphokinase (PRS). In the **second control mechanism**, an excess of GMP in the cell inhibits IMPDH, diminishing the conversion of IMP to XMP in the first committed step of guanine synthesis. Conversely, an accumulation of adenylate results in inhibition of formation of adenylosuccinate (SAMP) by adenylosuccinate synthetase (ADSS), in the first committed step of adenine synthesis. In the **third mechanism**, GTP is required in the conversion of IMP to AMP, whereas ATP is required to form GMP from IMP, a reciprocal arrangement that tends to balance synthesis of the two nucleotides.

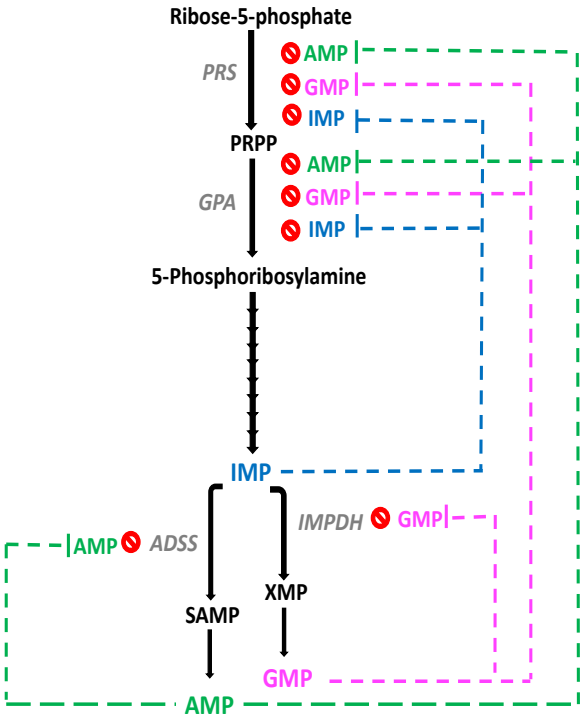

Figure 14. Negative regulation excreted by nucleotides in the *de novo* synthesis of purines. Modified from (Bhagavan and Ha 2015).

In this way, the enzymes responsible for the first committed step toward guanine nucleotide synthesis (IMPDH) or adenine nucleotide synthesis (ADSS) are competitively inhibited by product.

Recently, a breakthrough structural study has revealed that eukaryotic IMPDHs are not only regulated competitively by GMP, but are also regulated allosterically by the binding of GDP and GTP to their Bateman domains (Buey et al. 2015). Nucleotide binding at the Bateman domains regulates the activity of a variety of proteins such as voltage-gated chloride channels (ClC), AMP-activated protein kinase (AMPK) and CBS (Scott et al. 2004). In these proteins the Bateman domain acts as an ATP sensor, and mutations in the adenyl binding sites in this domain have been linked to homocystinuria (CBS); familial hypertrophic cardiomyopathy with Wolff-Parkinson-White syndrome (AMPK); and myotonia congenital (ClC-1) (Scott et al. 2004).

The milestone of recent structural studies on IMPDH proteins was the discovery that eukaryotic IMPDHs responded to GDP/GTP in addition to ADP/ATP; and that while ADP/ATP binding promoted activation of the enzyme, GDP/GTP binding allosterically inhibited catalytic activity. Buey et al. identified three allosteric nucleotide binding sites in the Bateman domain of eukaryotic IMPDHs: sites 1, 2 and 3. Sites 1 and 2 are canonical nucleotide binding sites that bind either ADP/ATP or GDP/GTP (Scott et al. 2004). Site 3 is a non-canonical site located at the interface between CBS domains that binds only GDP/GTP (Buey et al. 2015).

The basis for nucleotide allosteric regulation of IMPDH enzymes reside on the reversible dimerization of tetramers. Nucleotide binding makes IMPDH tetramers assemble into octamers, by inducing the dimerization of Bateman domains (**Fig 15**). ADP/ATP binding promotes the formation of octamers with an extended conformation, that are catalytically active. In contrast, GDP/GTP binding induces the formation of compressed octamers which are inactive. The conformation and activity of the octamers is set specifically by the occupancy of sites 2 and 3, which resides on the binding competition of ADP/ATP and GDP/GTP. Because non-canonical site 3 is GDP/GTP specific (can be either empty or GDP/GTP-bound), GDP/GTP can inhibit IMPDHs even in the presence of ATP.

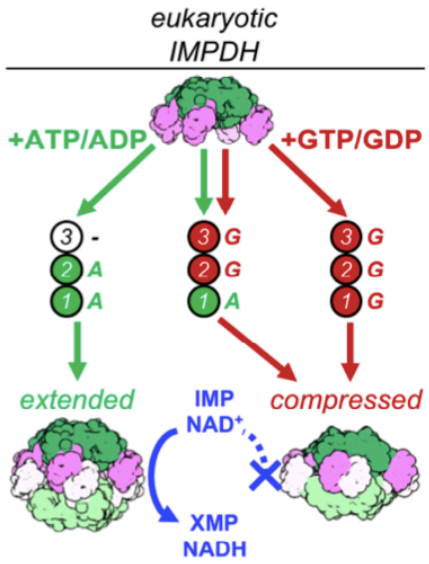

Figure 15. Model of eukaryotic IMPDH allosteric regulation by nucleotides. Eukaryotic IMPDHs Bateman domains present three nucleotide binding sites: sites 1, 2 and 3. Sites 1 and 2 can bind either ADP/ATP or GDP/GTP. Site 3 can only bind GDP/GTP. When adenine nucleotides are bound to sites 1 and 2, and site 3 is empty, IMPDH forms extended octamers with normal catalytic activity. The binding of guanine nucleotides in Sites 2 and 3; or in all sites results in the formation of compressed octamers with compromised catalytic activity. Image from (Johnson and Kollman 2020).

Interestingly, several of the residues mutated in adRP10 map at the GDP/GTP binding sites at the Bateman domain, and *in vitro* studies have determined that these **mutations disrupt GDP/GTP-mediated allosteric regulation of the enzyme** (Buey et al. 2017). It has therefore been proposed that the physiopathology of adRP10 resides on the disruption of the GDP/GTP negative allosteric feedback to *de novo* GTP synthesis.

1.6.5 IMPDH capacity to reversibly polymerize into filaments

Many enzymes involved in cell metabolism can form reversible filamentous structures *in vitro* and *in vivo* in response to cellular stress or under conditions that require a boost of enzymatic capacity to cope with specific cellular requirements (Liu 2010). Various filamentous structures have been characterized *in vitro* by biophysical methods, including electron microscopy (Park and Horton 2019). Cytoophidia, for instance, are large-scale self-assembled structures that are observed by superresolution techniques as foci, rods, and rings. Some of the enzymes described to form

cytoophidia include: glutamate dehydrogenase (Olson and Anfinsen 1952), acetyl CoA carboxylase (Kleinschmidt, Moss, and Lane 1969), nitrilase (Harper 1977), β-glucosidase (Kim et al. 2000), cytosine triphosphate synthase (Noree et al. 2010), glutaminase (Ferreira et al. 2013), glutamine synthase (O'Connell et al. 2014), phosphofructokinase (Webb et al. 2017), glucokinase (Stoddard et al. 2019) and ribonucleotide reductase (Thomas et al. 2019).

IMPDH can form macromolecular filamentous structures in mammalian cells under metabolic deficiency. IMPDH forms macromolecular assemblies under conditions that require higher IMPDH activity to keep with GTP demand (Liu 2010; Chang et al. 2015; Aughey and Liu 2016; Keppeke et al. 2018), like high rates of proliferation, or Gln/Ser/folate-metabolite deficiency (Calise et al. 2016; Chang et al. 2015; Keppeke et al. 2018). Formation of these reversible fiber-like subcellular structures is believed to transiently boost IMPDH activity (Chang et al. 2015; Keppeke et al. 2018). IMPDH cytoophidia can also be induced in cells by the addition of inhibitors that block *de novo* GTP biosynthesis, such as mycophenolic acid (Ji et al. 2006) and ribavirin (Carcamo et al. 2014). Disassembly of cytoophidia can be induced by the addition of the downstream product guanosine or GTP (Calise et al. 2014); or by disrupting the cell cycle through the PI3K-AKT-mTOR pathway using PI3K inhibitors (Chang et al. 2015).

More recently, structural studies in IMPDH2 have revealed that increases in IMP stabilize IMPDH2 filaments, even in the presence of high GTP levels (Johnson and Kollman 2020).

IMPDH1 filaments could be induced *in vitro* (Fernández-Justel et al. 2019). It was shown that high ATP levels promoted the assembly of IMPDH into filaments, whereas addition of GTP led to filament disassembly into free octamers. **Blindness-associated mutations in IMPDH1 resulted in proteins that had the capacity to form filaments, but were not able of reverting the filaments to free octamers** (Fernández-Justel et al. 2019), **due to the inability of these mutants to bind GTP.**

Although structural-functional *in vitro* analysis are paving the way to dissect key aspects on IMPDH regulation, the relevance of these mechanisms of regulation of the enzyme *in vivo* have not yet been addressed. Addressing these questions *in vivo* and particularly in the retina is of the outmost importance to understand the adRP10 form of blindness.

2. AIMS

2.1 AIMS OF THE STUDY

The **MAIN AIM** of this work is to deepen the knowledge of guanine metabolism and cGMP synthesis in photoreceptor cells of the retina, and how genetic defects at this level lead to different forms of retinal dystrophies. We focus this work on the study of GCAPs and IMPDH1 proteins and their relationship to Leber´s Congenital Amaurosis (LCA) and Retinitis Pigmentosa (RP).

2.1.1 SPECIFIC AIMS

1. **Explore the putative role of Guanylate Cyclase Activating Proteins (GCAPs) as calcium sensor proteins that mediate the physiopathology in Leber´s Congenital Amaurosis 12 (LCA12):** i) establish whether GCAPs are involved in the physiopathology of LCA12, by assessing the effect of GCAPs ablation in the *rd3* mice; ii) study how GCAPs may mediate photoreceptor cell death in this scenario.

2. **Characterize the role and *in vivo* modulation of inosine monophosphate dehydrogenase 1 (IMPDH1) in photoreceptor cells of the retina, to get insight into how *IMPDH1* mutations lead to retinitis pigmentosa:** i) IMPDH1 localization in the retina; ii) IMPDH1 *in vivo* regulation in dark/light conditions, iii) effect of IMPDH1 activity and *in vivo* regulation on the light response.

3. RESULTS

Chapter 1: Antibody generation against the proteins of study: RetGC1, RD3 and IMPDH1

Chapter 2: Exploring the putative role of GCAPs as damage mediators in the *rd3* mouse model of LCA12

Chapter 3: Characterizing the *in vivo* modulation of IMPDH1 in dark/light and its effect on the light response

3.1 RESULTS CHAPTER 1. ANTIBODY GENERATION AGAINST THE PROTEINS OF STUDY: RETGC1, RD3 AND IMPDH1

3.1.1 Contributions

We are in debt with Dr. Álvaro Gimeno and Lidia Gómez at the Vivarium facility for performing the immunization protocol in rabbits. We aknowledge Dra. Dunja Lukovic from the Slaven Erceg Laboratory [University of Valencia] for providing us with human retinal eyecup sections derived from iPSCs for testing anti-RetGC1 antibodies. We are in debt with Dr. Jordi Andilla [ICFO] and Dr. Benjamin Torrejón [CCiT-UB] for their assistance with image acquisitions at the confocal microscope.

My contribution to this chapter was the preparation of antigens for immunization of rabbits: either by crosslinking the peptides of interest to KLH (RetGC, RD3); or by purification of recombinant IMPDH1 expressed in bacteria. I prepared the columns (by –SH or –NH4 covalent binding of the antigen) for affinity purification of the antibodies from rabbit serum, and performed the affinity purification. I rigorously characterized the specificity of the antibodies in western blots, and immunofluorescence and immunoprecipitation assays. I acquired the images by confocal microscopy with the help of Benjamin Torrejon and Jordi Andilla.

ANTIBODY GENERATION AGAINST THE PROTEINS OF STUDY: RETGC1, RD3 AND IMPDH1

3.1.2 Antibody against murine RetGC1

An antibody anti-RetGC1 was generated by immunizing rabbits with the last 21 COOH-terminal amino acids of murine RetGC1. Since there are two RetGC isoforms in murine retinas (RetGC1 and RetGC2, with RetGC1 present in rods and cones, and RetGC2 restricted to rods), a region specific to RetGC1 was chosen. The last COOH-terminal peptide presents less than 20% homology with the RetGC2 amino acidic sequence. Therefore, an *in vitro* synthetized 21 aa peptide corresponding to the last twenty-one amino acids of RetGC1 followed by a Cys: H2N-IPPERRKKLEKARPGQFTGKC-OH was conjugated to Keyhole Limpet Hemocyanin (KLH) by using the Imject Maleimide-activated mcKLH Spin kit (Thermo Scientific), see Methods. KLH is an extremely immunogenic and effective carrier protein for immunogen preparation, given that each KLH protein molecule contains several hundred of lysines that provide primary amines as targets for covalent attachment of haptens. Once prepared, the antigen was used to immunize New Zealand rabbits following a standard 3-boost protocol (detailed in Methods).

Rabbit serum was subjected to an affinity purification protocol, by using the immunizing peptide covalently attached to agarose by –SH chemistry, using a SulfoLink Immobilization kit for peptides (Thermo Scientific), see Methods. After extensive dialysis of the antibody against phosphate saline buffer pH 7.2, the concentration of different antibody batches was determined, preservatives were added (either 40% glycerol or 0.4% BSA in 0.025% sodium azide), and antibodies were aliquoted and kept at -80ºC.

Anti-RetGC affinity purified antibodies were first tested by **Western blot** analysis on whole murine retinal extracts. **Fig 16A** shows a 12% SDS-PAGE with 40 μg of murine retinal extract (corresponding to 1/10 of a retina).

The antibody recognized a prominent band between 100-150 kDa, with the expected molecular weight for RetGC1 being 120 kDa (**Fig 16A**). This result shows that anti-mRetGC1 Ab works efficiently and specifically in Western blots.

Antibodies were then tested in **immunolocalization assays**, by performing indirect immunofluorescence of murine retinal cryosections. The Ab yielded a strong signal at the photoreceptor outer segment layer, staining both rod and cone outer segments (OS) (**Fig 16B**).

Note that cone outer segments are shorter than rod's and are typically discerned at the inner segment (IS) layer (white arrows). Note that cones in the image are stained in red, with an Alexa647-conjugated cone-marker: peanut agglutinin (PNA) lectin, that binds to specific-cone surface oligosaccharides (Blanks and Johnson 1984). The green anti-mRetGC1 signal overlaps with the red PNA signal, yielding the yellow staining of cone outer segment compartments (white arrows).

The antibody was also tested in bovine retinal sections, giving a strong cone outer segment signal. See green signal at magnified cone from bovine retina, **Fig 16C**. Anti-mRetGC1 Ab also recognized the human isoform of the protein in immunolocalization assays. In human retinal eyecups derived from induced pluripotent stem cells iPSCs [a kind gift from the Slaven Erceg Lab, Principe Felipe Institute, Valencia] the antibody specifically recognized the incipient outer segment structures that are characteristic of these organoids (**Fig 16D**).

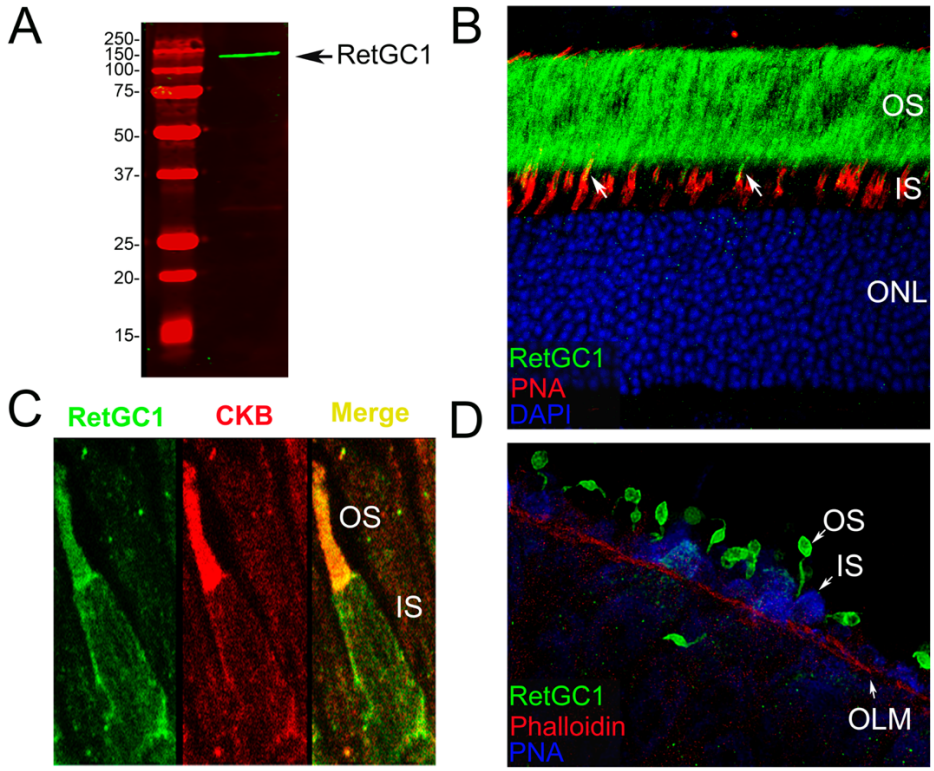

Figure 16. RetGC1 antibody specifically recognizes RetGC1 of various species in Western blot and immunolocalization assays. A. Anti-mRetGC1 Ab recognizes only one band at 120 kDa in a 12% SDS-PAGE gel loaded with whole murine retinal extract (40 µg protein). **B.** Immunolocalization of RetGC1 in murine retinal fixed tissue. Both cone outer segments (white arrows at the IS compartment) and rod outer segments (OS layer) were stained with the anti-mRetGC1 antibody (green signal). RetGC1 colocalizes with lectin PNA (red), a cone specific marker. **C.** Detail of a bovine cone stained with RetGC1 (green) and Creatine Kinase B (CKB) (red) obtained by super-sensitivity [ICFO]. **D.** Section from a human eyecup derived from iPSCs labeled with RetGC1, showing staining of incipient photoreceptor outer segments (green). Phalloidin stains actin filaments, labelling the outer limiting membrane (red) whereas PNA lectin stains cones (blue). OS (Outer segment), IS (Inner segment), OLM (Outer limiting membrane) and ONL (Outer nuclear layer).

3.1.3 Antibody against murine RD3

The anti-RD3 antibody was generated against the last COOH-terminal 16 amino acids of murine RD3. The peptide Cys: H2N-PPRTWSMPEFRAPQAD -OH was conjugated to KLH, and a rabbit immunizing protocol was followed as indicated above. Antibody affinity purification was performed as indicated for anti-mRetGC1 pAb.

The affinity purified antibody was first tested by western blot in murine retinal extracts from wild-type and *rd3/rd3* retinas. The *rd3* mice present a point mutation [c.319C→T] at exon 3 of the *Rd3* gene, that results in a truncated protein lacking the last 89 aa of the protein (Friedman et al. 2006). The truncated RD3 protein is rapidly degraded in these mice; but even if traces of RD3 protein were present they would not be detected with this Ab generated against the C-terminal. The antibody detected a band between 20-25 kDa; which corresponds to RD3, a protein of 23 kDa (**Fig 17A**). This band is not detected in *rd3/rd3* retinal extracts.

Then the anti-mRD3 pAb was tested in immunolocalization assays. RD3 localization has been controversial since it was reported by Robert Molday´s Lab. They first identified RD3 in bovine rod outer segments in a proteome-based study (Kwok et al. 2008). Then the authors studied the localization of RD3 by producing a policlonal antibody against the last 15 aa murine amino acids of the protein and determined that RD3 localizes at the rod outer segment layer of the retina (S. Azadi, Molday, and Molday 2010). However, other studies have pointed to a different localization of RD3. A polyclonal antibody against a human peptide encompassing the RD3 171-183 amino acid region was tested in human retinal sections, resulting in a strong inner segment staining (Aravindan et al. 2017). At Karl Wilhelm Koch´s Lab, RD3 has been immunolocalized to both photoreceptor inner and outer segments using a commercial monoclonal antibody against RD3 (Wimberg, Janssen-Bienhold, and Koch 2018). Recently, Dizhoor´s Lab has determined that RD3 localizes at the inner segment of photoreceptors by developing a RD3-GFP engineered mouse (Dizhoor, Olshevskaya, and Peshenko 2019).

When we tested our antibody by immunofluorescence on wild-type retinas we observed a rather clear staining of photoreceptor outer segments (outer segment layer shown in green, **Fig 17B**). However, the antibody gave an identical signal on *rd3/rd3* retinal sections (**Fig 17C**). This result indicated that the antibody generated against the last 16 aa of the protein, even though it recognizes RD3 epitopes very specifically under protein denaturing conditions on SDS-PAGE, is not recognizing RD3 specifically in retinal sections of fixed tissue. The antibody may be recognizing conformational epitopes from other proteins on retinal sections.

Antibodies against RD3 have proved to be problematic for immunolocalization in several different laboratories, and this issue has been attributed to the inaccessibility of the epitopes and/or low levels of RD3 expression (Aravindan et al. 2017). We made three attempts at generating antibodies against RD3 in the lab: against two different peptides of RD3; and against the full-length protein solubilized in urea. They all worked to different extents in Western blot. None of them worked in immunolocalization assays, despite different antigen retrieval protocols were tried. For determination of RD3 subcellular localization we ultimately relied on the transient transgenic expression of RD3.V5 in rods by *in vivo* DNA electroporation after subretinal injection (see **Fig 23**, Chapter 2).

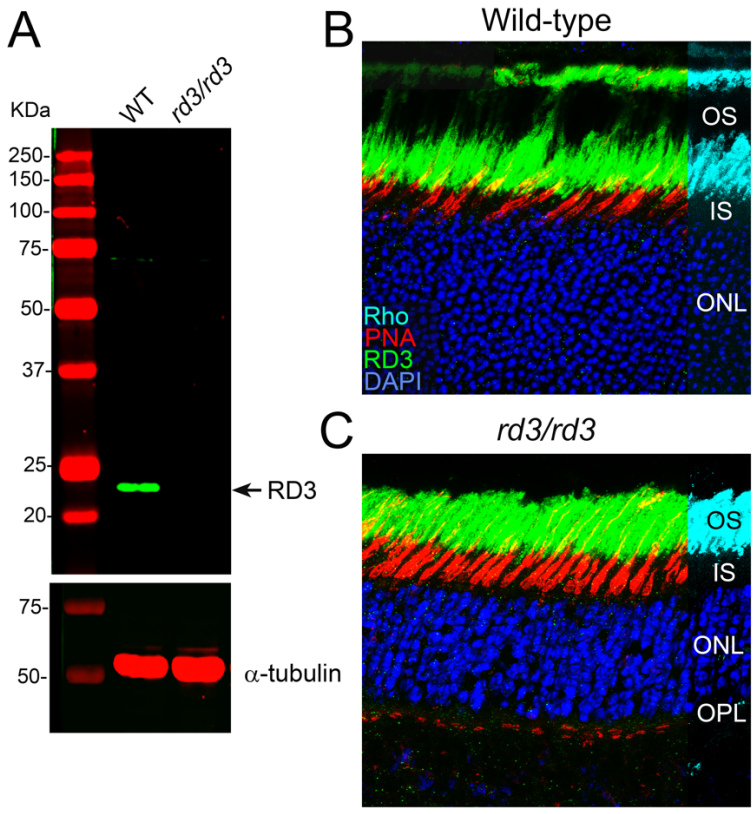

Figure 17. Anti-mRD3 antibody testing on murine retinal extracts and retinal sections of wt and *rd3/rd3* retinas. A. Western blot showing RD3 antibody specificity. RD3 protein is detected between 20-25 kDa on wild-type retinal extracts, but not in *rd3/rd3* retinal extracts. Tubulin levels in the extracts are shown as a loading control. **B.** Immunolocalization of RD3 on a retinal section from wild-type fixed eyecup. The anti-mRD3 antibody strongly stained the photoreceptor outer segment layer, and colocalized with the PNA lectin cone-marker. The same signal was detected with the same extent in *rd3/rd3* mice **(C)**. Anti-mRD3 antibody was tested in three independent *rd3/rd3* animals that were confirmed to be deficient in RD3 by genotyping. OS (Outer segment), IS (Inner segment), ONL (Outer nuclear layer) and OPL (outer plexiform layer).

3.1.4 Antibody against bovine IMPDH1

For antibody generation against IMPDH1, we purified the bovine canonical isoform of IMPDH1-(514 aa). bIMPDH1-514 aa was expressed in *E.coli* and purified from inclusion bodies (Krishnaiah 1975) by solubilization in guanidinium hydrochloride, purification in its denatured form by metal chelation with a HiTrap column, and subsequent dialysis in a gradient of urea (see methods).

Purified bIMPDH1 in <1M urea was used to immunize two New Zeland rabbits following a standard 3-boost protocol as described above. Rabbit serum was purified against recombinant bIMPDH1-crosslinked to Aminolink coupling resin (see methods).

IMPDH1 is a highly conserved protein (Hedstrom 2009). Five human retinal isoforms were identified (Bowne, Liu, et al. 2006), with the 546 aa (presenting an extra C-terminus) and 595 aa (extra N-terminus and extra C-terminus) being the more abundant. In the mouse system, the major isoforms are the 603/604 aa and 546 aa isoforms, that predominate among the seven isoforms identified. By the use of an antibody against the whole recombinant protein we expected to detect the different IMPDH1 splicing isoforms in murine and bovine retinal extracts.

The anti-bIMPDH1 antibody was tested by western blot in murine and bovine retinal homogenates (**Fig 18A**). In murine extracts the predominant isoforms of 603/604 aa and 546 aa were clearly detected. In the bovine system the different IMPDH1 splicing isoforms have not been annotated. In bovine retinal extracts we detected two major isoforms between 50-75 kDa. The antibody also recognized the tetrameric form of IMPDH1 on bovine homogenates, despite the presence of SDS in the loading buffer. These results show that the anti-bIMPDH1 antibody was highly specific.

On murine retinal sections, anti-bIMPDH1 strongly stained the inner segment layer and the outer plexiform layer. The signal was also present in the perinuclear region of the ONL (**Fig 18B**). Note that despite IMPDH1 abundance, IMPDH1 signal did not colocalize with the cone-marker PNA at synaptic terminals. IMPDH1 immunolocalization results are consistent with previous studies (Bowne, Liu, et al. 2006).

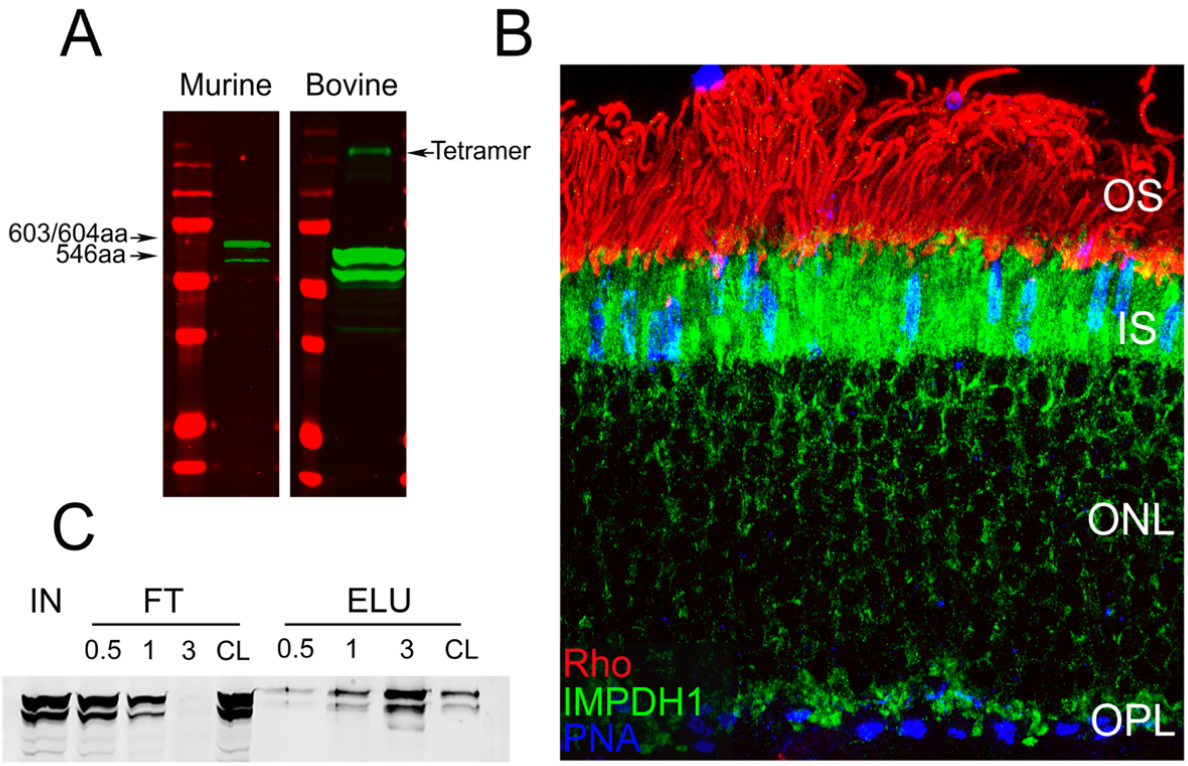

Figure 18. Specificity of anti-bIMPDH1 antibody in Western, immunolocalization and immunoprecipitation assays. A. Western blot showing IMPDH1 antibody specificity. The two major bands observed (50-75 kDa) correspond to the two predominant retinal splicing isoforms in the murine and bovine systems, with predicted masses of 55 and 60 kDa. In bovine retinal extracts (more material loaded), the tetrameric form of the protein is also detected, at ~220 kDa. **B.** Immunolocalization assay on a wild-type murine fixed retina. IMPDH1 stains rod inner segments, the perinuclear region and synaptic terminals. OS (Outer segment), IS (Inner segment), ONL (Outer nuclear layer) and OPL (outer plexiform layer). **C.** Immunoprecipitation assay with anti-IMPDH1 antibody. A fixed input (IN) corresponding to one-tenth of a retinal bovine homogenate was used as starting material. Increasing concentrations of antibody (0.5; 1 and 3 μg) were used with a fixed amount of Protein G magnetic beads. FT: Flow Through (Unbound fraction) and ELU: Elution (Bound fraction). CL: crosslinked antibody (10 μg). IMPDH1 increases in the elution fractions an decreases in the FT fractions with increasing amounts of Ab.

Because the anti-bIMPDH1 antibody was generated against the whole recombinant protein, it is expected to detect many IMPDH1 epitopes, putatively valid for immunoprecipitation purposes. We performed an immunoprecipitation assay to titrate the antibody required to immunodeplete IMPDH1 from a given retinal extract. For that, we incubated a fixed amount of bovine retinal extract, and increasing amounts of Ab (0.5, 1 and 3 μg), with a fixed amount of protein-G dynabeads. We determined that 3 μg of the anti-IMPDH1 antibody completely immunodepleted the IMPDH1 from one-tenth of a bovine retina (corresponding to 0.5 mg total protein) (**Fig 18C**). Unfortunately, this antibody could not be cross-linked to protein G-dynabeads for immunoprecipitation assays at a larger scale for proteomic purposes, because the Ab lost immunogenicity when crosslinked (CL in panel 3C).

3.2 RESULTS CHAPTER 2. EXPLORING THE PUTATIVE ROLE OF GCAPS AS DAMAGE MEDIATORS IN THE *RD3* MOUSE MODEL OF LCA12

3.2.1 Contributions

Dr. Pedro de la Villa from the University of Alcalá, Madrid, recorded the dark-adapted ERG responses from the different mouse lines here shown (C57BL/6; GCAPs-/-; *rd3*/*rd3* and *rd3*/*rd3* GCAPs-/-) in a visit to the lab. Dr. Santiago López-Begines, a former PhD student in the lab, performed the pull-down assays with GCAP2-P and GCAP2 from bovine retinal homogenates and created the volcano plot presented. Dr. Josep M. Estanyol and Dr. M. José Fidalgo, from the CCiT-UB Technical Platform performed the LC-MS/MS experiments. We aknowledge the help of Alex Rovira (TFG student) in the cloning of pRho_mRd3V5_dsRed expression vector, and of Nerea Ugartondo (Master student) in the *in vivo* DNA electroporation of the plasmid in *rd3* mice. I am in debt with Dr.Jordi Andilla and Dr. Benjamin Torrejon for their help at image acquisition and analysis at the confocal microscope.

My contribution to this chapter was the establishment and analysis of the *rd3*/*rd3* GCAPs-/- line; that involved developing a method to detect the SNP present in the *rd3* line; and the genotyping of F1, F2 and F3 generations. I analyzed the extended eye collection from wt; wt/*rd3*; *rd3*/*rd3*; *rd3*/*rd3* GCAPs+/- and *rd3*/*rd3* GCAPs-/- at different time points in order to assess the rate of retinal degeneration, both by light and electron microscopy, performing the morphometric measurement statistical analysis. I determined the expression levels and subcellular localization of our proteins of interest in these mice. I established that GCAP2 is mainly in its phosphorylated form in *rd3* mice by running isoelectrofocusing gels of murine retinal extracts. I assessed ER stress and apoptosis markers in the different lines. I significantly contributed to experimental design, data analysis, and conceptualization of the proposed model.

3.2.2 Rationale

Mutations in a number of genes that impair or alter cGMP synthesis in rods and cones have been associated to different forms of blindness (Isabella Perrault et al. 1996; Payne et al. 1998; Kelsell et al. 1998). Loss-of-function mutations in the *RD3* gene (name coming from the natural strain of blind mice called "retinal degeneration 3", *Rd3* locus mutated) cause Leber's Congenital Amaurosis 12 (LCA12) (B. Chang et al. 1993; Friedman et al. 2006). LCA12 is characterized by severe vision loss at an early age and rapid retinal degeneration, due to rod and cone impaired function.

It is known that the 23 kDa RD3 protein is required for the stability and ciliary trafficking of the guanylate cyclases RetGC1 and RetGC2 (S. Azadi, Molday, and Molday 2010). RetGCs are regulated by the guanylate cyclase activating proteins GCAP1 and GCAP2, that confer Ca^{2+} regulation to cGMP synthesis. In *rd3* mice the levels of RetGC1 and RetGC2 are dramatically decreased, and retained at the cell soma (S. Azadi, Molday, and Molday 2010). GCAPs, that depend on RetGCs for their stability and distribution to the outer segment, are also diminished and retained (Baehr et al. 2007; López-Begines, et al. 2018; S. Azadi, Molday, and Molday 2010). This is expected to result in reduced cGMP synthesis, closure of CNG-channels and severely impaired vision. This phenotype mimics that of LCA1 caused by null mutations in *GUCY2D* (RetGC1) in humans (Samuel G. Jacobson et al. 2013), or by retinal guanylate cyclase deficiency in mice [RetGC1/RetGC2 double knockout mice, (Baehr et al. 2007)]. However, while mice deficient in RetGC1/RetGC2 show a progressive retinal degeneration, in *rd3* mice the loss of rod and cone cells progresses fast (Linberg *et al.*, 2005).

Little is known about the molecular mechanisms that link the lack of RD3 with photoreceptor cell death in *rd3* mice. We have previously proposed that the GCAP proteins could contribute to the pathophysiology of several retinal dystrophies characterized by rod/cone chronic hyperpolarization and low $[Ca^{2+}]_i$ at the photoreceptor soma. This hypothesis was based on the fact that when a form of GCAP2 impaired to bind Ca^{2+} (with all functional EF-hands mutated, EF$^-$GCAP2) was expressed in living photoreceptors, it was retained at the cell soma by phosphorylation and 14-3-3 binding, resulting in severe toxicity and fast retinal degeneration (Hoyo et al. 2014). GCAPs are retained at the cell soma in *rd3* mice, in a context of chronic low $[Ca^{2+}]_i$. Considering that GCAP2 has previously been identified as a modifier gene of the *rd3* mouse phenotype (Danciger et al. 2008), we hypothesized that Ca^{2+}-free GCAPs could be contributing to the pathophysiology of this disease. We here test this hypothesis.

EXPLORING THE PUTATIVE ROLE OF GCAPS AS DAMAGE MEDIATORS IN THE *RD3* MOUSE MODEL OF LCA12

3.2.3 Retinal degeneration due to RD3 deficiency is substantially rescued by GCAPs ablation.

To test the hypothesis that the GCAP proteins contribute to the pathophysiology of LCA12 blinding disease associated to the lack of functional RD3, we bred *rd3* mice to GCAP1/GCAP2 double knockout mice (GCAPs-/- mice), to compare the rate of retinal degeneration caused by RD3 deficiency in the presence or absence of GCAP proteins.

We first characterized the rate of retinal degeneration in the specific *rd3* strain used in this study [B6.Cg-Rd3rd3/Boc], hereinafter referred to as *rd3* mice, because rates of degeneration vary in the different strains carrying the *Rd3* mutation (Linberg *et al.*, 2005). Our analysis showed that *rd3* mice developed normal retinas up to two postnatal weeks, but showed signs of retinal degeneration as early as postnatal day 20 (p20). While wt/*rd3* heterozygous littermate controls showed a nearly normal outer nuclear layer (ONL) with 11-12 rows of photoreceptor nuclei and a width of 40-42 μm at p20, *rd3*/*rd3* homozygous mice showed a slightly shorter ONL (8-10 rows of nuclei, 32-36 μm-thickness) at this age (**Fig 19A**). At p26, the ONL of *rd3*/*rd3* mice was reduced to 6-8 rows of nuclei (28-30 μm), and at p44 to about 5 rows of nuclei (20 μm) (**Fig 19A**). An statistical analysis of ONL thickness was performed on morphometric measurements from 2 p20 and 2 p26 retinas of each genotype (p20-p26 traces, n=4), and 4 retinas at p44 of *rd3*/*rd3* mice (**Fig 19B**). We conclude that the retinal degeneration in *rd3* mice manifests as early as at p20 and halves the number of photoreceptor cells in about 6 weeks, which is consistent with the reported rate of degeneration of pigmented strains with the *rd3* mutation (Linberg et al., 2005).

We confirmed that RetGC expression was severely reduced in this *rd3* strain at p20 (S. Azadi, Molday, and Molday 2010), with RetGC1 levels reduced to ~12% the expression in control mice (**Fig 19C**). The expression levels of GCAP1 and GCAP2 were reduced to 37% and 42% the levels in control mice (**Fig 19C**). A novel observation is that RetGC1 was detected by immunofluorescence analysis on retinal sections of *rd3* mice at the inner segment layer and perinuclear region of photoreceptors, showing a characteristic punctated staining (**Fig 19D**). GCAP1 and GCAP2 were largely retained to proximal photoreceptor compartments in *rd3* mice, as previously described (S. Azadi, Molday, and Molday 2010) (**Fig 19D**).

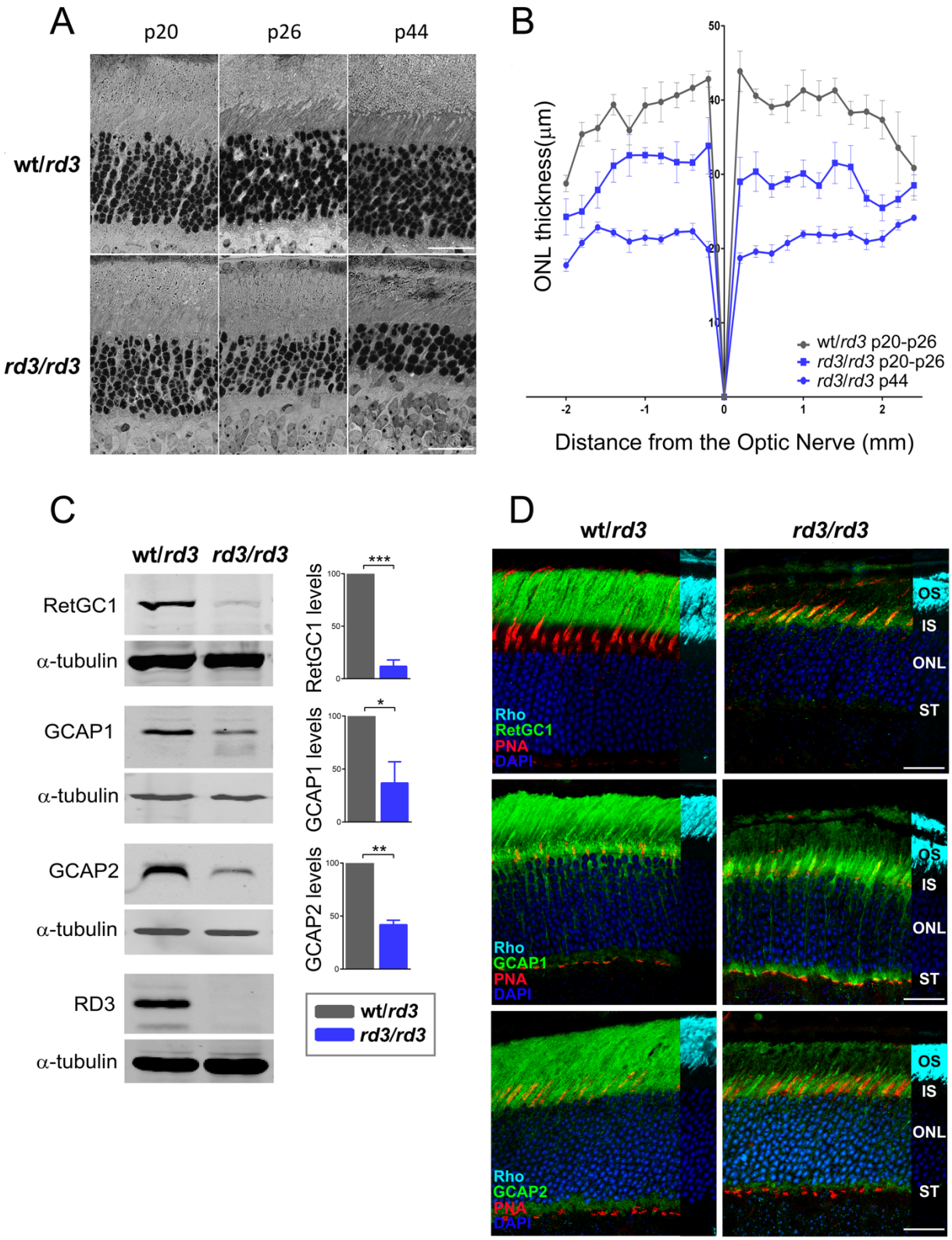

Figure 19. Time course and molecular alterations that characterize the retinal degeneration in *rd3* mice strain B6.Cg-Rd3rd3/Boc. (see figure legend in next page)

Figure 19. Time course and molecular alterations that characterize the retinal degeneration in *rd3* mice strain B6.Cg-Rd3rd3/Boc. A. Retinal micrographs of wt/*rd3* and *rd3/rd3* mice at p20, p26 and p44 show the progressive retinal degeneration in *rd3/rd3* mice, that halves the number of photoreceptor cells at p44. Scale bar 20 μm. **B.** Retinal morphometric analysis of wt/*rd3* and *rd3/rd3* mice at the indicated ages, showing outer nuclear layer (ONL) length (μm) at 200 μm-intervals from the optic nerve in the vertical meridian of the eye, superior retina to the right. Each trace represents the average measurements of four mice analyzed, with error bars indicating the standard error of the mean (SEM) [n= 2 biological replicates at p20, and n= 2 biological replicates at p26 for wt/*rd3* and *rd3/rd3*; n= 4 biological replicates at p44 for *rd3/rd3*]. **C.** Expression levels of RetGC1, GCAP1 and GCAP2 in *rd3/rd3* mice compared to wt/*rd3* mice at p30. Histograms indicate the percentage of expression of each protein in *rd3/rd3* mice versus wt/*rd3* mice, after normalization with α-tubulin. No RD3 protein is detected in *rd3/rd3* mice with an antibody generated against RD3 C-terminus. For the determination of protein levels, three independent experiments were performed. Unpaired t-test for RetGC1 (wt/*rd3* versus *rd3/rd3*; P<0.0001***); GCAP1 (wt/*rd3* versus *rd3/rd3*; P=0.032*); GCAP2 (wt/*rd3* versus *rd3/rd3*; P=0.0017**). **D.** Immunofluorescence localization of RetGC1, GCAP1 and GCAP2 in wt/*rd3* and *rd3/rd3* mice at p24. RetGC1, GCAP1 and GCAP2 signals are greatly reduced in *rd3/rd3* mice, and mostly restricted to the photoreceptor inner layer. Cones are labeled with peanut agglutinin (PNA) in red; the rod outer segment layer with anti-Rhodopsin mAb 1D4 (1 cm overlay) in cyan; and nuclei are labeled with DAPI (blue). Scale bar 20 μm. OS, outer segment; IS, inner segment; ONL, outer nuclear layer; ST, synaptic terminals.

To assess whether ablation of GCAPs affected the time course of retinal degeneration in the *rd3* mice, we bred *rd3* mice to GCAPs-/- mice. To minimize strain variation effects, the breeding was established between *rd3/rd3* GCAPs+/- mice, so that homozygous *rd3/rd3* mice that were either GCAPs+/- or GCAPs-/- littermates could be directly compared (**Fig 20**). The ONL width of *rd3/rd3* mice at p44 from (**Fig 19B**) is plotted as a reference. Compared to *rd3/rd3* mice at p44 [ONL thickness of 20 μm, 5 nuclei]; *rd3/rd3* GCAPs+/- showed a very minor improvement at this age [22-24 μm, 5-6 nuclei, n=4]; but *rd3/rd3* GCAPs-/- mice showed a striking improvement [30-32 μm, 7-8 nuclei, n=4], (**Fig 20A-B**). This rescue effect of GCAPs ablation was preserved at p60 (**Fig 20C-D**), when 4 biological replicates per genotype were analyzed (*rd3/rd3* GCAPs+/- and *rd3/rd3* GCAPs-/- littermates). *Rd3/rd3* GCAPs-/- mice preserve 75% of their photoreceptors at p60; when *rd3/rd3* mice have lost more than 50%.

This substantial preservation of photoreceptors in the absence of GCAPs correlated with an increase in RetGC levels in *rd3/rd3* GCAPs-/- retinas (**Fig 20E-F**). Quite surprisingly, RetGC1 in *rd3/rd3* mice was distributed to rod outer segments to a higher extent in the absence of GCAPs (**Fig 20I**).

At eight months *rd3/rd3* mice have completely lost the photoreceptor cell layer, and *rd3/rd3* GCAPs-/- mice still preserved 5 rows of photoreceptors with visible outer segments (**Fig 21A-B**). We conclude that GCAPs ablation markedly slows down photoreceptor cell death in the *rd3* mice, substantially delaying retinal degeneration in this mouse model of LCA12. Consequently, the GCAP proteins are involved in the pathophysiology of LCA12.

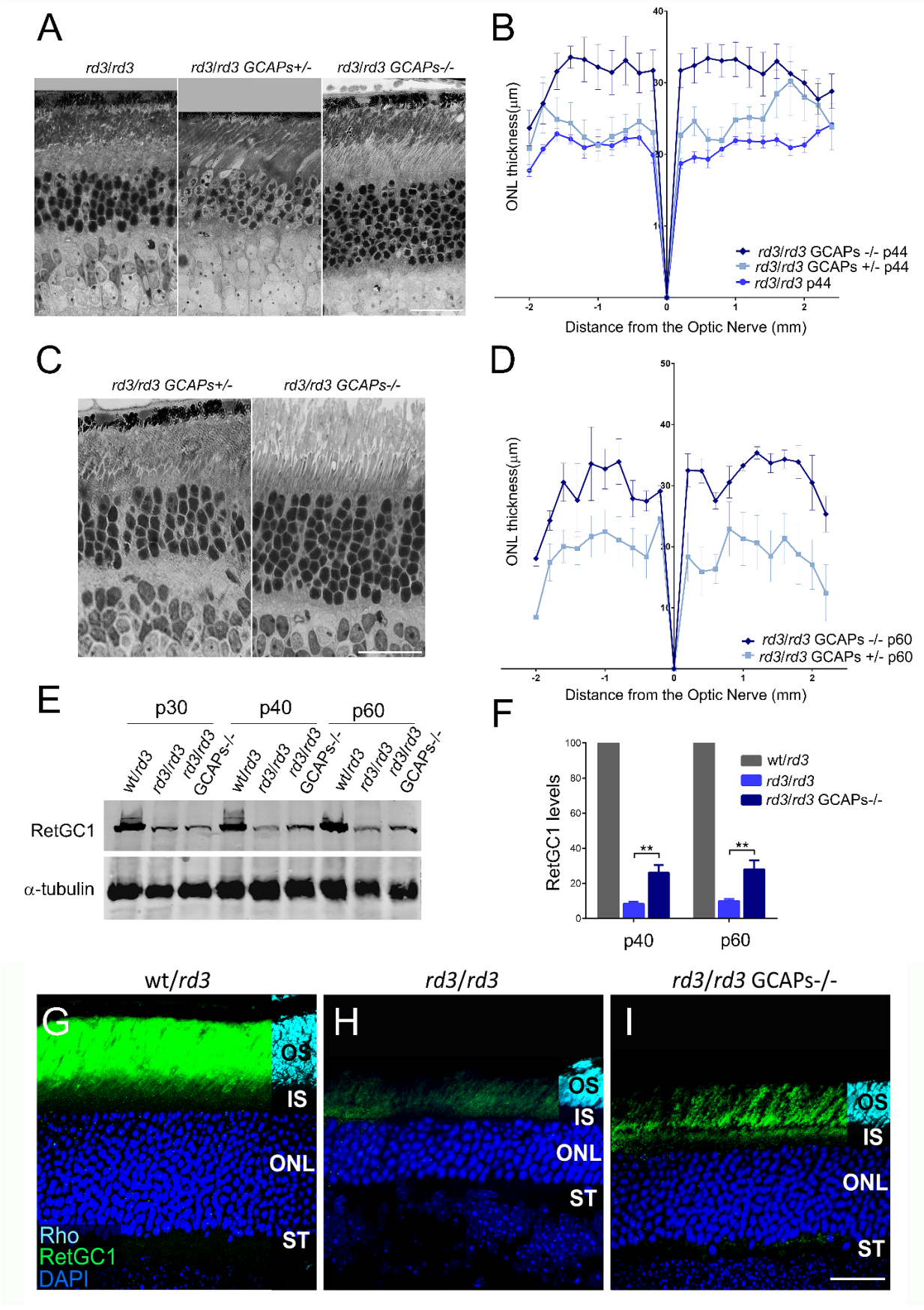

Figure 20. Retinal degeneration in *rd3* mice is substantially prevented by GCAPs ablation. (see figure legend in next page)

Figure 20. Retinal degeneration in *rd3* mice is substantially prevented by GCAPs ablation. **A.** Retinal morphology of *rd3/rd3*; *rd3/rd3* GCAPs+/- and *rd3/rd3* GCAPs-/- mice at p44. Photoreceptor cell loss is substantially prevented in the GCAPs-/- background. Scale bar 20 μm. **B.** Retinal morphometry analysis of the indicated genotypes at p44 showing ONL length (μm) along the vertical meridian of the eye. Each trace shows the average from measurements taken from four mice, with error bars showing the standard error of the mean (SEM). GCAPs removal resulted in preservation of 25% more photoreceptors at p44. **C.** Morphology of the retina in *rd3/rd3* GCAPs+/- and *rd3/rd3* GCAPs-/- at p60. The protective effect of GCAPs ablation persisted at this age. Scale bar 20 μm. **D.** Statistical analysis of ONL length in *rd3/rd3* GCAPs+/- and *rd3/rd3* GCAPs-/- retinas at p60. Results are Mean ± SEM of four biological replicates. **E.** Level of expression of RetGC1 in *rd3/rd3* GCAPs+/- and *rd3/rd3* GCAPs-/- retinas at p30, p40 and p60. RetGC1 expression levels correlated with the fraction of photoreceptors preserved. **F.** Statistical analysis of RetGC1 expression levels, Mean ± SEM of three biological replicates per genotype. RetGC1 levels were not altered by the presence or absence of GCAPs at p30, consistent with *rd3/rd3* and *rd3/rd3* GCAPs-/- mice having a similar ONL thickness at this age. RetGC1 levels were significantly higher in the GCAPs-/- background at p40 and p60 compared to *rd3/rd3*, reflecting the extent to which photoreceptor cells were preserved at this ages. Unpaired t-test (*rd3/rd3* versus *rd3/rd3* GCAPs-/- at p40, P=0.0023**); (*rd3/rd3* versus *rd3/rd3* GCAPs-/- at p60, P=0.0043**) **G-I.** In the absence of GCAPs, more RetGC1 distributed to the rod outer segment layer in *rd3* mice (I), than in the presence of GCAPs (H). Scale bar 20 μm. OS, outer segment; IS, inner segment; ONL, outer nuclear layer; ST, synaptic terminals.

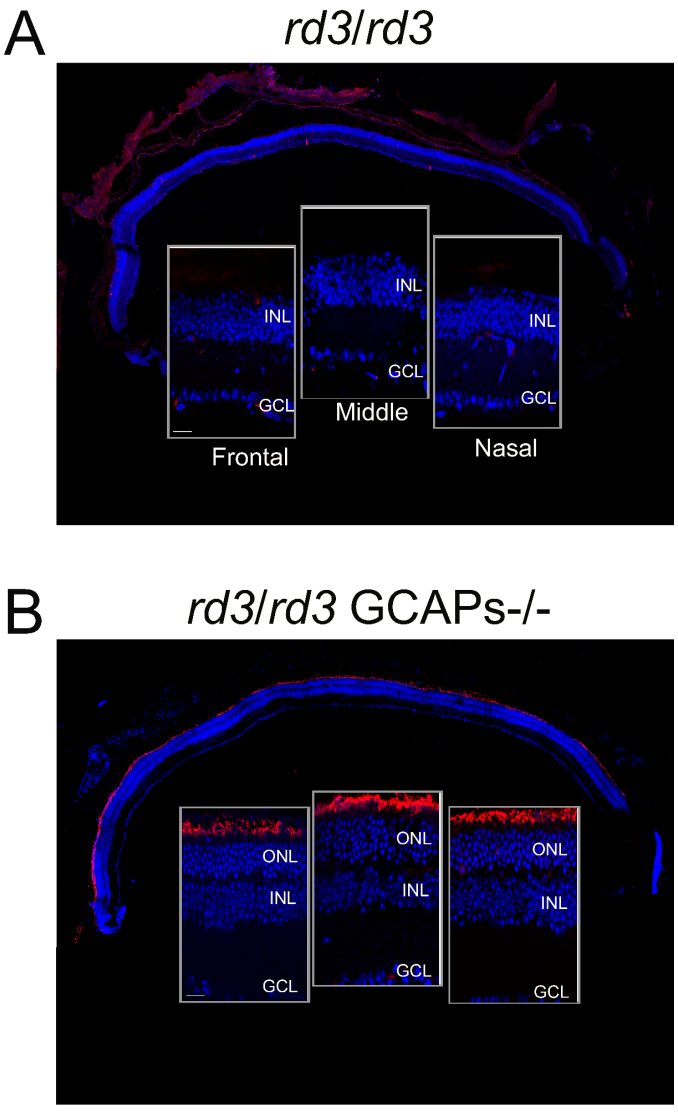

Figure 21. Protective effect of GCAPs ablation persists at eight months. A. Retinal section of *rd3/rd3* mice at eight months of age, with nuclei stained with DAPI (blue) and rod outer segment layer stained with anti-rhodopsin antibody 1D4 (in red, note the absence of rhodopsin in *rd3/rd3* mice at 8 months). Retinas from *rd3/rd3* mice show a complete loss of the photoreceptor cell layer at 8 months. Insets of frontal, middle and nasal regions of the retina are shown to evidence the loss in photoreceptor cell nuclei. **B.** Retinal morphology of *rd3/rd3* GCAPs-/- mice at the same age, showing an outer nuclear layer with five rows of nuclei. Note the rod outer segment layer (ROS) stained with anti-rhodopsin mAb 1D4 (red). Retinal sections are representative of three mice per genotype. Scale bar 20 μm. ONL, outer nuclear layer; INL, inner nuclear layer; GCL, ganglion cell layer.

3.2.4 Morphological rescue of *rd3* retinas by GCAPs ablation does not correlate with an amelioration of visual function

To test whether the substantial morphological rescue of *rd3* mice that resulted from GCAPs ablation correlated with an amelioration of visual function, light-elicited electroretinogram (ERG) responses were recorded from wildtype, *rd3/rd3*, GCAPs-/- and *rd3/rd3* GCAPs-/- mice at p40.

Rd3 mice showed substantially reduced scotopic and photopic responses (**Fig 22**), as expected based on the drastically reduced RetGC levels in this mice, as previously reported (L. L. Molday et al. 2013). Although the *rd3* mice had substantially reduced sensitivity to light, *rd3* mice at p40 elicited diminished but reliable responses to flashes in the scotopic and photopic range (**Fig 22**), indicating that *rd3* mice at this age retained some rod and cone visual function.
GCAPs-/- mice presented reduced visual responses in the scotopic and photopic range due to the lack of GCAPs stimulation of guanylate cyclase activity, but they largely retained visual function (**Fig 22**).

Strikingly, *rd3/rd3* GCAPs-/- mice at p40 yielded barely noticeable responses to flashes at either the scotopic or photopic range (**Fig 22**), despite maintaining 25% more photoreceptor cells than *rd3/rd3* mice and higher levels of RetGC at the retina. A possible explanation for these results is that *rd3/rd3* GCAPs-/- responses reflect the lack of stimulation of RetGC activity by the GCAP proteins; whereas *rd3/rd3* mice retain GCAP stimulation of the remaining RetGC proteins.

Taken together our results show that GCAPs ablation in the *rd3* mice substantially prevented retinal degeneration but at the cost of impairing rather than ameliorating visual function.

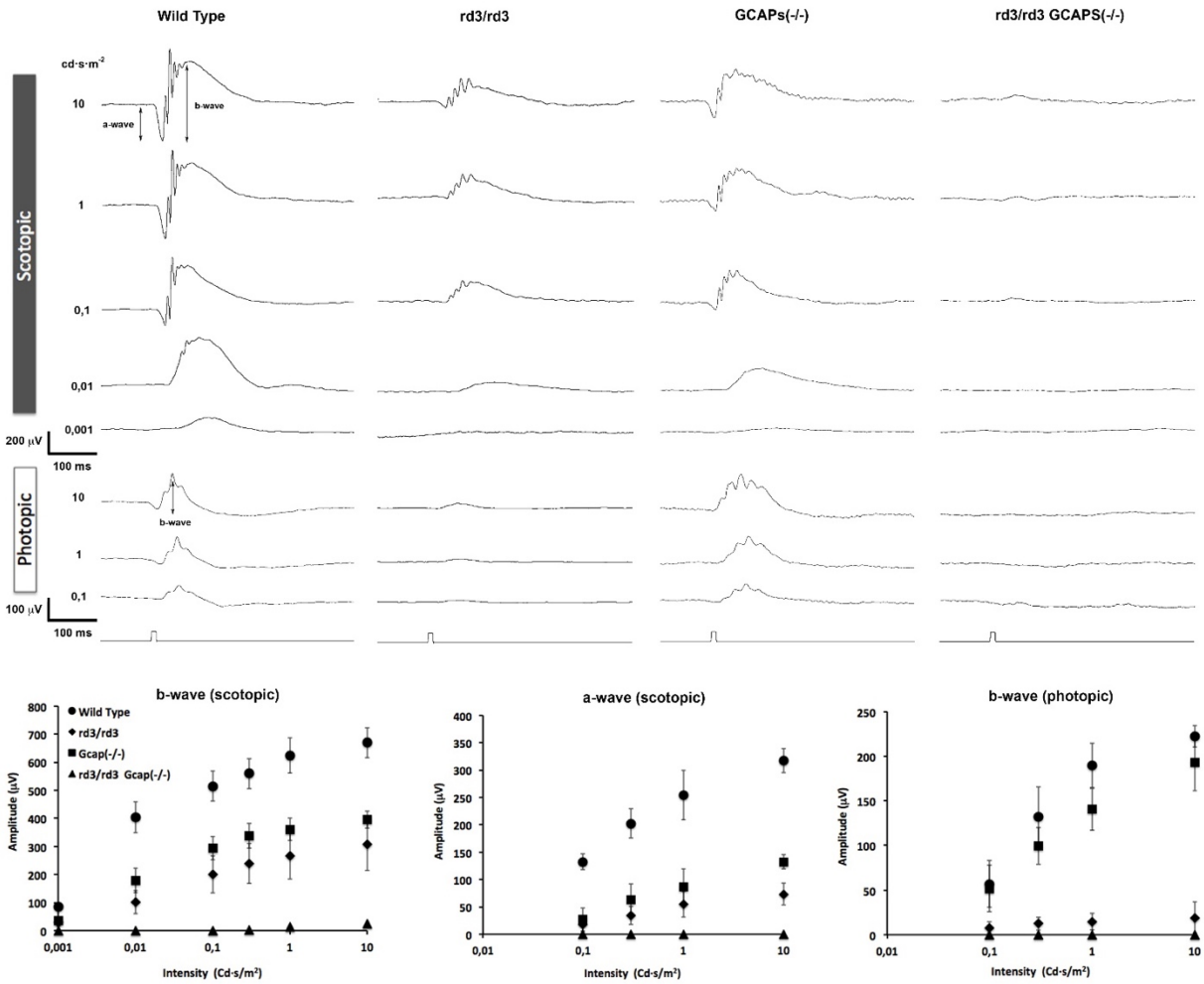

Figure 22. Light responses are drastically reduced in *rd3/rd3* GCAPs-/- mice. Electroretinographic recordings from 40 days-old wild type, *rd3/rd3*, GCAPs-/- and *rd3/rd3* GCAPs-/- mice in response to light stimuli of increasing intensity at scotopic or photopic conditions. Representative recordings are shown from one mouse of each genotype, evoked by light pulses of increasing intensity (indicated in cd.s.m^{-2}). Scotopic a-wave and b-wave amplitudes (mean $\pm$ SD) and photopic b-wave amplitudes are plotted at different light intensities from a total of four wild type mice; seven *rd3/rd3* mice; five GCAPs-/- and five *rd3/rd3* GCAPs-/- mice. Both GCAPs-/- and *rd3/rd3* mice showed substantially reduced responses when compared to wild type responses. GCAPs ablation in *rd3/rd3* mice resulted in nearly abolished responses at the scotopic or photopic range.

3.2.5 Subcellular localization of RD3 in retinal sections

There have been some inconsistencies in recent reports regarding RD3 subcellular localization. RD3 was immunolocalized to the outer segment layer of the retina in wildtype mice by specific antibodies against the COOH-terminus of the protein (S. Azadi, Molday, and Molday 2010). Subsequently RD3 was described as a potent inhibitor of RetGC activity *in vitro*, and was predicted to localize to the inner segment layer where it could silence the cyclase during its transport to the cilium (Peshenko, Olshevskaya, Azadi, et al. 2011).

To determine RD3 subcellular localization by avoiding the use of anti-RD3 antibodies, we here generated transient transgenic mice that expressed RD3 fused to a short tag (RD3.V5) in rod photoreceptors. To express RD3.V5 in rods we made use of *in vivo* DNA electroporation after subretinal injection to transfect newborn *rd3/rd3* mice with the construct pRho_mRD3.V5_dsRed. RD3 was then immunolocalized at p20 in retinal sections using well-established anti-V5 antibodies (see methods).

RD3.V5 showed the mosaic pattern of expression that characterizes *in vivo* DNA electroporation transgenesis, in which only transfected cells express the transgene. The expression of RD3.V5 in *rd3/rd3* transfected rods restored RetGC expression and its localization to the outer segment, which indicates that the RD3.V5 protein was active (**Fig 23**). RD3.V5 localized to the inner and outer segments of transfected cells, giving a stronger signal at the inner segments. Particularly, there appears to be a membrane region, probably at the connecting cilium, where the RetGC1 and RD3.V5 signals strongly colocalize (see the white signal that results at the merged green and magenta channels with the shape of "staples").

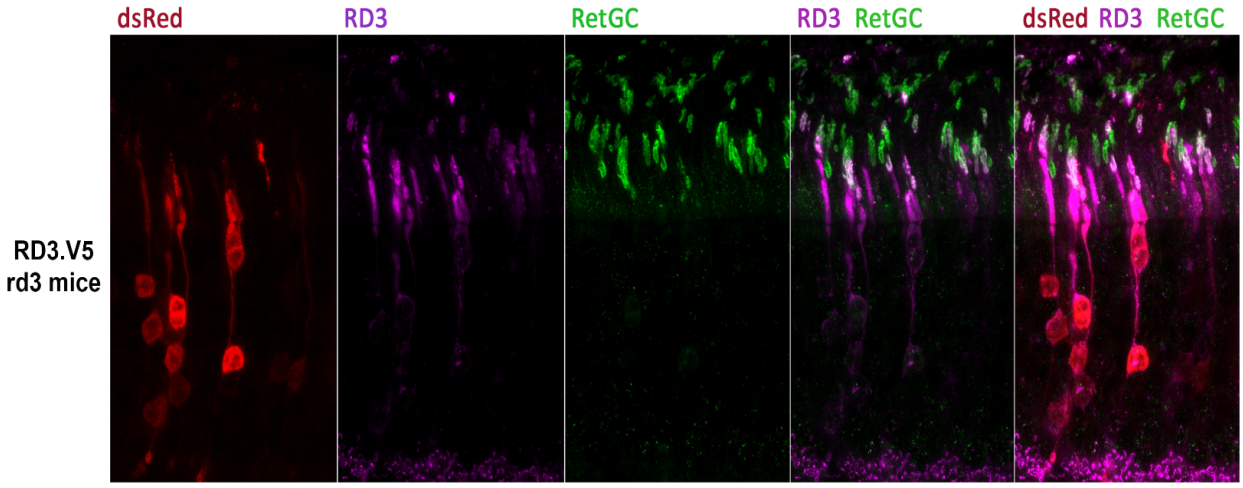

Figure 23. Subcellular localization of RD3 protein in murine retinas. Immunolocalization of RD3.V5 protein in retinal sections from *rd3/rd3* mice electroporated with pRho_mRD3.V5_dsRed. RD3.V5 distributes between the inner and outer segment compartments of transfected photoreceptor cells, with a stronger signal at inner segments. Note that the signal particularly marks a structure that could be an apical membrane domain of the inner segment, co-localizing with RetGC1. Note that the expression of RD3.V5 in transfected cells restores RetGC1 expression levels and its transport to the outer segment. The red channel shows the dsRed signal from pRho_dsRed, a plasmid co-electroporated with pRho_mRD3.V5_dsRed to serve as a reporter in the identification of the eye injected area (see methods).

Therefore our results are in line with the results obtained by (Dizhoor, Olshevskaya, and Peshenko 2019) that localize RD3 mainly at the inner segment, but we do observe some signal at the outer segments as well. The mosaic expression excludes that this signal is unspecific, as electroporated cells

are surrounded by negative-control cells. Anti-V5 antibodies unspecifically stain synaptic ribbons. This signal is clearly unspecific because it is detected in transfected and untransfected cells.

3.2.6 GCAP2 in *rd3* mice is mostly in its phosphorylated Ca2+-free form, a target for 14-3-3 binding

We have previously reported that an accumulation of Ca^{2+}-free GCAP2 at the inner segment and proximal cell compartments is highly deleterious for rod cells (Hoyo et al. 2014). In *rd3* mice GCAP2 is retained at the inner segment and proximal cell compartments (**Fig 19D**).

To test whether GCAP2 is in its Ca^{2+}-free "deleterious" conformation in *rd3* mice we analyzed GCAP2 levels of phosphorylation. *In vitro* and *in vivo* studies have shown that GCAP2 is phosphorylated at Ser201 preferentially in its Ca^{2+}-free form (Peshenko, Olshevskaya, and Dizhoor 2004; Hoyo et al. 2014). In wild type mice, about 50% of GCAP2 is phosphorylated when mice are reared under standard cyclic light, independently of their sacrifice in the dark or light period (Hoyo et al. 2014).

However, a GCAP2 mutant locked in its Ca^{2+}-free form (EF^{-}GCAP2) transgenically expressed in rods showed a much higher extent of GCAP2 phosphorylation. This indicates that the extent of GCAP2 phosphorylation *in vivo* reflects the fraction of GCAP2 molecules in the Ca^{2+}-free conformation (Hoyo et al. 2014).

The extent of GCAP2 phosphorylation in *rd3/rd3* versus wild type mice was analyzed by resolving retinal homogenates at p21 in isoelectrofocusing gel strips that covered a linear pH gradient of 3-10 (**Fig 24A**). Three-fold more *rd3/rd3* protein sample (75 μg) than wild type sample (25 μg) was loaded in order to equilibrate the GCAP2 signal. Unphosphorylated GCAP2 presented an isoelectric point (IP) of 4.92, whereas phosphorylated GCAP2 an IP of 4.85. In wild type mice, GCAP2 and GCAP2-P were present at a 1:1 ratio as originally reported. In contrast, GCAP2 and GCAP2-P were observed at a 1:3 ratio in *rd3* mice (**Figure 24B**). This ratio of GCAP2 to GCAP2-P was very similar to the ratio reported for EF^{-}GCAP2 mice (Hoyo et al. 2014), and indicates that GCAP2 in *rd3* mice is mostly in its phosphorylated Ca^{2+}-free state.

To gain insight into the mechanism by which Ca^{2+}-free GCAP2 could contribute to the physiopathology of *rd3* mice, we searched for molecular targets of Ca^{2+}-free GCAP2 in the retina. We performed pull-down assays with purified myristoylated recombinant bGCAP2 that was *in vitro* phosphorylated -or with its mock control- on Triton-X100 solubilized bovine retinas, under EGTA conditions (see Methods).

Experiments were performed in triplicate. Bound proteins were identified by liquid chromatography and mass spectrometry (LC-MS/MS) and subjected to label-free quantitative statistical analysis. For each identified protein (776 total proteins, data not shown), the equation detailed in Methods was used to determine its normalized spectral abundance factor (NSAF) in the GCAP2-P and the GCAP2 sample. The scatter plot in **Fig 24C** presents the Log2 (Mean NSAFGCAP2-P/Mean NSAFGCAP2) on the X axis, versus the -10Log(P value) in the Y axis, considering threshold values of 1.35 and 5 for the X and Y axis, respectively. Proteins that showed an statistically significant preference for GCAP2-P are shown as red dots, while those with preference for unphosphorylated GCAP2 as blue dots (**Fig 24C**).

The 14-3-3 proteins, known to interact with GCAP2-P (Hoyo et al. 2014), were identified with robust statistics as GCAP2-P binding proteins; as were proteins NDUFS5 (NADH dehydrogenase[ubiquinone] iron-sulfur protein 5), Ndel1 (nuclear distribution protein nude-like1) and RPL31 (60S ribosomal protein L31). On the other side, among the proteins with preference for unphosphorylated Ca^{2+}-free GCAP2, were HSP90(α, β) and HspB8, chaperones that may be required to stabilize this unstable form of the protein, and superoxide dismutase 1 (SOD1) and peroxiredoxin-6 (PRDX6), involved in maintaining the redox state of the cell.

RetGC1 was only identified in two out of three experiments, with < 6 spectral counts, and showed a slight preference for the unphosphorylated form of GCAP2. However, it is well established that the RetGC-GCAPs interaction is very sensitive to detergents, and virtually impossible to detect in pull-down assays.

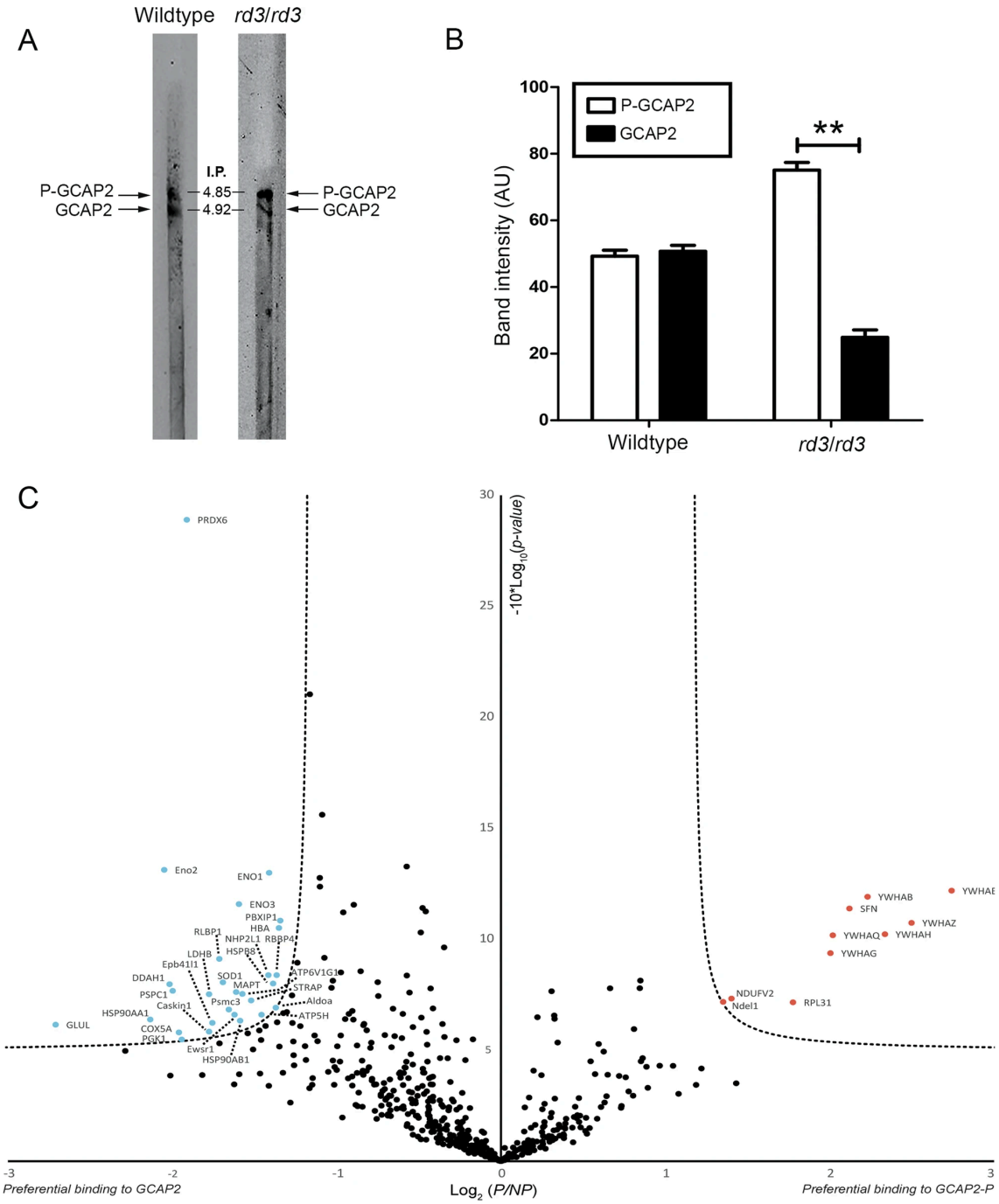

Figure 24. GCAP2 in *rd3/rd3* retinas is largely in its Ca^{2+}-free phosphorylated state, which is a target for 14-3-3 binding. **A**. Isoelectric focusing (IEF) separation of retinal homogenates from wt and *rd3/rd3* mice at p30 in linear pH 3-10 gradient gel strips. Following isoelectric focusing, proteins were transferred to a nitrocellulose membrane and immunoblotted with anti-GCAP2 pAb. **B**. The GCAP2-P to GCAP2 ratio was determined by densitometric analysis (Mean± SEM) of three independent isoelectrofocusing experiments. Unpaired t-test (GCAP2 versus GCAP2-P in the wildtype, P=0.72) and (GCAP2 versus GCAP2-P in *rd3/rd3* mice, P=0.0082**). **C**. Label-free quantitative proteomic analysis to identify putative protein interactions of Ca^{2+}-free GCAP2-P and GCAP2. Pull-down assays were performed on bovine retinal homogenates with purified myristoylated GCAP2 that was phosphorylated *in vitro* or with a MOCK-phosphorylation control, under EGTA conditions. The Volcano plot represents the statistical analysis of three independent pull-down assays. Log2 (P/NP) refers to Log2 (Mean $NSAF_{GCAP2\text{-}P}$/Mean $NSAF_{GCAP2}$), with NSAF being the normalized spectral abundance factor, see Methods. The already reported 14-3-3 phosphobinding proteins (different isoforms of YWHA) were clearly revealed as Ca^{2+}-free GCAP2-P interactors, validating the assay. Other putative interactors identified with statistical significance are marked in red (GCAP2-P) and blue (GCAP2-NP).

3.2.7 Endoplasmic reticulum stress and mitochondrial swelling are prominent early signs of retinal degeneration in the *rd3* mice that are substantially rescued by GCAPs ablation

One early alteration that we observed in the retinas of *rd3* mice at p20 was rhodopsin mislocalization. Although rhodopsin transport is not affected by the lack of RD3 and rhodopsin antibodies largely stain the outer segment layer in *rd3* mice (e.g., **Fig 19**), a number of photoreceptor cells showed rhodopsin perinuclear staining in any taken frame of the *rd3* outer retina at p20 (**Fig 25A**). This was not observed in age-matching wild type or *rd3*/*rd3* GCAPs-/- mice (**Fig 25A**). The number of cells per unit area that showed mislocalized rhodopsin in *rd3* mice was highest at p20 and diminished with age (**Fig 25B-C**).

Because this signal could be reflecting rhodopsin retention at the endoplasmic reticulum (ER) due ER dysfunction, we assessed ER stress by comparing the levels of ER stress marker C/EBP homologous protein (CHOP) in wild type, *rd3*/*rd3* and *rd3*/*rd3* GCAPs-/- mice. CHOP is a transcription factor that links severe ER impairment with the induction of apoptosis (Thapa et al. 2012). We observed a clear induction of CHOP expression in *rd3* mice at p20 (**Fig 25D-E**), that was substantially prevented by GCAPs ablation (**Fig 25D-E**). Apoptotic cell death was assessed by evaluating caspase 3 activation (detection of the p17 large fragment from caspase 3 cleavage) and the cleavage of poly (ADP-ribose) polymerase PARP, a main target of caspases. **Fig 25D-E** shows activated p17 fragment of caspase 3 at a much higher level in *rd3* mice than in wt or *rd3*/*rd3* GCAPs-/- mice, with statistical significance (experiment performed in triplicate). The extent of PARP1 cleavage in *rd3* mice versus wt and *rd3*/*rd3* GCAPs-/- mice confirms the induction of apoptotic cell death in *rd3* mice at p20, that is partially rescued by GCAPs ablation.

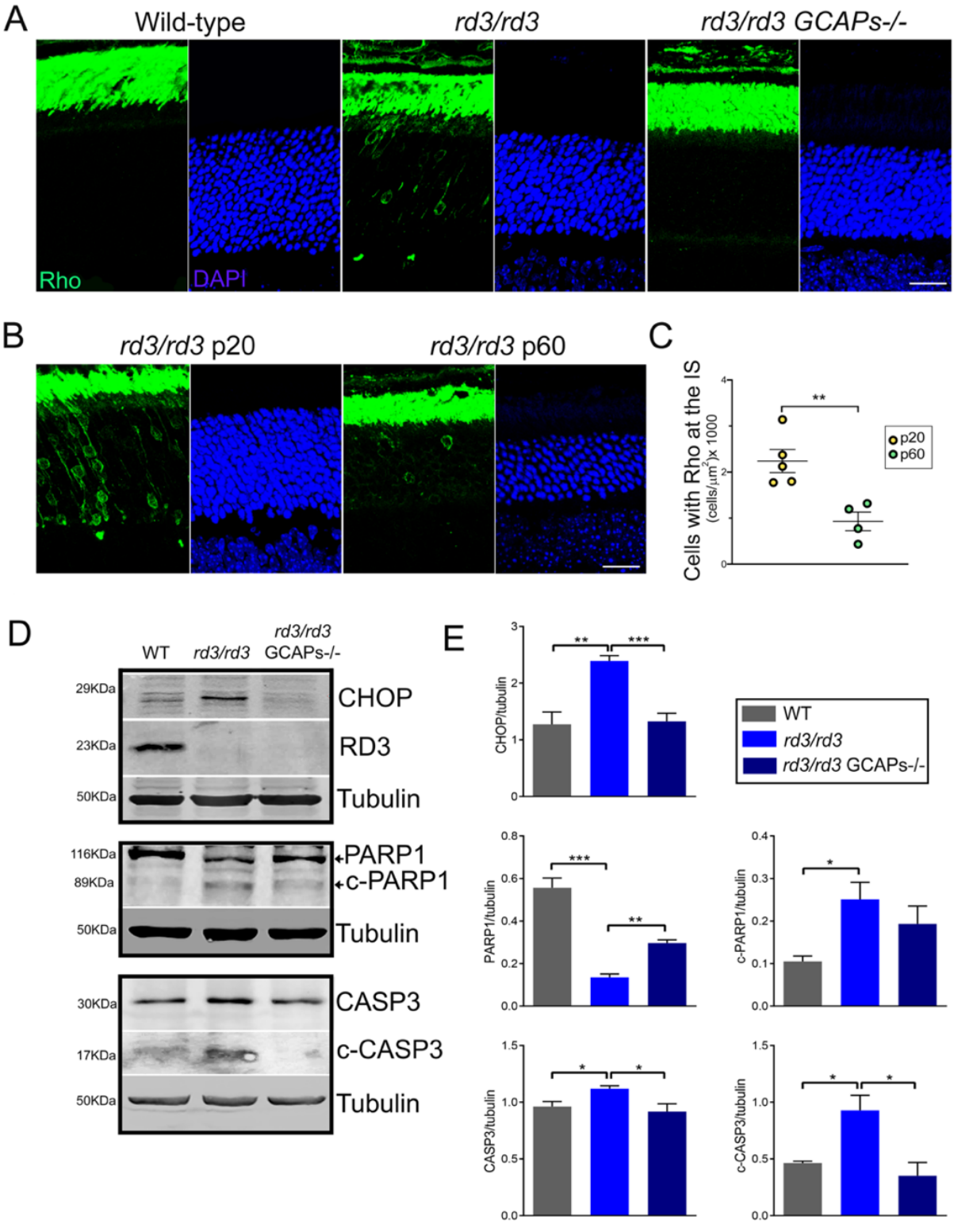

Figure 25. Rhodopsin mislocalization and endoplasmic reticulum stress are early signs of retinal degeneration in *rd3* mice that are palliated by GCAPs ablation. (see figure legend in next page)

Figure 25. Rhodopsin mislocalization and endoplasmic reticulum stress are early signs of retinal degeneration in *rd3* mice that are palliated by GCAPs ablation. **A**. Retinal sections from wt, *rd3/rd3* and *rd3/rd3* GCAPs-/- mice at p20 stained with anti-rhodopsin antibody (green) and DAPI (blue). Rhodopsin mislocalization at the perinuclear region and proximal compartments is observed in a number of photoreceptor cells at any given frame of the outer retina in *rd3/rd3* mice at p20, but not in wildtype or *rd3/rd3* GCAPs-/- mice at this age. Scale bar 20 μm. **B-C**. Representative images and quantification of cells that present rhodopsin mislocalization at p20 versus p60 in *rd3/rd3* mice, expressed per unit area [n=5 *rd3/rd3* mice at p20; n=4 *rd3/rd3* mice at p60. Unpaired t-test p20 versus p60, P=0.0058**]. **D**. Levels of CHOP; full-length and p17 kDa fragment of cleaved caspase 3; and full length and 89 kDa fragment of cleaved PARP1 proteins in retinal extracts from wt, *rd3/rd3* and *rd3/rd3* GCAPs-/- at p20. Note that the full length casp3 and c-casp3 signals were obtained from different exposure conditions of the same membrane, given that c-casp3 represents a small percentage of full length casp3. No RD3 protein was observed in *rd3/rd3* or *rd3/rd3* GCAPs-/- extracts. **E**. Six independent experiments were performed to determine CHOP expression levels (wild type versus *rd3/rd3*, P=0.0012**; and *rd3/rd3* versus *rd3/rd3* GCAPs-/- P=0.0001***). Three independent experiments were performed to determine PARP1 and c-PARP1 levels [PARP1: wt versus *rd3*, P=0.001***; and *rd3/rd3* versus *rd3/rd3* GCAPs-/-, P=0.0018**)]; [c-PARP1: wt versus *rd3*, P=0.026*; and *rd3/rd3* versus *rd3/rd3* GCAPs-/-, P=0.37 ns)]. Three independent experiments were performed to determine casp3 and c-casp3 levels [Casp3: wt versus *rd3*, P=0.035*; and *rd3/rd3* versus *rd3/rd3* GCAPs-/-, P=0.05*)]; [c-Casp3: wt versus *rd3*, P=0.026*; and *rd3/rd3* versus *rd3/rd3* GCAPs-/-, P=0.031*)].

Actually, one of the most prominent alterations in *rd3* mice at p20-p26 revealed by ultrastructural analysis was mitochondrial swelling, indicative of apoptosis. **Fig 26** shows representative electron micrographs of *rd3/rd3* mice at p20-p26 (**Fig 26B, D**), opposed to wt/*rd3* heterozygous littermate controls (**Fig 26A, C**).

Retinas from *rd3/rd3* mice showed distinctive features like emerging vertical outer segment membrane discs (black arrows in **panels B and D**, and enlarged area at **panel E**); as well as disc structures that have been internalized at the inner segment (black arrowheads in **panels F, G, H and K**). Prominent morphological alteration in *rd3/rd3* mice was mitochondrial swelling at the inner segment, noticeable at p20 at a fraction of cells (**panel F, magnified at G**), and at p26 at the majority of cells (**panels I and J**). This mitochondrial swelling preceded cell death.

Interestingly, the striking mitochondrial swelling in *rd3* photoreceptor cells (**Fig 27A**) was greatly diminished in *rd3/rd3* GCAPs-/- mice (**Fig 27B**) when four animals of each genotype were compared (**Fig 27C**).

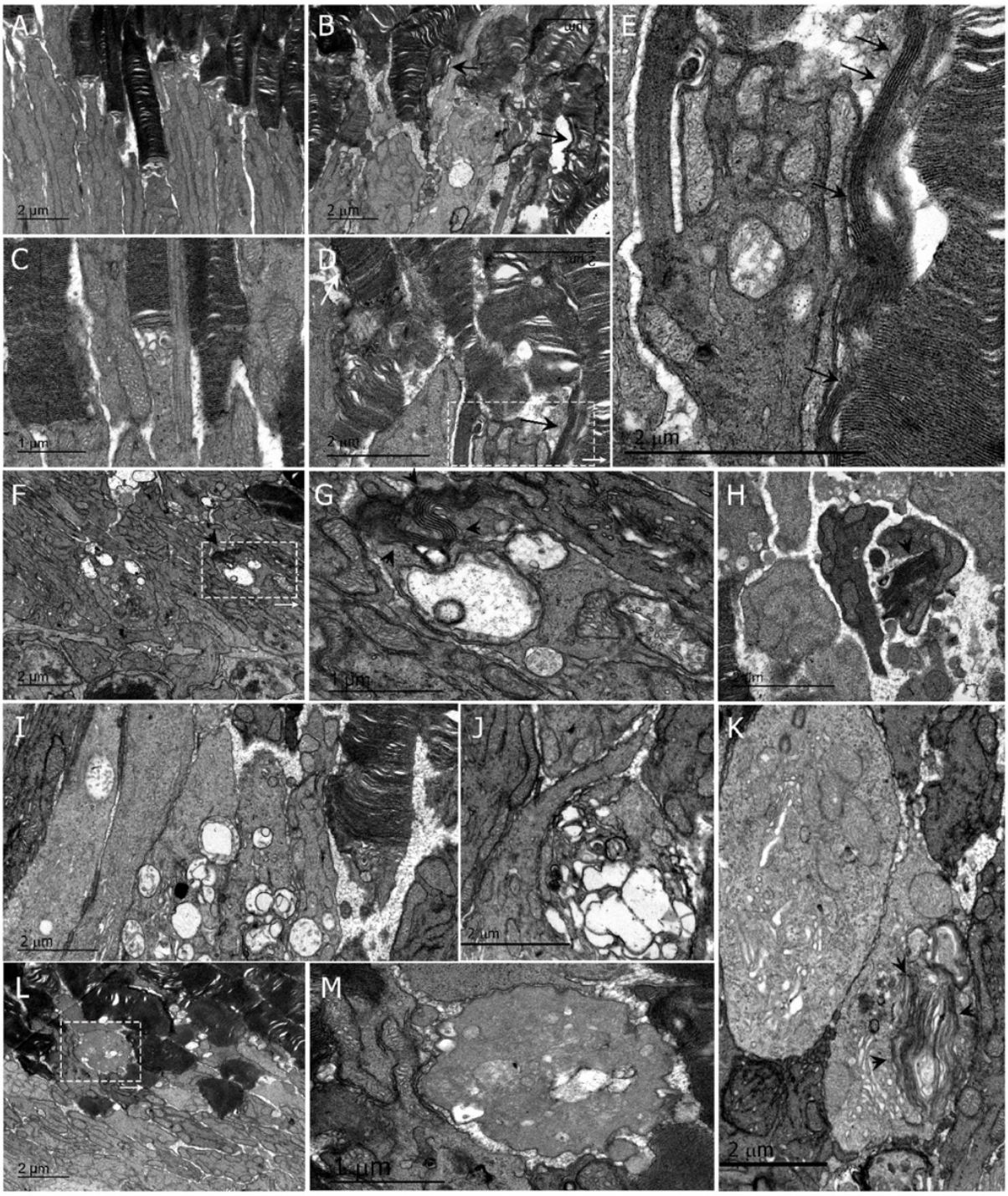

Figure 26. Mitochondrial swelling is an early sign of retinal degeneration in *rd3/rd3* mice. **A to E**. Comparison of *rd3/rd3* retinas at p20 (B, D) versus wt/*rd3* littermate controls (A, C). Retinas from *rd3/rd3* mice present distinctive features like emerging vertical outer segment membrane discs (black arrows in panels B and D, and in the enlarged area in panel E); as well as swelling mitochondria (arrowheads, panels B and E). **F, G, I, J**. Mitochondrial swelling is a hallmark ultrastructural alteration in *rd3/rd3* mice at early stages of retinal degeneration, as observed at p20 at the ellipsoid region of several photoreceptor cells (panels B, D), and more dramatically at a higher number of photoreceptor cells at p26 (panels F, G, I, J). Other striking alterations are the internalization at the inner segment of what appears to be stacks of outer segment disc membranes (black arrowheads in panels F, G, H and K); and the occasional infiltration of cells of the immune system at the inner/outer segment boundary (panel L, enlarged at M).

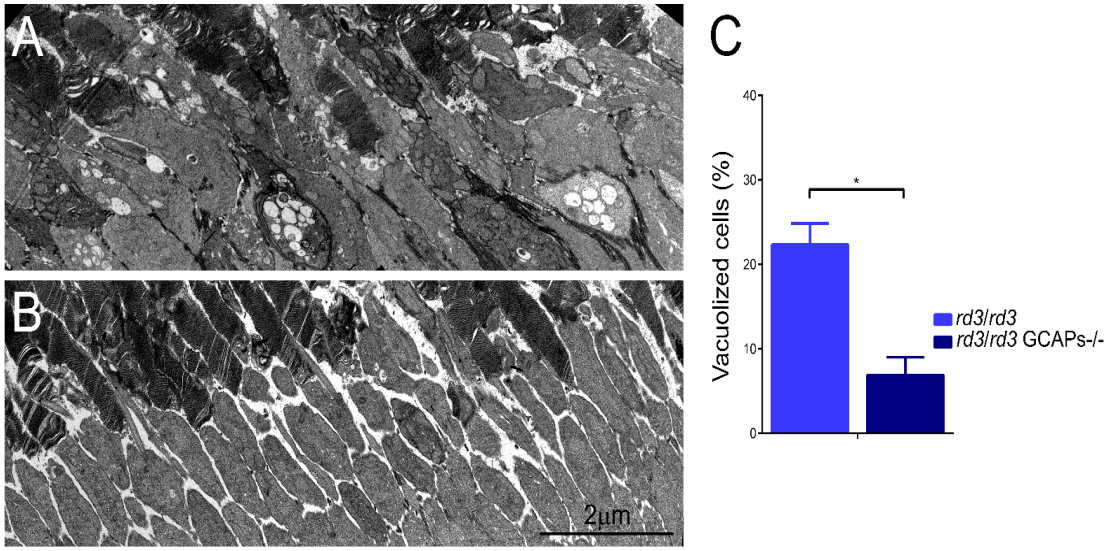

Figure 27. Mitochondrial swelling is substantially prevented by GCAPs ablation in the *rd3* mice. **A.** Representative electron micrographs of retinal sections from *rd3/rd3* and *rd3/rd3* GCAPs-/- (**B**) mice at p26. Images are the result of fusing four transmission electron microscopy fields obtained at 10 000x magnification. Scale bar 2 µm. **C.** The number of photoreceptor cells that present mitochondrial swelling is substantially reduced in *rd3/rd3* GCAPs-/- mice versus the *rd3/rd3* mice. Four independent regions were analyzed per retina; and retinas were obtained from four mice of each genotype. Histograms represent the percentage of cells with presence of vacuoles, from the total number of cells. Unpaired t-test (*rd3/rd3* versus *rd3/rd3* GCAPs-/-, P=0.019*).

Taken together, our results show that GCAPs induce the ER stress response in *rd3* mice, inducing CHOP expression and triggering apoptosis at a very early stage of the disease, and that GCAPs ablation substantially suppresses this induction and prevents photoreceptor cell death.

3.2.8 Discussion

We here show that the GCAP proteins play a central role in the physiopathology of blinding diseases associated to loss of functional RD3 (LCA12), by showing that GCAPs ablation substantially delays retinal degeneration in the *rd3* mouse model. While preservation of the retinal morphology is not accompanied by restoration of visual function, it is very revealing of the molecular mechanisms that link the lack of functional RD3 with photoreceptor cell death, and may assist at designing therapies to expand the window for gene therapy intervention in LCA12 patients.

We first confirmed all the previously reported manifestations of the phenotype of the *rd3* mice (S. Azadi, Molday, and Molday 2010), with further attention to meaningful details. RetGC1 levels are drastically reduced in *rd3* retinas as reported, but can still be detected, and are estimated at ~12% of the wild-type levels in *rd3* mice at p20 (**Fig 19C**). RetGC1 is retained at proximal cell compartments, mostly at the inner segment and perinuclear regions (**Fig 19D and Fig 23**). GCAP1 and GCAP2 levels are reduced in *rd3* mice to ~37 and ~42% of wild-type levels. Although mostly retained at the inner segment as previously reported (S. Azadi, Molday, and Molday 2010), traces of RetGC1, GCAP1, and GCAP2 are also observed at the outer segment layer (**Fig 19D**), explaining why *rd3* mice elicit bigger ERG responses than *rd3/rd3* GCAPs-/- mice (**Fig 22**).

The *rd3* strain of mice showed a fast rate of retinal degeneration, going from approximately ten rows of photoreceptor nuclei at p20 to approximately five rows at p44. GCAPs ablation substantially slowed down retinal degeneration, so that at 8 months of age *rd3/rd3* GCAPs-/- mice still retained five rows of photoreceptor nuclei. Therefore, the loss of RD3 still caused cell death in the absence of GCAPs, but at a substantially slower rate. We infer that: (i) the loss of RD3 causes an initial insult, with its origin in the closure of CNG-channels and the ensuing chronic decrease in $[Ca^{2+}]_i$; and (ii) the GCAP proteins mediate/amplify the response to this initial insult.

At a molecular level we show that >75% of GCAP2 in *rd3* mice is phosphorylated and therefore in its Ca^{2+}-free state (**Fig 24A-B**), which is indicative of low $[Ca^{2+}]_i$ at *rd3* photoreceptor cell somas. Both GCAPs would therefore be in their Ca^{2+}-free, guanylate cyclase activator state at photoreceptor cell somas of *rd3* mice, where they result in cellular damage. How would GCAPs induce damage in this context? We envision two possible pathways, sketched in our proposed model in **Fig 28** (see below).

First, as proposed by Dizhoor et al. (Dizhoor, Olshevskaya, and Peshenko 2019) Ca^{2+}-free GCAPs could, in the absence of RD3, stimulate RetGCs and promote constitutive cGMP synthesis at the inner segment, where it would result in toxicity. Dizhoor's demonstration that RD3.GFP expressed as a transgene in rods localizes to the inner segment compartment (Dizhoor, Olshevskaya, and

Peshenko 2019) supports RD3 proposed role of silencing RetGCs while at the inner segment (Peshenko, Olshevskaya, Azadi, et al. 2011). Dizhoor et al. also bred the *rd3* mice to GCAPs$^{-/-}$ mice and reported the retinal morphological rescue, interpreting the outcome as a demonstration of the importance of cyclase silencing at the inner segment for photoreceptor viability.

While we believe that other scenarios cannot be discarded at this point, we consider our data to be consistent with Dizhoor's interpretation. We here show that the levels of RetGC in *rd3* mice are ~12% of the wild-type levels, that are present at the inner segment layer. By showing that GCAP2 is mostly phosphorylated, we can infer that GCAPs are in their Ca^{2+}-free form. Although 75% of the GCAP2 present in *rd3* mice (reduced to 42% of GCAP2 wild-type levels) is phosphorylated and bound to 14-3-3 and therefore not free to bind the cyclase, there is still ~10% of GCAP2 (referred to wild-type GCAP2 levels) that could bind the cyclase and activate it in a constitutive manner. Constitutive synthesis of cGMP would therefore rely on ~12% of the wild type levels of RetGC and ~10% of GCAP2, which is apparently low. However, constitutive synthesis of cGMP at the inner segment compartment of cones has been shown to be very toxic and the basis of the physiopathology in mouse models of achromatopsia caused by null mutations in cone CNG-channel subunits CNGA3 and CNGB3. In these models, activation of cGMP-dependent protein kinase (PKG) alters ER ionic homeostasis causing ER stress (Ma et al. 2015a; Thapa et al. 2012; Butler et al. 2017).

Actually, we here show that GCAPs mediate damage by activating ER stress-mediated apoptosis, by demonstrating CHOP induction as well as caspase 3 and PARP1 cleavage in *rd3* mice that are prevented in *rd3*/*rd3* GCAPs-/- mice (**Fig 26**). Nevertheless, evidence of cGMP synthesis specifically at the inner segment compartment and/or PKG involvement is still missing in the *rd3* model and will require further investigation. An intriguing thought, assuming that preventing RetGC activity at the inner segment is critical for photoreceptor's viability, is that GCAP2 phosphorylation and 14-3-3 binding might serve as an additional mechanism to prevent cyclase activation in this compartment.

Whether GCAP1 is phosphorylated is not known, and will require further investigation. However, it is *Guca1b* gene encoding GCAP2 that was identified as a modifier gene of the *rd3* mouse phenotype (Danciger et al. 2008), and GCAP2 expression that was downregulated in *rd3* mice (R. S. Molday and Cheng 2013).

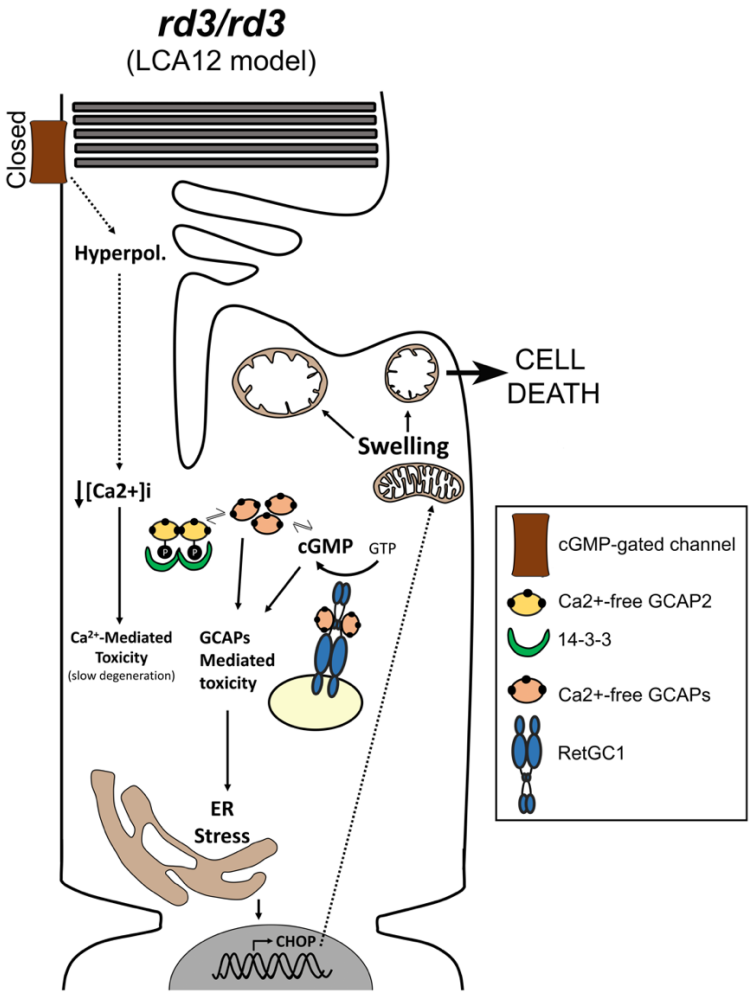

Figure 28. Sketch summarizing the mechanisms that likely contribute to the physiopathology of *rd3* mice and LCA12 patients. The lack of RD3 represents an immediate insult for photoreceptor cells by causing chronic hyperpolarization and chronic low $[Ca^{2+}]_i$ due to the closure of CNG-channels by the severe drop in cGMP synthesis. This chronic low $[Ca^{2+}]_i$ likely represents the original insult causing damage to the cell. Chronic low Ca^{2+} cause the GCAP proteins to remain permanently in their Ca^{2+}-free conformation. GCAPs in their Ca^{2+}-free guanylate cyclase activator state in the absence of RD3 may stimulate cGMP synthesis at the inner segment, ultimately causing ER stress and ER stress-mediated apoptosis. Ca^{2+}-free GCAP2 conformational instability may also ultimately induce ER stress. GCAP2 phosphorylation and 14-3-3 binding might serve as a protective role from both pathways of damage.

A second putative pathway of damage involves the conformational instability of Ca^{2+}-free GCAP2, manifested by its high tendency to aggregate when expressed in bacteria (Hoyo et al. 2014). We have previously shown that a form of GCAP2 locked in its Ca^{2+}-free form expressed as a transgene in rods is retained at the inner segment compartment by phosphorylation and 14-3-3 chaperone binding, leading to a fast retinal degeneration (Hoyo et al. 2014). EF^{-}GCAP2 toxicity occurs in the presence of RD3 silencing the cyclase. One possibility would be that the Ca^{2+}-free form of GCAP2 formed toxic protein oligomers, with 14-3-3 binding serving as a protective role by preventing this formation. In this manner, GCAP2 could cause damage in a similar way as how α-synuclein contributes to Parkinson's disease (Yacoubian et al. 2010; Plotegher et al. 2014). The instability of Ca^{2+}-free GCAP2 is also reflected in its high affinity for the HSP90 dimer observed in pull-down assays (**Fig 24C**), that raises the possibility that Ca^{2+}-free GCAP2 under chronic low $[Ca^{2+}]_i$ may trigger the heat shock response.

A few other proteins were selectively identified as putative interactors of GCAP2-P, like the cytoskeletal regulator Ndel1, nuclear-distribution gene E homolog like-1 protein, a modulator of dynein that has been involved in securing the selectivity of cargo delivered to axons (Kuijpers et al. 2016), and at inhibiting primary cilia assembly in proliferating cells (Inaba et al. 2016). Ndel1 would be a putative candidate to mediate the morphological disc alterations observed in *rd3* mice. Future experiments will test this hypothesis, and aim at confirming other putative interactions.

Finally, by expressing RD3.V5 as a transgene in the rods of *rd3* mice, we report that RD3 localizes mainly to photoreceptor inner segments, although it also distributes to some extent to the outer segments (**Fig 23**). The outer segment RD3 signal might not have been so apparent in the recent study of RD3.GFP localization in rods (Dizhoor, Olshevskaya, and Peshenko 2019) due to the protein modification by the much bigger tag. RD3 main localization to the inner segment provides some insight into the mechanisms underlying trafficking of the cyclase to the cilium. The cyclase is probably transported in two stages: a first stage, in which it is escorted and silenced by RD3 to the base of the connecting cilium; and a second, in which the GCAPs displace RD3 to bind the cyclase, previous to RetGC/GCAPs complex entry into the outer segment compartment. Future studies will be addressed at elucidating the mechanistic steps of this trafficking.

3.3 RESULTS CHAPTER 3. CHARACTERIZING THE IN VIVO MODULATION OF IMPDH1 IN DARK/LIGHT AND ITS EFFECT ON THE LIGHT RESPONSE

3.3.1 Contributions

The technical execution of the retinal phosphoproteome analysis was carried out by Eduard Sabidó and Guadalupe Espadas from the CRG/UPF Proteomics Unit. Ruben Martínez-Buey from the University of Salamanca provided us with the bacterial expression vectors for the retinal spliced isoforms of hIMPDH1, and key technical advice on how to purify the enzymes for enzymatic assays. David Justel in Rubén Martínez-Buey´s laboratory performed the GDP/GTP inhibitory assay. Isidre Casals and Esther Miralles at the Separation Techniques platform at the UB (CCiT-UB, Parc Cientific) were instrumental at helping us to set up a protocol for determination of nucleotides by High Pressure Liquid Chromatography (HPLC). I was able to run the retinal extracts and analyze the chromatograms in their facility under their supervision. Alexandra Junza and Oscar Yanes at the Institut d´Investigació Sanitària Pere Virgili (IISPV) at the Hospital Universitari Sant Joan de Reus performed the analysis of nucleotides by mass spectrometry, and I performed the quantitation. The electroretinogram dark-adapted responses were recorded in the laboratory of Pedro de la Villa, at the University of Alcalá de Henares, where I had the chance to stay for a week and learn how to analyze the recordings. A former PhD student from our lab, Santiago López-Begines, contributed to the project at its early stages, by cloning and expressing the bovine isoforms of IMPDH1. I was very fortunate to count with the assistance of Jordi Andilla and Pablo Loza from the Institute of Photonic Sciences with image acquisition and analysis at the confocal microscope.

My contribution to this chapter was: i) the obtention of the fresh and rigorously processed bovine retinal dark/light samples for the phosphoproteomic study; ii) the *in vivo* metabolic labeling analysis of IMPDH1 in mice; iii) the isoelectrofocusing analysis of IMPDH1 phosphorylation in dark/light-adapted living mice; iv) the cloning, bacterial expression and purification of the bovine/human IMPDH1 isoforms and its mutants (disease mutant collection; and phosphomimic/phosphoKO collection) for enzymatic assays; v) most of the IMPDH1 enzymatic assays; vi) the *in vitro* phosphorylation assays; vii) the immunolocalization of IMPDH1 at different light conditions, and analysis of the spicula. I significantly contributed to experiment design, conceptualization, statistical analysis and interpretation of the data.

3.3.2 Rationale

Mutations in inosine monophosphate dehydrogenase 1 (IMPDH1), the enzyme responsible for the first and rate-limiting step in *de novo* GTP synthesis, are associated to severe forms of inherited blindness. At least nine mutations have been associated to the RP10 form of autosomal dominant retinitis pigmentosa, that primarily manifests as night blindness and gradually progresses to loss of central vision: R224P (Kennan et al. 2002a); D226N (Bowne et al. 2002); R231P (Grover, Fishman, and Stone 2004); T116M, V268I, G324D, H372P (Bowne, Sullivan, et al. 2006); K238E (Wada et al. 2005) and K238R (Wada et al. 2005). Together they account for about 1% of adRP cases (Sullivan et al. 2013). IMPDH1 mutations have also been associated to rare autosomal dominant Lebers Congenital Amaurosis (adLCA), characterized by nearly complete blindness from early age: R105W and N198K (Bowne, Sullivan, et al. 2006). Despite the ubiquitous nature of guanine nucleotide synthesis, clinical manifestations of *IMPDH1* mutations are limited to the retina, for reasons that are not yet understood.

RP10 mutations are allegedly "gain-of-function" mutations, given that IMPDH1 knock-out mice present only a mild retinopathy (Aherne et al. 2004). Mutations do not directly affect IMPDH1 catalytic activity *in vitro* (Mortimer and Hedstrom 2005; D. Xu et al. 2008; Aherne et al. 2004). IMPDH1 capacity to bind single-stranded nucleic acids (Mortimer et al. 2008; Hedstrom 2008) and IMPDH1 tendency to aggregate (Tam et al. 2008; Aherne et al. 2004) have been suggested to contribute to the pathophysiology.

More recently, a structural study has provided a new framework to interpret the effect of mutations, by revealing the allosteric inhibition of eukaryotic IMPDHs by GDP/GTP binding to the Bateman domain (Buey et al. 2015). GDP/GTP binding sites at the Bateman domain overlap with several of the residues mutated in adRP10 (Buey et al. 2015).

The competition of adenine or guanine nucleotides at the nucleotide binding sites of the Bateman domain controls a conformational switch that modulates catalytic activity (Buey et al. 2015). ATP binding induces the formation of extended octamers that are fully active; while GTP binding induces the formation of compacted octamers with significantly reduced catalytic activity (Labesse et al. 2013; Buey et al. 2015). Most of the residues in hIMPDH1 associated to blindness map at or in the proximity of GDP/GTP binding sites and diminish GDP/GTP negative allosteric control of human IMPDH1 *in vitro* (Buey et al. 2015).

IMPDH can form macromolecular filamentous structures in mammalian cells (spicules or cytoophidia) under conditions that require higher IMPDH activity to keep with GTP demand (Liu

2010; Chang et al. 2015; Aughey and Liu 2016; Keppeke et al. 2018), like at high rates of proliferation, or Gln/Ser/folate-metabolite deficiency (Calise et al. 2016; Chang et al. 2015; Keppeke et al. 2018). Formation of these reversible fiber-like subcellular structures is believed to transiently boost IMPDH activity (Chang et al. 2015; Keppeke et al. 2018). Once the guanine levels are reestablished, GTP itself promotes disassembly of the "cytoophidia-like" structures (Calise et al. 2014).

Reversible formation of IMPDH fibers could be recently induced *in vitro* from recombinant proteins, revealing that most adRP10 IMPDH1 mutants form filaments but fail to disassemble them due to their inability to sense GTP at the Bateman domain (Fernández-Justel et al. 2019).

Importantly, structural and functional characterization of IMPDHs has largely been performed on recombinant proteins expressed in *E Coli*. Little is known about the relevance of IMPDH1 catalytic activity in photoreceptor cells of the retina or its physiological regulation *in vivo*.

This study aimed to study IMPDH1 role in photoreceptor cells and its regulation *in vivo* in dark/light conditions, in order to gain insight into the effect of IMPDH1 mutations in the retina.

CHARACTERIZING THE *IN VIVO* MODULATION OF IMPDH1 IN DARK/LIGHT AND ITS EFFECT ON THE LIGHT RESPONSE

3.3.3 Dark/light-dependent phosphorylation of retinal IMPDH1.

Phosphoproteomic analysis of dark- and light-adapted bovine retinas (see methods) revealed three phosphorylation sites in IMPDH1: Thr^{159}/Ser^{160}, Ser^{416} and Ser^{477} (**Fig 29A-B**). One phosphorylation event was detected at the Bateman domain, assigned to Thr^{159} or Ser^{160} with a 50:50 probability [numbering corresponding to canonical bovine IMPDH1 (β) of 514 aa]. The peak areas of the precursor ions for the monophosphorylated peptide 154-169 in 3 dark (1-3) and 3 light (4-6) biological replicates revealed a light preference of the observed phosphorylation event (light/dark log2 fold change =1.67; p=0.03*). Residues Thr^{159} and Ser^{160} map within the CBS1 (cystathionine β-synthase) sequence of the Bateman domain, in close proximity to N198, R224 and D226 mutated in adLCA or adRP10 (**Fig 29C-D**).

A second phosphorylation event was detected at residue Ser^{416}, but was observed to a similar extent in dark and light conditions (light/dark log2 fold change = 0.33; p= 0.08). This residue maps at the mobile flap in the catalytic domain (residues 412-432, shown in green in **Fig 29E**), required in the conformational rearrangement of IMPDH1 during the hydrolysis step (E-XMP* to XMP) (Hedstrom 2009).

The third phosphorylation event was detected at residue Ser^{477}, which occurred preferentially in the dark-adapted state although statistical significance was not reached (light/dark log2 fold change= -0.50; p= 0.19). Ser^{477} maps to a region that has not been involved in the catalytic process.
Remarkably, all the phosphorylated residues are conserved in mammalian IMPDHs (**Fig 29F**).

The light/dark log2 fold change of phosphopeptides representative of well characterized light- or dark-dependent phosphorylation events in rhodopsin (Wilden 1995; K. A. Lee et al. 2002; A Mendez et al. 2000), phosducin (R. H. Lee, Brown, and Lolley 1990; B. Y. Lee, Thulin, and Willardson 2004) and GRK1 (R. H. Lee, Brown, and Lolley 1982; Palczewski et al. 1992) are shown (**Fig 30**) as a quality control of the phosphoproteomic analysis.

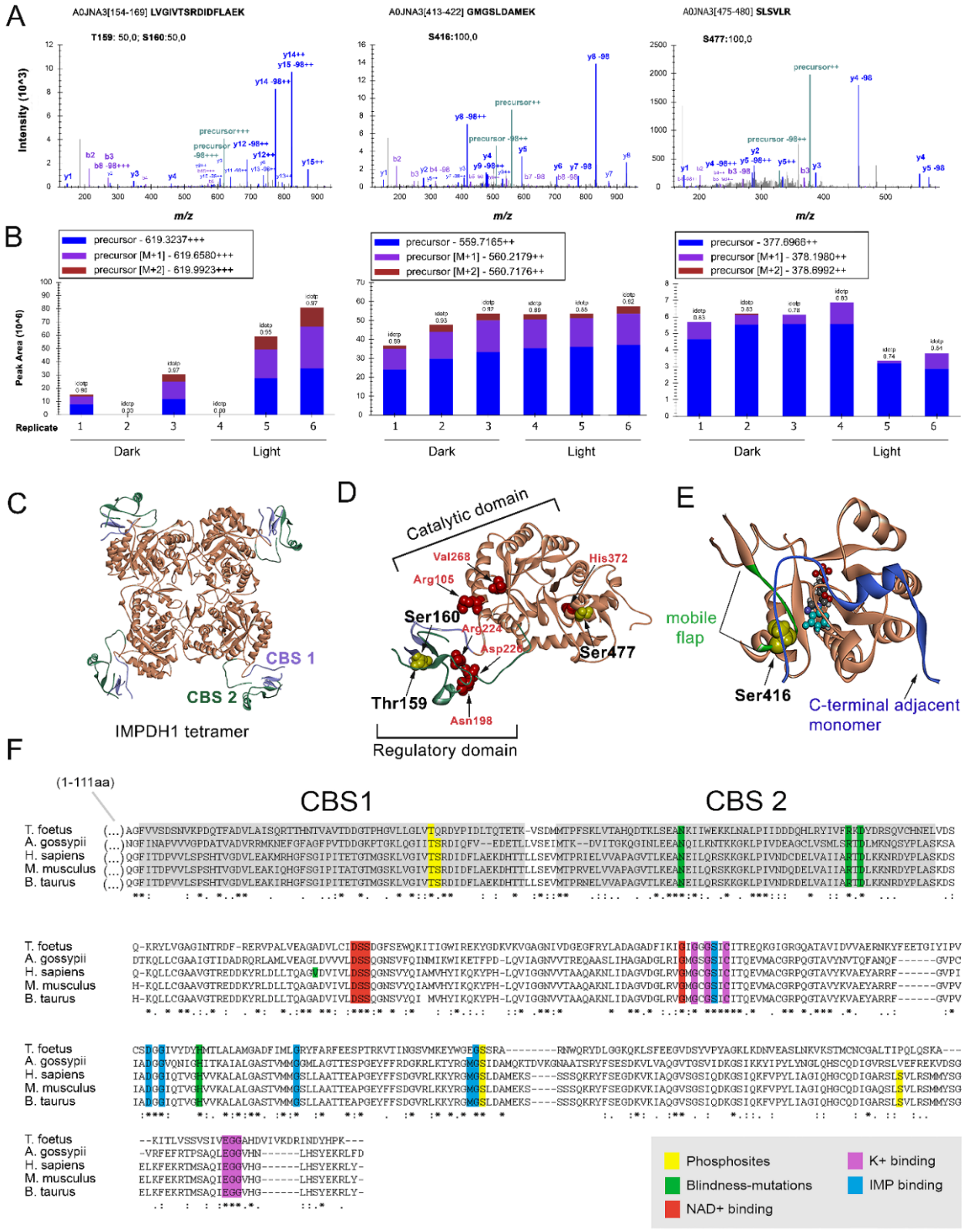

Figure 29. IMPDH1 phosphorylation sites identified in a phosphoproteomic study of dark/light-adapted bovine retinas. (see figure legend in next page)

Figure 29. IMPDH1 phosphorylation sites identified in a phosphoproteomic study of dark/light-adapted bovine retinas. **A.** Mass spectra of identified IMPDH1 phosphorylated peptides. Residue numbers refer to the canonical bovine isoform β (514 aa) [Uniprot A0JNA3]. For peptide 154-169 only one phosphorylation was detected, that could not be unequivocally assigned to Thr^{159} or Ser^{160}. Phosphorylation at peptides 413-422 and 475-480 were at Ser^{416} and Ser^{477}, respectively. **B.** Peak areas of the precursor ions corresponding to the identified phosphopeptides of IMPDH1. Samples 1-3 are dark-adapted retinas; 4-6 light-exposed retinas (biological replicates). Thr^{159}/Ser^{160} are preferentially phosphorylated in light, Ser^{477} in dark, and Ser^{416} indistinctly. **C.** Ribbon diagram of IMPDH in its tetrameric conformation [pdb: 1jcn], showing the TIM barrel catalytic domain in coral, and the regulatory Bateman domain with two copies of cystathione beta-synthase (CBS) sequence in slate blue (CBS1) and green (CBS2). **D.** Monomer conformation [pdb: 1jcn] showing Thr^{159} and Ser^{160} at CBS1 in the Bateman domain; and Ser^{477} at the COOH-terminus. Disease associated mutations, depicted in red, are proximal to Thr^{159}/Ser^{160} (Asn198; Arg224; Asp226) or to Ser^{477} (His372). **E.** The catalytic domain of AgIMPDH [pdb:4xfi] in coral, the mobile flap where Ser^{416} maps in green and the COOH-terminus of an adjacent monomer in blue. **F.** Alignment of IMPDH from *T. foetus* (prokaryotic), *A. gossypii* (filamentous fungus), *H. sapiens*, *M. musculus* and *B. taurus* IMPDH1 canonical isoforms. Phosphosites highlighted in yellow.

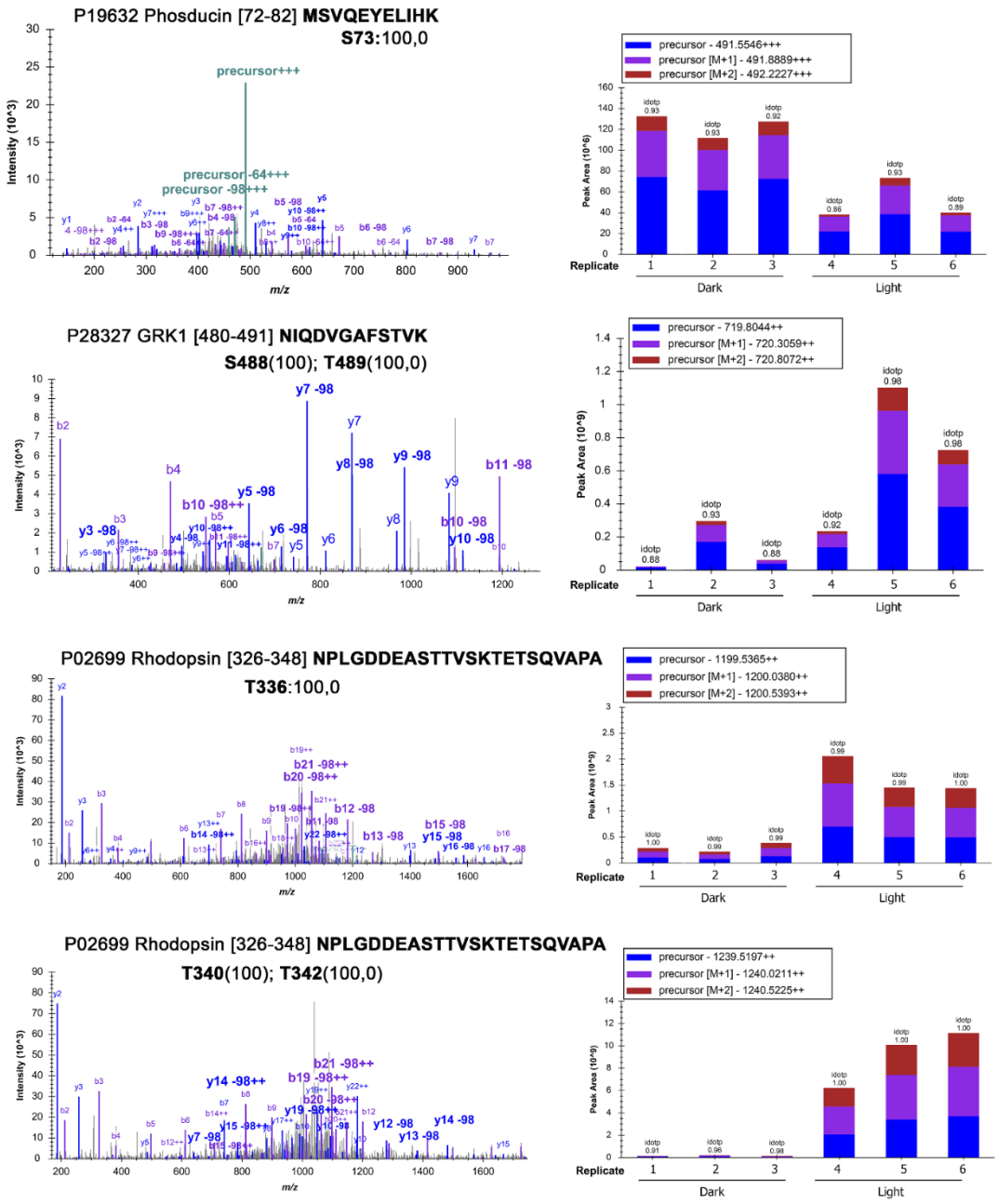

Figure 30. Dark/light fold-change of peak areas from control phosphopeptides from phosducin, GRK1 and rhodopsin shown as a quality control of the phosphoproteomic analysis. Mass spectra of phosphorylated peptides of: phosducin 72-82 peptide MSVQEYELIHK [Uniprot P19632]; GRK1 480-491 peptide NIQDVGAFSTVK [Uniprot P28327]; and rhodopsin 326-348 peptide NPLGDDEASTT-VSKTETSQVAPA [Uniprot P02699]. For each peptide, the peak area of the precursor peptide ion was extracted and plotted for each sample. Samples 1-3 are dark-adapted retinas; 4-6 light-exposed retinas (biological replicates). Light/dark log2 fold-change values were: phosducin Ser^{73} (**-1.39**; P=0.01); GRK1 Ser^{488}/Thr^{489} (**2.70**; P=0.08); Rhodopsin Thr^{336} (**2.49**; P=0); and Rhodopsin Thr^{340}/Thr^{342} (**5.53**; P=0).

3.3.4 IMPDH1 is phosphorylated *in vivo* at a high extent in both dark and light conditions

To further characterize IMPDH1 phosphorylation *in vivo* we performed an *in situ* metabolic labeling assay. Retinas from dark-adapted mice were dissected and incubated in Locke´s buffer with ^{32}P-inorganic phosphate for 90 min in the dark, to allow for ^{32}P incorporation in the ATP pool. Retinas were then kept in the dark or exposed to 2000 lux light for 5 min.

IMPDH1 was immunoprecipitated from supernatant and membrane fractions with an anti-bIMPDH1 pAb generated against the canonical bovine IMPDH1β of 514aa (see results Chapter 1). This antibody immunoprecipitated all IMPDH1 isoforms in the murine retina (immunoblots in **Fig 31A-B**). ^{32}P-incorporation was limited to the largest and most abundant isoform in murine retinas, the 603/604 aa retinal-specific spliced form (autoradiographs in **Fig 31A-B**). Phosphorylation of 603/604 aa IMPDH1 occurred to a high extent in dark- and light-retinas, both in the soluble and membrane fractions. Phosphorylation of IMPDH1 in the soluble fraction was slightly skewed towards the light condition (P=0.18); while in the membrane fraction toward the dark condition (P=0.30), with no statistical significance, **Fig 31C**.

To obtain insight into the predominant phosphorylated species in dark and light, immunoprecipitated IMPDH1 from ^{32}P-labeled retinas was resolved by isoelectrofocusing (IEF), **Fig 31D**. Three abundant species were detected in dark and light conditions: unphosphorylated IMPDH1-603/604aa, monophosphorylated IMPDH1-603/604aa-1P, and diphosphorylated IMPDH1-603/604aa-2P.
The same ratio of IMPDH1-0P, -1P and -2P was observed by IEF separation of retinal homogenates from living mice that were either dark-adapted or exposed to 2000lux light for 5, 20 and 60 min. Measured isoelectric points (IP) of IMPDH1-603/604aa-0P, -1P and -2P correlated well with IP predicted values, **Fig 31E**.

Taken together our results show that the most abundant isoform of IMPDH1 in the retina, which is a retina-specific spliced form, is phosphorylated to a high extent *in vivo*. Nearly two thirds of the protein are phosphorylated *in vivo*, with mono- and di-phosphorylated forms being present but monophosphorylated species predominating under dark or physiological light conditions. Dark/light phosphorylation of IMPDH1 is consistent with our mass spectrometry results (**Fig 29 A-B**).

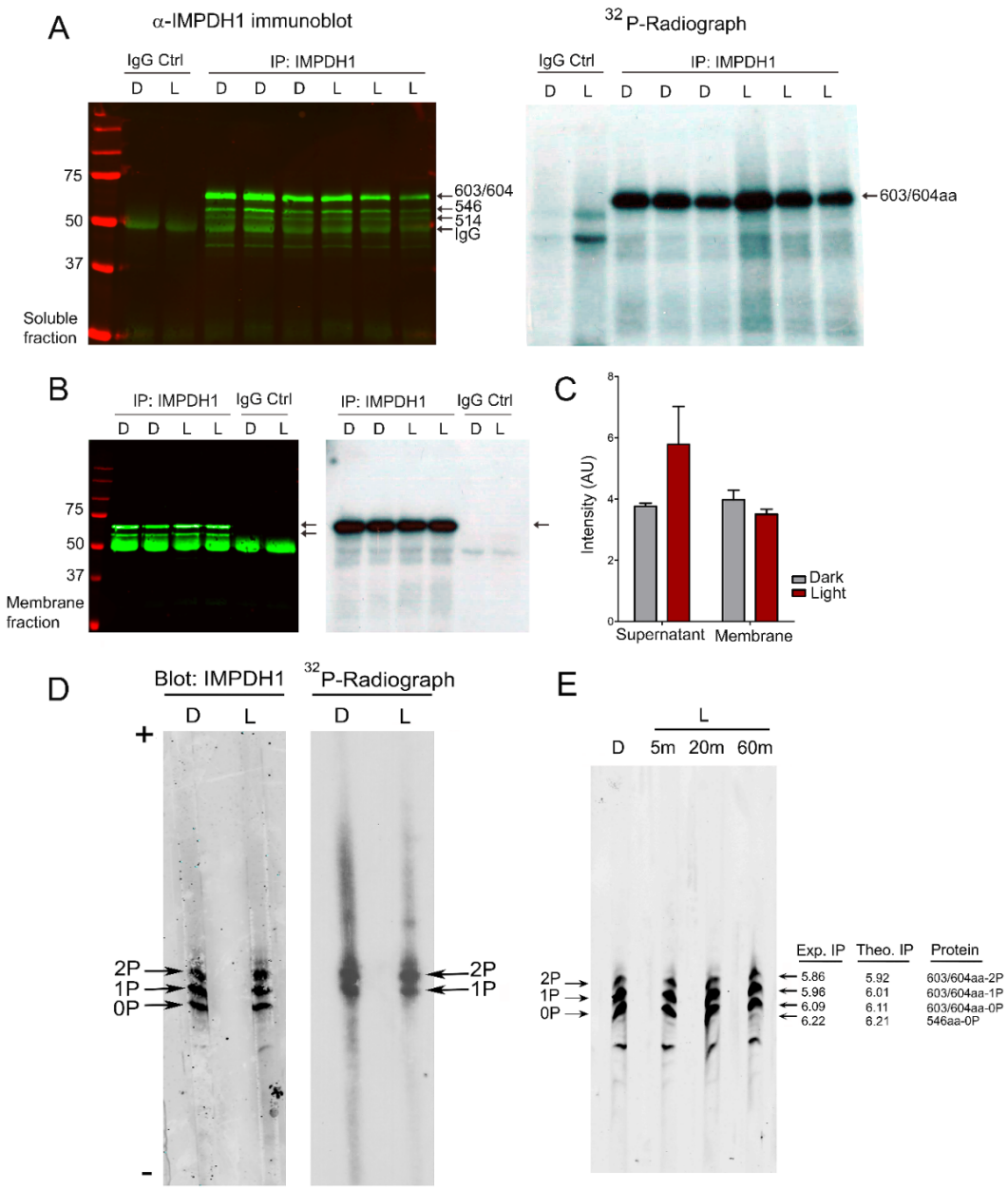

Figure 31. The retinal spliced variant of IMPDH1 is phosphorylated to a high extent in intact retinas. **A.** Immunoblot of IMPDH1 immunoprecipitated from soluble fractions of ^{32}P-labeled retinas, and corresponding autoradiograph. $^{32}P_i$ incorporation was observed at mIMPDH1-603/604 aa isoform, in both dark and light conditions (autoradiograph), 3 biological replicates. **B.** Immunoblot and autoradiograph of IMPDH1 immunoprecipitated from membrane fractions. $^{32}P_i$ incorporation was observed at IMPDH1-603/604 aa, at dark and light conditions, 2 biological replicates. **C.** Average intensity of ^{32}P-labeled 603/604 aa bands normalized by immunoblot signal, for dark and light samples. IMPDH1 is substantially phosphorylated under dark and light, both in soluble and membrane fractions. **D.** Isoelectrofocusing (IEF) of immunoprecipitated IMPDH1 samples from $^{32}P_i$-labeled retinas revealed the presence of mono- and di-phosphorylated forms of IMPDH1-603/604 aa in dark and light. Observed bands were: mIMPDH1-603/604-0P; mIMPDH1-603/604-1P and mIMPDH1-603/604-2P. Please note that the di-phosphorylated form incorporates 2 radiolabeled phosphates per protein molecule, so that the band intensity of the di-phosphorylated form in the autoradiograph reflects twice its abundance. **E.** IEF of retinal homogenates (soluble fractions) from 16 hrs dark-adapted mice or mice that were exposed to 5, 20 or 60 min of 2000 lux light after pupil dilation. Measured isoelectric points (IP) of bands correlated well with theoretical IP for the mIMPDH1 isoforms indicated.

3.3.5 *In vitro* effects of phosphorylation on IMPDH1 catalytic activity

While IMPDH1-603/604 aa is the prevalent isoform in murine retinas, two isoforms predominate in human retinas: IMPDH1α (546 aa) and IMPDH1γ (595 aa) (Bowne, Liu, et al. 2006), with IMPDH1α (546aa) being the most abundant. In order to study the effect of phosphorylation on the catalytic activity of IMPDH1, recombinant human IMPDH1α (546 aa) and its individual phosphomimetic mutants (Thr (T) or Ser (S) substituted by Asp (D)) were expressed in bacteria and purified to homogeneity.

The S160D-hIMPDH1α and S477D-hIMPDH1α mutants showed very similar reaction kinetics and Michaelis-Menten parameters as the wildtype protein (**Fig 32A-B**), indicating that phosphorylation at these sites were unlikely to affect the K_m or V_{max} of the enzyme. However, the S416D-hIMPDH1α mutant showed a slower reaction. This result was not surprising, given that Ser^{416} maps at the mobile flap that determines the open or closed conformation of the enzyme during enzyme catalysis (Hedstrom 2009).

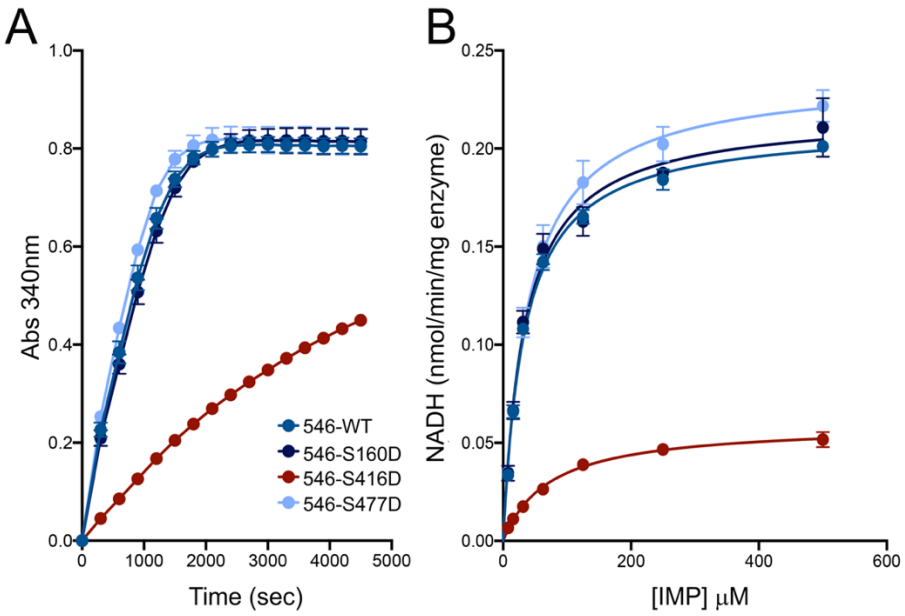

Figure 32. Effect of phosphomimetic substitutions on enzymatic activity. A. Reaction kinetics of wildtype; S160D; S416D and S477D mutants of hIMPDH1α (546 aa). Assays were performed with 2 μg of recombinant protein in assay buffer with 125 μM IMP and 0.5 mM NAD+. Absorbance at 340 nm was used to monitor NADH production at 6 min intervals. Results represent the mean and S.E.M of three independent experiments with three technical replicates each. S160D and S477D mutants showed wildtype kinetics; while S416D mutant showed delayed kinetics. **B.** Michaelis-Menten plots for the wildtype and phosphomimetic mutants. NADH production plotted to concentration of IMP. Assays were performed at 0.5 mM NAD+ and varying concentrations of IMP, from 0 to 500 μM. NADH production (nmol/min/mg enzyme) was obtained from ΔAbs/Δt by applying Lambert- Beer's law ($\varepsilon NADH_{340nm}$=6220 $M^{-1}cm^{-1}$, l=0.58 cm), and results were fitted to Michaelis-Menten curves with GraphPad Prism [Mean and S.E.M of three independent experiments, three technical replicas each].

We further confirmed the effect of Ser^{416} phosphorylation by measuring the effect on kinetics and IMP dependence of the S416D substitution in main hIMPDH1 isoforms: hIMPDH1β (514 aa) and hIMPDH1γ (595 aa) (**Fig 33A**).

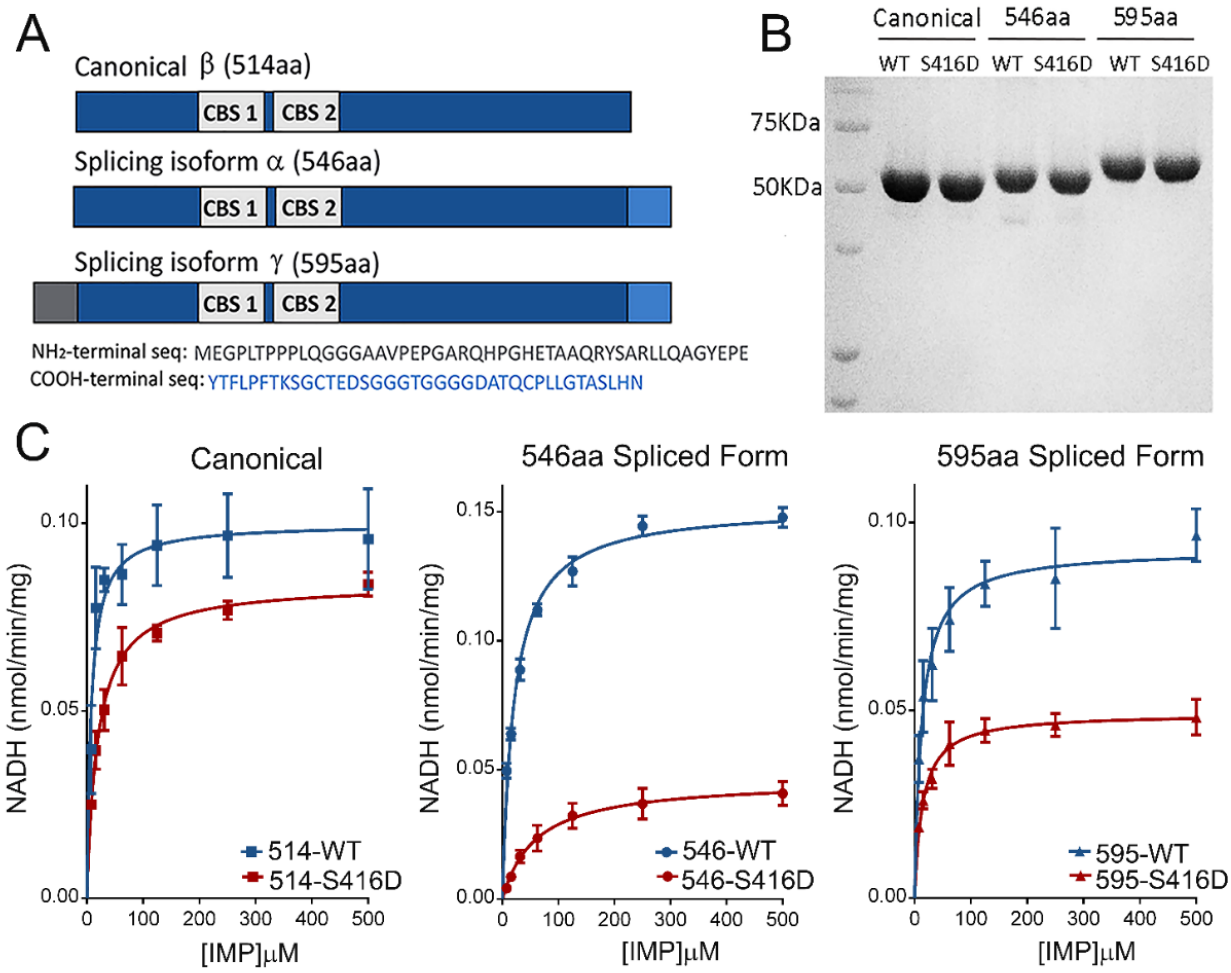

Figure 33. Effect of S416D phosphomimetic substitution on enzymatic activity. A. Main splice variants of hIMPDH1: hIMPDH1α (546 aa) and hIMPDH1γ (595 aa) contain extended sequences at the COOH-terminal (546 aa) or both the NH_2- and COOH-terminal (595 aa). **B.** S416D mutant recombinant proteins were rigorously normalized to their wildtype counterparts preceding enzymatic analysis. **C.** Effect of S416D substitution on the Michaelis-Menten kinetics of hIMPDH1β (514 aa); hIMPDH1α (546 aa); and hIMPDH1γ (595 aa) isoforms. Kinetic parameters were: hIMPDH1β (514 aa) [V_{max}=0.099±0.004, K_m=7.62±1.69]; S416D/hIMPDH1β (514 aa) [V_{max}=0.084±0.002, K_m=19.13±1.75]; hIMPDH1α (546 aa) [V_{max}=0.152±0.002, K_m=20.72±1.32]; S416D/hIMPDH1α (546 aa) [V_{max}=0.046±0.002, K_m=59.59±9.74]; hIMPDH1γ (595 aa) [V_{max}=0.093±0.003, K_m=12.86±2.18]; S416D/hIMPDH1γ (595 aa) [V_{max}= 0.049±0.001, K_m=13.95±1.71]. Results represent the media and S.E.M of three independent experiments.

Recombinant proteins were rigorously normalized by Bradford and SDS-PAGE prior to the enzymatic assays, to ensure that identical amounts of proteins were used (**Fig 33B**). Michaelis-Menten kinetics of S416D-hIMPDH1β (514 aa); S416D-hIMPDH1α (546 aa) and S416D-hIMPDH1γ (595 aa) showed that S416D substitution in the mobile flap had a significant effect at inhibiting the enzyme, that was higher for the retinal spliced forms of 546 and 595 aa than for the canonical form (**Fig 33C**). However, because phosphorylation at this residue was similar in dark and light conditions, we believe that the decrease in IMPDH1 catalytic activity associated to Ser^{416} phosphorylation might occur in response to other signals such as nutritional stress, but would have an effect unrelated to dark/light physiological conditions (see Discussion).

3.3.6 T159 and S160 phosphorylation impairs GDP/GTP regulation of IMPDH1

It has been recently established that GTP and GDP allosterically inhibit the catalytic activity of eukaryotic IMPDH enzymes *in vitro* (Anthony et al. 2017; Buey et al. 2015; Fernández-Justel et al. 2019). Thereby, we then tested whether phosphorylation could affect allosteric inhibition *in vitro*. To do that we assayed IMPDH activity of wild-type and phosphomimetic proteins (Thr (T) or Ser (S) substituted by Asp (D) or Glu (E)) in the presence of GDP and GTP.

Fig 34 plots the normalized V_{max} values (V_{max}^{app} in the presence of 2 mM GTP or GDP divided by V_{max} in the absence of nucleotide) for all hIMPDH1β (514 aa) wild-type and phosphomimetic mutants. As expected, phosphorylation at Thr^{159}/Ser^{160} had an obvious effect on the allosteric inhibition of IMPDH1 by GDP/GTP *in vitro* (**Fig 34A**). As Thr^{159} phosphomimetic mutants affected both GDP and GTP inhibition we then assayed the catalytic activity of the T159E/D at different concentrations of GDP (**Fig 34B**) and GTP (**Fig 34C**). $K_{1/2}$ values for enzyme inhibition were around 5-fold higher in T159D than for the wild-type (**Table 6**).

Enzyme kinetics data were fitted by non-linear regression to the Michaelis-Menten equation to derive V_{max} and K_M values. The V_{max} values *versus* GTP/GDP concentration were then adjusted to a sigmoidal dose-response function using the GraphPad software package.

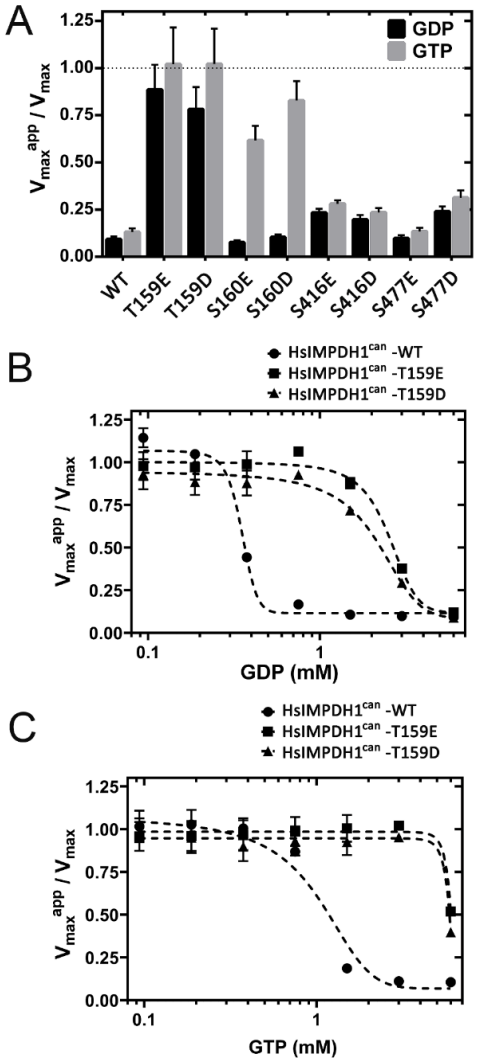

Figure 34. **Effect of phosphomimetic mutations on GDP and GTP allosteric regulation of IMPDH1 activity**. **A.** V_{max}^{app}/V_{max} for the indicated phosphomimetics mutants. **B.** V_{max}^{app}/V_{max} for the T159E and T159D mutants, as a function of GDP concentration. **C.** V_{max}^{app}/V_{max} for the T159E and T159D mutants, as a function of GTP concentration. Results shown are representative of two independent experiments.

Table 6: K1/2 values (mM) for GDP and GTP

	GDP	**GTP**
HsIMPDH1 β (514aa)-WT	0.45 ± 0.03	0.97 ± 0.1
HsIMPDH1 β (514aa)-T159D	2.19 ± 0.2	≈ 6

$K_{1/2}$ values are given in mM units (Mean ± SD), and are representative of two independent experiments.

Taken together our results show that phosphorylation at Thr^{159}/Ser^{160} desensitizes the enzyme to the allosteric inhibition exerted by GTP and GDP. Given the light-dependence of this phosphorylation event, these results predict an activation of IMPDH1 activity upon light exposure *in vivo*.

3.3.7 Photoreceptor cells present roughly equimolar levels of GTP and ATP in the dark and light steady-states

The structural studies that uncovered the allosteric regulation of eukaryotic IMPDHs by purines established that ATP/ADP and GTP/GDP compete for the nucleotide-binding sites at the Bateman domain. ATP/ADP and GTP/GDP have opposite effects on catalytic activity. ATP/ADP binding leads to the formation of extended octamers with full enzymatic activity, while GTP/GDP binding induces the formation of compacted octamers with compromised enzymatic activity (Buey et al. 2015).

In most cell types the ratio of ATP:GTP is between 3:1 to 5:1 (Traut 1994), and even under these conditions it has been proposed that IMPDHs could be partially inhibited by GDP/GTP in their quiescent state (Johnson and Kollman 2020). Photoreceptor cells present GDP and GTP levels that are much higher than normal. Numerous studies since the 70s have shown that the GTP pool equals the ATP pool in whole retinas (Biernbaum and Bownds 1979; Berger et al. 1980) and in bovine rod outer segment preparations (Ostroy, Svoboda, and Wilson 1990).

If the ratio of ATP:GTP was 1:1 in photoreceptor cells, it would favor the GDP/GTP allosteric inhibition of IMPDH1, because GDP/GTP would effectively compete with ADP/ATP at nucleotide binding sites 1, 2 and 3 at the Bateman domain. We therefore assessed the GTP and ATP nucleotide levels in whole retinas, both in the dark- and bright light steady-states (**Fig 35**). We also determined GMP and AMP levels. Nucleotide levels were determined by high pressure liquid chromatography (HPLC) as well as by mass spectrometry, given that each analytical method presents unique advantages and limitations.

First, we determined the nucleotide levels by HPLC from *in situ* murine retinas obtained from dark-adapted mice, that were either kept in darkness for 5 min or exposed to bright light (2000 lux light) for 5 min. Whole retinas were used to obtain nucleotide extracts. It must be noted that although our nucleotide determinations are done in whole retinas, guanine nucleotide levels largely reflect nucleotide content in photoreceptor cells, given that photoreceptor cells account for 70% of the retinal cells (Curcio et al. 1990) and that it has been demonstrated that cGMP and GTP levels are reduced to less than 20% their values in retinas that lack the photoreceptor cell layer (*rd1* mouse model (Du et al. 2016)).

Our results show that ATP and GTP levels are at about a 1:1 molar ratio both in darkness and under light conditions, **Fig 35** and (**Table 7**) as previously established.

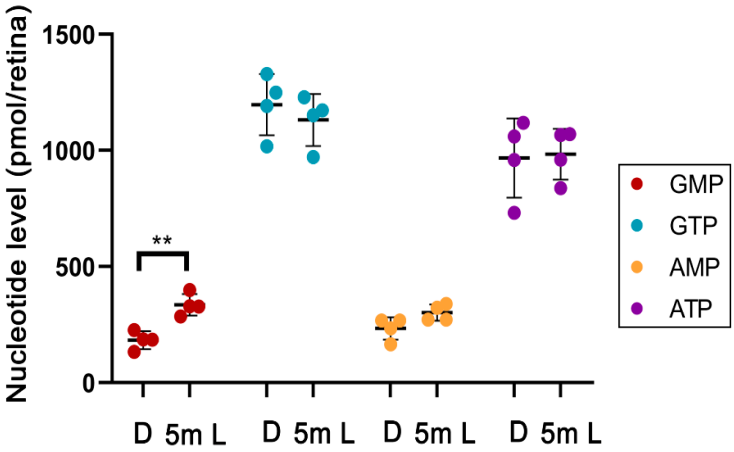

Figure 35: Nucleotide levels assessed by HPLC from *in situ* murine retinas in the dark-steady state and after 5 min of bright light exposure (2000 lux). A. GMP, AMP, GTP and ATP nucleotide levels (pmol/retina) determined by ion-pairing high performance liquid chromatography in dark- and 5 min light-exposed murine retinas. Values represent the Mean ± SEM of at least 4 biological replicates. Unpaired t-test for dark versus 5 min light: GMP (P=0.0014**), GTP (P=0.4747), AMP (P=0.075) and ATP (P=0.8768).

Table 7: Levels of purine nucleotides in the retina

NUCLEOTIDE	DARK (pmol nt/retina)	5m LIGHT (pmol nt/retina)
GMP	183.10 ± 19.3	335.75 ± 23.4
GTP	1197.48 ± 66.1	1131.49 ± 55.9
AMP	233.88 ± 24.2	301.64 ± 17.4
ATP	967.58 ± 85.3	983.97 ± 54.7
Ratio GTP/ATP	**1.24**	**1.15**

One major advantage of the HPLC method is that it allows a direct comparison of the relative levels of the mono-, di- and tri-phosphate nucleotides. Identification of each peak is based on its retention time and spectral sensitivity, by comparison with individual nucleotide standards. Nucleotide concentrations in the extract are inferred from integration of the peaks after using individual concentration standards, but a glimpse at the chromatogram already conveys the relative levels of the different nucleotides (see **Fig 36** for a representative chromatogram of the dark-adapted state).

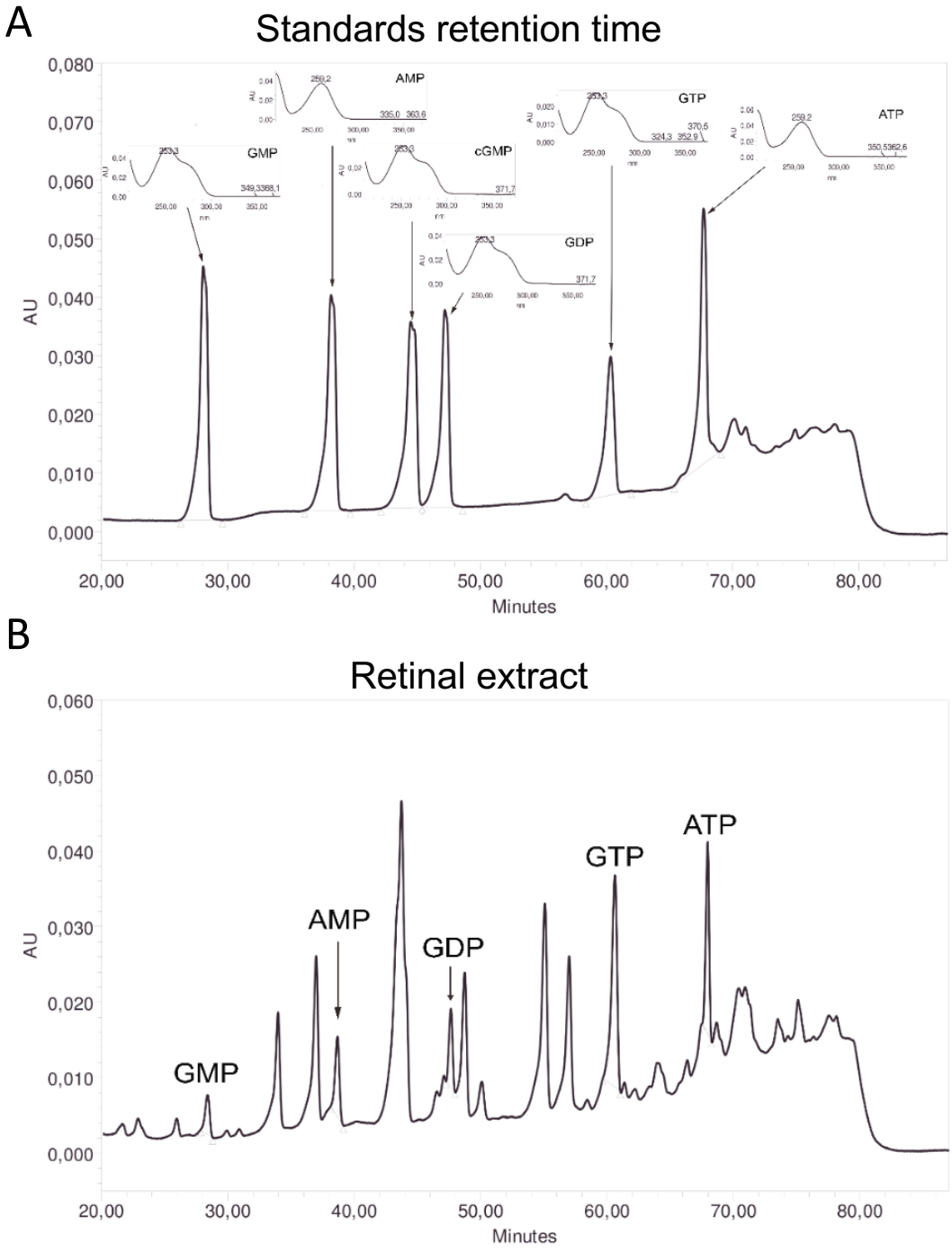

Figure 36. Representative HPLC chromatogram from a retinal extract showing the separation of GMP, AMP, GDP, GTP and ATP. A. Chromatogram of a mix of nucleotide standards, showing each nucleotide retention time and typical spectral sensitivity. **B**. Representative chromatogram of a retinal extract from a dark-adapted retina showing the retention time and relative abundances of the different nucleotides. GTP levels are > 6-fold higher than GMP levels in the dark-adapted retina. GTP and ATP present very similar levels in the retina. cGMP levels are under detection level.

One limitation of the HPLC analytical method, though, is that the IMP levels could not be determined. IMP was masked by the GMP peak under the HPLC gradient required to unequivocally separate GTP from ATP ((Di Pierro et al. 1995) see methods).

Mass spectrometry on the other side allows the unequivocal assignment of nucleotide identity to each peak, but nucleotide relative levels cannot be inferred unless specific mass standards are run for each nucleotide of interest, which is expensive. We have also determined the nucleotide levels by mass spectrometry (See **Fig 41**, in section below).

From our nucleotide determinations by HPLC we conclude that ATP:GTP are at a 1:1 molar ratio in darkness, and that neither their absolute levels nor their relative levels change with light.

3.3.8 Prolonged bright light exposure of living mice causes the accumulation of IMPDH1 aggregates at the rod outer segment layer of the retina

It has been reported that mammalian IMPDHs can form mesoscale macromolecular assemblies in mammalian cells, denoted as cytoophidia, when an increase in IMPDH activity is required to keep with GTP demand (Aughey and Liu 2016; Keppeke et al. 2018; Y. S. Ji et al. 2006; Chang et al. 2015). Recently it has been proposed that IMPDH1 cytoophidia are more resistant to GTP/GDP-mediated allosteric inhibition, which indicates that they would allow a boost of GTP synthesis when required (Fernández-Justel et al. 2019; Keppeke et al. 2018).

Because the light-dependent phosphorylation of IMPDH1 pointed to enzyme activation in light, we reasoned that an increase in the *de novo* synthesis of GTP might be required to sustain the light response particularly under prolonged **bright light exposures**. We hypothesized that IMPDH1 could form aggregates –cytoophidia-like- under these conditions, to keep with GTP demand.

IMPDH1 cytoophidia are not observed in the retina in mice reared **in standard 12h dark/12h light cycles**, although they can be induced and clearly detected if retinas are treated with mycophenolic acid (MPA) (**Fig 37A**) as previously reported in cells (Y. Ji et al. 2006)

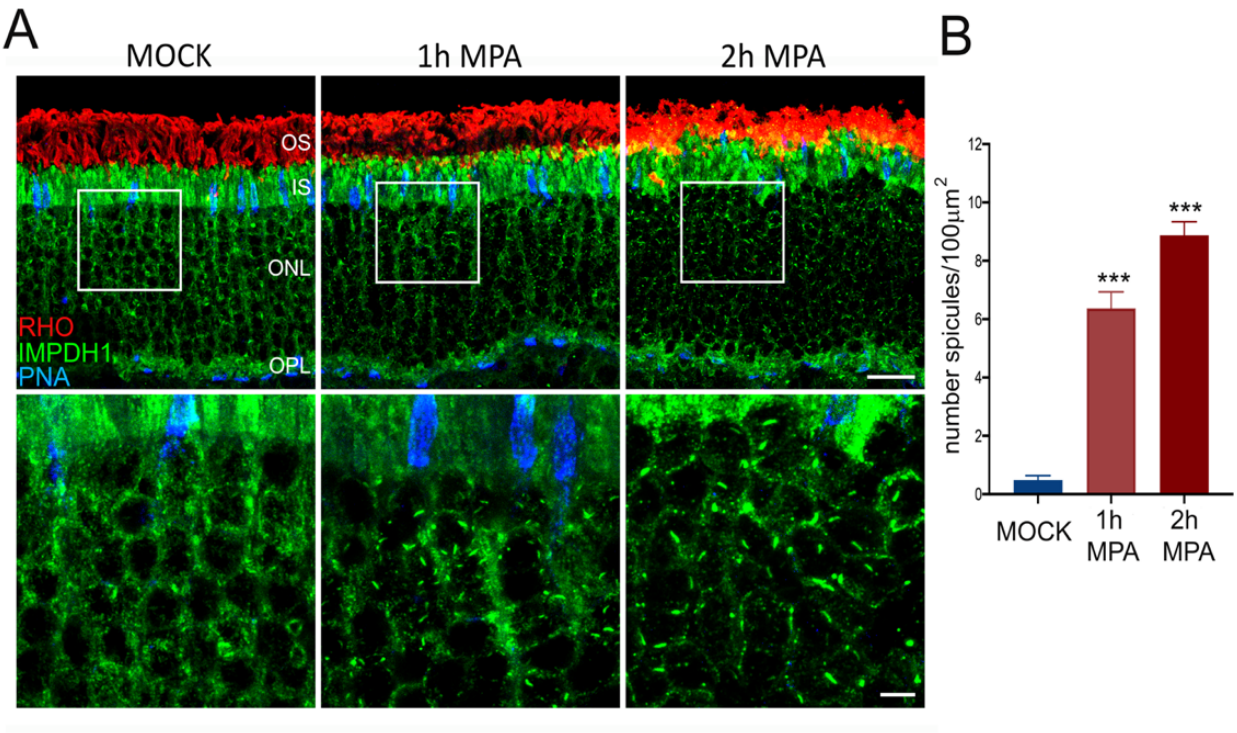

Figure 37. Formation of IMPDH1 spicules in intact retinas in response to mycophenolic acid-treatment. **A.** Murine retinal sections from dark-adapted mock- or 10 µM MPA-treated retinas for 1 or 2 hrs. MPA inhibition of IMPDH1 resulted in the formation and accumulation of IMPDH1 spicules with time, particularly noticeable at the perinuclear region of photoreceptor cells at the ONL. Spicules are clearly appreciated at bottom panels (8.5x zoom images). IMPDH1 shown in green; PNA staining of cones in cyan and rhodopsin in red. Confocal images are the average z-projections of three optical slices acquired with a step size of 0.13 µm. **B.** Histogram showing the number of spicules/100 µm². Unpaired t-test for mock vs 1h MPA, P=0.0001***; and mock vs 2h MPA P<0.0001***, with at least 6 planes from 2 animals analyzed per condition. OS: outer segment, IS: inner segment, ONL: outer nuclear layer, OPL: outer plexiform layer. Scale bar upper panels (20 µm) and bottom panels (5 µm).

In dark and cyclic light conditions IMPDH1 signal is particularly intense at the inner segment, outer nuclear and outer plexiform layers, and stronger in rods than cones (**Fig 37A mock** panel and **Fig 38A dark** panel), and no spicula or cytoophidia are particularly noticeable. Strikingly, exposure of living mice to **2000 lux bright light** after pupil dilation led to the gradual accumulation of IMPDH1 aggregates at the rod outer segment (ROS) layer, that increased in number and size with time (**Fig 38A** and **C**). IMPDH1 accumulation was even more evident when mice were reared for 15 days under constant light (2000 lux) (**Fig 38B** and **D**).

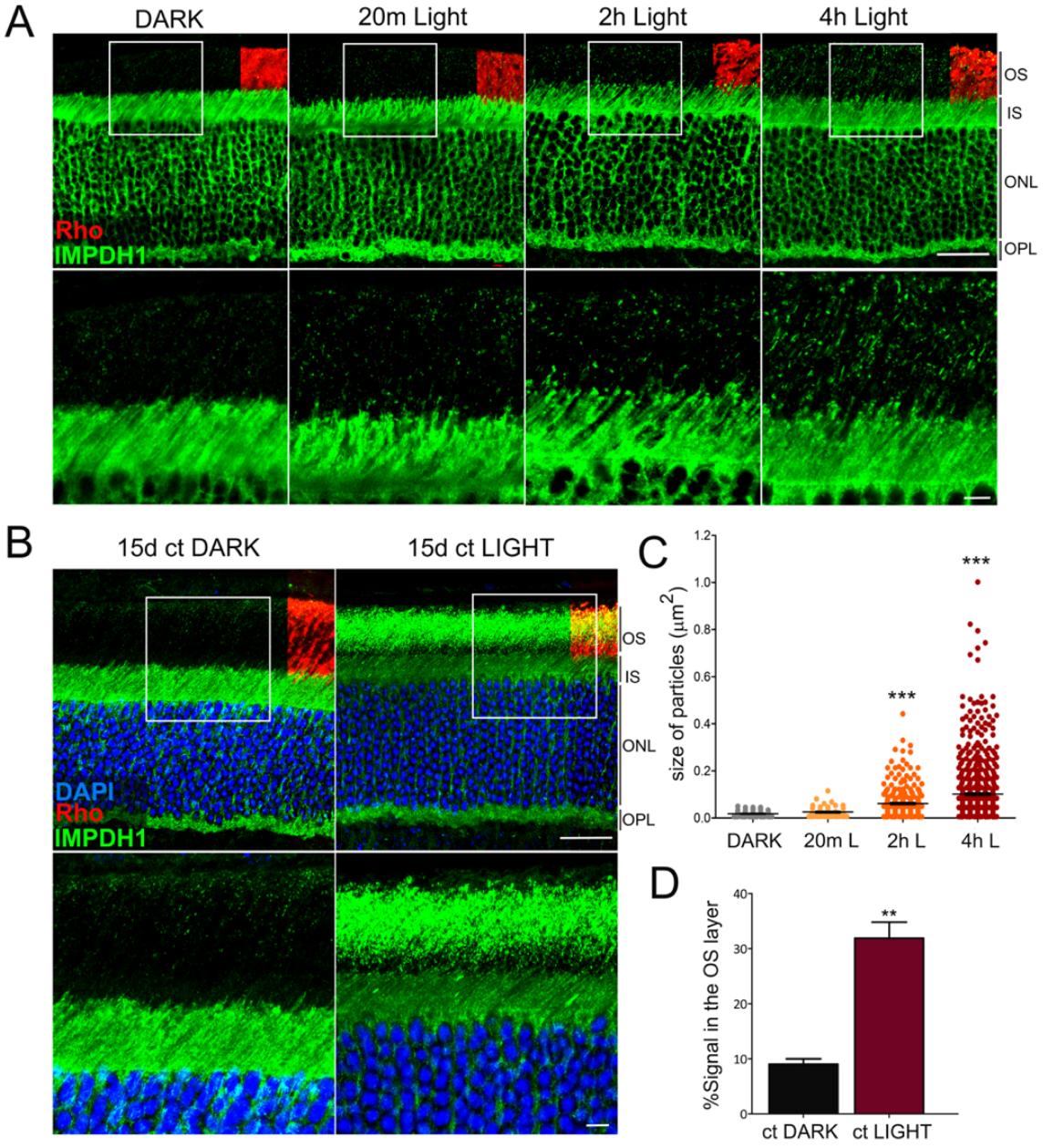

Figure 38. Accumulation of IMPDH1 aggregates at the outer segment layer in living mice exposed to constant bright light. **A**. Murine retinal sections from dark-adapted mice or mice exposed to 2000lux-light for 20 min, 2 hrs or 4 hrs were immunostained for IMPDH1 (green) and co-immunostained for rhodopsin (red). Confocal images are average z-projections of 5 optical slices with 0.13 µm-step size. Magnified frames from the outer segment layer show gradual accumulation of IMPDH1 aggregates with time of bright light exposure. Scale bar: 20 µm upper panels; 5 µm bottom panels. **B**. Retinal sections from constant dark or 2000 lux constant light-reared mice for 15 days, immunostained for IMPDH1 (green) and rhodopsin (red). Magnified inner/outer segment layers show a prominent accumulation of IMPDH1 signal at the outer segment layer, representing 30% of the total IMPDH1 signal in the retina. A basal IMPDH1 signal is already detected at the outer segment layer in dark-adapted mice. Scale bar: 20 µm upper panels; 5 µm bottom panels. **C.** Size and number of IMPDH1 aggregates with time. Unpaired t-test for dark vs 2 hrs light, P<0.0001***; and dark versus 4 hrs light, P<0.0001***, with at least 6 planes from 2 animals analyzed per condition **D.** Quantification of IMPDH1 signal at the outer segment layer, expressed as a fraction of total IMPDH1 in the retina. Unpaired t-test dark versus light, P=0.0017**, three independent experiments.

This light-dependent accumulation of IMPDH1 aggregates at the outer segment layer (evident at 72 hours of bright light exposure) could be reverted by a subsequent dark-adaptation of 16 hours (**Fig 39A**). The levels of expression of IMPDH1 did not change in this process, indicating that the protein that accumulated at ROS was translocated from the inner compartments but did not result from transcriptional upregulation (**Fig 39B- C**).

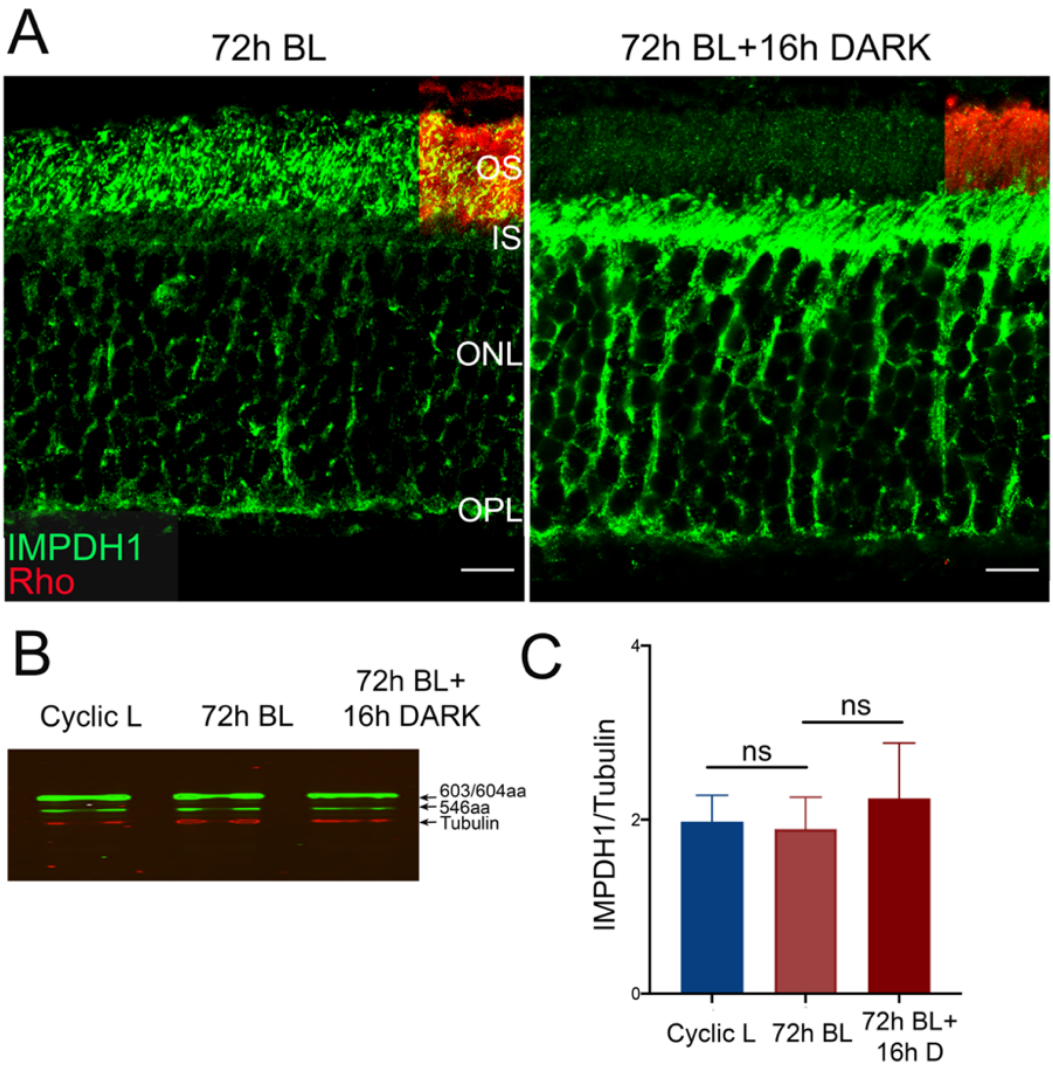

Figure 39. The light-dependent IMPDH1 accumulation and aggregation at ROS is reversible by subsequent dark-adaptation. A. IMPDH1 aggregate formation at the outer segment layer by 72 hrs of bright light exposure could be reverted by subsequent dark-adaptation (16 hrs). Shown is a representative result observed in three independent groups of mice. Scale bar 20 μm. **B.** The levels of murine IMPDH1 (603/604 aa and 546 aa) were not altered during bright light exposure/ subsequent dark-adaptation. Cyclic light (12 hrs dark/12 hrs light standard cycles), 72h BL (72 hrs of exposure to 2000 lux bright light) and 72h BL+16h dark (72 hrs of exposure to 2000 lux bright light followed by dark-adaptation for 16 hrs). **C.** IMPDH1 normalized to the loading control did not show noticeable changes in protein expression. Quantification from three independent experiments.

Taken together our results show that IMPDH1 assembles into aggregates at the outer segment layer of the retina (where phototransduction takes place) during bright light exposure, accumulating over time. These aggregates are reverted in subsequent dark-adaptation periods. Therefore we reasoned that the activity of this enzyme appears to be required to sustain the light response in these conditions.

3.3.9 Constant bright light exposure substantially increases the flux towards *de novo* GTP and ATP synthesis

As already mentioned, the picture from structural studies is emerging that the cellular aggregates from IMPDH proteins are bundles of filaments that serve to increase GTP synthesis under conditions of increased GTP demand.

In order to assess whether the bright light conditions that induced IMPDH1 aggregation at the outer segment layer correlated with an increase in IMPDH1 activity, we determined nucleotide levels both by HPLC (**Fig 40**) and by mass spectrometry in living mice after 4 hrs of bright light exposure (**Fig 41**).

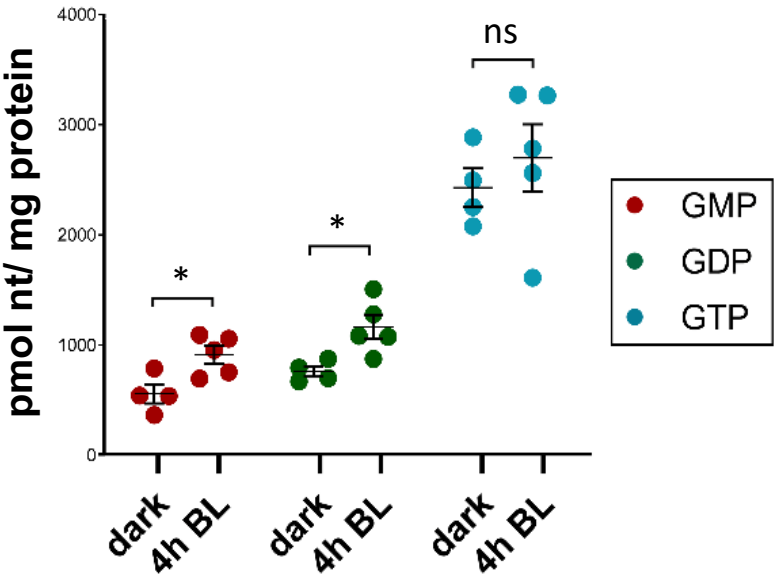

Figure 40: Nucleotide levels in whole murine retinas from dark-adapted mice, or mice that were exposed to bright light for 4h. Retinal GMP, GDP and GTP levels were determined by HPLC. Values represent the Mean ± SEM of at least 4 biological replicates. Unpaired t-test for dark versus 4h bright light: GMP (P=0.0205*), GDP (P=0.0161*) and GTP (P=0.8023, ns).

Similarly to our *in situ* experiment (**Fig 35**), the HPLC analysis showed that GMP and GDP showed a tendency to increase with light, while GTP levels were maintained.

We then repeated the exposure on living mice to bright light under the same conditions and determined the nucleotides by mass spectrometry. LC-MS/MS allowed us to determine the levels of IMP in dark and light conditions for the first time, revealing a substantial increase in IMP levels in the bright light condition (**Fig 41**). Interestingly the mass spectrometry analysis detected the decrease in cGMP that follows any adaptation to a light steady-state (Barbehenn et al. 1986), as well as an increase in the GMP and AMP levels.

These data pointed to an increase in the flux towards *de novo* ATP and GTP synthesis upon light exposure.

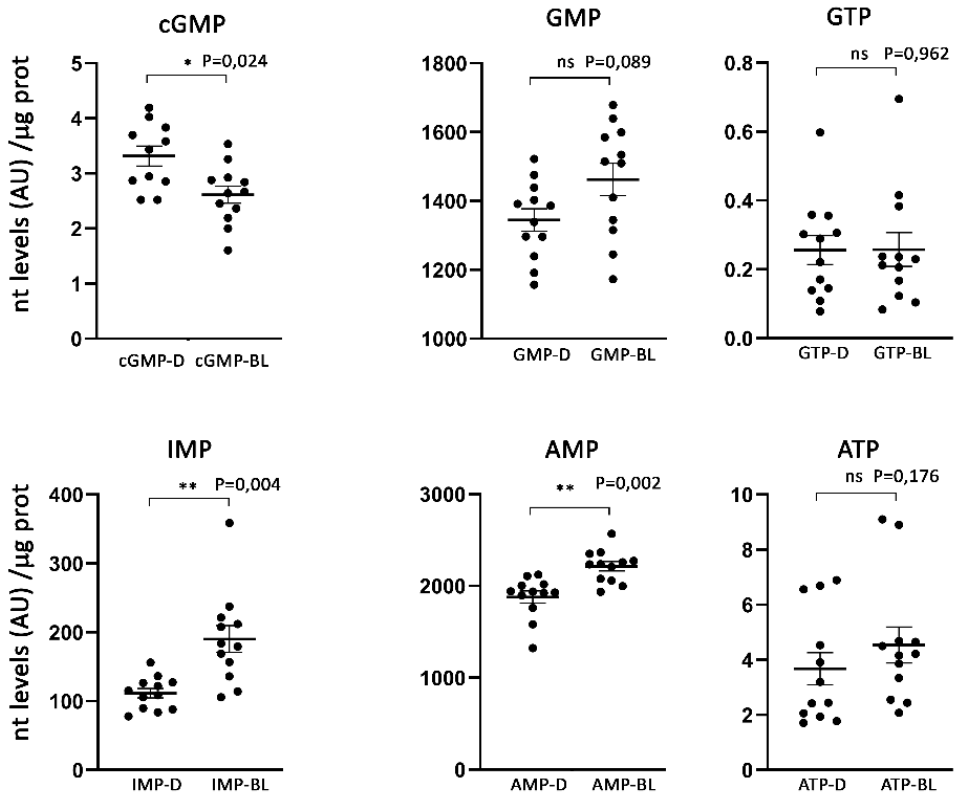

Fig 41. Mass spectrometry (MS) determination of nucleotide levels in murine retinas from dark-adapted mice or mice that were exposed to bright light for 4h. Retinal cGMP, GMP, GTP, IMP, AMP and ATP levels are expressed in arbitrary units (peak integration at MS), normalized per µg of protein. Note that a direct comparison between dark and light levels is established for each nucleotide, but that no direct comparison can be established between different nucleotides. Points represent individual retinas, n=12. Unpaired t-test of dark versus 4 hrs bright light: cGMP (p=0.024*), GMP (p=0.089), GTP (p=0.962), IMP (p=0.004**), AMP (p=0.002**) and ATP (p=0.176). D: dark; BL: bright light.

To test whether the *de novo* biosynthesis of purines was enhanced upon continuous light exposure, we performed an *in vivo* fluxomic analysis by performing the same experiment following intravitreal injection of an stable-isotope of glycine (a precursor in *de novo* biosynthesis of IMP). 1 µl of 20 mM [13C2,15N]-Glycine was intravitreally injected to living mice immediately preceding the 4 hrs bright

light exposure (or 4 hrs maintenance in the dark). Because the vitreous volume is 5 µl, the effective concentration of Gly* in contact with the retina was 4 mM. Following 4 hrs of dark or bright light exposure, retinas were dissected and immediately frozen for mass spectrometry analysis. The levels of labeled Gly*, IMP*, AMP* and GMP* were then determined by MS, and expressed as a function of unlabeled nucleotides. The percentage of IMP*, GMP* and AMP* were then normalized by the percentage of Gly* (**Fig 42**).

Our results showed that IMP, GMP and AMP were labeled to a substantially higher extent in the bright light condition that under dark-adaptation, which revealed that the flux to *de novo* ATP and GTP synthesis increased under light conditions (**Fig 42**).

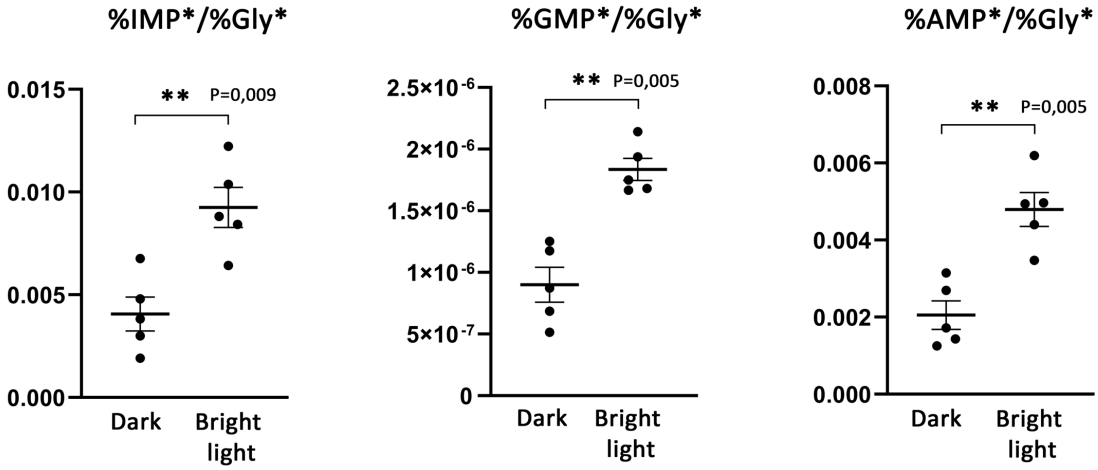

Fig 42. Incorporation of [13C2,15N]-Glycine into purine nucleotides by *de novo* biosynthesis in the retinas of mice in a period of 4 hrs in darkness (dark) or under 2000 lux light exposure (bright light). The levels of labelled glycine, IMP, AMP and GMP were assessed and expressed as a function of total nucleotide. Incorporation of [13C2,15N]-Glycine into IMP, AMP and GMP was compared in dark and light conditions by normalizing the percentage of labeled nucleotide to the percentage of Gly*. Unpaired t-test of dark versus 4 hrs bright light: IMP (P=0.009**), GMP (P=0.0051**) and AMP (P=0.0053**).

Taken together our results show that the flux to *de novo* synthesis of purine nucleotides increases in response to light. **Therefore the role of IMPDH1 phosphorylation at the Bateman domain could be to promote and stabilize a conformation of the protein that is permissive to this increase in flux from IMP to GMP, GDP and GTP.** Furthermore, its desensitization to GDP/GTP and concurrent increase in IMP levels would promote the formation of filaments (based on recent structural findings *in vitro*, (Johnson and Kollman 2020), that would further desensitize the enzyme to GDP/GTP inhibition. Thus, the ultimate role of GDP/GTP feedback inhibition and its release in light would be to adjust the enzyme conformation and activity to the overall flux of *de novo* purine

nucleotide biosynthesis in dark/light conditions. It follows that light conditions must require higher levels of ATP and GTP.

To test whether *de novo* GTP synthesis is required to sustain the light response kinetics under physiological light conditions, we recorded dark-adapted responses by electroretinogram (ERG).

3.3.10 Inhibition of IMPDH catalytic activity delays mass rod recovery in electroretinogram responses.

Two processes that increase GTP consumption upon light exposure would be GTP hydrolysis by the GTPase transducin at the activation step, and GTP conversion to cGMP synthesis during recovery of the light response by RetGC (A Mendez et al. 2001; Burns et al. 2002b).

To assess if IMPDH1 catalytic activity is required to sustain the light response (transducin activation) or rod mass response recovery (cGMP production by RetGC), we recorded electroretinogram (ERG) responses simultaneously from both eyes of mice that were injected intravitreally with an IMPDH1 inhibitor mycophenolate mofetil (MMF) or benzamide ribose (BZM) in their right eye; or control physiological saline buffer in their left eye.

The result of transiently inhibiting IMPDH1 on the rate of mass rod recovery after a saturating flash was tested using a paired-flash ERG paradigm (Lyubarsky and Pugh 1996) (**Fig 43A-B**). Briefly, a test flash was triggered [3 Cd·s/m^2], and an identical probe flash [3 Cd·s/m^2] was activated at different interstimulus times (IST) 400, 600, 800, 1200, 1500 or 2000 msec. An effect on transducin activation would result on a-wave diminution after the test flash, whereas an effect on RetGC activity would result on a-wave diminution after the probe flash.

IMPDH1 inhibitors did not significantly affect the amplitude of the a-wave or b-wave of the test flash [3 Cd·s/m^2] (**Fig 43E**), indicating no major effect on transducin activation. However, a slightly effect on the recovery rate was detected in both BZM and MMF injected eyes (**Fig 43A-B**).

The percentage of recovery of a- and b-wave amplitudes was plotted to interstimulus time (IST), (**Fig 43C-D**). Both BZM and MMF had a modest but statistically significant effect at delaying mass rod response recovery.

No alterations were observed in pure cone responses (**Fig 43F**), and both drugs caused the characteristic SDS-PAGE mobility shift of the enzyme caused by drug binding (Y. Ji et al. 2006), when retinas were obtained 20 min after intravitreal injection (**Fig 43G**), which demonstrates direct binding of the drugs to its target.

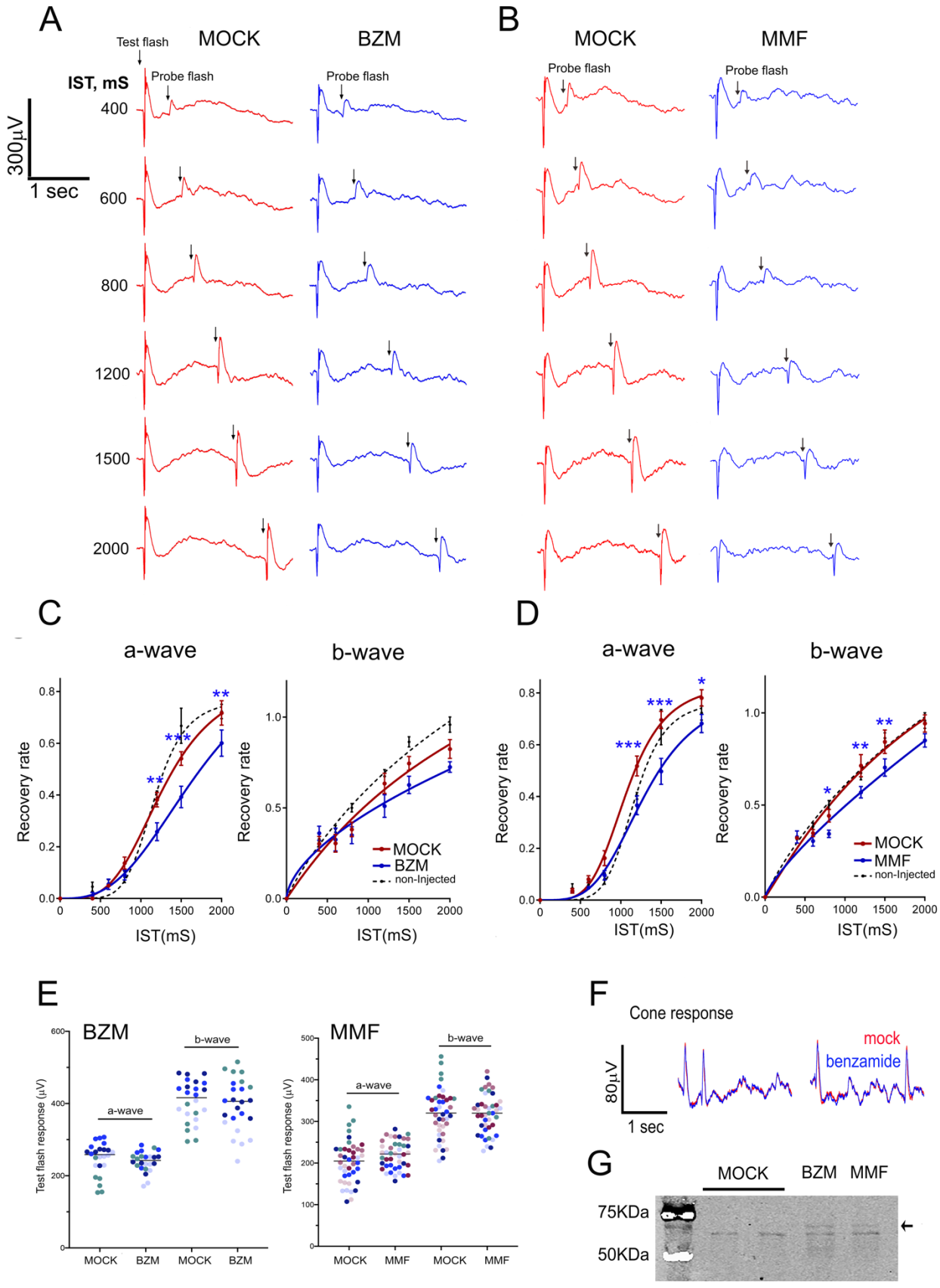

Figure 43. Effect of IMPDH inhibition on mass rod response recovery. (see figure legend in next page)

Figure 43. Effect of IMPDH inhibition on mass rod response recovery. A. Simultaneous electroretinogram (ERG) recordings from both eyes of a mouse injected with benzamide or drug dilution buffer (mock), in response to a probe flash triggered at increasing interstimulus times (IST) after a test flash. **B.** Representative raw traces from simultaneous electroretinogram (ERG) recordings from both eyes of a mouse injected with MMF or drug dilution buffer (mock), in response to a probe flash triggered at increasing interstimulus times (IST) after a test flash. **C.** Statistical analysis of mass rod response recovery (recovery rate plotted to interstimulus time, ERG paired flash paradigm) in BZM-injected eyes versus corresponding control eyes. Overimposed black dashed lines are the curves obtained for control non-injected mice. Two-way ANOVA (mock vs benzamide injections and IST as factors) with uncorrected Fisher´s test for multiple comparisons, a-wave benzamide vs mock [1200 msec (P=0.0027**); 1500 msec (P=0.0004***); 2000 msec (P=0.0046**), 4 mice analyzed]. **D.** Statistical analysis of mass rod response recovery in mycophenolate mofetyl MMF-injected eyes versus corresponding control eyes. Two-way ANOVA with uncorrected fisher's test for multiple comparisons, a-wave MMF vs mock [1200 msec (P=0.0002***); 1500 msec (P<0.0001***); 2000 msec (P=0.0132*), 7 mice analyzed]. **E.** Left panel: Statistical comparison of a- and b-wave amplitudes of the test flash in the mock-injected left eye versus the benzamide (BZM)-injected right eye in four mice. Each mouse is shown in a different color. Mean (+SD) for a-wave and b-wave of the test flash were: a-wave [MOCK: 246.8±44.5 and BZM: 239.1±28.2]; and b-wave [MOCK: 405.0+58.5 and BZM: 395.0±73.1]. Right panel: Statistical comparison of a- and b-wave amplitudes of the test flash in the mock-injected left eye versus the mycophenolate mofetyl (MMF)-injected right eye in seven mice. Each mouse represented in a different color. Mean (+SD) for a-wave and b-wave of the test flash were: a-wave [MOCK: 203.0±51.1 and MMF: 218.8±33.4]; and b-wave [MOCK: 318.3+58.9 and MMF: 318.2±47.3].**F.** Superimposed pure-cone responses of the mouse in panel A. No effects on cone response were detected. **G.** IMPDH1 mobility by SDS-PAGE is shifted by both benzamide and MMF in retinal extracts from intravitreally injected eyes.

Taken together our results suggest that IMPDH1 activity contributes to mass rod recovery by sustaining the GTP pool upon light exposure.

3.3.11 T159 and S160 sites are phosphorylated by PKC *in vitro*

In order to identify the kinase/s responsible for the phosphorylation of the described residues of IMPDH1, the human IMPDH1α (546 aa) isoform, and mutant forms with all of these 4 residues mutated to Gly (4KO, i.e. quadruple mutant T159**G**/S160**G**/S416**G**/S477**G**) or with individual phosphorylation sites restored in the 4KO (for instance, T159-only; T159**T**/S160**G**/S416**G**/S477**G**) were purified to perform *in vitro* phosphorylation assays with the kinases PKA, PKCα, CaMKII, CK II, PKB-Akt and AMPK.

PKCα phosphorylated the wild-type but not the 4KO enzyme, and phosphorylation was only restored in the mutants T159-only and S160-only, showing PKCα specificity for the Thr^{159} and Ser^{160} residues (**Fig 44A**). Other kinases fail to selectively phosphorylate any of the "-only" mutants (data not shown).

Given the proximity of Thr^{159} and Ser^{160} to residues that are most prevalently mutated in adRP10 and rare LCA at the Bateman domain, we analyzed whether Thr^{159}/Ser^{160} phosphorylation was affected in blindness associated mutations. For this, we purified the recombinant human IMPDH1α (546 aa) isoform carrying individual mutations associated to RP10 (R224P, D226N, V268I and H372P) or

LCA (R105W, N198K), and used them as substrates for phosphorylation reactions with PKCα *in vitro* (**Fig 44B**). Following a ^{32}P-densitometry analysis, our data showed that the mutations N198K and R224P significantly reduced phosphorylation of IMPDH1 by PKCα, whereas H372P increased the phosphorylation level (**Fig 44C**). Out of the few adRP10 mutations that do not affect GDP/GTP binding directly (Fernández-Justel et al. 2019), H372P enhances PKC phosphorylation, which means it would cause GDP/GTP desensitization also.

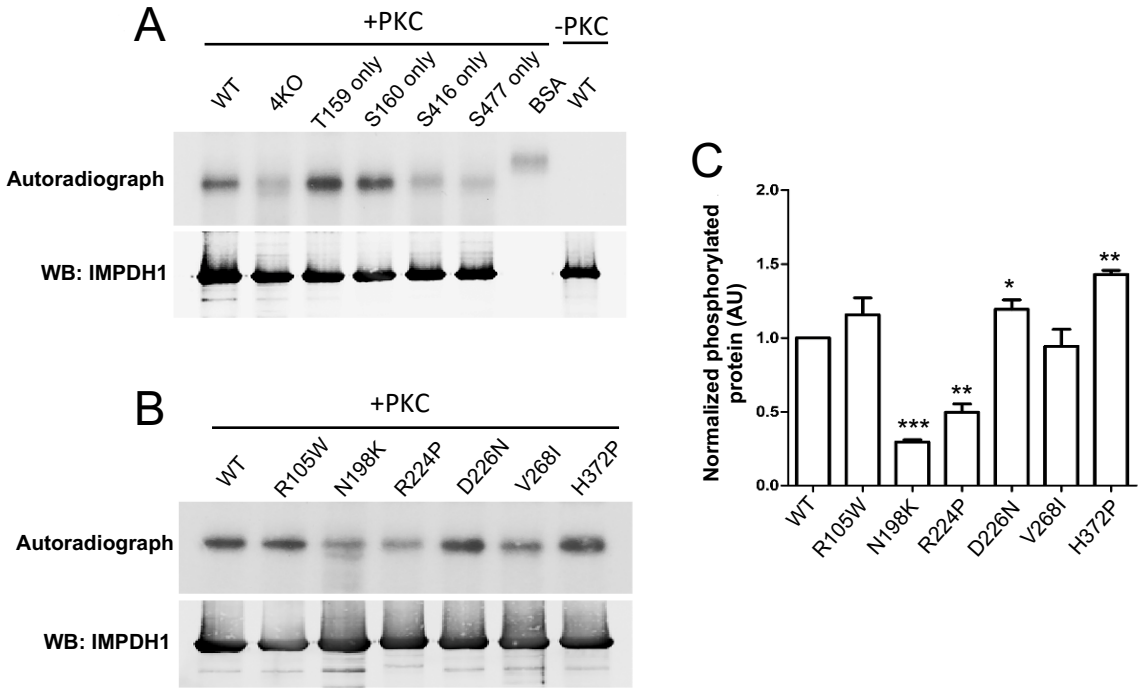

Figure 44. **PKC phosphorylates Thr^{159} and Ser^{160} of hIMPDH1 in *in vitro* phosphorylation assays. A.** *In vitro* phosphorylation assays with PKCα kinase of hIMPDH1α (546aa) ; T159G/S160G/ S416G/S477G-hIMPDH1α (546 aa) (4KO); and forms of the protein with phosphorylation sites individually restored. 5 μg of each mutant were incubated with 4 μg/ml recombinant hPKCα with 1 μl of ^{32}P-γ-ATP (3000 Ci/mmol), for 30 min at 30ºC. Samples were resolved by SDS-PAGE, exposed to an X-ray film (autoradiograph), and immunoblotted for IMPDH1. PKC phosphorylated hIMPDH1α (546 aa) selectively at Thr^{159} and Ser^{160}. Results shown are representative of two independent experiments. BSA (bovine serum albumin) was used as a negative control. **B.** *In vitro* PKC phosphorylation assay of hIMPDH1α (546 aa) disease mutants R105W; N198K; R224P; D226N; V268I and H372P. **C.** Average intensity of autoradiograph signal normalized by the immunoblot signal for blindness-associated mutations, expressed as a function of the wildtype levels. N198K and R224P mutations resulted in a decrease of phosphorylation [P=0.0001*** and P=0.004** versus the wildtype, n=3 independent experiments]; while H372P led to an statistically significant increase in phosphorylation [P=0.0013**, n=3 independent experiments].

Therefore our results showed that sites Thr[159]/Ser[160] at IMPDH1 are PKC substrates *in vitro*.

To test whether PKC is the kinase responsible of IMPDH1 phosphorylation *in vivo*, we treated *in situ* retinas with Bisindolylmaleimide I (BM), a selective PKC inhibitor, immediately before dark- or light-adaptation. We reasoned that if PKC was the enzyme responsible for the light-dependent phosphorylation required to boost GTP synthesis during light exposure, then in the presence of the drug the GTP levels should drop substantially in the light condition.

This is what we observed (**Fig 45A**). Retinas from dark-adapted mice were dissected in DMEM medium supplemented with glycine and serine in the dark. BM was then added to a final concentration of 50 nM to the "inhibitor-treated samples" and DMSO to the mock samples, and retinas were incubated at 37°C in a 5% CO_2 incubator for 20 min in the dark. Retinas were then kept in the dark or exposed to 2000 lux light for 5 min, and immediately processed for nucleotide determination by HPLC (see methods). Whereas the GTP levels were maintained at their dark values in the mock retinas after light exposure; the addition of BM caused a substantial drop in the GTP at the light condition (**Fig 45A**). Dark retinas treated with BM showed a slight but not significant decrease in the GTP levels also (**Fig 45A**).

The effect of BM on the light response was tested *in vivo* as described above (**Fig 43**). Mice were injected intravitreally with an effective concentration of 200 nM of BM in their right eyes; or control physiological saline buffer in their left eyes. After 30 min of drug injection ERG responses were recorded using the paired-flash paradigm described above. The percentage of recovery of a- and b-wave amplitudes was plotted to interstimulus time (IST), (**Fig 45B**). BM had a modest but statistically significant effect at delaying mass rod response recovery.

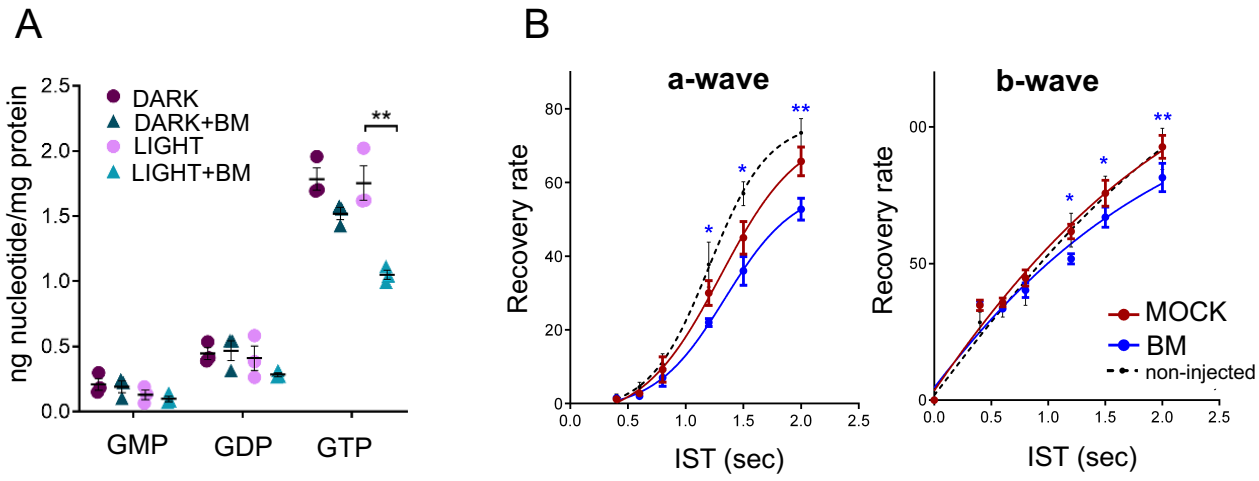

Figure 45. ***In vivo* effect of PKC inhibition on nucleotide levels and light response.** (see figure legend in next page)

Figure 45. ***In vivo*** **effect of PKC inhibition on nucleotide levels and light response. A.** Guanine nucleotide levels (GMP, GDP and GTP) in dark-adapted or light exposed retinas in either the presence or absence of a selective PKC inhibitor, Bisindolylmalemide I (BM). Each point represent the nucleotide pool obtained from three retinas. Unpaired t-test for GTP levels [light versus light+BM, p=0.0071**] and [dark versus dark+BM, p=0.0546, ns]. **B.** Statistical analysis of mass rod response recovery (recovery rate plotted to interstimulus time, ERG paired flash paradigm) in BM-injected eyes versus corresponding control eyes. Overimposed black dashed lines are the curves obtained for control non-injected mice. Two-way ANOVA (mock vs BM injections and IST as factors) with uncorrected Fisher´s test for multiple comparisons, a-wave BM vs mock [1.2 sec (P=0.0468*); 1.5 sec (P=0.0263*); 2 sec (P=0.0019**), 4 mice analyzed].

Taken together our results point to a light-dependent phosphorylation of IMPDH1 at the Bateman domain taking place in response to a light-triggered signaling pathway that involves PKC activation.

3.3.12 Discussion

In this study we report that retinal IMPDH1 is phosphorylated at up to three residues *in vivo*: Thr^{159}/Ser^{160} at the Bateman domain; Ser^{416} at the mobile flap in the catalytic domain; and Ser^{477} at the COOH-terminus. In the bovine system, in which calf eyes were dark-adapted *in situ* for 1 h and retinas were processed in darkness or after 5 min of bright light exposure, Thr^{159}/Ser^{160} was preferentially phosphorylated in response to light, Ser^{477} in the dark-adapted state, and Ser^{416} indistinctly at both conditions (**Fig 29A-B**).

Actually, isoelectrofocusing separation of retinal extracts from dark-adapted or light-adapted living mice revealed that > 60% of the protein is phosphorylated under physiological conditions; with the predominant monophosphorylated form corresponding to phosphorylated Thr^{159}/Ser^{160} in the light state and Ser^{477} in the dark state (based on the mass spectrometry data); and di-phosphorylated forms likely reflecting slow dephosphorylation kinetics of the reciprocal site.

The effect of these phosphorylation events on hIMPDH1 catalytic activity *in vitro* was determined in enzymatic assays with the corresponding phosphomimetic mutants. The S416D mutation significantly reduces retinal hIMPDH1 catalytic activity (**Fig 33C**). However, because Ser^{416} phosphorylation does not appear to be regulated by light, we speculate that this phosphorylation event may respond to metabolic stress or nutrient deficiency (manifested in the phosphoproteomic analysis due to the 1 h maintenance of the retinas in Locke´s -lacking Ser/Gly- during dark adaptation), to direct IMP towards ATP synthesis. In this respect, Ser^{416} maps at a region that resembles a consensus site for AMPK (Hardie 2011), although the AMPK (A2/B2/G1) recombinant human isoform did not recognize hIMPDH1-546aa as a substrate in *in vitro* phosphorylation assays in this study. We believe that Ser^{416} phosphorylation would have a limited contribution to regulation of the enzyme by light *in vivo* under physiological conditions.

S477D substitution did not have a direct effect on enzymatic activity neither on GTP allosteric regulation of the enzyme. Thereby, we speculate that Ser^{477} phosphorylation might be involved in other aspects of enzyme regulation *in vivo*: e.g. inducing filament disassembly. To this respect, a recently reported structure of IMPDH2 polymers has revealed details of the interface that mediates cytoophidia assembly: the 12 amino-terminal residues of the canonical IMPDH2 isoform extend from the catalytic domain to bind into the adjacent molecule, in a shallow surface groove formed by a short helix (aminoacids 476-485), two beta strands (51-63), and two short loops (355-360, 379-380) (Johnson and Kollman 2020). Strikingly, Ser^{477} maps into the short helix at the IMPDH2 cytoophidia longitudinal contact interface, allowing us to speculate that phosphorylation of Ser^{477} in IMPDH1 might disrupt cytoophidia assembly.

Additionally, Ser^{477} phosphorylation might also be implied in protein translocation from outer to proximal photoreceptor compartments during dark-adaptation after a period of bright light exposure, or regulating local IMPDH1 interactions with other proteins. Further experiments are needed to corroborate these hypotheses.

We here demonstrate that the T159D and S160D (or T159E and S160E) substitutions increased about 5-fold the $K_{1/2}$ for GDP/GTP inhibitory allosteric regulation of the enzyme *in vitro*, and propose that light-dependent phosphorylation of these residues *in vivo* would effectively desensitize the enzyme to GDP/GTP allosteric control and increase *de novo* GTP synthesis.

Light-dependent activation of IMPDH1 might seem at odds with the assumption in the field that GMP, generated from cGMP hydrolysis during light exposure, would act as a negative feedback regulator of purine nucleotide synthesis by inhibiting IMPDH1, 5-phosphoribosyl 1-pyrophosphate synthetase (PRS), and glutamine phosphoribosyl amidotransferase (GPA) (Du et al. 2016). However, by performing an *in vivo* metabolic flux analysis of purine nucleotide synthesis in dark/light conditions following an intravitreal injection of a stable isotope of Glycine, we found that the *de novo* synthesis of purine nucleotides was substantially increased with light, with IMP levels nearly doubling in light conditions (**Fig 41**). We found that IMP, GMP and AMP levels all increased with light; as did Gly* incorporation into these nucleotides (**Fig 41** and **Fig 42**). The overall *de novo* purine nucleotide synthesis increased in the retinas of living mice exposed to bright light.

Considering these results, we believe that most of the GMP increase observed upon light exposure by HPLC actually reflects the light-driven overall increase in *de novo* purine nucleotide synthesis, rather than the GMP coming from cGMP hydrolysis alone. It is likely that the fraction of GMP coming from the hydrolysis of cGMP would be under detection by HPLC, given that cGMP itself is under detection by HPLC in retinal extracts (**Fig 36**). cGMP levels in retinal extracts have been classically determined by radioimmunoassay (Debora B. Farber and Lolley 1974).

Eukaryotic IMPDH isoforms contain three allosteric nucleotide binding sites at the Bateman domain, numbered 1, 2 and 3, that can bind either adenine or guanine nucleotides. Nucleotide binding at these sites promote the dimerization of tetramers, forming reversible IMPDH octamers. Depending on which nucleotide binds at sites 1, 2 and 3 the dimerization results in octamers with an extended conformation that are active (ATP bound) or octamers in a compressed conformation that are inhibited (GDP/GTP-bound). Thr^{159}/Ser^{160} maps at the nucleotide binding site 1 of IMPDH1. In this way, Thr^{159}/Ser^{160} phosphorylation by light would dramatically decrease the affinity for GDP/GTP for the canonical site 1 reducing IMPDH1 allosteric inhibition.

In most cell types the ratio of ATP:GTP is between 3:1 to 5:1 (Traut 1994). *In vitro* structural studies predict that under homeostatic quiescent conditions -purines largely provided by the *savage* pathways- IMPDH would bind both nucleotides and remain mostly in inhibited free octamers (Johnson and Kollman 2020). It would be the decrease in intracellular GTP during proliferation that would allow the extension of the Bateman domain causing activation and transient assembly into enzymatically active filaments (Johnson and Kollman 2020).

GTP levels in the retina are particularly high, with GTP being equimolar or higher than ATP (**Fig 35** and **Table 7**), consistent with previous reports in frog rod inner/outer segment suspensions (Biernbaum and Bownds 1979) and bovine rod outer segments (Ostroy, Svoboda, and Wilson 1990).

Thereby, we propose that under dark-adapted conditions IMPDH1 would bind GDP/GTP and shift the equilibrium towards free octamers in compacted inhibited conformation (GDP/GTP imposing negative feedback on IMPDH1 activity). Upon light exposure, phosphorylation at Thr^{159}/Ser^{160} would dramatically decrease the affinity for GDP/GTP, allowing the extension of the Bateman domain and promoting activation of the enzyme. The loss of GDP/GTP sensing capacity would also -based on structural models, (Johnson and Kollman 2020)- be expected to induce the assembly of extended octamers into enzymatically active filaments. The gradual accumulation of these filaments upon constant light exposure would yield the aggregate structures that we observe at the rod outer segment layer (**Fig 38** and **39**).

IMPDH subcellular aggregates are a landmark of cells or tissues with increased GTP demand and/or circumstances of metabolic GTP deficiency that require stimulation of GTP biosynthesis (Aughey and Liu 2016; Keppeke et al. 2018; Y. S. Ji et al. 2006; Chang et al. 2015). A recent *in vivo* study has shown, for instance, that IMPDH1 formation of filaments is inherent to T cell activation and proliferation, triggered at a post-translational level by NFAT or mTOR signaling, and serves to increase guanine nucleotide levels (Duong-Ly et al. 2018). We therefore propose that the accumulation of IMPDH1 aggregates at the outer segment would serve to increase the GTP synthesis locally.

Our determinations of Gly* incorporation into IMP*, GMP* and AMP* performed by fluxomic analysis revealed an increase in the flux towards the *de novo* synthesis of purine nucleotides in response to light. These results are consistent with a major demand of GTP by photoreceptor cells in light conditions.

The fact that light-dependent IMPDH1 aggregates accumulate at the outer segment layer suggests that light increases GTP demand due to phototransduction. In light conditions GTP at the outer segment would be consumed in its conversion to GDP by transducin GTPase, and to cGMP by guanylate cyclase. Our electroretinogram recordings, performed simultaneously from both eyes of

mice injected with an IMPDH inhibitor or control saline buffer, showed no inhibitor effects on the size of the test flash responses (**Fig 43E**), discarding a noticeable effect of IMPDH inhibition on activation of the light response. However, inhibiting IMPDH1 caused a delay in mass rod response recovery, that was modest but statistically significant (**Fig 43A-D**).
Thereby, we conclude that *de novo* GTP biosynthesis contributes to cGMP replenishment during the recovery phase of the light response, even if cGMP can be substantially sustained by the *salvage* pathways.

In this respect, retinal GTP levels upon light exposure were reported to be maintained when it was living mice that were exposed to light, or *in situ* retinas kept in supplemented tissue culture medium (with glycine and serine), like in Du et al. 2016 study (Du et al. 2016) and this study (**Fig 35**, **Table 7**, **Fig 40** and **Fig 41**). In contrast, reports of light causing a large decrease in GTP come from determinations performed in isolated ROS/RIS preparations or retinas kept in Ringers, that cannot sustain one-carbon metabolism (Biernbaum and Bownds 1979; Salceda et al. 1982).

According to this model it might seem surprising that Impdh1-/- mice display only a slowly progressive retinal degeneration. However, despite maintenance of the retinal structure, these mice present gradually diminished ERG responses from normal at 5 months to nearly extinguished at 13 months of age (Aherne et al. 2004). Furthermore, compensatory changes like upregulation of IMPDH2 cannot be excluded in this chronic scenario.

We here demonstrate that the light-dependent phosphorylated residues Thr^{159} and Ser^{160} in retinal hIMPDH1 were selective *in vitro* substrates for PKCα kinase; but not for the other kinases tested [PKA, CamKII, CKII, PKB-Akt and AMPK]. We also show that treatment of *in situ* retinas with a PKC inhibitor (bisindolylmaleimide I (BM)) led to a noticeable decrease of GTP retinal levels upon light exposure (**Fig 45A**); and that *in vivo* PKC inhibtion had an effect on the rate of recovery responses (**Fig 45B**). We know from our phosphoproteomic analysis that the phosphorylation events that prime PKCα occur in the retina in response to light (Thr^{500}, Thr^{641} and Ser^{660} (Keranen et al. 1995)). Therefore, we propose a model in which light triggers a signaling pathway that activates PKCα, that in turn phosphorylates IMPDH1 at the Bateman domain, desensitizing the enzyme to GTP/GDP inhibition.

Our proposed model that GDP/GTP allosteric regulation of IMPDH1 is controlled by phosphorylation *in vivo* to adapt GTP synthesis to the illumination conditions supports previous hypothesis that IMPDH1 mutations would cause the pathology by resulting in higher than normal IMPDH1 activity and/or by forming irreversible filaments. Abnormally high IMPDH1 activity could conceivably result in abnormally high cGMP synthesis, which is one of the well-known causes of

photoreceptor cell damage (Olshevskaya et al. 2004; Woodruff et al. 2007; Paquet-Durand et al. 2009; Trifunović et al. 2010; Sothilingam et al. 2015). On the other hand, the formation of filaments –in moments of sporadic bright light exposure in the natural world- would be reversible in healthy individuals, but irreversible in adRP10 patients by their impaired capacity to sense GDP/GTP levels.

This could result in the gradual accumulation of protein aggregates that would eventually turn toxic, in line with the reported compromised stability of IMPDH1 mutants when recombinantly expressed (Aherne et al. 2004) and their high tendency to aggregate *in vivo* (Tam et al. 2010). Most IMPDH1 mutations in adRP10 and adLCA, including the mutations N198K, R224P and D226N analyzed in this study, desensitize the enzyme to GDP/GTP allosteric inhibition (Buey et al. 2015).

Interestingly, we here show that out of the few IMPDH1 mutations that do not significantly reduce GDP/GTP allosteric inhibition directly, like R105W, V268I and H372P, mutant H372P resulted in abnormally high phosphorylation at Thr^{159}/Ser^{160} by PKCα *in vitro* (**Fig 44B-C**). This means that the H372P mutation would ultimately result in desensitization of the enzyme to GDP/GTP allosteric inhibition as well, even if H372P mutation would do it indirectly.

This study provides key insights into the complex IMPDH1 regulation in the retina, and proposes that phosphorylation-controlled GDP/GTP allosteric regulation of the enzyme plays an important role *in vivo* by serving to adjust the rate of *de novo* GTP synthesis to illumination conditions. We propose that IMPDH1 mutations lead to retinal dystrophies by disrupting this mechanism of control. This study calls for the development of adRP10 and rare adLCA animal models in which to test this model and assay novel therapies.

4. GLOBAL DISCUSSION AND FUTURE PERSPECTIVES

GLOBAL DISCUSSION AND FUTURE PERSPECTIVES

4.1 Role of GCAPs as damage mediators in the *rd3* mouse model of LCA12

Our study on *rd3* mice has established that the calcium sensor protein GCAPs mediate the physiopathology in LCA12. It is the Ca^{2+}-free conformational state of GCAPs that trigger a cell death signal, so we can state that GCAPs act as sensors of the chronic low $[Ca^{2+}]_i$ that results from RD3 deficiency.

There are many other genes that when mutated lead to chronic low $[Ca^{2+}]_i$, the so-called "light-equivalent" disorders (Table 4, introduction). One of the future lines of study should be testing whether GCAPs are generic "light-damage mediators", involved in the physiopathology of most of these disorders. These disorders could include: i) mutations in rhodopsin kinase (*GRK1*) and arrestin (*SAG*) that impair termination of the light response; ii) mutations in *RPE65* and *LRAT* that impair chromophore recycling therefore leaving photoreceptors with the apoprotein opsin which presents a low constitutive activity; iii) mutations in the alpha subunits of transducin (*GNAT1*) that lead to Nougaret disease; iv) null mutations in *REEP6* that lower the expression of RetGCs… and likely others to be discovered. If GCAPs were generically involved in these disorders, elucidation of the mechanism by which they trigger ER stress and identification of therapeutic targets in the pathway would be of the outmost importance.

- How do GCAPs induce ER stress and cell death in a context of chronic low Ca^{2+}? As we point in our model, we envision two possibilities: i) by triggering cGMP synthesis chronically at the inner segment where cGMP is toxic; or ii) by accumulating in a conformational state that is unstable and tend to form toxic oligomers and/or trigger the heat shock response.

i) Could GCAPs mediate the physiopathology by inducing deregulated/unabated cGMP synthesis at photoreceptor cell somas?

In this study we have localized RD3 at the inner segments of photoreceptors, which is consistent with Dizhoor et al. model in which RD3 acts as a potent inhibitor of RetGC during its trafficking to the outer segment (Dizhoor, Olshevskaya, and Peshenko 2019). Based on this model, Dizhoor et al. proposed that the calcium sensors, in the absence of RD3, may stimulate cGMP synthesis by RetGC at the inner segments (IS).

Abnormal production of cGMP in the IS may in turn activate PKG leading to aberrant phosphorylation of key targets governing the Ca^{2+} dynamics of the endoplasmic reticulum, ER malfunction and ER stress. The involvement of PKG in the physiopathology of mouse models of achromatopsia that involve ER stress has been previously reported (Ma et al. 2015). In their studies Ma et al. treated mice lacking functional CNGA3 and CNGB3 (CNG-channels subunits) with PKG inhibitors. They showed morphological rescue of animals treated with either KT5823 (a selective PKG inhibitor) or (Rp)-8-Br-cGMPS (a cGMP analogue that blocks PKG in its inactive state) and palliated ER stress effects. Therefore one future direction to test the involvement of PKG in the physiopathology of *rd3* mice would be to follow the protocols of the Ding lab based on PKG inhibitors. Alternatively, *rd3* mice could be bred with the PKG knock out model, to assess morphological rescue. For this approach we would select the *Prkg1-/-* mice, because this is the prevalent form of PKG in the retina and has been immunolocalized to the inner segments of photoreceptors (Gamm et al. 2000) where abnormal synthesis of cGMP is predicted to occur.

ii) Could GCAPs trigger deleterious effects simply by accumulating in their Ca^{2+}-free unstable conformation?

Early studies showed that although GCAPs are active in its Ca^{2+}-free form, this conformation made these proteins susceptible to proteolysis (Rudnicka-Nawrot et al. 1998) and made them propense to aggregate (Ana Mendez and Chen 2002; Hoyo et al. 2014).

These characteristics make GCAPs "unstable" in the conditions of prolonged low calcium characteristic of "light-equivalent" disorders. We have observed that Ca^{2+}-free GCAPs present high affinity for HSP90 in our pull down assays. This raises the possibility that Ca^{2+}-free GCAPs under chronic low $[Ca2+]_i$ may trigger the heat shock response that would ultimately cause ER stress.

To unequivocally establish a mechanism of toxicity mediated by Ca^{2+}-free GCAPs that is independent of GCAPs activation of the cyclase, we could analyse the effect of GCAPs ablation in the RetGC1/RetGC2 dKO model (lacking both RetGC1 and RetGC2 isoforms). In the RetGC1/RetGC2 dKO animals cGMP production is impaired, Ca^{2+} is expected to be abnormally low and GCAPs are retained at the proximal compartment of cells (Baehr et al. 2007). These animals present a retinal degeneration that resembles the human LCA1 phenotype. If GCAPs contributed to photoreceptor cell toxicity simply by accumulating in an unstable conformation, then GCAPs ablation should ameliorate the retinas of RetGC1/RetGC2 dKO with time. If GCAPs just act by inducing unabated cGMP synthesis in "light-equivalent" disorders, then GCAPs ablation should not improve RetGC1/RetGC2 dKO mice.

Finally, a particularly interesting model in which to test our hypothesis of GCAPs as damage mediators in "light-equivalent disorders" would be the Reep6-/- mice. Mutations in *REEP6* have been associated with adRP (Arno et al. 2016). Reep6 acts on a similar manner as RD3. Reep6-/- mice present a loss of RetGC1 and RetGC2 isozymes, and manifest a fast retinal degeneration (<40% photoreceptors remain at 4 months) (Agrawal et al. 2017). Thereby, Reep6 has been proposed to act in a similar way as RD3 by stabilizing and/or trafficking guanylate cyclase.

Agrawal et al. found altered ER stress with upregulation of CHOP in these mice. It will be very interesting to test whether RD3 levels are altered in Reep6-/- mice, because if this is not the case, then the chronic low Ca^{2+} and GCAPs retention at the IS (GCAPs require RetGCs for its trafficking to the OS) in this scenario would be causing cell death even when RD3 is silencing the remaining RetGCs.

- Other roles of RD3?

Given that *rd3* mice display one of the fastest retinal degeneration among mouse models of retinal dystrophies, we cannot discard that RD3 might have additional roles. Recently it has been shown that rdl-1 (RD3 homolog in *C.elegans*) and the retromer (Vps26, Vps29 and Vps35 subunits) work antagonistically on different endomembrane components to regulate rGC trafficking to BAG neuron cilia (rGC, specific guanylate cyclase in BAG neurons of *C.elegans*) (Martínez-Velázquez and Ringstad 2018). Martínez-Velázquez et al. observed that in the absence of rdl-1, rGC failed to distribute to the chemosensory cilia in these specific neurons. However, if in the absence of rdl-1 they depleted Vps29 and Vps35 (specific retromer components) they reconstituted rGC trafficking to the sensory cilia. Whether a similar relationship between RD3 and retromer exists in mammal photoreceptor cells requires investigation. However, blocking the retromer components in LCA12 patients would not be a therapeutic option because VPS35 loss of function mutations have been associated with Parkinson (Tang et al. 2015) and Alzheimer diseases (Muhammad et al. 2008), suggesting strong adverse effects of blocking these proteins.

4.2 *In Vivo* regulation of IMPDH1 in the retina, and effect of adRP10 IMPDH1 mutations on retinal physiology

We here report a novel mechanism of regulation of IMPDH1 in the retina *in vivo*. First, we have characterized a light-dependent phosphorylation event at the Bateman domain that desensitizes the enzyme to its allosteric inhibition by GDP/GTP. We have shown that IMPDH1 inhibition *in vivo* delays light response recovery, which depends on cGMP synthesis. Interestingly, by determining guanine and adenine nucleotide levels in dark/light we have observed that IMP levels nearly double during bright light exposure. Measurements of Gly* (stable isotope) incorporation to IMP, GMP and AMP allowed us to conclude that the whole *de novo* biosynthesis of purines is boosted under light exposure. Therefore we propose that this phosphorylation is part of a physiological program triggered by light to enhance *de novo* ATP and GTP synthesis to keep with the phototransduction demand. In this context, the release from GDP/GTP inhibition keeps IMPDH1 in a permissive state in light, to keep up with the increased metabolic flux.

We have observed that upon prolonged light exposure IMPDH1 forms aggregates at the outer segment compartment of photoreceptors, where cGMP turn-over multiplies by 10-20 in response to light. cGMP synthesis requires GTP as a substrate, there the increase in GTP demand.

IMPDH1 aggregates could result from the bundling of IMPDH1 filaments. Recent structural studies have shown that the conditions that promote IMPDH filament formation *in vitro* are the simultaneous depletion of GDP/GTP (marks an increase in GTP demand in cells: e.g. proliferation) and an increase in IMP (stabilizes filaments, precluding their disassembly) (Johnson and Kollman 2020). By establishing a parallelism of our results with structural studies we propose the model of IMPDH1 regulation depicted in **Fig 46**.

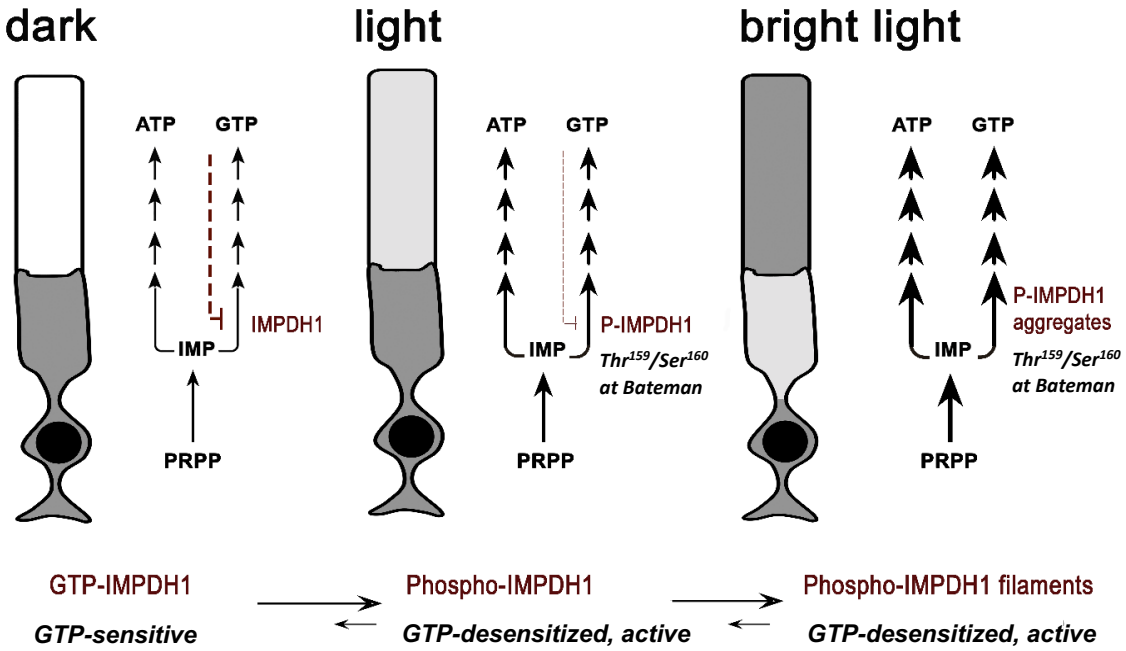

Figure 46. Proposed model of regulation of IMPDH1 activity in photoreceptor cells by light-dependent phosphorylation at Thr^{159}/Ser^{160}. In the dark, GTP can bind to the nucleotide binding sites at the Bateman domain and shift IMPDH1 conformation towards GTP-bound IMPDH1 compacted octamers that are inactive (negative feedback regulation in red). Upon light exposure, phosphorylation at Thr^{159}/Ser^{160} desensitizes the enzyme to GTP, coinciding with the increase in IMP levels. We propose that these concurring conditions would cause filamentation of the enzyme, leading to protein aggregation at the outer segment layer. In this way, light exposure would stabilize IMPDH1 in an active conformation permissive to the increased flux towards guanine and adenine nucleotide synthesis (thicker arrows in light). This increased flux is likely required to compensate for ATP and GTP consumption in the phototransduction process, to sustain the pools of ATP and GTP. IMPDH1 localization at the outer segment layer in these macrostructures would be reverted by dephosphorylation and gradual decrease of IMP levels during dark-adaptation. IMPDH1 localization at different light conditions is depicted in grey.

Two important aspects of the model await further experimentation/ reinforcement:

i) Whether phosphorylation at the Bateman domain is required to trigger IMPDH1 aggregates *in vivo* can be easily tested by treating mice with an specific PKC inhibitor previous to bright light exposure. Alternatively, phosphomimic and phosphoKO mutants of IMPDH1 could be transfected in living rod photoreceptors by *in vivo* DNA electroporation, to test whether the phosphomimic mutants trigger aggregate formation in dark conditions. Finally, generation of specific antibodies to the phosphorylated peptide would allow us to establish where phosphorylation is taking place.

ii) More exhaustive metabolic flux analysis can be performed with a series of stable isotopes (Gly, glucose) by doing time course analysis upon exposure to light steps of increasing intensity.

- How we can gain insight from this study for understanding the adRP10 and LCA11 pathologies?

Beyond understanding the physiological role and regulation of IMPDH1 in the retina, there is an urge to understand how *IMPDH1* mutations lead to the adRP10 and LCA11 forms of blindness. Based on ours and previous studies (Buey et al. 2015; Fernández-Justel et al. 2019) we envision two possible pathways of damage: 1) Blindness-associated mutations with impaired GDP/GTP regulation result in unabated IMPDH1 activity that yields abnormally high cGMP levels which is a well-known cause of cell death in photoreceptors (Olshevskaya et al. 2004; Woodruff et al. 2007; Paquet-Durand et al. 2009; Trifunović et al. 2010; Sothilingam et al. 2015); and 2) Blindness-associated mutations result in formation of filaments -in moments of sporadic bright light exposure in the natural world- that are irreversible due to their GDP/GTP desensitization (GDP/GTP cannot induce the disassembly of filaments), and toxic upon accumulation.

To test the *in vivo* effect of the adRP10 and LCA11 mutations it would be necessary to develop knock-in mouse models with selected mutations, i.e. N198K and R224P (the most prevalent). These animal models would serve to assess whether mutations result in increased IMPDH1 activity independent of the light conditions, and the formation and reversibility of IMPDH1 aggregates upon different light environments. These knock-in models would also serve to test novel therapies for adRP10 and LCA11 based on more specific IMPDH1 inhibitors.

5. CONCLUSIONS

CONCLUSIONS

1. GCAPs ablation in the *rd3* mice largely delays retinal degeneration; providing substantial morphological rescue.

2. GCAPs ablation in the *rd3* mice does not improve visual function.

3. GCAPs mediate the physiopathology in *rd3* mice by sensing the chronic low $[Ca^{2+}]_i$ and inducing ER stress and CHOP-mediated apoptosis at an early stage of the disease.

4. IMPDH1 is phosphorylated *in vivo* at three residues: Thr^{159}/Ser^{160} in response to light, Ser^{416} indistinctly in dark/light conditions, and Ser^{477} preferentially in the dark.

5. Phosphorylation of Ser^{416} at the mobile flap of IMPDH1 reduces enzymatic activity in *in vitro* assays.

6. Phosphorylation at the Bateman domain (Thr^{159}/Ser^{160}) desensitizes IMPDH1 to inhibitory allosteric regulation by GDP/GTP *in vitro,* which indicates that *in vivo* IMPDH1 activity should increase with light.

7. Bright light exposure causes the progressive and reversible accumulation of IMPDH1 aggregates at the rod outer segment layer of the retina; that correlates with an increase in IMP, AMP and GMP levels in the retina.

8. Light increases the flux through *de novo* synthesis of purine nucleotides in the retina, likely to sustain the ATP and GTP pools despite their increased consumption.

9. IMPDH1 inhibition in the retina *in vivo* delays rod mass recovery, implying that *de novo* synthesis of cGMP contributes to sustain the recovery kinetics of the light response.

10. IMPDH1 residues Thr^{159}/Ser^{160} are substrates of PKC *in vitro.*

11. adRP10 mutation H372P results in increased phosphorylation at Thr^{159}/Ser^{160} by PKC *in vitro*, which points to its desensitization to GDP/GTP *in vivo.*

12. *In vivo* treatment with a selective PKC inhibitor reduces the GTP pool under light exposure and also delays rod mass recovery.

6. MATERIALS AND METHODS

6.1. Materials and methods for Chapter 1

6.1.1. Ethics statement

Pertaining to animal research, this study was conducted in accordance with the ARVO statement for the use of animals in ophthalmic and vision research and in compliance with acts 5/1995 and 214/1997 for the welfare of experimental animals of the autonomous community (Generalitat) of Catalonia; and approved by the ethics committee on animal experiments of the University of Barcelona (Generalitat Reference #9906, protocols Bell 216/17; 217/17 and 218/17).

6.1.2 Generation and affinity purification of antibodies against RetGC1 and RD3

The polyclonal antibodies against RetGC1 and RD3 were generated against a peptide corresponding to the last 21aa of murine RetGC1 (Cys: H2N-IPPERRKKLEKARPGQFTGKC-OH) and to the last 16aa of murine RD3 (Cys: H2N-PPRTWSMPEFRAPQAD -OH). Peptides were conjugated to keyhole limpet hemocyanin (KLH) carrier protein (#77666, Thermo Fisher Scientific) and inoculated in New Zealand White rabbits following a standard 70 day antigen delivery protocol (**Fig 47A**): initial injection of antigen (0.25 mg) emulsified in Freund's complete adjuvant (Sigma), and three boosts of antigen (0.1 mg) in Freund's incomplete adjuvant (Sigma). Serum from immunized rabbits was purified by affinity chromatography, by using the immunizing peptide covalently coupled to agarose columns by –SH chemistry (Sulfolink technology, Thermo Fisher Scientific) (**Fig 47B**). Immunoglobulins were eluted from columns in acidic conditions (0.5 M glycine pH 2.5), neutralized (Tris HCl pH 8.8), dialyzed against 1x PBS pH 7.2, and concentrated with 10 K Amicon devices (Merck Millipore).

6.1.3 Generation and affinity purification of antibody against bIMPDH1 canonical protein

Anti-IMPDH1 antibody was generated against purified bovine canonical IMPDH1 (bIMPDH1-514 aa). Bovine IMPDH1 cDNA was amplified from total RNA from fresh bovine retinas and cloned into pET15b bacterial expression plasmid (Novagen®) for expression in *E. coli* BL21 (DE3) cells. The expression of recombinant protein was induced in bacterial cultures at OD_{600}=0.6 for 5 hrs at 37ºC. Cells were then collected and bacterial inclusion bodies were obtained and solubilized in 6 M guanidinium hydrochloride buffer as previously described (Krishnaiah 1975).

bIMPDH1-514aa.His was purified by metal chelation using a HiTrap column (GE Healthcare) and dialyzed against dialysis buffer (1 M urea, 0.4 M L-arginine, 20 mM Hepes and 200 mM NaCl).

Purified bIMPDH1-514aa was used to immunize two New Zealand White rabbits following a standard 70 day protocol as described above. At exsanguination, blood serum was affinity purified with bIMPDH1-crosslinked to Aminolink coupling resin (Thermo Fisher Scientific). Antibodies were eluted, dialyzed and concentrated as described above.

6.1.4 Antibodies preservation

Following dialysis and concentration in PBS pH 7.2, antibody concentrations were assessed by a BCA assay (#23225, Thermo Fischer Scientific). Batches of ~4-6 mg antibody/ml were properly aliquoted in fresh tubes and conserved in different preservatives. Purified antibodies were preserved in either 0.4% BSA, 0.025% sodium azide; or in 40% glycerol and kept at -80ºC until use.

A fraction of non-purified serum was precipitated in ammonium sulphate to avoid the use of BSA or glycerol that would interfere in future crosslinking/conjugating procedures. For this, a saturated solution of ammonium sulphate (100%) was added drop by drop to serums until 40% saturation. As addition of ammonium sulphate would acidify antibodies causing antibody denaturalization, a final concentration of 50 mM Trisma base pH=8 was added to the mix. Precipitation of antibodies was allowed to proceed in a rotating wheel for 1 h, at 4ºC. Antibodies were further centrifuged at 12,000×*g* (4ºC) for 20 min, and then supernatants were discarded and pellets containing the precipitated antibody were kept at -80ºC until use. To reconstitute the precipitated fractions, antibodies were resuspended in PBS pH 7.2 and centrifuged at 12,000×*g* (4ºC) for 20 min. Supernatants containing clarified antibodies were transferred to fresh tubes and stored at 4ºC until use.

6.1.5 Testing of antibodies by Western Blot

Murine and bovine retinas were homogenized in homogenization buffer [20 mM Hepes, 115 mM KCl, 10 mM NaCl, 10 mM $MgCl_2$, 1 mM PMSF and a protease cocktail inhibitor (Complete mini EDTA-free, Roche)]. Extracts were clarified by centrifugation at 12,000×*g* 20 min at 4ºC. Samples were boiled for 5 min after addition of 4x Laemmli SDS buffer, and fractions corresponding to one tenth of a murine retina (20 μg) or one hundredth of a bovine retina (50 μg) were resolved by SDS-PAGE in tris-glycine gels. Proteins were transferred to nitrocellulose membranes (0.2 μm nitrocellulose, Bio-Rad). Membranes were blocked for 1 hr at room temperature with 5% dry milk and then were incubated with anti-RetGC1 (1:1000), anti-RD3 (1:2000) or anti-IMPDH1 (1:5000)

Abs. Secondary antibody was a goat anti-rabbit IgG (Heavy and Light chains, H&L) antibody Dylight™ 800 conjugated (#611-145-002, Rockland) at 1:5000. Images were acquired at an Odyssey Scanner (LI-COR).

6.1.6 Testing of antibodies in indirect immunofluorescence localization assays

For immunolocalization assays, murine or bovine eyes were enucleated, the cornea was excised and eyecups were fixed (4% paraformaldehyde, 0.02% glutaraldehyde in PBS, pH 7.4) for 30 min at room temperature. Then the lens was removed and eyecups were further fixed for 1.30 hrs at room temperature. Eyecups were washed in PBS prior to being infiltrated in acrylamide (8.4% acrylamide, 0.014% bisacrylamide in PBS pH 7.4) overnight at 4ºC. Following overnight infiltration, acrylamide polymerization was induced by addition of ammonium persulphate and TEMED. Eyecups in acrylamide blocks were submerged in molds with O.C.T. compound (Tissue-Tek, Electron microscopy Sciences) and immediately frozen in liquid nitrogen. Cryosections were obtained at 20 μm-thickness using a CM15105 Leica Cryostat (Leica Microsystems).

RetGC1 and RD3 antibodies did not required antigen retrieval protocols. The antibody against IMPDH1 worked optimally when applying a brief antigen retrieval protocol that consisted on incubation of the retinal sections with proteinase K in PBS (0.05 mg/ml) for 2 min, followed by a heat shock at 70ºC for 10 sec. Sections were extensively washed in PBS and incubated with blocking solution (3% normal goat serum, 1% BSA, 0.1% Triton-X100 in PBS pH 7.4) for 1 hr at room temperature. First antibodies were incubated over night at 4ºC in blocking solution without Triton-X100 (RetGC1; 1:200); (RD3; 1:500) and (IMPDH1; 1:250). Secondary antibody was goat anti rabbit Alexa-488 (Thermo Fisher Scientific) incubated for 1.5 hrs at room temperature. Then retinas were fixed for 15 min in 4% paraformaldehyde prior to being mounted with Mowiol (#475904, Calbiochem)

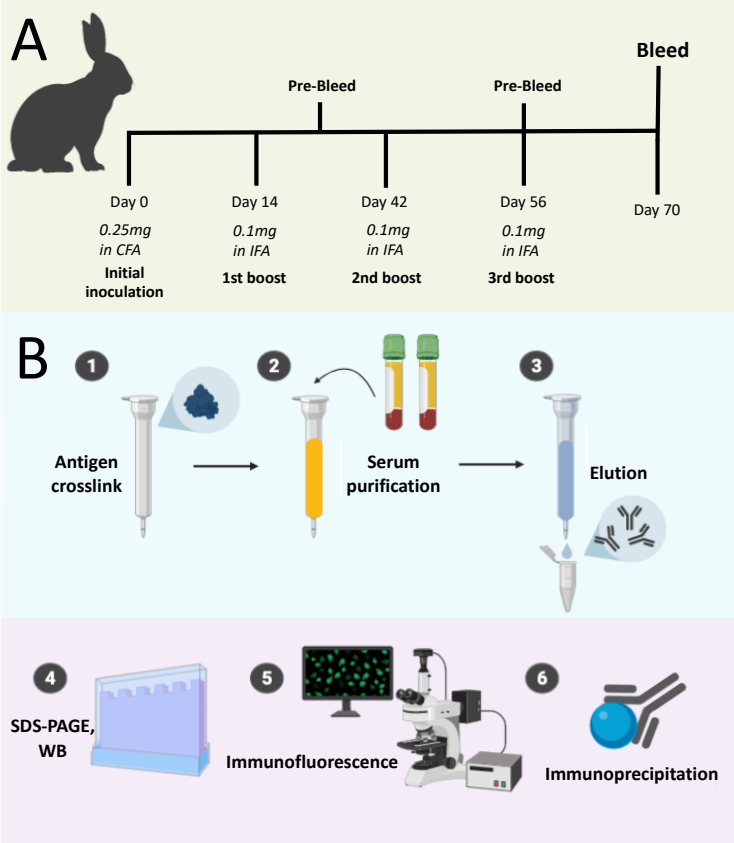

Figure 47. Scheme of antibody generation, purification and testing. A. A standard 70 day (three boost) antigen delivery was followed to inject two rabbits per antigen. At day 0 animals were pre-bleed (1ml) to obtain control serum; and were injected with 0.25 mg antigen (RetGC-KLH; RD3-KLH or IMPDH1) in Complete Freund's Adjuvant (CFA) at four subcutaneous sites. At days 14, 42 and 56 animals were boosted with 0.1 mg antigen in Incomplete Freund's Adjuvant (IFA) at four subcutaneous sites. At days 28 and 56 a pre-bleed (1 ml) was collected to test antibody title and specificity. At day 70 animals were euthanized and bled (~70 ml blood/animal). Blood was centrifuged at 2500 rpm to obtain the serum fraction. **B.** Antibody purification consisted in crosslinking the antigen (RetGC and RD3 peptides; or whole recombinant IMPDH1) to agarose, using —SH or Aminolink chemistry (1). Serum was incubated in agarose columns for 15 min (2), extensively washed in PBS pH 7.2, and bound antibodies were eluted in acidic conditions (0.5 M glycine pH 2.5) further neutralized (Tris HCl pH 8.8) and dialyzed against PBS pH 7.2 (3). Antibodies were aliquoted and preserved in 0.4% BSA, 0.025% azide; in 40% glycerol and were kept at -80ºC until use. Antibody specificity was tested by western blot (4), immunofluorescence on fixed retinas (5) and in immunoprecipitation assays (6).

6.1.7 Titration of bIMPDH1 antibody in Immunoprecipitation

To perform immunoprecipitation assays, increasing amounts of IMPDH1 antibody (0.5 µg, 1 µg and 3 µg) were incubated with a fixed amount of magnetic beads-protein G (Dynabeads, Life Technologies) for 15 min at room temperature. After three washes with 1x PBS, the beads-antibody complex was incubated with a fixed amount of bovine retinal extract (0.5 mg protein, corresponding to 1/10 of a bovine retina) for 1 h at room temperature in a rotating wheel. Flow through fractions were collected and beads were extensively washed. Elutions were performed by adding 20 µl of 1x SDS loading buffer to the antigen-antibody-beads complexes. Input, flow through and elution

fractions were run on a 12% SDS-PAGE, transferred to a nitrocellulose membrane and incubated with anti-IMPDH1 Ab. Instead of a secondary antibody, protein G-800 [protein G conjugated to 800 fluorophore, (#PG00-32, Rockland, 1:200)] was used for the detection, to avoid detecting the immunoglobulin chains of the IMPDH1 Ab used in the immunoprecipitation reaction).

The antibody against IMPDH1 was also cross-linked to magnetic beads using the pierce BS3 crosslinker (Thermo Fisher Scientific) following manufacturer instructions. For that, 10 μg of the antibody were crosslinked to 50 μl of Dynabeads protein-G (Thermo Fisher Scientific) for 30 min at room temperature. The reaction was stopped and beads were extensively washed before proceeding with the immunoprecipitation. IP was performed in parallel with non- crosslinked antibody as described above.

6.2 Materials and methods for Chapter 2

6.2.1 Mice

The B6.Cg-Rd3rd3/Boc strain of *rd3* mice used in this study were obtained from the Jackson's Laboratories (JAX Stock #8627 Maine, USA) as heterozygous wt/*rd3* mice(B. Chang et al. 1993). These mice present a point mutation after residue 106 (C→T) that results in a premature stop codon after residue 106. The *rd3* mutation results in expression of a truncated form of the RD3 protein that is rapidly degraded (Friedman et al. 2006). Heterozygous animals were bred in order to obtain homozygous *rd3*/*rd3* mice. Mice were genotyped by real-time polymerase chain reaction (RT-PCR) by making use of the TaqMan® SNP genotyping assay (Life Technologies, Carlsbad, USA). For that purpose, forward and reverse primers were designed to amplify a fragment of 68 bp from the *Rd3* locus of genomic DNA that encompasses the *rd3* mutation (Fw: 5'-CTGGAGACGCTCATGATGGA-3'; and Rv: 5'-CGACGCTCCCTCTGTTGT-3') and primer probes were designed to hybridize with either the amplified wild-type allele (VIC-5'-CTCTCTCATCTGCCCAGCC-3') or knock-out allele (FAM-5'-CTCTCTCATCTACCCAGCC-3'). RT-PCR was performed in 25 µl reactions containing 12.5 µl TaqMan universal master Mix (Life Technologies); 300 nM each forward/reverse primer; 250 nM of each primer probe, and 20 ng of genomic DNA obtained from digested mouse tails (Nucleospin® Tissue, Macherey-Nagel, Düren, Germany). After 10 min incubation at 95 °C, thermal cycling was performed on the StepOne Real-time PCR System (Thermo Fisher Scientific, Waltham, Massachusetts) and consisted of 40 cycles (95 °C for 15 s; 60 °C for 1 min). End-point allelic discrimination genotyping was assessed by inspecting the fluorescence plots for the wild type versus mutated probe (**Fig 48B**).

To obtain mice expressing the *rd3* mutation to homozygosis in the GCAPs$^{-/-}$ background, *rd3*/*rd3* mice were bred to GCAPs$^{-/-}$ mice (**Fig 48A)**.

GCAPs$^{-/-}$ mice lack GCAP1 and GCAP2 expression, and their phenotype and genotyping protocols have been described (A Mendez et al. 2001) (**Fig 48C-D**).

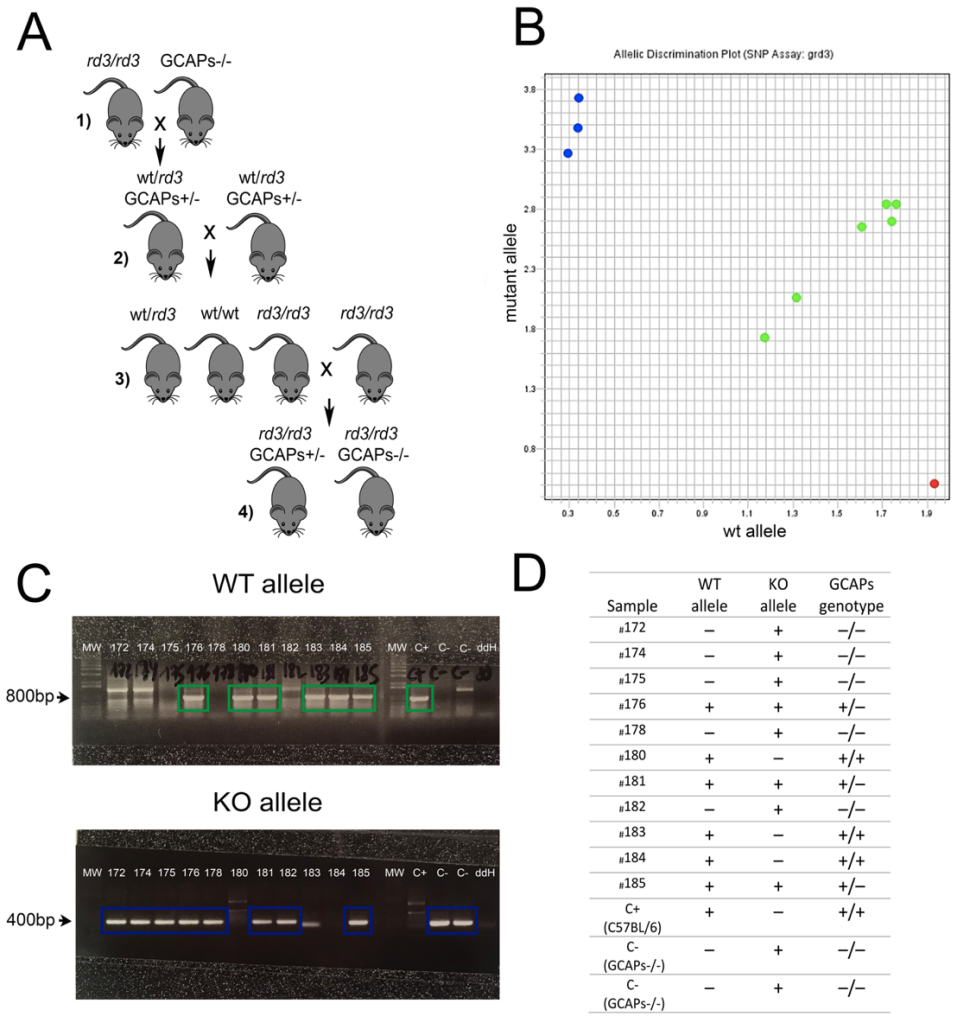

Sample	WT allele	KO allele	GCAPs genotype
#172	–	+	–/–
#174	–	+	–/–
#175	–	+	–/–
#176	+	+	+/–
#178	–	+	–/–
#180	+	–	+/+
#181	+	+	+/–
#182	–	+	–/–
#183	+	–	+/+
#184	+	–	+/+
#185	+	+	+/–
C+ (C57BL/6)	+	–	+/+
C- (GCAPs-/-)	–	+	–/–
C- (GCAPs-/-)	–	+	–/–

Figure 48. Establishing the *rd3/rd3* GCAPs-/- line. A. *rd3/rd3* mice were bred to GCAPs-/- mice (1). The progeny was heterozygous for both *rd3* and GCAPs null allele, and were subsequently crossed (2) to fix the *rd3* mutation (*rd3/rd3*). Selected progeny (3) that were GCAPs+/- and rd3/rd3 were then crossed in order to obtain *rd3/rd3* GCAPs+/- and *rd3/rd3* GCAPs-/- mice (4). **B.** Representative allelic discrimination plot in *rd3* genotyping: blue dots, *rd3/rd3*; green dots, wt/*rd3*; red dot wt/wt. **C.** Representative GCAPs genotyping result. The pair of primers used yield a PCR band of ~800bp band from the wt allele (green boxes) (Ana Mendez *et al.*, 2001) [note that 172, 174 and 182 samples amplify in a higher Kb band (>800bp), this band also appears in negative GCAPs-/- control (2)]; whereas the KO allele yields a ~400bp band (blue boxes). **D.** Example of GCAPs genotype determination after PCR analysis.

6.2.2 Antibodies

Anti-GCAP1 and anti-GCAP2 polyclonal antibodies have been previously described (López-Begines, Plana-Bonamaisó, and Méndez 2018). The polyclonal antibodies against RetGC1 and RD3 were generated in rabbit against C-terminal peptides corresponding to the last 21 aa of murine RetGC1 and the last 16 aa of murine RD3 (see methods Chapter 1).

6.2.3 Specimen preparation for light and electron microscopy

Mice of the indicated genotypes were reared under standard cyclic light (12 h dark:12 h light) and sacrificed by cervical dislocation. The vertical meridian of the eye was marked at the top for orientation purposes. The eye was enucleated, punctured, and immediately submerged in 2% paraformaldehyde, and 2.5% glutaraldehyde in 0.1 M cacodylate buffer pH 7.2 for 5 min. The cornea was excised and fixation was allowed to proceed for 1 h, before removal of the lense and further fixation of the eye cup for 12 h at 4 °C. Eye cups were washed with 0.1 M cacodylate buffer and fixed with 1% osmium tetroxide in 0.1 M cacodylate buffer for 2 h at room temperature. Specimens were dehydrated in ethanol (30–100%) or acetone, infiltrated with propylene oxide, and embedded in Epoxi embedding medium (Fluka Analytical, Munich, Germany). Retinal sections for histological analysis by light microscopy morphometry measurements were obtained with a Reichert Ultracut S ultramicrotome (Leica, Wetzlar, Germany) at 1-µm thickness and contrasted with Richardson's stain (0.5% methylene blue, 0.5% Azine II, and 0.5% borax in dH_2O). For transmission electron microscopy analysis, ultrathin sections were obtained (see below).

6.2.4 Retinal morphometry analysis

For morphometrical analysis, measurements of ONL thickness were taken on 1-µm sections at the vertical meridian of the eye that encompassed the optic nerve. Overlapping frames at 20x magnification were acquired covering the whole section with a Zeiss Axio Zoom.V16 stereo microscope (Zeiss, Oberkochen, Germany). An integrated image of the whole retinal section was assembled with the HUGIN fusion software. Measurements of ONL thickness were taken at 200-µm intervals from the optic nerve (12 divisions in the superior retina, and 10 divisions in the inferior retina) (**Fig 49**). For each morphometry analysis a minimum of four mice per genotype were used at indicated ages. Error bars represent the standard error of the mean (SEM).

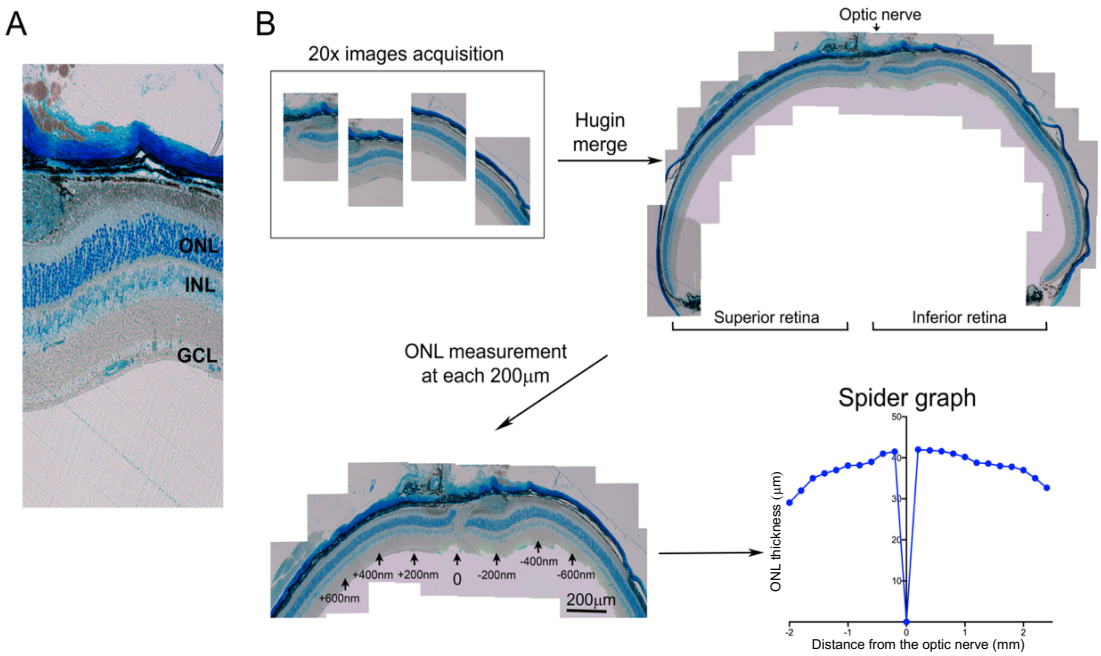

Figure 49. Retinal morphometric analysis on retinal sections from the vertical meridian of the eye that traverse the optic nerve. A. Identification of photoreceptor nuclei on murine retinas. ONL, Outer nuclear layer; INL, Inner nuclear layer; GCL, Ganglion cell layer. **B.** 20x images are acquired by bright field microscopy covering the whole retina. Images of entire retinas are reconstructed using the Hugin application. Scale is set with Fiji (Image J) software, and retinas are divided at 12 equal divisions (+ numbering, superior retina) and 10 equal divisions (- numbering, inferior retina) at 200 µm intervals. Fiji is then used to measure ONL thickness (µm) and a "Spider graph" is generated by plotting ONL width to optic nerve distance using Graph Pad Prism.

6.2.5 Ultrathin sectioning and image acquisition at the transmission electron microscope

Ultrathin sections (70–90 nm) were obtained with a Reichert Ultracut S ultramicrotome (Leica), collected on 200 mesh copper grids, counterstained by heavy metal staining (2% uranyl acetate in 50% ethanol for 30 min), and contrasted with 2% lead citrate for 10 min. Ultrathin sections were analyzed in a JEOL 1010 transmission electron microscope and images acquired with a Bioscan Gatan wide angle slow scan CCD camera.

6.2.6 Immunofluorescence analysis in fixed tissue

For immunofluorescence analysis, eye cups were fixed in 4% paraformaldehyde, 0.02% glutaraldehyde in phosphate-buffered saline (PBS), pH = 7.4 for 2 h at room temperature. Eye cups were infiltrated in acrylamide (8.4% acrylamide, 0.014% bisacrylamide in PBS pH 7.4) overnight at 4 °C. Acrylamide polymerization was induced and eye cup acrylamide blocks immediately frozen in O.C.T. compound (Tissue-Tek, Electron microscopy Sciences, Hatfield, PA) using liquid nitrogen. Cryosections were obtained at 18-µm thickness with a CM15105 Leica Cryostat (Leica Microsystems, Wetzlar, Germany).

Immunolocalization of GCAP1 and GCAP2 required an antigen retrieval protocol, consistent on incubation with proteinase K (0.05 mg/ml in PBS) for 2 min, followed by a 10 s heating shock at 70 °C. Sections were incubated with blocking solution (3% normal goat serum, 1% bovine serum albumin (BSA), 0.3% Triton-X100 in PBS pH7.4) for 1 h; first antibody in dilution buffer (3% normal goat serum, 0.4% BSA, 0.1% Triton-X100 in PBS pH 7.4) for 16 h at 4 °C; and secondary antibody (1.5 h at room temperature), and fixed with 4% paraformaldehyde prior to being mounted with Mowiol (Calbiochem #475904, San Diego, CA, USA). Antibodies used were anti-RetGC1 pAb; anti-GCAP1 pAb; anti-GCAP2 pAb; anti-rhodopsin mAb 1D4; anti-PNA-647 (# L32460, Thermo Fisher Scientific); anti-rabbit Alexa Fluor 488 (#A-11034, Thermo Fisher Scientific, Walthman, MA, USA); and anti-mouse Alexa Fluor 555 (#A-32727, Thermo Fisher Scientific). Samples were mounted on 0.13–0.16 mm thick cover glasses.

6.2.7 Confocal microscopy and data analysis

Confocal microscopy images were acquired at a confocal laser scanning microscope Zeiss LSM 880 equipped with one GaAsP detector, with a 63×/1.4 NA oil objective. For localization of RetGC and GCAPs in **Fig 19** and **Fig 20** spectral bands were set to 493–550 nm for the 488 channel, 566–638 nm for the 555 channel, and to 638–755 nm for the 647 channel. The *Z*-stacks covered 16 μm of tissue with a 368 nm step size (~40 planes/stack). The image acquisition settings provided a pixel size of about 0.132 × 0.132 μm in 1024 × 1024 images.

6.2.8 Western blot

Retinas (at least $n = 3$ per condition) were homogenized in Laemmli sodium dodecyl sulfate (SDS) buffer with 1 mM phenylmethylsulfonyl fluoride (PMSF), and protease cocktail inhibitor (Complete mini EDTA-free, Roche). Samples were boiled for 10 min at 95 °C, and fractions corresponding to one tenth of a retina were resolved by 12 or 16% SDS–polyacrylamide gel electrophoresis. Proteins were transferred to nitrocellulose membranes (0.2 μm nitrocellulose, Bio-Rad, Hercules, CA, USA). Membranes were blocked for 1 h at room temperature with 5% non-fat dry milk in TBST and then were incubated overnight at 4 °C with custom polyclonal antibodies to RetGC1, RD3, GCAP1, and GCAP2, and antibodies anti-CHOP (#L63F7, Cell Signaling); anti-Caspase 3 (#9662, Cell Signaling); anti-PARP1 (#9542, Cell Signaling); goat anti-rabbit IgG (Heavy and Light chains, H&L) antibody Dylight™ 800 conjugated (#611-145-002, Rockland, Pottstown, PA, USA); goat anti-mouse IgG (H&L) antibody Dylight™ 680 conjugated (#610-144-002-0.5, Rockland); and donkey anti-goat

conjugated to Horseradish Peroxidase (HRP) was from Thermo Fisher (#86326). Detection was performed in an Odyssey Scanner (LI-COR Biosciences, Lincoln, Nebraska) or ImageQuant™ LAS500 (Ge Healthcare, Chicago, Illinois) image acquisition system. Band densitometric analysis was performed using the Fiji (Image J) software, and band intensity analysis presented in histograms always reflect band intensity of the protein of interest normalized by the intensity of tubulin in the loading control.

6.2.9 Isoelectric focusing separation of murine retinal homogenates

Retinas from wt and *rd3*/*rd3* mice were dissected at p21, at an early onset of retinal degeneration of *rd3* mice. Retinas were homogenized in homogenization buffer with phosphatase inhibitors [20 mM Hepes, 115 mM KCl, 10 mM NaCl, 10 mM $MgCl_2$, 50 mM NaF, 5 mM β-glycerophosphate, 1 mM PMSF, and a protease cocktail inhibitor (Complete mini EDTA-free, Roche, Basel, Switzerland); pH 7.4]. Samples were centrifuged at 13,200 rpm, 4 °C for 30 min, and supernatant fractions were kept. An aliquot was taken at this point for protein determination (BCA kit, Thermo Fisher Scientific). Protein material in supernatant fractions was precipitated by addition of three volumes of ice-chilled trichloroacetic acid (TCA)-acetone (13.3% w/v trichloroacetic acid in acetone, with dithiothreitol (DTT) to 20 mM final concentration); equilibration of samples to −20 °C for 72 h; and centrifugation at 13,000×*g* for 1 h at 4 °C. Protein pellets were washed twice with cold 20 mM DTT in acetone; and allowed to air-dry for 10 min. Samples were dissolved in urea/thiourea/CHAPS/DTT (7 M urea, 2 M thiourea, 40 mM DTT, 4% CHAPS, and 2% IPG buffer pH 3–10) to ensure complete reduction, denaturing, and solubilization of proteins in the samples.

Samples were kept at −80 °C until use. For isoelectric focusing (IEF) separation, gel strips with a preformed linear pH gradient of pH 3–10 (prehydrated IPG Immobiline (TM) DryStrips pH 3–10, 18 cm, GE Healthcare) were used. Threefold more sample was loaded for *rd3*/*rd3* retinas than wt retinas in order to equilibrate the GCAP2 signal. IEF separation was conducted on an Ettan IPGphor3 system (GE Healthcare), following a 500 V step for 1 h, a gradient to 1000 V for 1 h, a gradient to 10,000 V for 3 h, and a 10,000 V step for 3 h. Gel strips were incubated in transfer buffer for 15 min, and proteins were transferred to nitrocellulose membranes by capillary action. GCAP2 was immunoblotted with anti-GCAP2 pAb and goat anti-rabbit IgG (Heavy and Light chains) antibody Dylight™ 800. Bands were visualized at an Odyssey scanner (LI-COR), and densitometry analysis was performed with the Fiji (ImageJ) software.

6.2.10 Expression, purification, and in vitro phosphorylation of myristoylated GCAP2 for pull-down assays

Myristoylated GCAP2 expression was induced in *Escherichia coli* BL21(DE3) cells transformed with pET-15b-bGCAP2 and the pBB131 plasmid encoding N-myristoyl transferase (a gift from Dr. J. Gordon, Washington University School of Medicine, Missouri, USA). Free myristic acid was added to 50 μg/ml to the cell culture and expression was induced for 4 h at 37 °C. bGCAP2 protein, was recovered from solubilized inclusion bodies and purified by on-column refolding using immobilized metal affinity chromatography (IMAC) on a Nickel-NTA [Nickel bound to agarose beads by chelation using nitrilotriacetic acid] as previously described (Hoyo et al. 2014).

To obtain phosphorylated bGCAP2 for pull-down assays, in vitro phosphorylation reactions were performed with protein kinase G (PKGIα, Calbiochem, Billerica, MA, USA). Each 50 μl reaction contained 30 mM Tris-HCl pH 7.5, 5 mM $MgCl_2$, 5 mM sodium phosphate buffer pH 7.5, 6 mM DTT, 2 mM EGTA, 10 μM ATP, and 500 μM cGMP, with 10 μg of bGCAP2 in the presence or absence of purified PKGIα (100 units) to obtain phosphorylated GCAP2 (GCAP2-P) and the mock-control (GCAP2). Phosphorylation reactions were allowed to proceed for 2 h at 30 °C, and GCAP2 and GCAP2-P were covalently linked to Epoxi-magnetic beads (Life Technologies, Carlsbad, CA, USA). GCAP2- or GCAP2-P-beads were then incubated with bovine retinal homogenates obtained by homogenization of fresh bovine retinas in binding buffer (10 mM HEPES, 135 mM NaCl, 5 mM KCl, 1 mM PMSF, 1 mM NaF, 1 mM β-mercaptoethanol, 1% Triton X-100, 4 mM EGTA, 2 mM EDTA, and Complete Mini protease inhibitors, pH 7.4). After 1 h incubation at room temperature, beads were washed and bound proteins were eluted under acidic conditions. Magnetic beads were extensively washed, and bound material was eluted in 0.2 M glycine pH 2.5 and immediately neutralized. Proteins in the bound fraction were identified by LC-MS/MS. The experiment included three biological replicates.

6.2.11 LC-MS/MS

Samples were reduced with 10 mM DTT at 60 °C for 30 min, and alkylated with 55 mM iodoacetamide for 30 min at room temperature. Samples were precipitated with 10% TCA. Pellets were dissolved in 2 μl of 8 M urea and brought to a final volume of 10 μl with 25 mM ammonium bicarbonate. Samples were digested with sequencing grade trypsin in 25 mM ammonium bicarbonate for 12 h. For LC-MS/MS, samples were resuspended in 0.1% formic acid and injected into a series Proxeon LC nanoEASY system (Thermo Fisher Scientific) coupled to a LTQ-Velos Orbitrap (Thermo Fisher Scientific). The resulting mass spectral peak lists were searched with the Sequest search engine

(v.2.1.04, Matrix Sciences, London, UK) against the merged BOVIN-MOUSE UP SP r 2011-1.fasta sequence library. For database searching, raw mass spectrometry files were submitted to the in-house MOUSE-BOVIN_UP_SP_r_2014-5.fasta Swiss-Prot database (released February 2014; 22460 protein entries) using SEQUEST version 28.0 (Thermo Fisher Scientific). The criteria used to accept identification included a minimum of two peptides matched per protein, with a false discovery rate of 1%. All proteins were treated as ungrouped.

6.2.12 Characterizing differential protein interactions of GCAP2-P and GCAP2

For label-free quantitative proteomic analysis of proteins identified with GCAP2-P versus GCAP2, we first filtered the protein lists to remove any duplications resulting from the use of bovine and mouse fasta sequence libraries. Only those proteins unequivocally assigned by at least a unique peptide were retained. For each protein identified the NSAF was calculated with the following equation:

$$Equation\ 1: NSAF_k = \frac{(SpC_k + 1)/L_k}{\sum_{i=0}^{n} (SpC_i + 1)/L_i}$$

where $NSAF_k$ is the Normalized Spectral Abundance Factor (Zybailov et al. 2006) for a given protein k; SpC_k is the Spectral Count for protein k, L_k is the length of the protein in number of amino acids; and the denominator is the summation of the NSAFs of all identified proteins in that sample. This expression corrects for differences in sampling depth between both conditions assayed, and avoids the discontinuity seen in simple count ratios when a protein shows spectral count = 0 in one of the samples.

Mean NSAF values were then calculated from triplicate biological samples, followed by a t-test comparison (two tails, unequal variance). To obtain the Volcano-plot, the $\log_2 \frac{Mean_P}{Mean_{NP}}$ was plotted in the X axis; and the $-10\log(p\ value)$ from the t-test was plotted in the Y axis, with $Mean_P$ referring to Mean $NSAF_{GCAP2\text{-}P}$, and $Mean_{NP}$ referring to Mean $NSAF_{GCAP2.}$ Threshold curves for the volcano plot were obtained by fitting values to $Equation\ 2: f(x) = \frac{1}{x^2 - n} + m$; were n is the value of the $\log_2 \frac{Mean_P}{Mean_{NP}}$ ratio threshold and m is the -10log(p-value) threshold. m and n values were fixed to 5 and 1.35 respectively. (Notes: taking $a \equiv \log_2\left(\frac{P}{NP}\right)$ and $b \equiv -10\log(p - value)$, the proteins passing the thresholds are those proteins that: $a < -\sqrt{n}$ and $b > f(x)$, for the negative side; and $a > \sqrt{n}$ and $b > f(x)$, for the positive side.

6.2.13 Electroretinography

A total of 4–7 mice were tested for each animal group. Dark-adapted (>12 h) animals were anesthetized with an intraperitoneal injection of ketamine (70 mg/kg; Ketalar, Parke-Davis, Wellington, New Zealand) and xylazine (7 mg/kg; Rompun, Bayer, Leverkusen, Germany) in saline solution (NaCl 0.9%) and pupils were dilated with one drop of 1% tropicamide. A corneal electrode was used to record ERGs from right eyes (Burian-Allen, Hansen Ophthalmic Development Lab, Coralville, IA). Electrode was placed in the visual axis 1–2 mm from the cornea and a drop of 2% methyl-cellulose (Methocel, Ciba Vision, Hetlingen, Switzerland) was dropped between cornea and electrode. Mice were maintained for >5 min in absolute darkness before the recordings. Mouse temperature during the recording was maintained at 37 °C with a liquid heating pad. Full-field flash ERG responses were recorded with the retina illuminated with a LED-driven Ganzfeld dome. A series of light flashes of increasing intensity (from 0.001 to 10 $cd/s/m^2$) were averaged both in scotopic and photopic conditions. Photopic cone responses were recorded following 5 min of light adaptation with a background white light (50 cd/m^2). Light intensity was controlled for each animal group (Mavo-Monitor USB, Gossen, Germany). Recorded electrophysiological responses were amplified, filtered (CP511 AC amplifier; Grass Instruments, Quincy, MA), and digitalized (ADInstruments Ltd, Oxfordshire, UK). The recording process was controlled with Scope version 3.8.1 software (Power Lab, ADInstruments Ltd). The stimulation protocols were designed according to the International Society for Clinical Electrophysiology of Vision.

6.2.14 Generation of pRho-mRd3.V5-dsRed expression vector and in vivo DNA electroporation

The expression vector used for in vivo DNA electroporation was based on the plasmid pRho-DsRed. pRho-DsRed was a gift from Connie Cepko (Addgene plasmid#11156; (Matsuda and Cepko 2004)). This plasmid contains the 2.2 kb-version of the rod opsin promoter from Bos Taurus (Zack et al. 1991); a multicloning site; a Kozak sequence; the DsRed2 reporter gene; and the β-globin poly(A) signal (Matsuda and Cepko 2004). To make pRho-mRD3.V5-DsRed, murine *rd3* cDNA was amplified by PCR with a forward primer that introduced an XbaI restriction site and the reverse primer introducing the V5 epitope in frame with RD3 COOH-terminal sequence, followed by an EcoRI restriction site. The mRD3.V5 DNA was inserted in the XbaI and EcoRI sites of pRho-DsRed, and the resulting expression vector was verified by sequencing. For *in vivo* electroporation, pRho-mRd3.V5-dsRed vector was amplified with the pureLinkTM Expi Endotoxin-Free Mega Plasmid Purification Kit (Invitrogen, Carlsbad, California).

In vivo DNA electroporation in the retina following DNA injection in the subretinal space was performed as originally described (Matsuda and Cepko 2004) with minor modifications. A DNA solution (6 μg/μl) was prepared by mixing pRho-DsRed and pRho-mRD3.V5-DsRed at a molar ratio of 1:4 in phosphate saline buffer with 0.1% v-v fast green. Even though pRho-mRD3.V5-DsRed expressed dsRed, we found the levels of expression too low for detection of the eye injected area at the fluorescence dissection scope. Therefore pRho-DsRed was coinjected with pRho-mRD3.V5-DsRed. Pups were injected the day they were born at the subretinal space, with 0.2–0.5 μl of DNA by using a Hamilton syringe with a blunt 30-gauge needle under a dissecting microscope (Zeiss KL1500LCD. Stemi2000, Germany). Tweezer-type electrodes were placed softly holding the head of the pup, and five 80 V square pulses of 50 ms duration with 950 ms intervals were applied using a CUY21 electroporator (Nepagene, Chiba, Japan). Electroporated eyes were processed at p20–p25 for immunofluorescence localization analysis as described above. Antibodies were anti-RetGC1 pAb and the anti-V5 mAb (#2F11F7, Invitrogen) by secondary antibodies α-rabbit Alexa Fluor 488 (Life Technologies) and α-mouse Alexa Fluor 647 (Life Technologies) both at 1:500 for 1.5 h at room temperature.

Images were acquired with a LEICA SP5 microscope using a 63 × 1.4 NA oil objective. The pixel and step sizes are 100 nm and 198 nm respectively providing an effective image volume of 131 μm × 131 μm × 9.5 μm. Two Hybrid detectors in photon counting mode and a photomultiplier tube (PMT) were used to acquire the different channels. The spectral configuration for the channel 1 used a 488 nm laser line and an emission window from 498 to 535 nm. The channel 2 used the 633 nm laser line and an emission window between 642 and 722 nm. Finally, the channel 3 used the 543 nm laser line with the emission window set between 551 and 616 nm.

6.3 Materials and methods for chapter 3

6.3.1 Label-free quantitative proteomic analysis of enriched phosphopeptides from dark- and light-adapted bovine retinas

Fresh calf eyes were obtained immediately postmortem and processed at the slaughterhouse premises. Upon collection, eyes were processed in a dark room by excising the cornea and submerging eyecups in chilled oxygenated Locke's buffer (10 mM Hepes, 20 mM $NaHCO_3$, 112.5 mM NaCl, 3.6 mM KCl, 2.4 mM $MgCl_2$, 1.2 mM $CaCl_2$, 0.1 mM EDTA and 10 mM glucose, pH 7.4) for 1 hr of dark-adaptation. Retinas were then excised under dim red light. Three retinas were kept for 5 min at room temperature in the dark; while three retinas were exposed to light of 2000 lux for 5 min. Following dark/light exposure retinas were homogenized in homogenization buffer (HB) (20 mM Hepes, 115 mM KCl, 10 mM NaCl, 10 mM $MgCl_2$, 50 mM NaF, 5 mM ß-glycerophosphate, 1 mM PMSF and complete protease inhibitor cocktail [Complete mini EDTA-free, Roche], pH 7.4). Retinal homogenates were kept at -80ºC until further analysis. Subsequently, a basic fractionation protocol was performed to obtain fractions corresponding to soluble, peripheral and membrane proteins from each sample. Sample preparation for mass spectrometry analysis involved in solution digestion (peripheral and supernatant samples) or Filter Aided Sample Prep (FASP) digestion (membrane samples) (Wiśniewski et al. 2009). For in soluble digestion, samples were reduced with dithiothreitol (1 hr, 37°C) and alkylated in the dark with iodoacetamide (30 min, 25ºC). Resulting protein extracts were diluted 1/3 with 200 mM NH4HCO3 and digested with LysC (#129-02541, Wako) overnight at 37ºC; and then diluted 1/2 and digested with trypsin (# V5113, Promega) for 8 hrs at 37°C. The peptide mix was acidified with formic acid and desalted with a MacroSpin C18 column (The Nest Group, Inc). For FASP digestion, samples were treated as previously described (Wiśniewski et al. 2009). Samples were reduced with dithiothreitol (5 min, 95°C); alkylated in the dark with iodoacetamide (30 min, 25 ºC) and digested with LysC (# 129-02541, Wako) overnight at 37ºC and with trypsin (# V5113, Promega) for 8 hrs at 37°C, as previously reported. Phosphopeptide enrichment was performed in each sample with the Pierce TiO_2 Phosphopeptide Enrichment kit (# 88301,Thermo Fisher Scientific).

Phosphopeptide mixes were analyzed in an Orbitrap Fusion Lumos mass spectrometer (Thermo Scientific, San Jose, CA, USA) coupled to an EasyLC (Thermo Scientific (Proxeon), Odense, Denmark). Peptides were directly loaded onto the analytical column and separated by reversed-phase chromatography using a 50-cm column with an inner diameter of 75 µm, packed with 2 µm C18 particles spectrometer (Thermo Scientific, San Jose, CA, USA). Chromatographic gradients started at 95% buffer A and 5% buffer B with a flow rate of 300 nl/min and gradually increased to 22% buffer

B in 79 min and then to 35% buffer B in 11 min. After each analysis, the column was washed for 10 min with 5% buffer A and 95% buffer B. Buffer A: 0.1% formic acid in water. Buffer B: 0.1% formic acid in acetonitrile.

The mass spectrometer was operated in DDA mode and full MS scans with 1 micro scans at resolution of 120.000 were used over a mass range of m/z 350-1500 with detection in the Orbitrap. Auto gain control (AGC) was set to 2E5 and dynamic exclusion to 60 sec. In each cycle of DDA analysis, following each survey scan Top Speed ions with charged 2 to 7 above a threshold ion count of $1e^4$ were selected for fragmentation at normalized collision energy of 28%. Fragment ion spectra produced via high-energy collision dissociation (HCD) were acquired in the Ion Trap, AGC was set to $3e^4$, isolation window of 1.6 m/z and a maximum injection time of 40 msec was used. All data were acquired with Xcalibur software v3.0.63.

6.3.2 Data Analysis

Proteome Discoverer software suite (v2.2, Thermo Fisher Scientific) and the Mascot search engine (v2.5, Matrix Science (2)) were used for peptide identification and quantification (Perkins et al. 1999). Samples were searched against the Uniprot proteome database corresponding to Bos Taurus (UP000009136), and a list of common contaminants (total entries 24,097), plus all the corresponding decoy entries. Trypsin was chosen as enzyme and a maximum of three miscleavages were allowed. Carbamidomethylation (C) was set as a fixed modification, whereas oxidation (M), phosphorylation (STY) and acetylation (N-terminal) were used as variable modifications. Searches were performed using a peptide tolerance of 7 ppm and a product ion tolerance of 0.5 Da, and identified phosphopeptides were filtered for FDR < 5 %. Phosphopeptides were quantified by extraction of its precursor areas using Skyline (version 4.2.0.19009). Light/dark fold change and p values were calculated for phosphopeptides present in two or more replicates of each condition.

6.3.3 *In situ* metabolic labeling

Eight six-week-old C57BL6 mice were dark-adapted overnight. Retinas were dissected under dim red light using a night vision dissecting scope, and placed in individual wells of two 12-well dishes –eight retinas per dish- in 600 µl of Locke's buffer (10mM Hepes, 20mM $NaHCO_3$, 112.5mM NaCl, 3.6mM KCl, 2.4mM $MgCl_2$, 1.2mM $CaCl_2$, 0.1mM EDTA, 10mM glucose, sodium succinate, sodium glutamate, vitamin and amino acid supplement, pH 7.4) containing 1 mCi/ml ^{32}P-orthophosphoric acid (9.000 Ci/mmol, NEX053010 Perkin Elmer, Waltham, MA, USA). Retinas were incubated for

90 min at 37°C in a 5% CO_2 incubator in the dark, to allow incorporation of the ^{32}P radionuclide into the ATP pool of retinal cells.

One multiwell dish was then placed over the bench at room temperature for 5 min in darkness (dark retinas); and the other was exposed to 2000 lux white light (light retinas) for 5 min. Pools of two retinas were homogenized in HB. Samples were then centrifuged at 14.000 rpm for 20 min, 4°C, to obtain supernatant and pellet fractions. Pellets were resuspended in HB with 1% TritonX100. Immunoprecipitation of IMPDH1 was carried out with 3 μg of anti-IMPDH1 pAb and 50 μl of Dynabeads-protein G (Thermo Scientific, Waltham, MA, USA). Samples were resolved by SDS-PAGE and transferred to nitrocellulose membranes, that were directly exposed to an X-ray film (AGFA Healthcare NV, Mortsel, Belgium) and subsequently immunoblotted for IMPDH1 using anti-IMPDH1 pAb 1:5000 followed by goat-anti Rabbit IREDye 800 (LI-COR, Lincoln, NE, USA) 1:5000. Bands visualized using an Odyssey Scan System (LI-COR). An immunoprecipitation control was carried with an anti-IgG isotype control (#02-6102, Thermo Fisher Scientific).

6.3.4 Isolectrofocusing separation of IMPDH1

^{32}P-labeled immunoprecipitated IMPDH1 from an *in situ* metabolic labeling procedure as described above was separated by isoelectrofocusing (IEF) to discern the differentially phosphorylated forms of the protein. For that, IMPDH1 immunoprecipitated samples were dissolved in IEF loading buffer (7M urea, 2M thiourea, 4% CHAPs, 40mM DTT, 2% IPG buffer). Samples were loaded into prehydrated pH-gradient IEF gel strips (18 cm linear gradient pH 3-10 DryStrips from GE Healthcare, Chicago, IL, USA), and run in an Ettan IPGphor3 IEF system (GE Healthcare, Chicago, IL, USA). Gel strips were incubated for 10m in transfer buffer (25 mM Tris base pH 8.3, 190 mM glycine, 0.2% SDS, 20% methanol) and proteins transferred to nitrocellulose membranes by capillary action. Membranes were first exposed to an X-ray film and subsequently immunoblotted for IMPDH1 as indicated above.

For isoelectric focusing analysis of IMPDH1 from retinas of living mice after dark/light adaptation, mice were dark-adapted for 16 hrs and exposed to 2000 lux bright light after pupil dilation for 5, 20 or 60 min. Retinas were dissected and homogenized in HB. Retinal homogenates were centrifuged at 13000 rpm for 20 min 4°C and supernatant fractions were kept. Protein was precipitated with 3 volumes of ice-chilled TCA-acetone buffer (13.3% w/v trichloroacetic acid in acetone, 20mM DTT), and samples were cooled at -20°C for 16 hrs, and centrifuged at 13200 rpm for 1 hr at 4°C. Protein pellets were washed in acetone, air-dried, resuspended in IEF buffer and resolved by IEF as described.

6.3.5 Cloning of HsIMPDH1 different spliced forms into pETEV and site-directed mutagenesis

Human IMPDH1 (1-514) ORF was obtained from a cDNA library and cloned into an *in house* modified pET15b expression vector (Alonso-García et al. 2009). A PCR-based strategy was used to insert NH2- and COOH- extra sequences to the ORF of the canonical protein, to generate the hIMPDH1 spliced retinal isoforms (1-546 and 1-595). All DNA constructs were corroborated by DNA sequencing.

Phosphomimetic mutants for enzymatic analysis were obtained by introducing mutations that created individual substitutions T159D, S160D, S416D, S477D into the pETEV15b_HsIMPDH1(546) vector; or in the pETEV15b_HsIMPDH1(514), using the QuickChange II Site-directed mutagenesis Kit (Agilent Technologies).

Phospho-knockout mutants for *in vitro* phosphorylation assays were obtained by introducing mutations that created triple substitutions that left only one phosphorylation site S160G/S416G/S477G (T159 only); T159G/S416G/S477G (S160 only); T159G/S160G/S477G (S416 only) and T159G/S160G/S416G (S477 only) into the pETEV15b_HsIMPDH1(546). A mutant was also generated with the 4 phosphorylation sites mutated to Gly (4KO mutant).

Blindness associated mutations R105W, N198K, R224P, D226N, V268I and H372P were introduced by site-directed mutagenesis in the pETEV15b_HsIMPDH1(546) vector.

Primers used for site-directed mutagenesis are listed (**Table 8**).

Site-directed mutagenesis was confirmed by sequencing both DNA strands in all generated constructs.

Table 8: Primers used for site-directed mutagenesis

Mutant	Fw/Rv	Sequence primer
S160D	Fw	5'-GGTGGGCATCGTCACCGACCGAGACATCGACTTT-3'
	Rv	5'-AAAGTCGATGTCTCGGTCGGTGACGATGCCCACC-3'
T159D/S160D	Fw	5'-GCAAGCTGGTGGGCATCGTCGACGACCGAGACATCGACTTTCTTG-3'
	Rv	5'-CAAGAAAGTCGATGTCTCGGTCGTCGACGATGCCCACCAGCTTGC-3'
S416D	Fw	5'-TACCGGGGCATGGGCGATCTGGATG-3'
	Rv	5'-CATCCAGATCGCCCATGCCCCGGTA-3'
S477D	Fw	5'-GGCCCGCAGCCTGGATGTCCTTCGGTCC-3'
	Rv	5'-GGACCGAAGGACATCCAGGCTGCGGGCC-3'
T159G	Fw	5'-TGGTGGGCATCGTCGGCTCCCGAGACATCG-3'
	Rv	5'-CGATGTCTCGGGAGCCGACGATGCCCACCA-3'
S160G	Fw	5'-GTGGGCATCGTCACCGGCCGAGACATCGACTT-3'
	Rv	5'-AAGTCGATGTCTCGGCCGGTGACGATGCCCAC-3'
T159G/S160G	Fw	5'-AGCTGGTGGGCATCGTCGGCGGCCGAGACATCGACTTTC-3'
	Rv	5'-GAAAGTCGATGTCTCGGCCGCCGACGATGCCCACCAGCT-3'
S416G	Fw	5'-CGGGGCATGGGCGGACTGGATGCCATGGAG-3'
	Rv	5'-CTCCATGGCATCCAGTCCGCCCATGCCCCG-3'
S477G	Fw	5'-GGCCCGCAGCCTGGGTGTCCTTCGGTCC-3'
	Rv	5'-GGACCGAAGGACACCCAGGCTGCGGGCC-3'
R105W	Fw	5'-CAGGCCAACGAGGTGTGGAAGGTCAAGAAGT-3'
	Rv	5'-ACTTCTTGACCTTCCACACCTCGTTGGCCTG-3'
N198K	Fw	5'-GTGACGTTGAAAGAGGCAAAGGAGATCCTGCAGCGTAGCA-3'
	Rv	5'-TGCTACGCTGCAGGATCTCCTTTGCCTCTTTCAACGTCAC-3'
R224P	Fw	5'-GCCATCATCGCCCCCACCGACCTGAAG-3'
	Rv	5'-CTTCAGGTCGGTGGGGGCGATGATGGC-3'
D226N	Fw	5'-ATCATCGCCCGCACCAACCTGAAGAAGAACC-3'
	Rv	5'-GGTTCTTCTTCAGGTTGGTGCGGGCGATGAT-3'
V268I	Fw	5'-CACCCAGGCGGGCATCGACGTCATAGT-3'
	Rv	5'-ACTATGACGTCGATGCCCGCCTGGGTG-3'
H372P	Fw	5'-CAGACCGTGGGACCCGTGGTCAAGGCC-3'
	Rv	5'-GGCCTTGACCACGGGTCCCACGGTCTG-3'

6.3.6 Purification of IMPDH1 enzymes

Human IMPDH1 enzymes were expressed in *Escherichia coli* strain BL21 (DE3) and purified by nickel-chelating affinity chromatography as described before (Krishnaiah 1975), and as described in methods for Chapter 1. His-tag was removed from the recombinant proteins for the GDP/GTP assays.

6.3.7 Enzymatic assays

IMPDH activity was studied by monitoring the increase in absorbance at 340nm upon reduction of NAD^+ at 32ºC, using 96-well microtiter plates. The reaction buffer was 100 mM Tris-HCl, 100 mM KCl, 2 mM DTT, pH 8.0. Final enzyme concentrations were set to 100 μgmL^{-1}, NAD^+ concentration was fixed at 0.5 mM and IMP concentration varied from 0.04 to 5 mM. Purine nucleotides were assayed at concentrations ranging from 0.09 to 6 mM. Free Mg^{2+} concentration was kept constant at 1 mM, as previously described (Buey et al. 2017). The experimental data were non-linearly fitted to the Michaelis-Menten equation of enzyme kinetics using the GraphPad Prism program (GraphPad software) in order to obtain the maximum apparent initial velocity (V_{max}^{app}) as a function of the nucleotide concentration. Normalized V_{max} values were calculated by dividing the V_{max}^{app} value in the presence of GTP/GDP nucleotides by V_{max} in the absence of nucleotides.

6.3.8 *In vitro* phosphorylation with PKC

For *in vitro* phosphorylation assays with PKC, 5 μg of recombinant protein HsIMPDH1(546) or its mutants were diluted in 12 μl of dilution buffer (TrisHCl pH 8, 500 mM KCl and 2 mM DTT), mixed with an equal volume of 2x kinase buffer (20 mM TrisHCl pH 7; 20 mM $MgCl_2$; 0.05 mM phorbol 12-myristate 13-acetate (PMA); 0.2 mM $CaCl_2$; 0.2 mM ATP); 1 μl of ^{32}P-ATP γ 3000 Ci/mmol (Perkin Elmer, Boston, Masachusetts, USA) and 1 μl of recombinant hPKC α (100ng/μl, Enzo Life Sciences, Farmingdale, NY, USA). Samples were incubated for 15 min at 30ºC, and reactions were stopped by addition of 4x SDS loading buffer. Sample fractions corresponding to 2.5 μg of HsIMPDH1(546) were resolved by 12% SDS-PAGE, and proteins were transferred to 0.2 μm nitrocellulose membranes (Bio-rad). The membranes were first exposed to X-ray films (AGFA Healthcare NV, Mortsel, Belgium) for 2 hrs; and subsequently immunoblotted for IMPDH1. Membranes were scanned at an Odyssey Scan System (LI-COR) and quantified with the Fiji (ImageJ) software.

6.3.9 Nucleotide determination in retinal extracts by HPLC

GMP, GDP, GTP, AMP and ATP levels were analytically measured in perchloric acid murine retinal extracts by ion-pairing high-performance liquid chromatography (HPLC). For *in situ* experiments, 6-8 week old C57Bl mice were dark-adapted for 16 hrs and their retinas were dissected under dim red light. Retinas were placed in DMEM high glucose and either kept in the dark for 5 min at room temperature, or exposed to 2000 lux white light. Immediately after the 5 min dark/light exposure retinas were washed with ice-cold PBS and pools of four retinas were homogenized in 120 μl of 1.2 M perchloric acid in PBS. Samples were centrifuged at 16000 rpm for 40 min at 4ºC. Deproteinized supernatants were transferred to new tubes, extracted with 1 vol of HPLC-grade chloroform, neutralized, clarified and filtered through 0.22 μm filters (Nanosep MF 0.22 μm, Pall, Westborough, Massachusetts, USA). Samples were kept at -80ºC until HPLC analysis. For the *in situ* experiment to test the effect of PKC inhibition on the dark/light levels of guanine nucleotides, bisindolylmaleimide I (BM) was added to the medium at 50 nM concentration, and the dark-adapted retinas were incubated in a 5% CO_2 incubator for 30 min, protected from light. Retinas were then kept in the dark for 5 min, or exposed to 2000 lux white light for 5 min and processed as above. For the *in vivo* experiment, retinas were obtained from 16 hrs dark-adapted mice or from mice exposed to 2000 lux white light for 4 hrs with pupils dilated, and processed the same way.

HPLC analysis was performed as previously described (Di Pierro et al. 1995), with minor modifications. A BRISA LC2 C18, 250 x 4.6mm, 5 μm particle size column (Teknokroma, Sant Cugat del Vallés, Spain) was equilibrated with mobile phase eluent A (10 mM tetrabuthylammonium hydroxide, 10 mM KH_2PO_4, 0.25% v:v methanol, adjusted to pH 7.00 with HCl). A linear gradient was formed with eluent B (2.8 mM tetrabuthylammonium hydroxide, 100 mM KH_2PO_4, 30% v:v methanol, adjusted to pH 5.5 with HCl) as follows: 5 min 100% eluent A; 5 min 90% eluent A; 5 min 70% eluent A; 10 min 63% eluent A; 5 min 55% eluent A; 10 min 45% eluent A; 20 min 25% eluent A; 20 min 0% eluent A (100% eluent B). A Waters Acquity HPLC with a 210nm-380nm diode array detector was used, at a flow rate of 0.8 ml/min and constant temperature of 40ºC. Injector temperature was 10ºC. Standard stock solutions (GMP, GDP, GTP, AMP, ATP) were diluted in 0.1 M KH_2PO_4. Nucleotide concentrations in each sample were determined by measuring the area of the corresponding peak and comparing it to the peak area of the corresponding standard.

6.3.10 *In vivo* metabolic flux analysis by injection of a stable isotope of Gly

A group of 6 week-old C57Bl mice was dark-adapted overnight. They were anesthesized with an intraperitoneal injection of ketamine (70 mg/kg; Ketalar, Parke-Davis, Wellington, New Zealand) and xylazine (7 mg/kg; Rompun, Bayer, Leverkusen, Germany) in saline solution (NaCl 0.9%), and injected intravitreally with 1 µl of a 20 mM solution of 13C2,15N-Glycine (#CNLM-1673-H-0.5, Cambridge Isotope Laboratories) in phosphate saline buffer. The injection was performed under dim red light. Mice were kept in darkness, or immediately transferred to a bright light setting (2000 lux white light) for 4 hrs. Mouse recovery from anesthesia in the dark or light setting was promoted by keeping the mouse body temperature with a heating pad. After 4 hrs, retinas were collected, frozen in dry ice and kept at -80ºC until mass spectrometry analysis. Mass spectrometry analysis was performed as previously described (Roig et al. 2017).

6.3.11 Electroretinogram analysis

A group of four mice was used for benzamide (BZM) injection, a group of seven mice for mycophenolate mofetyl (MMF) injection, and a group of four mice for bisindolylmaleimide I (BM) injection. Dark-adapted (>12 hrs) animals were anaesthetized with an intraperitoneal injection as described above. For each mouse the right eye was injected with the inhibitor (BZM, MMF or BM), and the left eye with the physiological saline buffer used for drug dilution. MMF was injected intravitreously to an effective concentration of 200 nM (1 µl injection of 1 µM stock); BZM was injected to an effective concentration of 80 µM (1 µl injection of 400 µM stock); and BM was injected to an effective concentration of 200 nM (1 µl injection of 1 µM stock). Two corneal electrodes were used to record simultaneous ERGs from both eyes (Burian-Allen, Hansen Ophthalmic Development Lab, Coralville, IA). Electrodes were placed in the visual axis 2-3 mm from the cornea, with a drop of 2% methyl-cellulose (Methocel, Ciba Vision, Hetlingen, Switzerland) between corneas and electrodes. Mice were maintained for >10 min in absolute darkness before the recordings, initiated 20 min after drug injection (30 min for BM treated mice). Mouse temperature during the recording was maintained at 37 °C with a heating pad (Hot-Cold, Pelton Shepherd Industries, Stockton, CA). Full-field flash ERG was performed, with the retina illuminated with a Ganzfeld dome. To test the effect of IMPDH inhibitors on rod mass recovery after a saturating light flash, we applied the paired-flash paradigm (Lyubarsky and Pugh 1996), by triggering a test flash (3 $Cd \cdot s/m^2$) followed by a probe flash of identical intensity at increasing inter-stimulus (IST) intervals: 400, 600, 800, 1200, 1500 and 2000 ms (double flash). The rate of recovery for the a- and b-waves at each IST was obtained by calculating the ratio of a- or b-wave of the probe flash to the a- or b-wave of the test flash. Cone

responses were recorded following 5 min of light-adaptation with background white light (50 Cd/m^2) to a flash light of 3 $Cd \cdot s/m^2$. Recorded electrophysiological responses were amplified; filtered (CP511 AC amplifier; Grass Instruments, Quincy, MA), and digitalized (ADInstruments Ltd, Oxfordshire, UK). The recording process was controlled with Scope version 3.8.1 software (Power Lab, ADInstruments Ltd). The stimulation protocols were designed according to the International Society for Clinical Electrophysiology of Vision.

6.3.12 IMPDH1 immunofluorescence localization in retinal sections

For the analysis of spicula formation in response to mycophenolic acid (MPA) treatment, retinas from 16 hrs dark-adapted mice were dissected under dim red light and placed in DMEM-high glucose in the presence or absence of 10 μM MPA, protected from light in a 5% CO2 incubator for 1 or 2 hrs. For analysis of the effect of living mice exposure to constant bright light, 16 hrs dark-adapted mice were exposed to 2000 lux bright light for 20 min, 2 hrs or 4 hrs after pupil dilation with a drop of phenylephrine and tropicamide.

For 15 d constant-dark or 15 d constant-light rearing, mice were either housed in a dark cabinet or in a set of constant bright light exposure (2000lux) for 15 days.

For studying the reversibility of IMPDH1 aggregates, mice were exposed to bright light (2000 lux) for 72h and then divided in two groups; first group was processed immediately after 72h bright light exposure; and the second group was kept in dark for 16 hr before processing.

The obtention of retinal sections for immunofluorescence experiments and antigen retrieval protocols have been described in methods for chapter 1. For IMPDH1 localization primary antibodies were anti IMPDH1 (1:250), anti-Rhodopsin 1D4 (1:15000) and PNA-647 (1:40) (# L32460, Thermo Fisher Scientific) incubated over night at 4ºC. Secondary antibodies were anti-rabbit Alexa Fluor 488 (#A-11034, Thermo Fisher Scientific) 1:500 and anti-mouse Alexa Fluor 555 (#A-32727, Thermo Fisher Scientific) 1:500 incubated for 2h at room temperature. Sections were mounted with Mowiol (Calbiochem).

Confocal microscopy images were acquired with a confocal laser scanning microscope Leica SP5 equipped with two HyD detectors. The spectral bands were set to 491-546 nm and 566-663 nm for 488 nm and 555 nm, respectively. The used objective was a HC PL APO 100x/1.4NA Oil and the samples were mounted on type 1.5 coverglasses (170 mm thick). The stacks covered approximately 2 μm in the z-axis with a 0.13 μm step size. The settings of the image acquisition provided a pixel size of about 74.8 nm x 74.8 nm.

The image analysis of the immunofluorescence data was performed using Fiji (ImageJ). In order to maximize the signal to noise ratio, we used the average projection of groups of 3 planes from large z-stacks. For the particle quantification, we selected a region of interest (e.g. magnified frames of rod outer segment layer) and we applied a light Gaussian filter (radius of one pixel). To determine the size of the areas with concentration of fluorescence we selected the pixels from the image that had a signal beyond a certain value. This value was determined from the statistics of intensity, taking only the 8% of the brighter pixels. Then, the areas of the spots were analyzed by using the plugin "analyze particles" from Fiji. Counted spots were plotted according to its size and the statistical analysis were performed with Graph Pad Prism (unpaired t-tests).

7. BIBLIOGRAPHY

BIBLIOGRAPHY

Aboshiha, Jonathan, Adam M. Dubis, Jacqueline Van Der Spuy, Koji M. Nishiguchi, Edward W. Cheeseman, Carmen Ayuso, Miriam Ehrenberg, Francesca Simonelli, James W. Bainbridge, and Michel Michaelides. 2015. "Preserved Outer Retina in AIPL1 Leber's Congenital Amaurosis: Implications for Gene Therapy." In *Ophthalmology*, 122:862–64. Elsevier Inc. https://doi.org/10.1016/j.ophtha.2014.11.019.

Abu-Safieh, Leen, May Alrashed, Shamsa Anazi, Hisham Alkuraya, Arif O. Khan, Mohammed Al-Owain, Jawahir Al-Zahrani, et al. 2013. "Autozygome-Guided Exome Sequencing in Retinal Dystrophy Patients Reveals Pathogenetic Mutations and Novel Candidate Disease Genes." *Genome Research* 23 (2): 236–47. https://doi.org/10.1101/gr.144105.112.

Agrawal, Smriti A., Thomas Burgoyne, Aiden Eblimit, James Bellingham, David A. Parfitt, Amelia Lane, Ralph Nichols, et al. 2017. "REEP6 Deficiency Leads to Retinal Degeneration through Disruption of ER Homeostasis and Protein Trafficking." *Human Molecular Genetics* 26 (14): 2667–77. https://doi.org/10.1093/hmg/ddx149.

Aherne, A., Avril Kennan, Paul F Kenna, Niamh McNally, David G Lloyd, Ian L Alberts, Anna-Sophia Kiang, et al. 2004. "On the Molecular Pathology of Neurodegeneration in IMPDH1-Based Retinitis Pigmentosa." *Human Molecular Genetics* 13 (6): 641–50. https://doi.org/10.1093/hmg/ddh061.

Aldahmesh, Mohammed A, Mohammed Al-Owain, Faisal Alqahtani, Salwa Hazzaa, and Fowzan S Alkuraya. 2010. "A Null Mutation in CABP4 Causes Leber's Congenital Amaurosis-like Phenotype." *Molecular Vision* 16 (February): 207–12. http://www.ncbi.nlm.nih.gov/pubmed/20157620.

Alonso-García, Noelia, Alvaro Inglés-Prieto, Arnoud Sonnenberg, and Jose M de Pereda. 2009. "Structure of the Calx-Beta Domain of the Integrin Beta4 Subunit: Insights into Function and Cation-Independent Stability." *Acta Crystallographica. Section D, Biological Crystallography* 65 (Pt 8): 858–71. https://doi.org/10.1107/S0907444909018745.

Anthony, Sajitha A., Anika L. Burrell, Matthew C. Johnson, Krisna C. Duong-Ly, Yin-Ming Kuo, Jacqueline C. Simonet, Peter Michener, Andrew Andrews, Justin M. Kollman, and Jeffrey R. Peterson. 2017. "Reconstituted IMPDH Polymers Accommodate Both Catalytically Active and Inactive Conformations." Edited by Diane Barber. *Molecular Biology of the Cell* 28 (20): 2600–2608. https://doi.org/10.1091/mbc.e17-04-0263.

Aravindan, Sheeja, Dinesh Babu Somasundaram, Kwok Ling Kam, Karthikeyan Subramanian, Zhongxin Yu, Terence S Herman, Kar-Ming Fung, and Natarajan Aravindan. 2017. "Retinal Degeneration Protein 3 (RD3) in Normal Human Tissues: Novel Insights." *Scientific Reports* 7 (1): 13154. https://doi.org/10.1038/s41598-017-13337-9.

Arno, Gavin, Smriti A. Agrawal, Aiden Eblimit, James Bellingham, Mingchu Xu, Feng Wang, Christina Chakarova, et al. 2016. "Mutations in REEP6 Cause Autosomal-Recessive Retinitis Pigmentosa." *American Journal of Human Genetics* 99 (6): 1305–15. https://doi.org/10.1016/j.ajhg.2016.10.008.

Arshavsky, Vadim Y., Trevor D. Lamb, and Edward N. Pugh. 2002. "G Proteins and Phototransduction." *Annual Review of Physiology* 64 (1): 153–87. https://doi.org/10.1146/annurev.physiol.64.082701.102229.

Aughey, Gabriel N., and Ji-Long Liu. 2016. "Metabolic Regulation via Enzyme Filamentation." *Critical Reviews in Biochemistry and Molecular Biology* 51 (4): 282–93. https://doi.org/10.3109/10409238.2016.1172555.

Azadi, Seifollah, Laurie L. Molday, and Robert S. Molday. 2010. "RD3, the Protein Associated with Leber Congenital Amaurosis Type 12, Is Required for Guanylate Cyclase Trafficking in Photoreceptor Cells." *Proceedings of the National Academy of Sciences* 107 (49): 21158–63. https://doi.org/10.1073/pnas.1010460107.

Baehr, Wolfgang, Sukanya Karan, Tadao Maeda, Dong Gen Luo, Sha Li, J. Darin Bronson, Carl B. Watt, King Wai Yau, Jeanne M. Frederick, and Krzysztof Palczewski. 2007b. "The Function of Guanylate Cyclase 1 and Guanylate Cyclase 2 in Rod and Cone Photoreceptors." *Journal of Biological Chemistry* 282 (12): 8837–47. https://doi.org/10.1074/jbc.M610369200.

Barbehenn, E K, K L Klotz, D M Noelker, R Nelson, G J Chader, and J V Passonneau. 1986. "In Vivo CGMP Levels in Frog Photoreceptor Cells as a Function of Light Exposure." *Experimental Eye Research* 43 (5): 729–38. https://doi.org/10.1016/s0014-4835(86)80004-5.

Berger, S J, G W DeVries, J G Carter, D W Schulz, P N Passonneau, O H Lowry, and J A Ferrendelli. 1980. "The Distribution of the Components of the Cyclic GMP Cycle in Retina." *The Journal of Biological Chemistry* 255 (7): 3128–33. http://www.ncbi.nlm.nih.gov/pubmed/6102093.

Bhagavan, N V, and Chung-Eun Ha. 2015. "Chapter 32 - Endocrine Metabolism V: Reproductive System." In *Essentials of Medical Biochemistry (Second Edition)*, edited by N V Bhagavan and Chung-Eun Ha, 589–606. Academic Press. https://doi.org/https://doi.org/10.1016/B978-0-12-416687-5.00032-4.

Biernbaum, M S, and M D Bownds. 1979. "Influence of Light and Calcium on Guanosine 5'-Triphosphate in Isolated Frog Rod Outer Segments." *The Journal of General Physiology* 74 (6): 649–69. https://doi.org/10.1085/jgp.74.6.649.

Blanks, J. C., and L. V. Johnson. 1984. "Specific Binding of Peanut Lectin to a Class of Retinal Photoreceptor Cells. A Species Comparison." *Investigative Ophthalmology and Visual Science* 25 (5): 546–57.

Bourne, Rupert R A, Gretchen A Stevens, Richard A White, Jennifer L Smith, Seth R Flaxman, Holly Price, Jost B Jonas, et al. 2013. "Causes of Vision Loss Worldwide, 1990-2010: A Systematic

Analysis." *The Lancet. Global Health* 1 (6): e339-49. https://doi.org/10.1016/S2214-109X(13)70113-X.

Bowes, Cathy, Tiansen Li, Michael Danciger, Leslie C. Baxter, Meredithe L. Applebury, and Debora B. Farber. 1990. "Retinal Degeneration in the Rd Mouse Is Caused by a Defect in the β Subunit of Rod CGMP-Phosphodiesterase." *Nature* 347 (6294): 677–80. https://doi.org/10.1038/347677a0.

Bowne, Sara J, Qin Liu, Lori S Sullivan, Jingya Zhu, Catherine J Spellicy, Catherine Bowes Rickman, Eric A Pierce, and Stephen P Daiger. 2006. "Why Do Mutations in the Ubiquitously Expressed Housekeeping Gene IMPDH1 Cause Retina-Specific Photoreceptor Degeneration?" *Investigative Ophthalmology & Visual Science* 47 (9): 3754–65. https://doi.org/10.1167/iovs.06-0207.

Bowne, Sara J, Lori S Sullivan, Susan H Blanton, Constance L Cepko, Seth Blackshaw, David G Birch, Dianna Hughbanks-Wheaton, John R Heckenlively, and Stephen P Daiger. 2002. "Mutations in the Inosine Monophosphate Dehydrogenase 1 Gene (IMPDH1) Cause the RP10 Form of Autosomal Dominant Retinitis Pigmentosa." *Human Molecular Genetics* 11 (5): 559–68.

Bowne, Sara J, Lori S Sullivan, Sarah E Mortimer, Lizbeth Hedstrom, Jingya Zhu, Catherine J Spellicy, Anisa I Gire, et al. 2006. "Spectrum and Frequency of Mutations in IMPDH1 Associated with Autosomal Dominant Retinitis Pigmentosa and Leber Congenital Amaurosis." *Investigative Ophthalmology & Visual Science* 47 (1): 34–42. https://doi.org/10.1167/iovs.05-0868.

Boycott, B B. 1988. "Horizontal Cells of Mammalian Retinae." *Neuroscience Research. Supplement : The Official Journal of the Japan Neuroscience Society* 8: S97-111. http://www.ncbi.nlm.nih.gov/pubmed/3068592.

Buey, Rubén M., David Fernández-Justel, Íñigo Marcos-Alcalde, Graeme Winter, Paulino Gómez-Puertas, José María de Pereda, and José Luis Revuelta. 2017a. "A Nucleotide-Controlled Conformational Switch Modulates the Activity of Eukaryotic IMP Dehydrogenases." *Scientific Reports* 7 (1): 2648. https://doi.org/10.1038/s41598-017-02805-x.

Buey, Rubén M., Rodrigo Ledesma-Amaro, Adrián Velázquez-Campoy, Mónica Balsera, Mónica Chagoyen, José M. de Pereda, and José L. Revuelta. 2015. "Guanine Nucleotide Binding to the Bateman Domain Mediates the Allosteric Inhibition of Eukaryotic IMP Dehydrogenases." *Nature Communications* 6 (1): 8923. https://doi.org/10.1038/ncomms9923.

Burns, Marie E., and Vadim Y. Arshavsky. 2005. "Beyond Counting Photons: Trials and Trends in Vertebrate Visual Transduction." *Neuron*. https://doi.org/10.1016/j.neuron.2005.10.014.

Burns, Marie E, Ana Mendez, Jeannie Chen, and Denis A Baylor. 2002a. "Dynamics of Cyclic GMP Synthesis in Retinal Rods." *Neuron* 36 (1): 81–91. https://doi.org/10.1016/s0896-6273(02)00911-x.

Butler, Michael R., Hongwei Ma, Fan Yang, Joshua Belcher, Yun Zheng Le, Katsuhiko Mikoshiba,

Martin Biel, et al. 2017. "Endoplasmic Reticulum (ER) Ca 2+ -Channel Activity Contributes to ER Stress and Cone Death in Cyclic Nucleotide-Gated Channel Deficiency." *Journal of Biological Chemistry* 292 (27): 11189–205. https://doi.org/10.1074/jbc.M117.782326.

Calise, S. John, Wendy C. Carcamo, Claire Krueger, Joyce D. Yin, Daniel L. Purich, and Edward K.L. Chan. 2014. "Glutamine Deprivation Initiates Reversible Assembly of Mammalian Rods and Rings." *Cellular and Molecular Life Sciences* 71 (15): 2963–73. https://doi.org/10.1007/s00018-014-1567-6.

Calise, S John, Daniel L Purich, Thuy Nguyen, Dania A Saleem, Claire Krueger, Joyce D Yin, and Edward K L Chan. 2016. "'Rod and Ring' Formation from IMP Dehydrogenase Is Regulated through the One-Carbon Metabolic Pathway." *Journal of Cell Science* 129 (15): 3042–52. https://doi.org/10.1242/jcs.183400.

Carcamo, Wendy C, S John Calise, Carlos A von Mühlen, Minoru Satoh, and Edward K L Chan. 2014. "Molecular Cell Biology and Immunobiology of Mammalian Rod/Ring Structures." *International Review of Cell and Molecular Biology* 308: 35–74. https://doi.org/10.1016/B978-0-12-800097-7.00002-6.

Castro-Miró, Marta De, Esther Pomares, Laura Lorés-Motta, Raul Tonda, Joaquín Dopazo, Gemma Marfany, and Roser Gonzàlez-Duarte. 2014. "Combined Genetic and High-Throughput Strategies for Molecular Diagnosis of Inherited Retinal Dystrophies." *PLoS ONE* 9 (2). https://doi.org/10.1371/journal.pone.0088410.

Chang, Bo, John R. Heckenlively, Norman L. Hawes, and Thomas H. Roderick. 1993. "New Mouse Primary Retinal Degeneration (Rd-3)." *Genomics* 16 (1): 45–49. https://doi.org/10.1006/geno.1993.1138.

Chang, Chia-Chun, Wei-Cheng Lin, Li-Mei Pai, Hsuan-Shu Lee, Shinn-Chih Wu, Shih-Torng Ding, Ji-Long Liu, and Li-Ying Sung. 2015a. "Cytoophidium Assembly Reflects Upregulation of IMPDH Activity." *Journal of Cell Science* 128 (19): 3550–55. https://doi.org/10.1242/jcs.175265.

Chen, C K, J Inglese, R J Lefkowitz, and J B Hurley. 1995. "Ca(2+)-Dependent Interaction of Recoverin with Rhodopsin Kinase." *The Journal of Biological Chemistry* 270 (30): 18060–66. https://doi.org/10.1074/jbc.270.30.18060.

Chen, Chunhe, Kei Nakatani, and Yiannis Koutalos. 2003. "Free Magnesium Concentration in Salamander Photoreceptor Outer Segments." *Journal of Physiology* 553 (1): 125–35. https://doi.org/10.1113/jphysiol.2003.053280.

Chen, T Y, M Illing, L L Molday, Y T Hsu, K W Yau, and R S Molday. 1994. "Subunit 2 (or Beta) of Retinal Rod CGMP-Gated Cation Channel Is a Component of the 240-KDa Channel-Associated Protein and Mediates Ca(2+)-Calmodulin Modulation." *Proceedings of the National Academy of Sciences of the United States of America* 91 (24): 11757–61. https://doi.org/10.1073/pnas.91.24.11757.

Cideciyan, Artur V., Xinyu Zhao, Lori Nielsen, Shahrokh C. Khani, Samuel G. Jacobson, and Krzysztof Palczewski. 1998. "Null Mutation in the Rhodopsin Kinase Gene Slows Recovery Kinetics of Rod and Cone Phototransduction in Man." *Proceedings of the National Academy of Sciences of the United States of America* 95 (1): 328–33. https://doi.org/10.1073/pnas.95.1.328.

Curcio, Christine A., Kenneth R. Sloan, Robert E. Kalina, and Anita E. Hendrickson. 1990. "Human Photoreceptor Topography." *Journal of Comparative Neurology* 292 (4): 497–523. https://doi.org/10.1002/cne.902920402.

Danciger, Michael, Diego Ogando, Haidong Yang, Michael T. Matthes, Nicole Yu, Kelly Ahern, Douglas Yasumura, Robert W. Williams, and Matthew M. LaVail. 2008. "Genetic Modifiers of Retinal Degeneration in the *Rd3* Mouse." *Investigative Opthalmology & Visual Science* 49 (7): 2863. https://doi.org/10.1167/iovs.08-1715.

Dizhoor, Alexander M., Elena V. Olshevskaya, and Igor V. Peshenko. 2010. "Mg2+/Ca2+ Cation Binding Cycle of Guanylyl Cyclase Activating Proteins (GCAPs): Role in Regulation of Photoreceptor Guanylyl Cyclase." *Molecular and Cellular Biochemistry* 334 (1–2): 117–24. https://doi.org/10.1007/s11010-009-0328-6.

Dizhoor, Alexander M., Elena V. Olshevskaya, and Igor V. Peshenko. 2019. "Retinal Guanylyl Cyclase Activation by Calcium Sensor Proteins Mediates Photoreceptor Degeneration in an *Rd3* Mouse Model of Congenital Human Blindness." *Journal of Biological Chemistry* 294 (37): 13729–39. https://doi.org/10.1074/jbc.RA119.009948.

Dryja, T. P., L. B. Hahn, T. Reboul, and B. Arnaud. 1996. "Missense Mutation in the Gene Encoding the α Subunit of Rod Transducin in the Nougaret Form of Congenital Stationary Night Blindness." *Nature Genetics* 13 (3): 358–60. https://doi.org/10.1038/ng0796-358.

Dryja, T P, D E Rucinski, S H Chen, and E L Berson. 1999. "Frequency of Mutations in the Gene Encoding the Alpha Subunit of Rod CGMP-Phosphodiesterase in Autosomal Recessive Retinitis Pigmentosa." *Investigative Ophthalmology & Visual Science* 40 (8): 1859–65. http://www.ncbi.nlm.nih.gov/pubmed/10393062.

Du, Jianhai, Austin Rountree, Whitney M Cleghorn, Laura Contreras, Ken J Lindsay, Martin Sadilek, Haiwei Gu, et al. 2016. "Phototransduction Influences Metabolic Flux and Nucleotide Metabolism in Mouse Retina." *The Journal of Biological Chemistry* 291 (9): 4698–4710. https://doi.org/10.1074/jbc.M115.698985.

Duong-Ly, Krisna C, Yin-Ming Kuo, Matthew C Johnson, Joy M Cote, Justin M Kollman, Jonathan Soboloff, Glenn F Rall, Andrew J Andrews, and Jeffrey R Peterson. 2018. "T Cell Activation Triggers Reversible Inosine-5'-Monophosphate Dehydrogenase Assembly." https://doi.org/10.1242/jcs.223289.

Essen, David C Van. n.d. "Organization of Visual Areas in Macaque and Human Cerebral Cortex."

Accessed October 8, 2019. http://brainmap.wustl.edu/sums/sums-.

Estrada-Cuzcano, Alejandro, Robert K Koenekoop, Frauke Coppieters, Susanne Kohl, Irma Lopez, Rob W J Collin, Elfride B W De Baere, et al. 2011. "IQCB1 Mutations in Patients with Leber Congenital Amaurosis." *Investigative Ophthalmology & Visual Science* 52 (2): 834–39. https://doi.org/10.1167/iovs.10-5221.

Fain, Gordon L. 2006. "Why Photoreceptors Die (and Why They Don't)." *BioEssays : News and Reviews in Molecular, Cellular and Developmental Biology* 28 (4): 344–54. https://doi.org/10.1002/bies.20382.

Farber, D B, J S Danciger, and G Aguirre. 1992. "The Beta Subunit of Cyclic GMP Phosphodiesterase MRNA Is Deficient in Canine Rod-Cone Dysplasia 1." *Neuron* 9 (2): 349–56. https://doi.org/10.1016/0896-6273(92)90173-b.

Farber, Debora B., and Richard N. Lolley. 1974. "Cyclic Guanosine Monophosphate: Elevation in Degenerating Photoreceptor Cells of the C3H Mouse Retina." *Science* 186 (4162): 449–51. https://doi.org/10.1126/science.186.4162.449.

Fernández-Justel, David, Rafael Núñez, Jaime Martín-Benito, David Jimeno, Adrián González-López, Eva María Soriano, José Luis Revuelta, and Rubén M. Buey. 2019. "A Nucleotide-Dependent Conformational Switch Controls the Polymerization of Human IMP Dehydrogenases to Modulate Their Catalytic Activity." *Journal of Molecular Biology*, January. https://doi.org/10.1016/j.jmb.2019.01.020.

Ferreira, Amanda Petrina Scotá, Alexandre Cassago, Kaliandra de Almeida Gonçalves, Marília Meira Dias, Douglas Adamoski, Carolline Fernanda Rodrigues Ascenção, Rodrigo Vargas Honorato, et al. 2013. "Active Glutaminase C Self-Assembles into a Supratetrameric Oligomer That Can Be Disrupted by an Allosteric Inhibitor." *The Journal of Biological Chemistry* 288 (39): 28009–20. https://doi.org/10.1074/jbc.M113.501346.

Ferri, K F, and G Kroemer. 2001. "Organelle-Specific Initiation of Cell Death Pathways." *Nature Cell Biology* 3 (11): E255-63. https://doi.org/10.1038/ncb1101-e255.

Festing, M.F.W. n.d. "Inbred Strains in Biomedical Research - Michael F. W. Festing - Google Libros." Accessed January 14, 2020. https://books.google.es/books?hl=es&lr=&id=GDFdDwAAQBAJ&oi=fnd&pg=PP7&ots=ZT7B3zetMd&sig=XPwpUqdd3fLpneiWF5behSZZyPE&redir_esc=y#v=onepage&q&f=false.

Friedman, James S., Bo Chang, Chitra Kannabiran, Christina Chakarova, Hardeep P. Singh, Subhadra Jalali, Norman L. Hawes, et al. 2006. "Premature Truncation of a Novel Protein, RD3, Exhibiting Subnuclear Localization Is Associated with Retinal Degeneration." *American Journal of Human Genetics* 79 (6): 1059–70. https://doi.org/10.1086/510021.

Fuchs, S, M Nakazawa, M Maw, M Tamai, Y Oguchi, and A Gal. 1995. "A Homozygous 1-Base Pair

Deletion in the Arrestin Gene Is a Frequent Cause of Oguchi Disease in Japanese." *Nature Genetics* 10 (3): 360–62. https://doi.org/10.1038/ng0795-360.

Gamm, D. M., L. K. Barthel, P. A. Raymond, and M. D. Uhler. 2000. "Localization of CGMP-Dependent Protein Kinase Isoforms in Mouse Eye." *Investigative Ophthalmology and Visual Science* 41 (9): 2766–73.

Gan, Lu, Gregory A Petsko, and Lizbeth Hedstrom. 2002. "Crystal Structure of a Ternary Complex of Tritrichomonas Foetus Inosine 5'-Monophosphate Dehydrogenase: NAD+ Orients the Active Site Loop for Catalysis." *Biochemistry* 41 (44): 13309–17. https://doi.org/10.1021/bi0203785.

Granovsky, A E, and N O Artemyev. 2001. "Partial Reconstitution of Photoreceptor CGMP Phosphodiesterase Characteristics in CGMP Phosphodiesterase-5." *The Journal of Biological Chemistry* 276 (24): 21698–703. https://doi.org/10.1074/jbc.M100626200.

Grau, Tanja, Nikolai O. Artemyev, Thomas Rosenberg, Hélène Dollfus, Olav H. Haugen, E. Cumhur Sener, Bernhard Jurklies, et al. 2011. "Decreased Catalytic Activity and Altered Activation Properties of PDE6C Mutants Associated with Autosomal Recessive Achromatopsia." *Human Molecular Genetics* 20 (4): 719–30. https://doi.org/10.1093/hmg/ddq517.

Gregory-Evans, K, R E Kelsell, C Y Gregory-Evans, S M Downes, F W Fitzke, G E Holder, M Simunovic, et al. 2000. "Autosomal Dominant Cone-Rod Retinal Dystrophy (CORD6) from Heterozygous Mutation of GUCY2D, Which Encodes Retinal Guanylate Cyclase." *Ophthalmology* 107 (1): 55–61. https://doi.org/10.1016/s0161-6420(99)00038-x.

Grover, Sandeep, Gerald A Fishman, and Edwin M Stone. 2004. "A Novel IMPDH1 Mutation (Arg231Pro) in a Family with a Severe Form of Autosomal Dominant Retinitis Pigmentosa." *Ophthalmology* 111 (10): 1910–16. https://doi.org/10.1016/j.ophtha.2004.03.039.

Gurevich, V V, and Jeffrey L Benovic. 1993. "Visual Arrestin Interaction with Rhodopsin." *The Journal of Biological Chemistry* 268 (16): 11628–38.

Hagins, W. A., R. D. Penn, and S. Yoshikami. 1970. "Dark Current and Photocurrent in Retinal Rods." *Biophysical Journal* 10 (5): 380–412. https://doi.org/10.1016/S0006-3495(70)86308-1.

Hardie, D Grahame. 2011. "AMP-Activated Protein Kinase: An Energy Sensor That Regulates All Aspects of Cell Function." *Genes & Development* 25 (18): 1895–1908. https://doi.org/10.1101/gad.17420111.

Harper, D. B. 1977. "Microbial Metabolism of Aromatic Nitriles. Enzymology of C-N Cleavage by Nocardia Sp. (Rhodochrous Group) N.C.I.B. 11216." *Biochemical Journal* 165 (2): 309–19. https://doi.org/10.1042/bj1650309.

Heckenlively, John R., Bo Chang, Chen Peng, Norman L. Hawes, and Thomas H. Roderick. 1993. "Variable Expressivity of Rd-3 Retinal Degeneration Dependent on Background Strain." In

Retinal Degeneration, 273–80. Springer US. https://doi.org/10.1007/978-1-4615-2974-3_27.

Hedstrom, Lizbeth. 2008. "IMP Dehydrogenase-Linked Retinitis Pigmentosa." *Nucleosides, Nucleotides and Nucleic Acids* 27 (6–7): 839–49. https://doi.org/10.1080/15257770802146486.

Hedstrom, Lizbeth. 2009. "IMP Dehydrogenase: Structure, Mechanism, and Inhibition." *Chemical Reviews* 109 (7): 2903–28. https://doi.org/10.1021/cr900021w.

Henderson, Robert H, Kathleen A Williamson, Joanna S Kennedy, Andrew R Webster, Graham E Holder, Anthony G Robson, David R FitzPatrick, Veronica van Heyningen, and Anthony T Moore. 2009. "A Rare de Novo Nonsense Mutation in OTX2 Causes Early Onset Retinal Dystrophy and Pituitary Dysfunction." *Molecular Vision* 15 (November): 2442–47. http://www.ncbi.nlm.nih.gov/pubmed/19956411.

Hetz, Claudio. 2012. "The Unfolded Protein Response: Controlling Cell Fate Decisions under ER Stress and Beyond." *Nature Reviews Molecular Cell Biology*. https://doi.org/10.1038/nrm3270.

Hetz, Claudio, and Bertrand Mollereau. 2014. "Disturbance of Endoplasmic Reticulum Proteostasis in Neurodegenerative Diseases." *Nature Reviews. Neuroscience* 15 (4): 233–49. https://doi.org/10.1038/nrn3689.

Hollander, Anneke I den, Ronald Roepman, Robert K Koenekoop, and Frans P M Cremers. 2008. "Leber Congenital Amaurosis: Genes, Proteins and Disease Mechanisms." *Progress in Retinal and Eye Research* 27 (4): 391–419. https://doi.org/10.1016/j.preteyeres.2008.05.003.

Hoyo, Natalia López-del del, Santiago López-Begines, Jose Luis Rosa, Jeannie Chen, and Ana Méndez. 2014. "Functional EF-Hands in Neuronal Calcium Sensor GCAP2 Determine Its Phosphorylation State and Subcellular Distribution In Vivo, and Are Essential for Photoreceptor Cell Integrity." Edited by Bruce A. Hamilton. *PLoS Genetics* 10 (7): e1004480. https://doi.org/10.1371/journal.pgen.1004480.

Hurley, J B, and L Stryer. 1982. "Purification and Characterization of the Gamma Regulatory Subunit of the Cyclic GMP Phosphodiesterase from Retinal Rod Outer Segments." *The Journal of Biological Chemistry* 257 (18): 11094–99. http://www.ncbi.nlm.nih.gov/pubmed/6286681.

Inaba, Hironori, Hidemasa Goto, Kousuke Kasahara, Kanako Kumamoto, Shigenobu Yonemura, Akihito Inoko, Shotaro Yamano, et al. 2016. "Ndel1 Suppresses Ciliogenesis in Proliferating Cells by Regulating the Trichoplein–Aurora A Pathway." *The Journal of Cell Biology* 212 (4): 409–23. https://doi.org/10.1083/jcb.201507046.

Iurlaro, Raffaella, and Cristina Muñoz-Pinedo. 2016. "Cell Death Induced by Endoplasmic Reticulum Stress." *The FEBS Journal* 283 (14): 2640–52. https://doi.org/10.1111/febs.13598.

Jacobson, S G, A V Cideciyan, Y Huang, D B Hanna, C L Freund, L M Affatigato, R E Carr, D J Zack, E M Stone, and R R McInnes. 1998. "Retinal Degenerations with Truncation Mutations in the

Cone-Rod Homeobox (CRX) Gene." *Investigative Ophthalmology & Visual Science* 39 (12): 2417–26. http://www.ncbi.nlm.nih.gov/pubmed/9804150.

Jacobson, Samuel G., Artur V. Cideciyan, Igor V. Peshenko, Alexander Sumaroka, Elena V. Olshevskaya, Lihui Cao, Sharon B. Schwartz, et al. 2013. "Determining Consequences of Retinal Membrane Guanylyl Cyclase (RetGC1) Deficiency in Human Leber Congenital Amaurosis En Route to Therapy: Residual Cone-Photoreceptor Vision Correlates with Biochemical Properties of the Mutants." *Human Molecular Genetics* 22 (1): 168–83. https://doi.org/10.1093/hmg/dds421.

Ji, Yan Shan, Jing Jin Gu, Alexander M. Makhov, Jack D. Griffith, and Beverly S. Mitchell. 2006. "Regulation of the Interaction of Inosine Monophosphate Dehydrogenase with Mycophenolic Acid by GTP." *Journal of Biological Chemistry* 281 (1): 206–12. https://doi.org/10.1074/jbc.M507056200.

Jiang, Li, Bradley J Katz, Zhenglin Yang, Yu Zhao, Nathan Faulkner, Jianbin Hu, Jennifer Baird, Wolfgang Baehr, Donnell J Creel, and Kang Zhang. 2005. "Autosomal Dominant Cone Dystrophy Caused by a Novel Mutation in the GCAP1 Gene (GUCA1A)." *Molecular Vision* 11 (February): 143–51. http://www.ncbi.nlm.nih.gov/pubmed/15735604.

Jiang, Li, Dianna Wheaton, Grzegorz Bereta, Kang Zhang, Krzysztof Palczewski, David G. Birch, and Wolfgang Baehr. 2008. "A Novel GCAP1(N104K) Mutation in EF-Hand 3 (EF3) Linked to Autosomal Dominant Cone Dystrophy." *Vision Research* 48 (23–24): 2425–32. https://doi.org/10.1016/j.visres.2008.07.016.

Johnson, Matthew C, and Justin M Kollman. 2020. "Cryo-EM Structures Demonstrate Human IMPDH2 Filament Assembly Tunes Allosteric Regulation." *ELife* 9 (January). https://doi.org/10.7554/elife.53243.

Kamenarova, Kunka, Marta Corton, Blanca García-Sandoval, Patricia Fernández-San Jose, Valentin Panchev, Almudena Ávila-Fernández, Maria Isabel López-Molina, Christina Chakarova, Carmen Ayuso, and Shomi S. Bhattacharya. 2013. "Novel GUCA1A Mutations Suggesting Possible Mechanisms of Pathogenesis in Cone, Cone-Rod, and Macular Dystrophy Patients." *BioMed Research International* 2013. https://doi.org/10.1155/2013/517570.

Karan, Sukanya, Beatrice M Tam, Orson L Moritz, and Wolfgang Baehr. 2011. "Targeting of Mouse Guanylate Cyclase 1 (Gucy2e) to Xenopus Laevis Rod Outer Segments." *Vision Research* 51 (21–22): 2304–11. https://doi.org/10.1016/j.visres.2011.09.001.

Kawamura, S. 1993. "Rhodopsin Phosphorylation as a Mechanism of Cyclic GMP Phosphodiesterase Regulation by S-Modulin." *Nature* 362 (6423): 855–57. https://doi.org/10.1038/362855a0.

Kelsell, R. E., K. Gregory-Evans, A. M. Payne, I. Perrault, J. Kaplan, R.-B. Yang, D. L. Garbers, A. C. Bird, A. T. Moore, and D. M. Hunt. 1998. "Mutations in the Retinal Guanylate Cyclase (RETGC-1) Gene in Dominant Cone-Rod Dystrophy." *Human Molecular Genetics* 7 (7): 1179–84.

https://doi.org/10.1093/hmg/7.7.1179.

Kennan, Avril, Aileen Aherne, Sara J Bowne, Stephen P Daiger, G Jane Farrar, Paul F Kenna, and Pete Humphries. 2003. "On the Role of IMPDH1 in Retinal Degeneration." *Advances in Experimental Medicine and Biology* 533: 13–18. https://doi.org/10.1007/978-1-4615-0067-4_2.

Kennan, Avril, Aileen Aherne, Arpad Palfi, Marian Humphries, Alex McKee, Alan Stitt, David A C Simpson, et al. 2002a. "Identification of an IMPDH1 Mutation in Autosomal Dominant Retinitis Pigmentosa (RP10) Revealed Following Comparative Microarray Analysis of Transcripts Derived from Retinas of Wild-Type and Rho(-/-) Mice." *Human Molecular Genetics* 11 (5): 547–57.

Keppeke, Gerson Dierley, Chia Chun Chang, Min Peng, Li-Yu Chen, Wei-Cheng Lin, Li-Mei Pai, Luis Eduardo Coelho Andrade, Li-Ying Sung, and Ji-Long Liu. 2018. "IMP/GTP Balance Modulates Cytoophidium Assembly and IMPDH Activity." *Cell Division* 13 (1): 5. https://doi.org/10.1186/s13008-018-0038-0.

Keranen, Lisa M., Erica M. Dutil, and Alexandra C. Newton. 1995. "Protein Kinase C Is Regulated in Vivo by Three Functionally Distinct Phosphorylations." *Current Biology* 5 (12): 1394–1403. https://doi.org/10.1016/S0960-9822(95)00277-6.

Kim, Y W, K S Kang, S Y Kim, and I S Kim. 2000. "Formation of Fibrillar Multimers of Oat Beta-Glucosidase Isoenzymes Is Mediated by the As-Glu1 Monomer." *Journal of Molecular Biology* 303 (5): 831–42. https://doi.org/10.1006/jmbi.2000.4130.

Kitiratschky, Veronique B D, Petra Behnen, Ulrich Kellner, John R Heckenlively, Eberhart Zrenner, Herbert Jägle, Susanne Kohl, Bernd Wissinger, and Karl-Wilhelm Koch. 2009. "Mutations in the GUCA1A Gene Involved in Hereditary Cone Dystrophies Impair Calcium-Mediated Regulation of Guanylate Cyclase." *Human Mutation* 30 (8): E782-96. https://doi.org/10.1002/humu.21055.

Kleinschmidt, A K, J Moss, and D M Lane. 1969. "Acetyl Coenzyme A Carboxylase: Filamentous Nature of the Animal Enzymes." *Science (New York, N.Y.)* 166 (3910): 1276–78. https://doi.org/10.1126/science.166.3910.1276.

Kohl, Susanne, Britta Baumann, Thomas Rosenberg, Ulrich Kellner, Birgit Lorenz, Maria Vadalà, Samuel G Jacobson, and Bernd Wissinger. 2002. "Mutations in the Cone Photoreceptor G-Protein Alpha-Subunit Gene GNAT2 in Patients with Achromatopsia." *American Journal of Human Genetics* 71 (2): 422–25. https://doi.org/10.1086/341835.

Kohl, Susanne, Frauke Coppieters, Françoise Meire, Simone Schaich, Susanne Roosing, Christina Brennenstuhl, Sylvia Bolz, et al. 2012. "A Nonsense Mutation in PDE6H Causes Autosomal-Recessive Incomplete Achromatopsia." *American Journal of Human Genetics* 91 (3): 527–32. https://doi.org/10.1016/j.ajhg.2012.07.006.

Krishnaiah, K. V. 1975. "Inosinic Acid 5'-Monophosphate Dehydrogenase of Escherichia Coli: Purification by Affinity Chromatography and Some Properties." *Archives of Biochemistry and*

Biophysics 170 (C): 567–75. https://doi.org/10.1016/0003-9861(75)90152-6.

Krizaj, David, and David R Copenhagen. 2002. "Calcium Regulation in Photoreceptors." *Frontiers in Bioscience : A Journal and Virtual Library* 7 (September): d2023-44. http://www.ncbi.nlm.nih.gov/pubmed/12161344.

Kuijpers, Marijn, Dieudonnée van de Willige, Amélie Freal, Anaël Chazeau, Mariella A. A. Franker, Jasper Hofenk, Ricardo J. Cordeiro J.Cordeiro Rodrigues, et al. 2016. "Dynein Regulator NDEL1 Controls Polarized Cargo Transport at the Axon Initial Segment." *Neuron* 89 (3): 461–71. https://doi.org/10.1016/j.neuron.2016.01.022.

Kumaran, Neruban, Anthony T. Moore, Richard G. Weleber, and Michel Michaelides. 2017. "Leber Congenital Amaurosis/Early-Onset Severe Retinal Dystrophy: Clinical Features, Molecular Genetics and Therapeutic Interventions." *British Journal of Ophthalmology*. BMJ Publishing Group. https://doi.org/10.1136/bjophthalmol-2016-309975.

Kumaran, Neruban, Anthony G Robson, and Michel Michaelides. 2018. "A novel case series of NMNAT1-associated early-onset retinal dystrophy: extending the phenotypic spectrum." *Retinal Cases and Brief Reports*, July. https://doi.org/10.1097/ICB.0000000000000754.

Kumaran, Neruban, Gary S. Rubin, Angelos Kalitzeos, Kaoru Fujinami, James W.B. Bainbridge, Richard G. Weleber, and Michel Michaelides. 2018. "A Cross-Sectional and Longitudinal Study of Retinal Sensitivity in RPE65-Associated Leber Congenital Amaurosis." *Investigative Ophthalmology and Visual Science* 59 (8): 3330–39. https://doi.org/10.1167/iovs.18-23873.

Kwok, Michael C M, Juha M Holopainen, Laurie L Molday, Leonard J Foster, and Robert S Molday. 2008. "Proteomics of Photoreceptor Outer Segments Identifies a Subset of SNARE and Rab Proteins Implicated in Membrane Vesicle Trafficking and Fusion." *Molecular & Cellular Proteomics : MCP* 7 (6): 1053–66. https://doi.org/10.1074/mcp.M700571-MCP200.

Labesse, Gilles, Thomas Alexandre, Laurène Vaupré, Isabelle Salard-Arnaud, Joséphine Lai Kee Him, Bertrand Raynal, Patrick Bron, and Hélène Munier-Lehmann. 2013. "MgATP Regulates Allostery and Fiber Formation in IMPDHs." *Structure (London, England : 1993)* 21 (6): 975–85. https://doi.org/10.1016/j.str.2013.03.011.

Lee, Bruce Y, Craig D Thulin, and Barry M Willardson. 2004. "Site-Specific Phosphorylation of Phosducin in Intact Retina. Dynamics of Phosphorylation and Effects on G Protein Beta Gamma Dimer Binding." *The Journal of Biological Chemistry* 279 (52): 54008–17. https://doi.org/10.1074/jbc.M405669200.

Lee, K. A., Kimberley B Craven, Gregory A Niemi, and James B Hurley. 2002. "Mass Spectrometric Analysis of the Kinetics of in Vivo Rhodopsin Phosphorylation." *Protein Science* 11 (4): 862–74. https://doi.org/10.1110/ps.3870102.

Lee, R H, B M Brown, and R N Lolley. 1982. "Autophosphorylation of Rhodopsin Kinase from Retinal

Rod Outer Segments." *Biochemistry* 21 (14): 3303–7.

Lee, R H, B M Brown, and R N Lolley.. 1990. "Protein Kinase A Phosphorylates Retinal Phosducin on Serine 73 in Situ." *The Journal of Biological Chemistry* 265 (26): 15860–66.

Linberg, Kenneth A., Robert N. Fariss, John R. Heckenlively, Debora B. Farber, and Steven K. Fisher. 2005. "Morphological Characterization of the Retinal Degeneration in Three Strains of Mice Carrying the *Rd-3* Mutation." *Visual Neuroscience* 22 (6): 721–34. https://doi.org/10.1017/S0952523805226044.

Liu, Ji-Long. 2010. "Intracellular Compartmentation of CTP Synthase in Drosophila." *Journal of Genetics and Genomics* 37 (5): 281–96. https://doi.org/10.1016/S1673-8527(09)60046-1.

López-Begines, Santiago, Anna Plana-Bonamaisó, and Ana Méndez. 2018. "Molecular Determinants of Guanylate Cyclase Activating Protein Subcellular Distribution in Photoreceptor Cells of the Retina." *Scientific Reports* 8 (1). https://doi.org/10.1038/s41598-018-20893-1.

Lyubarsky, A L, and E N Pugh. 1996. "Recovery Phase of the Murine Rod Photoresponse Reconstructed from Electroretinographic Recordings." *The Journal of Neuroscience : The Official Journal of the Society for Neuroscience* 16 (2): 563–71.

Ma, Hongwei, Michael R. Butler, Arjun Thapa, Josh Belcher, Fan Yang, Wolfgang Baehr, Martin Biel, Stylianos Michalakis, and Xi-Qin Ding. 2015. "CGMP/Protein Kinase G Signaling Suppresses Inositol 1,4,5-Trisphosphate Receptor Phosphorylation and Promotes Endoplasmic Reticulum Stress in Photoreceptors of Cyclic Nucleotide-Gated Channel-Deficient Mice." *Journal of Biological Chemistry* 290 (34): 20880–92. https://doi.org/10.1074/jbc.M115.641159.

Mackay, Donna S, Arundhati Dev Borman, Phillip Moradi, Robert H Henderson, Zheng Li, Genevieve A Wright, Naushin Waseem, et al. 2011. "RDH12 Retinopathy: Novel Mutations and Phenotypic Description." *Molecular Vision* 17: 2706–16. http://www.ncbi.nlm.nih.gov/pubmed/22065924.

Makino, Clint L., Xiao-Hong Wen, Elena V. Olshevskaya, Igor V. Peshenko, Andrey B. Savchenko, and Alexander M. Dizhoor. 2012. "Enzymatic Relay Mechanism Stimulates Cyclic GMP Synthesis in Rod Photoresponse: Biochemical and Physiological Study in Guanylyl Cyclase Activating Protein 1 Knockout Mice." Edited by Stephan CF. Neuhauss. *PLoS ONE* 7 (10): e47637. https://doi.org/10.1371/journal.pone.0047637.

Marino, Valerio, Giuditta Dal Cortivo, Elisa Oppici, Paolo Enrico Maltese, Fabiana D'Esposito, Elena Manara, Lucia Ziccardi, et al. 2018. "A Novel p.(Glu111Val) Missense Mutation in GUCA1A Associated with Cone-Rod Dystrophy Leads to Impaired Calcium Sensing and Perturbed Second Messenger Homeostasis in Photoreceptors." *Human Molecular Genetics* 27 (24): 4204–17. https://doi.org/10.1093/hmg/ddy311.

Marino, Valerio, Alexander Scholten, Karl-Wilhelm Koch, and Daniele Dell'Orco. 2015. "Two Retinal Dystrophy-Associated Missense Mutations in GUCA1A with Distinct Molecular Properties

Result in a Similar Aberrant Regulation of the Retinal Guanylate Cyclase." *Human Molecular Genetics* 24 (23): 6653–66. https://doi.org/10.1093/hmg/ddv370.

Martínez-Velázquez, Luis A., and Niels Ringstad. 2018. "Antagonistic Regulation of Trafficking to Caenorhabditis Elegans Sensory Cilia by a Retinal Degeneration 3 Homolog and Retromer." *Proceedings of the National Academy of Sciences of the United States of America* 115 (3): E438–47. https://doi.org/10.1073/pnas.1712302115.

Matsuda, Takahiko, and Constance L. Cepko. 2004. "Electroporation and RNA Interference in the Rodent Retina in Vivo and in Vitro." *Proceedings of the National Academy of Sciences of the United States of America*. https://doi.org/10.1073/pnas.2235688100.

McLaughlin, M E, M A Sandberg, E L Berson, and T P Dryja. 1993. "Recessive Mutations in the Gene Encoding the Beta-Subunit of Rod Phosphodiesterase in Patients with Retinitis Pigmentosa." *Nature Genetics* 4 (2): 130–34. https://doi.org/10.1038/ng0693-130.

Mendez, A, M E Burns, A Roca, J Lem, L W Wu, M I Simon, D A Baylor, and J Chen. 2000. "Rapid and Reproducible Deactivation of Rhodopsin Requires Multiple Phosphorylation Sites." *Neuron* 28 (1): 153–64.

Mendez, A, M E Burns, I Sokal, A M Dizhoor, W Baehr, K Palczewski, D A Baylor, and J Chen. 2001. "Role of Guanylate Cyclase-Activating Proteins (GCAPs) in Setting the Flash Sensitivity of Rod Photoreceptors." *Proceedings of the National Academy of Sciences of the United States of America* 98 (17): 9948–53. https://doi.org/10.1073/pnas.171308998.

Mendez, Ana, and Jeannie Chen. 2002. "Mouse Models to Study GCAP Functions in Intact Photoreceptors." *Advances in Experimental Medicine and Biology* 514: 361–88. https://doi.org/10.1007/978-1-4615-0121-3_22.

Michaelides, Michel, Susan E. Wilkie, Sharon Jenkins, Graham E. Holder, David M. Hunt, Anthony T. Moore, and Andrew R. Webster. 2005. "Mutation in the Gene GUCA1A, Encoding Guanylate Cyclase-Activating Protein 1, Causes Cone, Cone-Rod, and Macular Dystrophy." *Ophthalmology* 112 (8): 1442–47. https://doi.org/10.1016/j.ophtha.2005.02.024.

Molday, Laurie L, Hidayat Djajadi, Paul Yan, Lukasz Szczygiel, Sanford L Boye, Vince A Chiodo, Kevin Gregory-Evans, Marinko V Sarunic, William W Hauswirth, and Robert S Molday. 2013. "RD3 Gene Delivery Restores Guanylate Cyclase Localization and Rescues Photoreceptors in the Rd3 Mouse Model of Leber Congenital Amaurosis 12." *Human Molecular Genetics* 22 (19): 3894–3905. https://doi.org/10.1093/hmg/ddt244.

Molday, R S, and Christiana L Cheng. 2013. "Changes in Gene Expression Associated with Retinal Degeneration in the Rd3 Mouse." *Molecular Vision* 19 (October 2012): 955–69. http://eutils.ncbi.nlm.nih.gov/entrez/eutils/elink.fcgi?dbfrom=pubmed&id=23687432&retmode=ref&cmd=prlinks%5Cnpapers3://publication/uuid/136EAB2C-1465-4DE5-AC98-

35D92E064D6D.

Mortimer, Sarah E., and Lizbeth Hedstrom. 2005. "Autosomal Dominant Retinitis Pigmentosa Mutations in Inosine 5'-Monophosphate Dehydrogenase Type I Disrupt Nucleic Acid Binding." *Biochemical Journal* 390 (1): 41–47. https://doi.org/10.1042/BJ20042051.

Mortimer, Sarah E., Dong Xu, Dharia McGrew, Nobuko Hamaguchi, Hoong Chuin Lim, Sara J. Bowne, Stephen P. Daiger, and Lizbeth Hedstrom. 2008. "IMP Dehydrogenase Type 1 Associates with Polyribosomes Translating Rhodopsin MRNA." *Journal of Biological Chemistry* 283 (52): 36354–60. https://doi.org/10.1074/jbc.M806143200.

Muhammad, Alim, Ingrid Flores, Hong Zhang, Rui Yu, Agnieszka Staniszewski, Emmanuel Planel, Mathieu Herman, et al. 2008. "Retromer Deficiency Observed in Alzheimer's Disease Causes Hippocampal Dysfunction, Neurodegeneration, and Aβ Accumulation." *Proceedings of the National Academy of Sciences of the United States of America* 105 (20): 7327–32. https://doi.org/10.1073/pnas.0802545105.

Mustafi, Debarshi, Andreas H. Engel, and Krzysztof Palczewski. 2009. "Structure of Cone Photoreceptors." *Progress in Retinal and Eye Research*. Elsevier Ltd. https://doi.org/10.1016/j.preteyeres.2009.05.003.

Nahazawa, Mitsuru, Yuko Wada, and Malioto Tamai. 1998. "Arrestin Gene Mutations in Autosomal Recessive Retinitis Pigmentosa." *Archives of Ophthalmology* 116 (4): 498–501. https://doi.org/10.1001/archopht.116.4.498.

Nimmesgern, Elmar, James Black, Olga Futer, John R. Fulghum, Stephen P. Chambers, Christopher L. Brummel, Scott A. Raybuck, and Michael D. Sintchak. 1999. "Biochemical Analysis of the Modular Enzyme Inosine 5'-Monophosphate Dehydrogenase." *Protein Expression and Purification* 17 (2): 282–89. https://doi.org/10.1006/prep.1999.1136.

Nishiguchi, Koji M., Izabela Sokal, Lili Yang, Nirmalya Roychowdhury, Krzysztof Palczewski, Eliot I. Berson, Thaddeus P. Dryja, and Wolfgang Baehr. 2004. "A Novel Mutation (I143NT) in Guanylate Cyclase-Activating Protein 1 (GCAP1) Associated with Autosomal Dominant Cone Degeneration." *Investigative Ophthalmology and Visual Science* 45 (11): 3863–70. https://doi.org/10.1167/iovs.04-0590.

Noree, Chalongrat, Brian K Sato, Risa M Broyer, and James E Wilhelm. 2010. "Identification of Novel Filament-Forming Proteins in Saccharomyces Cerevisiae and Drosophila Melanogaster." *The Journal of Cell Biology* 190 (4): 541–51. https://doi.org/10.1083/jcb.201003001.

O'Connell, Jeremy D, Mark Tsechansky, Ariel Royal, Daniel R Boutz, Andrew D Ellington, and Edward M Marcotte. 2014. "A Proteomic Survey of Widespread Protein Aggregation in Yeast." *Molecular BioSystems* 10 (4): 851–61. https://doi.org/10.1039/c3mb70508k.

Olshevskaya, Elena V, Peter D Calvert, Michael L Woodruff, Igor V Peshenko, Andrey B Savchenko,

Clint L Makino, Ye-Shih Ho, Gordon L Fain, and Alexander M Dizhoor. 2004. "The Y99C Mutation in Guanylyl Cyclase-Activating Protein 1 Increases Intracellular Ca2+ and Causes Photoreceptor Degeneration in Transgenic Mice." *The Journal of Neuroscience : The Official Journal of the Society for Neuroscience* 24 (27): 6078–85. https://doi.org/10.1523/JNEUROSCI.0963-04.2004.

Olson, J. A., and C. B. Anfinsen. 1952. "The Crystallization and Characterization of L-Glutamic Acid Dehydrogenase." *The Journal of Biological Chemistry* 197 (1): 67–79.

Ostroy, Sanford E., Roberta A. Svoboda, and Meegan J. Wilson. 1990. "A Stage in Glycolysis Controls the Metabolic Adjustments of Vertebrate Rod Photoreceptors upon Illumination." *Biochemical and Biophysical Research Communications* 168 (1): 155–60. https://doi.org/10.1016/0006-291X(90)91687-N.

Palczewski, K, J Buczyłko, P Van Hooser, S A Carr, M J Huddleston, and J W Crabb. 1992. "Identification of the Autophosphorylation Sites in Rhodopsin Kinase." *The Journal of Biological Chemistry* 267 (26): 18991–98.

Paquet-Durand, François, Stefanie M Hauck, Theo van Veen, Marius Ueffing, and Per Ekström. 2009. "PKG Activity Causes Photoreceptor Cell Death in Two Retinitis Pigmentosa Models." *Journal of Neurochemistry* 108 (3): 796–810. https://doi.org/10.1111/j.1471-4159.2008.05822.x.

Park, Chad K., and Nancy C. Horton. 2019. "Structures, Functions, and Mechanisms of Filament Forming Enzymes: A Renaissance of Enzyme Filamentation." *Biophysical Reviews* 11 (6): 927–94. https://doi.org/10.1007/s12551-019-00602-6.

Parmeggiani, Francesco, Francesco S. Sorrentino, Diego Ponzin, Vanessa Barbaro, Stefano Ferrari, and Enzo Di Iorio. 2011. "Retinitis Pigmentosa: Genes and Disease Mechanisms." *Current Genomics* 12 (4): 238–49. https://doi.org/10.2174/138920211795860107.

Payne, A., S M Downes, D A Bessant, R Taylor, G E Holder, M J Warren, A C Bird, and S S Bhattacharya. 1998. "A Mutation in Guanylate Cyclase Activator 1A (GUCA1A) in an Autosomal Dominant Cone Dystrophy Pedigree Mapping to a New Locus on Chromosome 6p21.1." *Human Molecular Genetics* 7 (2): 273–77. https://doi.org/10.1093/hmg/7.2.273.

Pedley, Anthony M., and Stephen J. Benkovic. 2017. "A New View into the Regulation of Purine Metabolism: The Purinosome." *Trends in Biochemical Sciences* 42 (2): 141–54. https://doi.org/10.1016/j.tibs.2016.09.009.

Perkins, David N., Darryl J.C. Pappin, David M. Creasy, and John S. Cottrell. 1999. "Probability-Based Protein Identification by Searching Sequence Databases Using Mass Spectrometry Data." In *Electrophoresis*, 20:3551–67. Wiley-VCH Verlag. https://doi.org/10.1002/(SICI)1522-2683(19991201)20:18<3551::AID-ELPS3551>3.0.CO;2-2.

Perrault, I., J. M. Rozet, P. Calvas, S. Gerber, A. Camuzat, H. Dollfus, S. Chatelin, et al. 1996. "Retinal-Specific Guanylate Cyclase Gene Mutations in Leber's Congenital Amaurosis." *Nature Genetics* 14

(4): 461–64. https://doi.org/10.1038/ng1296-461.

Perrault, Isabelle, Alejandro Estrada-Cuzcano, Irma Lopez, Susanne Kohl, Shiqiang Li, Francesco Testa, Renate Zekveld-Vroon, et al. 2013. "Union Makes Strength: A Worldwide Collaborative Genetic and Clinical Study to Provide a Comprehensive Survey of RD3 Mutations and Delineate the Associated Phenotype." *PLoS ONE* 8 (1). https://doi.org/10.1371/journal.pone.0051622.

Peshenko, Igor V., Artur V. Cideciyan, Alexander Sumaroka, Elena V. Olshevskaya, Alexander Scholten, Seher Abbas, Karl Wilhelm Koch, Samuel G. Jacobson, and Alexander M. Dizhoor. 2019a. "A G86R Mutation in the Calcium-Sensor Protein GCAP1 Alters Regulation of Retinal Guanylyl Cyclase and Causes Dominant Cone-Rod Degeneration." *Journal of Biological Chemistry* 294 (10): 3476–88. https://doi.org/10.1074/jbc.RA118.006180.

Peshenko, Igor V., and Alexander M. Dizhoor. 2004. "Guanylyl Cyclase-Activating Proteins (GCAPs) Are Ca2+/Mg 2+ Sensors: Implications for Photoreceptor Guanylyl Cyclase (RetGC) Regulation in Mammalian Photoreceptors." *Journal of Biological Chemistry* 279 (17): 16903–6. https://doi.org/10.1074/jbc.C400065200.

Peshenko, Igor V., Elena V. Olshevskaya, Seifollah Azadi, Laurie L. Molday, Robert S. Molday, and Alexander M. Dizhoor. 2011. "Retinal Degeneration 3 (RD3) Protein Inhibits Catalytic Activity of Retinal Membrane Guanylyl Cyclase (RetGC) and Its Stimulation by Activating Proteins." *Biochemistry* 50 (44): 9511–19. https://doi.org/10.1021/bi201342b.

Peshenko, Igor V., Elena V. Olshevskaya, and Alexander M. Dizhoor. 2004. "Ca $^{2+}$ -Dependent Conformational Changes in Guanylyl Cyclase-Activating Protein 2 (GCAP-2) Revealed by Site-Specific Phosphorylation and Partial Proteolysis." *Journal of Biological Chemistry* 279 (48): 50342–49. https://doi.org/10.1074/jbc.M408683200.

Peshenko, Igor V., Elena V. Olshevskaya, and Alexander M. Dizhoor. 2008. "Binding of Guanylyl Cyclase Activating Protein 1 (GCAP1) to Retinal Guanylyl Cyclase (RetGC1): The Role of Individual EF-Hands." *Journal of Biological Chemistry* 283 (31): 21747–57. https://doi.org/10.1074/jbc.M801899200.

Peshenko, Igor V., Elena V. Olshevskaya, Andrey B. Savchenko, Sukanya Karan, Krzysztof Palczewski, Wolfgang Baehr, and Alexander M. Dizhoor. 2011. "Enzymatic Properties and Regulation of the Native Isozymes of Retinal Membrane Guanylyl Cyclase (RetGC) from Mouse Photoreceptors." *Biochemistry* 50 (25): 5590–5600. https://doi.org/10.1021/bi200491b.

Peshenko, Igor V, Artur V Cideciyan, Alexander Sumaroka, Elena V Olshevskaya, Alexander Scholten, Seher Abbas, Karl-Wilhelm Koch, Samuel G Jacobson, and Alexander M Dizhoor. 2019b. "A G86R Mutation in the Calcium-Sensor Protein GCAP1 Alters Regulation of Retinal Guanylyl Cyclase and Causes Dominant Cone-Rod Degeneration." *The Journal of Biological Chemistry* 294 (10): 3476–88. https://doi.org/10.1074/jbc.RA118.006180.

Peshenko, Igor V, Elena V Olshevskaya, and Alexander M Dizhoor. 2015. "Evaluating the Role of Retinal Membrane Guanylyl Cyclase 1 (RetGC1) Domains in Binding Guanylyl Cyclase-Activating Proteins (GCAPs)." *The Journal of Biological Chemistry* 290 (11): 6913–24. https://doi.org/10.1074/jbc.M114.629642.

Pierro, D Di, B Tavazzi, C F Perno, M Bartolini, E Balestra, R Caliò, B Giardina, and G Lazzarino. 1995. "An Ion-Pairing High-Performance Liquid Chromatographic Method for the Direct Simultaneous Determination of Nucleotides, Deoxynucleotides, Nicotinic Coenzymes, Oxypurines, Nucleosides, and Bases in Perchloric Acid Cell Extracts." *Analytical Biochemistry* 231 (2): 407–12. https://doi.org/10.1006/abio.1995.0071.

Plotegher, Nicoletta, Dhruv Kumar, Isabella Tessari, Marco Brucale, Francesca Munari, Laura Tosatto, Elisa Belluzzi, et al. 2014. "The Chaperone-like Protein 14-3-3η Interacts with Human α-Synuclein Aggregation Intermediates Rerouting the Amyloidogenic Pathway and Reducing α-Synuclein Cellular Toxicity." *Human Molecular Genetics* 23 (21): 5615–29. https://doi.org/10.1093/hmg/ddu275.

Power, Michael, Soumyaparna Das, K. Schütze, Valeria Marigo, Per Ekström, and François Paquet-Durand. 2019. "Cellular Mechanisms of Hereditary Photoreceptor Degeneration – Focus on CGMP." *Progress in Retinal and Eye Research*. Elsevier Ltd. https://doi.org/10.1016/j.preteyeres.2019.07.005.

Preising, Markus N., Nora Hausotter-Will, Manuel C. Solbach, Christoph Friedburg, Franz Rüschendorf, and Birgit Lorenz. 2012. "Mutations in RD3 Are Associated with an Extremely Rare and Severe Form of Early Onset Retinal Dystrophy." *Investigative Ophthalmology and Visual Science* 53 (7): 3463–72. https://doi.org/10.1167/iovs.12-9519.

Pugh, E N, and T D Lamb. 1990. "Cyclic GMP and Calcium: The Internal Messengers of Excitation and Adaptation in Vertebrate Photoreceptors." *Vision Research* 30 (12): 1923–48. https://doi.org/10.1016/0042-6989(90)90013-b.

Rattner, A, H Sun, and J Nathans. 1999. "Molecular Genetics of Human Retinal Disease." *Annual Review of Genetics* 33: 89–131. https://doi.org/10.1146/annurev.genet.33.1.89.

Ridge, Kevin D, Najmoutin G Abdulaev, Marcelo Sousa, and Krzysztof Palczewski. 2003. "Phototransduction: Crystal Clear." *Trends in Biochemical Sciences* 28 (9): 479–87. https://doi.org/10.1016/S0968-0004(03)00172-5.

Rodriguez, Diego, Diego Rojas-Rivera, and Claudio Hetz. 2011. "Integrating Stress Signals at the Endoplasmic Reticulum: The BCL-2 Protein Family Rheostat." *Biochimica et Biophysica Acta* 1813 (4): 564–74. https://doi.org/10.1016/j.bbamcr.2010.11.012.

Rudnicka-Nawrot, Maria, Irina Surgucheva, Jeffrey D. Hulmes, Françoise Haeseleer, Izabela Sokal, John W. Crabb, Wolfgang Baehr, and Krzysztof Palczewski. 1998. "Changes in Biological Activity

and Folding of Guanylate Cyclase- Activating Protein 1 as a Function of Calcium." *Biochemistry* 37 (1): 248–57. https://doi.org/10.1021/bi972306x.

Rueda, Elda M, Jerry E Johnson, Anand Giddabasappa, Anand Swaroop, Matthew J Brooks, Irena Sigel, Shawnta Y Chaney, and Donald A Fox. 2016. "The Cellular and Compartmental Profile of Mouse Retinal Glycolysis, Tricarboxylic Acid Cycle, Oxidative Phosphorylation, and ~P Transferring Kinases." *Molecular Vision* 22: 847–85. http://www.ncbi.nlm.nih.gov/pubmed/27499608.

Salceda, R., G. R.E.M. van Roosmalen, P. A.A. Jansen, S. L. Bonting, and F. J.M. Daemen. 1982. "Nucleotide Content of Isolated Bovine Rod Outer Segments." *Vision Research* 22 (12): 1469–74. https://doi.org/10.1016/0042-6989(82)90211-5.

Sato, Motoya, Mitsuru Nakazawa, Tomoaki Usui, Naoyuki Tanimoto, Haruki Abe, and Hiroshi Ohguro. 2005. "Mutations in the Gene Coding for Guanylate Cyclase-Activating Protein 2 (GUCA1B Gene) in Patients with Autosomal Dominant Retinal Dystrophies." *Graefe's Archive for Clinical and Experimental Ophthalmology = Albrecht von Graefes Archiv Fur Klinische Und Experimentelle Ophthalmologie* 243 (3): 235–42. https://doi.org/10.1007/s00417-004-1015-7.

Scott, John W., Simon A. Hawley, Kevin A. Green, Miliea Anis, Greg Stewart, Gillian A. Scullion, David G. Norman, and D. Grahame Hardie. 2004. "CBS Domains Form Energy-Sensing Modules Whose Binding of Adenosine Ligands Is Disrupted by Disease Mutations." *Journal of Clinical Investigation* 113 (2): 274–84. https://doi.org/10.1172/JCI19874.

Senft, Daniela, and Ze'ev A. Ronai. 2015. "UPR, Autophagy, and Mitochondria Crosstalk Underlies the ER Stress Response." *Trends in Biochemical Sciences*. Elsevier Ltd. https://doi.org/10.1016/j.tibs.2015.01.002.

Soens, Zachry T., Yuanyuan Li, Li Zhao, Aiden Eblimit, Rachayata Dharmat, Yumei Li, Yiyun Chen, et al. 2016. "Hypomorphic Mutations Identified in the Candidate Leber Congenital Amaurosis Gene CLUAP1." *Genetics in Medicine* 18 (10): 1044–51. https://doi.org/10.1038/gim.2015.205.

Sokal, I, N Li, C L Verlinde, F Haeseleer, W Baehr, and K Palczewski. 2000. "Ca(2+)-Binding Proteins in the Retina: From Discovery to Etiology of Human Disease(1)." *Biochimica et Biophysica Acta* 1498 (2–3): 233–51. https://doi.org/10.1016/s0167-4889(00)00099-9.

Sothilingam, Vithiyanjali, Marina Garcia Garrido, Kangwei Jiao, Elena Buena-Atienza, Ayse Sahaboglu, Dragana Trifunović, Sukirthini Balendran, et al. 2015. "Retinitis Pigmentosa: Impact of Different Pde6a Point Mutations on the Disease Phenotype." *Human Molecular Genetics* 24 (19): 5486–99. https://doi.org/10.1093/hmg/ddv275.

Stoddard, Stoddard, P. R., Lynch Lynch, E. M., Farrell Farrell, D. P., Justman Justman, et al. 2019. "Independent Evolution of Polymerization in the Actin ATPase Clan Regulates Hexokinase Activity." *BioRxiv Biochemistry*. https://doi.org/10.1101/686915.

Sullivan, Lori S., Sara J. Bowne, Melissa J. Reeves, Delphine Blain, Kerry Goetz, Vida NDifor, Sally Vitez, Xinjing Wang, Santa J. Tumminia, and Stephen P. Daiger. 2013. "Prevalence of Mutations in EyeGENE Probands With a Diagnosis of Autosomal Dominant Retinitis Pigmentosa." *Investigative Opthalmology & Visual Science* 54 (9): 6255. https://doi.org/10.1167/iovs.13-12605.

Szabo, Viktoria, Hans-Jürgen Kreienkamp, Thomas Rosenberg, and Andreas Gal. 2007. "P.Gln200Glu, a Putative Constitutively Active Mutant of Rod α-Transducin (GNAT1) in Autosomal Dominant Congenital Stationary Night Blindness." *Human Mutation* 28 (7): 741–42. https://doi.org/10.1002/humu.9499.

Tam, Lawrence C.S., Anna Sophia Kiang, Naomi Chadderton, Paul F. Kenna, Matthew Campbell, Marian M. Humphries, G. Jane Farrar, and Pete Humphries. 2010. "Protection of Photoreceptors in a Mouse Model of RP10." In *Advances in Experimental Medicine and Biology*, 664:559–65. https://doi.org/10.1007/978-1-4419-1399-9_64.

Tam, Lawrence C S, Anna Sophia Kiang, Avril Kennan, Paul F. Kenna, Naomi Chadderton, Marius Ader, Arpad Palfi, et al. 2008. "Therapeutic Benefit Derived from RNAi-Mediated Ablation of IMPDH1 Transcripts in a Murine Model of Autosomal Dominant Retinitis Pigmentosa (RP10)." *Hum Mol Genet* 17 (14): 2084–2100. https://doi.org/10.1093/hmg/ddn107.

Tang, Fu Lei, Wei Liu, Jin Xia Hu, Joanna Ruth Erion, Jian Ye, Lin Mei, and Wen Cheng Xiong. 2015. "VPS35 Deficiency or Mutation Causes Dopaminergic Neuronal Loss by Impairing Mitochondrial Fusion and Function." *Cell Reports* 12 (10): 1631–43. https://doi.org/10.1016/j.celrep.2015.08.001.

Thapa, Arjun, Lynsie Morris, Jianhua Xu, Hongwei Ma, Stylianos Michalakis, Martin Biel, and Xi-Qin Ding. 2012. "Endoplasmic Reticulum Stress-Associated Cone Photoreceptor Degeneration in Cyclic Nucleotide-Gated Channel Deficiency." *Journal of Biological Chemistry* 287 (22): 18018–29. https://doi.org/10.1074/jbc.M112.342220.

Thomas, William C, F Phil Brooks, Audrey A Burnim, John-Paul Bacik, JoAnne Stubbe, Jason T Kaelber, James Z Chen, and Nozomi Ando. 2019. "Convergent Allostery in Ribonucleotide Reductase." *Nature Communications* 10 (1): 2653. https://doi.org/10.1038/s41467-019-10568-4.

Traut, Thomas W. 1994. "Physiological Concentrations of Purines and Pyrimidines." *Molecular and Cellular Biochemistry* 140 (1): 1–22. https://doi.org/10.1007/BF00928361.

Trifunović, Dragana, Katja Dengler, Stylianos Michalakis, Eberhart Zrenner, Bernd Wissinger, and François Paquet-Durand. 2010. "CGMP-Dependent Cone Photoreceptor Degeneration in the Cpfl1 Mouse Retina." *The Journal of Comparative Neurology* 518 (17): 3604–17. https://doi.org/10.1002/cne.22416.

Tsang, Stephen H., Peter Gouras, Clyde K. Yamashita, Hild Kjeldbye, John Fisher, Debora B. Farber, and Stephen P. Goff. 1996. "Retinal Degeneration in Mice Lacking the γ Subunit of the Rod

CGMP Phosphodiesterase." *Science* 272 (5264): 1026–29. https://doi.org/10.1126/science.272.5264.1026.

Wada, Yuko, Asako Tada, Toshitaka Itabashi, Miyuki Kawamura, Hajime Sato, and Makoto Tamai. 2005. "Screening for Mutations in the IMPDH1 Gene in Japanese Patients with Autosomal Dominant Retinitis Pigmentosa." *American Journal of Ophthalmology* 140 (1): 163–65. https://doi.org/10.1016/j.ajo.2005.01.017.

Wald, George, Jack Durell, and Robert C.C. St. George. 1950. "The Light Reaction in the Bleaching of Rhodopsin." *Science* 111 (2877): 179–81. https://doi.org/10.1126/science.111.2877.179.

Walter, Peter, and David Ron. 2011. "The Unfolded Protein Response: From Stress Pathway to Homeostatic Regulation." *Science (New York, N.Y.)* 334 (6059): 1081–86. https://doi.org/10.1126/science.1209038.

Wässle, Heinz. 2004. *Parallel Processing in the Mammalian Retina. Nature Reviews Neuroscience*. Vol. 5. https://doi.org/10.1038/nrn1497.

Webb, Bradley A, Anne M Dosey, Torsten Wittmann, Justin M Kollman, and Diane L Barber. 2017. "The Glycolytic Enzyme Phosphofructokinase-1 Assembles into Filaments." *The Journal of Cell Biology* 216 (8): 2305–13. https://doi.org/10.1083/jcb.201701084.

Weleber, Richard G, Peter J Francis, Karmen M Trzupek, and Catie Beattie. 1993. *Leber Congenital Amaurosis. GeneReviews®*. http://www.ncbi.nlm.nih.gov/pubmed/20301475.

Wilden, U. 1995. "Duration and Amplitude of the Light-Induced CGMP Hydrolysis in Vertebrate Photoreceptors Are Regulated by Multiple Phosphorylation of Rhodopsin and by Arrestin Binding." *Biochemistry* 34 (4): 1446–54.

Wilkie, S E, R J Newbold, E Deery, C E Walker, I Stinton, V Ramamurthy, J B Hurley, S S Bhattacharya, M J Warren, and D M Hunt. 2000. "Functional Characterization of Missense Mutations at Codon 838 in Retinal Guanylate Cyclase Correlates with Disease Severity in Patients with Autosomal Dominant Cone-Rod Dystrophy." *Human Molecular Genetics* 9 (20): 3065–73. https://doi.org/10.1093/hmg/9.20.3065.

Wilkie, Susan E., Yang Li, Evelyne C. Deery, Richard J. Newbold, Daniel Garibaldi, J. Bronwyn Bateman, Heidi Zhang, et al. 2001. "Identification and Functional Consequences of a New Mutation (E155G) in the Gene for GCAP1 That Causes Autosomal Dominant Cone Dystrophy." *American Journal of Human Genetics* 69 (3): 471–80. https://doi.org/10.1086/323265.

Wimberg, Hanna, Ulrike Janssen-Bienhold, and Karl-Wilhelm Koch. 2018. "Control of the Nucleotide Cycle in Photoreceptor Cell Extracts by Retinal Degeneration Protein 3." *Frontiers in Molecular Neuroscience* 11: 52. https://doi.org/10.3389/fnmol.2018.00052.

Wimberg, Hanna, Dorit Lev, Keren Yosovich, Prasanthi Namburi, Eyal Banin, Dror Sharon, and Karl

Wilhelm Koch. 2018. "Photoreceptor Guanylate Cyclase (GUCY2D) Mutations Cause Retinal Dystrophies by Severe Malfunction of Ca2+-Dependent Cyclic GMP Synthesis." *Frontiers in Molecular Neuroscience* 11 (September). https://doi.org/10.3389/fnmol.2018.00348.

Wiśniewski, Jacek R., Alexandre Zougman, Nagarjuna Nagaraj, and Matthias Mann. 2009. "Universal Sample Preparation Method for Proteome Analysis." *Nature Methods* 6 (5): 359–62. https://doi.org/10.1038/nmeth.1322.

Woodruff, Michael L., Elena V. Olshevskaya, Andrey B. Savchenko, Igor V. Peshenko, Ronald Barrett, Ronald A. Bush, Paul A. Sieving, Gordon L. Fain, and Alexander M. Dizhoor. 2007. "Constitutive Excitation by Gly90Asp Rhodopsin Rescues Rods from Degeneration Caused by Elevated Production of CGMP in the Dark." *Journal of Neuroscience* 27 (33): 8805–15. https://doi.org/10.1523/JNEUROSCI.2751-07.2007.

Xu, Dong, Garrett Cobb, Catherine J. Spellicy, Sara J. Bowne, Stephen P. Daiger, and Lizbeth Hedstrom. 2008. "Retinal Isoforms of Inosine 5'-Monophosphate Dehydrogenase Type 1 Are Poor Nucleic Acid Binding Proteins." *Archives of Biochemistry and Biophysics* 472 (2): 100–104. https://doi.org/10.1016/j.abb.2008.02.012.

Xu, Mingchu, Lizhu Yang, Feng Wang, Huajin Li, Xia Wang, Weichen Wang, Zhongqi Ge, et al. 2015. "Mutations in Human IFT140 Cause Non-Syndromic Retinal Degeneration." *Human Genetics* 134 (10): 1069–78. https://doi.org/10.1007/s00439-015-1586-x.

Yacoubian, T A, S R Slone, A J Harrington, S Hamamichi, J M Schieltz, K A Caldwell, G A Caldwell, and D G Standaert. 2010. "Differential Neuroprotective Effects of 14-3-3 Proteins in Models of Parkinson's Disease." *Cell Death & Disease* 1 (1): e2–e2. https://doi.org/10.1038/cddis.2009.4.

Yang, R B, S W Robinson, W H Xiong, K W Yau, D G Birch, and D L Garbers. 1999. "Disruption of a Retinal Guanylyl Cyclase Gene Leads to Cone-Specific Dystrophy and Paradoxical Rod Behavior." *The Journal of Neuroscience : The Official Journal of the Society for Neuroscience* 19 (14): 5889–97. http://www.ncbi.nlm.nih.gov/pubmed/10407028.

Zack, Donald J., Jean Bennett, Yanshu Wang, Carol Davenport, Brenda Klaunberg, John Gearhart, and Jeremy Nathans. 1991. "Unusual Topography of Bovine Rhodopsin Promoter-IacZ Fusion Gene Expression in Transgenic Mouse Retinas." *Neuron*. https://doi.org/10.1016/0896-6273(91)90355-4.

Zhao, Hong, Jarrod B. French, Ye Fang, and Stephen J. Benkovic. 2013. "The Purinosome, a Multi-Protein Complex Involved in the de Novo Biosynthesis of Purines in Humans." *Chemical Communications* 49 (40): 4444. https://doi.org/10.1039/c3cc41437j.

Zybailov, Boris, Amber L Mosley, Mihaela E Sardiu, Michael K Coleman, Laurence Florens, and Michael P Washburn. 2006. "Statistical Analysis of Membrane Proteome Expression Changes in Saccharomyces Cerevisiae Research Articles," 2339–47.

8. APPENDIX

8.1 Cover

Shown in the cover is a wild-type murine retina stained with acetylated-γ-tubulin (green signal) and IMPDH1 (red signal). Cover wants to show how specific is the expression of IMPDH1 in photoreceptor cells.

In standard cyclic light conditions, IMPDH1 signal is restricted to photoreceptor cells staining inner segments, perinuclear zone of nuclei and synaptic terminals.

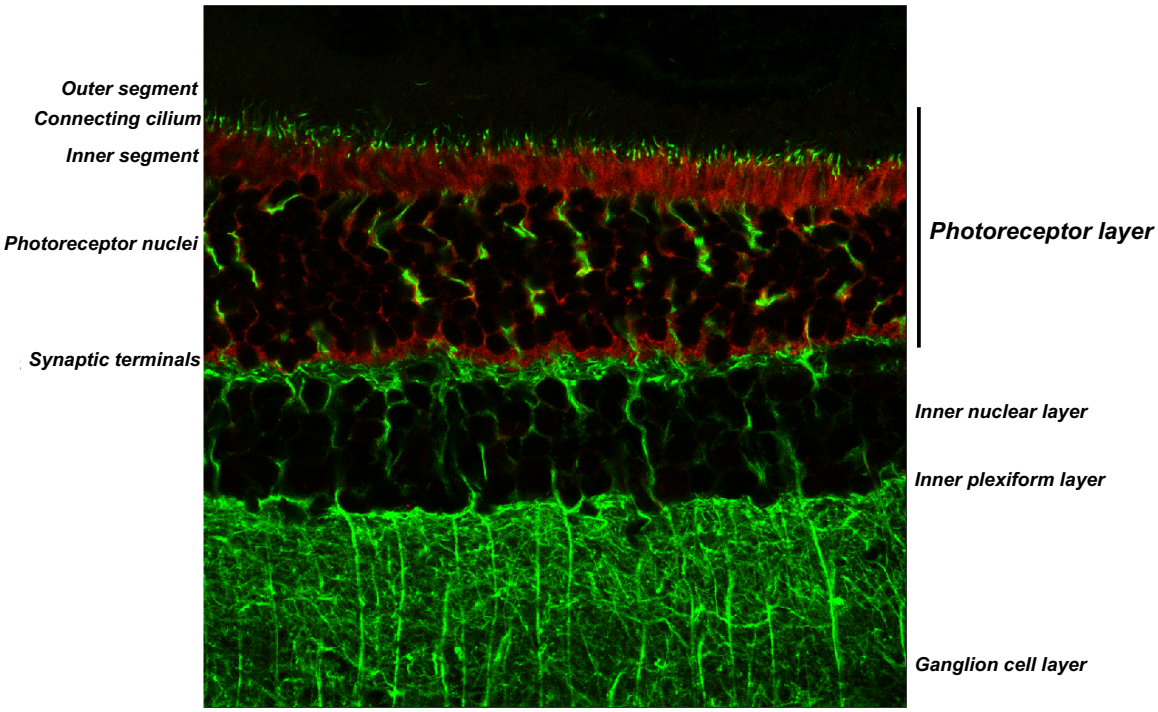

9. ACKNOWLEDGEMENTS- AGRAÏMENTS

AGRAÏMENTS

A part de totes les persones que m'han ajudat per tal de realitzar la tesis, a qui m'he anat dirigint durant els diferents capítols en els apartats de contribucions, m'agradaria fer uns agraïments més personals dirigits a aquelles persones que han estat al meu costat durant aquesta etapa.

Primer de tot voldria agrair a la meva directora de tesis **Ana Méndez** deixar-me formar part del seu laboratori. Durant aquests anys he tingut la oportunitat de rebre una formació extensa, de la que m'enduc moltes coses. Per una banda totes les tècniques que he après, i per altra banda el marc intel·lectual que l'Ana ha anat inculcant en mi (sobretot allò de... Anna, tenemos que ir a por la "pregunta de calado" ☺). Ana, he après moltíssim; també que la ciència no és un camí de roses... (pero hay que ser más resiliente). Gràcies per tots aquests aprenentatges professionals i també personals, que m'emporto!

A en **Santi** moltes gràcies per introduir-me en el mon del laboratori, per totes les idees que han acabat repercutint en aquest treball i totes les tècniques que va posar a punt. Va esser un plaer tenir-te com a mentor i company!!!

A tots aquells que han passat pel laboratori, espero no deixar-me a ningú: **Anna, Sergi, Ari, Francesc, Alex, Nerea, Marta, Alba, Laia, Paula i "Nerea pequeña"**. Alguns heu passat temporades més curtes que d'altres, però recordo moments molt especials amb tots vosaltres. Tots heu estat de gran ajuda gràcies al vostre esforç i dedicació. **Martona**, a tu et deixo el relleu del laboratori (i en breus et faré entrega de la clau de la càmera fosca :D) desitjo que aprenguis moltes coses en aquesta nova etapa i que siguis un boost d'energia i coneixement pel laboratori. Moltíssima sort!!

Als companys amb qui compartim laboratori, els diferents, variats, d'aquí i d'allà, **els fotoswitches**: heu estat el meu gran suport durant aquesta etapa. A part de ser grans científics sou tots persones increïbles i m'emporto uns grans amics. **Ros** et trobaré tantíssim a faltar, gràcies per donar-me suport sempre, fer que els dinars hagin estat tan entretinguts i per les tardes fins les tantes donant-nos ànims "forza Anita" ☺. **Núria**, ets fantàstica! Gràcies per ser-hi sempre i per ser l'alegria del laboratori! També per escoltar-me i guiar-me i "tranquil·litzar-me" també jeje :D **Alex** i **Ricardo**, us poso en el mateix pack ja que em sembla que heu estat els meus dos grans psicòlegs sobretot aquest últim any (deveu tenir unes ganes que marxi...) moltes gràcies per la vostra serenitat i paciència; us desitjo molta sort i espero que no perdem mai el contacte (Alex espero que recordis la meva cara d'aquí a dos mesos, gràcies). **Aideta**, la meva lleidatana, he rigut molt amb aquest idioma que parles i les coses que et passen, estic molt orgullosa del treball que has fet i malgrat m'has acabat avançant en la finalització de la tesis, jo no recordo haver fet mai cap aposta ;) A en **Miquel** vull agrair-li la seva proximitat i

amabilitat (i els seus acudits dolents...bé potser això no tant ;)). **Galyna**, la nova incorporació, m'ho he passat molt bé amb tu, gràcies per la teva simpatia i consells ☺ Nois, de veritat, ha estat un plaer compartir aquests anys al vostre costat! Ens veiem a plaça Osca, oi? ♡

Voldria agrair també als membres del **departament de Fisiologia** tot el suport que m'han donat sempre que ho he necessitat. Gràcies per ajudar-me en diferents tècniques i fins i tot per deixar-nos certs reactius en moments que ho hem necessitat. Gràcies a la **Carla Pérez** per ajudar-me amb el SNP genotyping, tots els "tips" que em vas donar van ser essencials per a desenvolupar aquesta tècnica. Gràcies **al grup de Jose Luis Rosa** per les mil i una vegades que ens han ajudat ja sigui aportant idees per avançar en el nostre treball, deixant-nos reactius, etc. I a tots aquells que d'una manera o altra heu ajudat a que aquest treball sigui possible. A l'**Ana Manzano** voldria agrair-li les paraules amables i de suport que sempre m'ha donat i per haver estat l'alegria del despatx :D

No podria deixar-me els membres del **grup de Biologia Cel·lular** moltíssimes gràcies per tot. Gràcies per deixar-me utilitzar tota la bateria d'aparells sofisticats i moderns que teniu. Gràcies també a la **Vanessa** i la **Marta** pel seu suport durant els últims mesos quan em van ajudar a encarrilar els últims experiments. I a en **Pep**, gràcies per l'ajuda i "tips" que m'ha donat.

A la **Rocio** del laboratori de Microbiologia moltes gràcies per ser sempre allà per escoltar-me i aconsellar-me en els moments més difícils. I molts ànims que ben aviat serà el teu moment :)

Voldria fer un especial agraïment a l'**Andreu**, per tota la paciència que ha tingut aquests anys. Encara que no entrava dintre els nostres plans que la tesis s'allargués més de l'esperat, has aguantat al meu costat, donant-me suport i cuidant-me. Per això et dedico aquesta tesis, per compensar una mica aquesta espera que sé que se t'ha acabat fent pesada.♡

Gràcies també a la **Clara**, amb qui compartim aventures des de que vam començar la carrera. Sempre m'has donat bons consells en moments complicats i ens hem donat suport mútuament. Ara que és el moment en què et poses a escriure la tesis, veurem com reacciones a les teves pròpies frases ;)

Finalment voldria fer un agraïment **a la meva família** per a tot el suport que m'han donat, per respectar sempre les meves decisions i creure en mi. I a les meves nenes: **Isa**, **Sandra**, **Pilar** i **Neu** que sabeu que us poso en el pack de la família, perquè és com si ho fóssiu. Gràcies per ser-hi des de petites i no deixar que aquesta amistat es trenqui, heu estat sempre fonamentals i també en aquesta etapa.

Moltes gràcies a tots!!!

10. PUBLICATION

Plana-Bonamaisó et al. *Cell Death and Disease* (2020)11:62
https://doi.org/10.1038/s41419-020-2255-0

Cell Death & Disease

ARTICLE Open Access

GCAP neuronal calcium sensor proteins mediate photoreceptor cell death in the rd3 mouse model of LCA12 congenital blindness by involving endoplasmic reticulum stress

Anna Plana-Bonamaisó[1,2,3], Santiago López-Begines[1], Jordi Andilla[4], María José Fidalgo[5], Pablo Loza-Alvarez[4], Josep María Estanyol[5], Pedro de la Villa[6,7] and Ana Méndez[1,2,3]

Abstract

Loss-of-function mutations in the retinal degeneration 3 (*RD3*) gene cause inherited retinopathy with impaired rod and cone function and fast retinal degeneration in patients and in the natural strain of *rd3* mice. The underlying physiopathology mechanisms are not well understood. We previously proposed that guanylate cyclase-activating proteins (GCAPs) might be key Ca^{2+}-sensors mediating the physiopathology of this disorder, based on the demonstrated toxicity of GCAP2 when blocked in its Ca^{2+}-free form at photoreceptor inner segments. We here show that the retinal degeneration in *rd3* mice is substantially delayed by GCAPs ablation. While the number of retinal photoreceptor cells is halved in 6 weeks in *rd3* mice, it takes 8 months to halve in *rd3/rd3* GCAPs$^{-/-}$ mice. Although this substantial morphological rescue does not correlate with recovery of visual function due to very diminished guanylate cyclase activity in *rd3* mice, it is very informative of the mechanisms underlying photoreceptor cell death. By showing that GCAP2 is mostly in its Ca^{2+}-free-phosphorylated state in *rd3* mice, we infer that the $[Ca^{2+}]_i$ at rod inner segments is permanently low. GCAPs are therefore retained at the inner segment in their Ca^{2+}-free, guanylate cyclase activator state. We show that in this conformational state GCAPs induce endoplasmic reticulum (ER) stress, mitochondrial swelling, and cell death. ER stress and mitochondrial swelling are early hallmarks of *rd3* retinas preceding photoreceptor cell death, that are substantially rescued by GCAPs ablation. By revealing the involvement of GCAPs-induced ER stress in the physiopathology of Leber's congenital amaurosis 12 (LCA12), this work will aid to guide novel therapies to preserve retinal integrity in LCA12 patients to expand the window for gene therapy intervention to restore vision.

Introduction

Synthesis of cyclic GMP (cGMP) is an essential process in photoreceptor cells of the retina, as cGMP is the signal-transducing molecule in the light response[1,2]. Mutations in a number of genes that impair or alter cGMP synthesis in rods and cones have been associated to different forms of blindness[3–12]. Loss-of-function mutations in the *RD3* gene (name from the natural strain of "retinal degeneration 3" mice, *rd3* locus mutated) cause Leber's congenital amaurosis 12 (LCA12)[13,14]. LCA12 is characterized by rod and cone impaired function and severe vision loss from an early age, as well as rapid retinal degeneration.

The RD3 protein is required for the stability and ciliary trafficking of guanylate cyclases RetGC1 and RetGC2, responsible for cGMP synthesis[15]. In *rd3* mice the levels

Correspondence: Ana Méndez (mendezzu@ub.edu)
[1]Department of Physiological Sciences, University of Barcelona School of Medicine - Health Science Campus of Bellvitge, L´Hospitalet de Llobregat, 08907 Barcelona, Spain
[2]Institute of Neurosciences, University of Barcelona, Castelldefels, 08035 Barcelona, Spain
Full list of author information is available at the end of the article.
Edited by G. Melino

SPRINGER NATURE CDDpress

of RetGC1 and RetGC2 are dramatically decreased, and proteins are retained at the cell soma[15]. GCAPs (guanylate cyclase-activating proteins), that are proteins that confer Ca^{2+} sensitivity to RetGCs[16–20] and depend on their binding to RetGCs for their stability and distribution to the outer segment, are also decreased in *rd3* mice[15,21,22]. As a consequence, there is reduced cGMP synthesis that results in closure of cyclic nucleotide-gated channels (CNG-channels) and presumed chronic hyperpolarization of *rd3* photoreceptors, concomitant to loss of visual function. This phenotype mimics that of LCA1 caused by null mutations in *GUCY2D* (RetGC1) in humans[23], or by retinal guanylate cyclase deficiency in mice (RetGC1/RetGC2 double knockout mice[21]). However, while mice deficient in RetGC1/RetGC2 show a progressive retinal degeneration, in *rd3* mice the loss of photoreceptor cells progresses fast[24].

RD3 was also reported to be a potent inhibitor of RetGC catalytic activity in vitro[25], diminishing RetGC basal activity and competing with GCAP1 for RetGC binding. It was proposed that one role of RD3 would be to prevent RetGC activation while RetGCs traffic through the inner segment[25].

Little is known about the molecular mechanisms that link the lack of RD3 with photoreceptor cell death in *rd3* mice. We previously proposed that the GCAP proteins could contribute to the physiopathology of retinal dystrophies characterized by rod/cone chronic hyperpolarization. This hypothesis was based on the fact that when a form of GCAP2 impaired to bind Ca^{2+} (with all functional EF-hands mutated, EF^{-}GCAP2) was expressed in living photoreceptors, it was retained at the cell soma by phosphorylation and 14-3-3 binding, resulting in severe toxicity and fast retinal degeneration[26]. In *rd3* mice, GCAPs are retained at the cell soma in a presumed context of chronic low $[Ca^{2+}]_i$. In addition, GUCA1B (GCAP2) has been reported as a modifier gene of the *rd3* mouse phenotype[27]. We hypothesized that Ca^{2+}-free GCAPs could be critically involved in the physiopathology of LCA12.

We here tested that hypothesis by breeding *rd3* mice to $GCAPs^{-/-}$ mice. We show that the retinal degeneration of *rd3* mice was drastically delayed by GCAPs ablation. While in *rd3* mice the number of photoreceptors was halved in 6 weeks, in *rd3/rd3* $GCAPs^{-/-}$ it was halved in 8 months. By assessing the extent of GCAP2 phosphorylation in *rd3* mice, we infer that the GCAP proteins are mostly in their Ca^{2+}-free cyclase activator state in *rd3* cell somas. By expressing RD3.V5 as a transient transgene in the rods of *rd3* mice, we confirm that RD3 localizes mostly to the inner segment compartment of rods, which is consistent with the proposed role of RD3 as a RetGC inhibitor. We show prominent induction of endoplasmic reticulum (ER) stress and mitochondrial swelling in *rd3* mice, that are substantially prevented by GCAPs ablation. We conclude that GCAPs mediate the physiopathology of LCA12 by triggering ER stress, and discuss the putative mechanisms by which they might do so, ultimately causing mitochondrial swelling, energy failure, and cell death.

Results

Retinal degeneration due to RD3 deficiency is substantially rescued by GCAPs ablation

To test the hypothesis that the GCAP proteins contribute to the physiopathology of blindness associated to the lack of functional RD3, we bred *rd3* mice to GCAP1/GCAP2 double knockout mice ($GCAPs^{-/-}$ mice), to assess whether the retinal degeneration was delayed.

We first characterized the rate of retinal degeneration in the specific *rd3* strain used in this study (B6.Cg-Rd3rd3/Boc), hereinafter referred to as *rd3* mice, as rates of degeneration vary in different *rd3* strains[24]. As early as at postnatal day 20 (p20), *rd3* mice presented a thinner outer nuclear layer (ONL) than wild-type mice (10 rows versus 12 rows of nuclei, Fig. 1a). An statistical analysis of ONL thickness performed on morphometric measurements from wt/*rd3* and *rd3/rd3* littermate mouse retinas at p20, p26, and p44 revealed that in *rd3* mice the number of photoreceptor cells was halved in ~6 weeks (Fig. 1a, b). This is consistent with the reported rate of degeneration of *rd3* pigmented mouse strains[24].

We confirmed that RetGC1 expression was severely reduced in *rd3* mice[15]. RetGC1 levels were reduced to ~12% of the expression in control mice at p20, Fig. 1c. The expression levels of GCAP1 and GCAP2 were reduced to 37 and 42% of the levels in control mice, Fig. 1c. A novel observation was that RetGC1 was detected by immunofluorescence analysis on retinal sections of *rd3* mice at the inner segment layer and perinuclear region of photoreceptors, showing a characteristic punctated staining, Fig. 1d. GCAP1 and GCAP2 were largely retained to proximal photoreceptor compartments in *rd3* mice, as previously described[15], Fig. 1d. Specificity of the antibodies to RetGC1 and RD3 used in Fig. 1c, d is shown in Supplementary Fig. 1.

To assess whether ablation of GCAPs affected the time course of retinal degeneration in the *rd3* mice, we bred *rd3* mice to $GCAPs^{-/-}$ mice. To minimize strain variation effects, the breeding was established between *rd3/rd3* $GCAPs^{+/-}$ mice, and homozygous *rd3/rd3* mice that were either $GCAPs^{+/-}$ or $GCAPs^{-/-}$ littermates were compared, Fig. 2. The ONL width of *rd3/rd3* mice at p44 from Fig. 1 is plotted as a reference. Compared to *rd3/rd3* mice at p44 (ONL thickness of 20 µm, 5 nuclei), *rd3/rd3* $GCAPs^{+/-}$ showed a very minor improvement at this age (22–24 µm, 5–6 nuclei, $n = 4$); while *rd3/rd3* $GCAPs^{-/-}$ mice showed a striking improvement (30–32 µm, 7–8

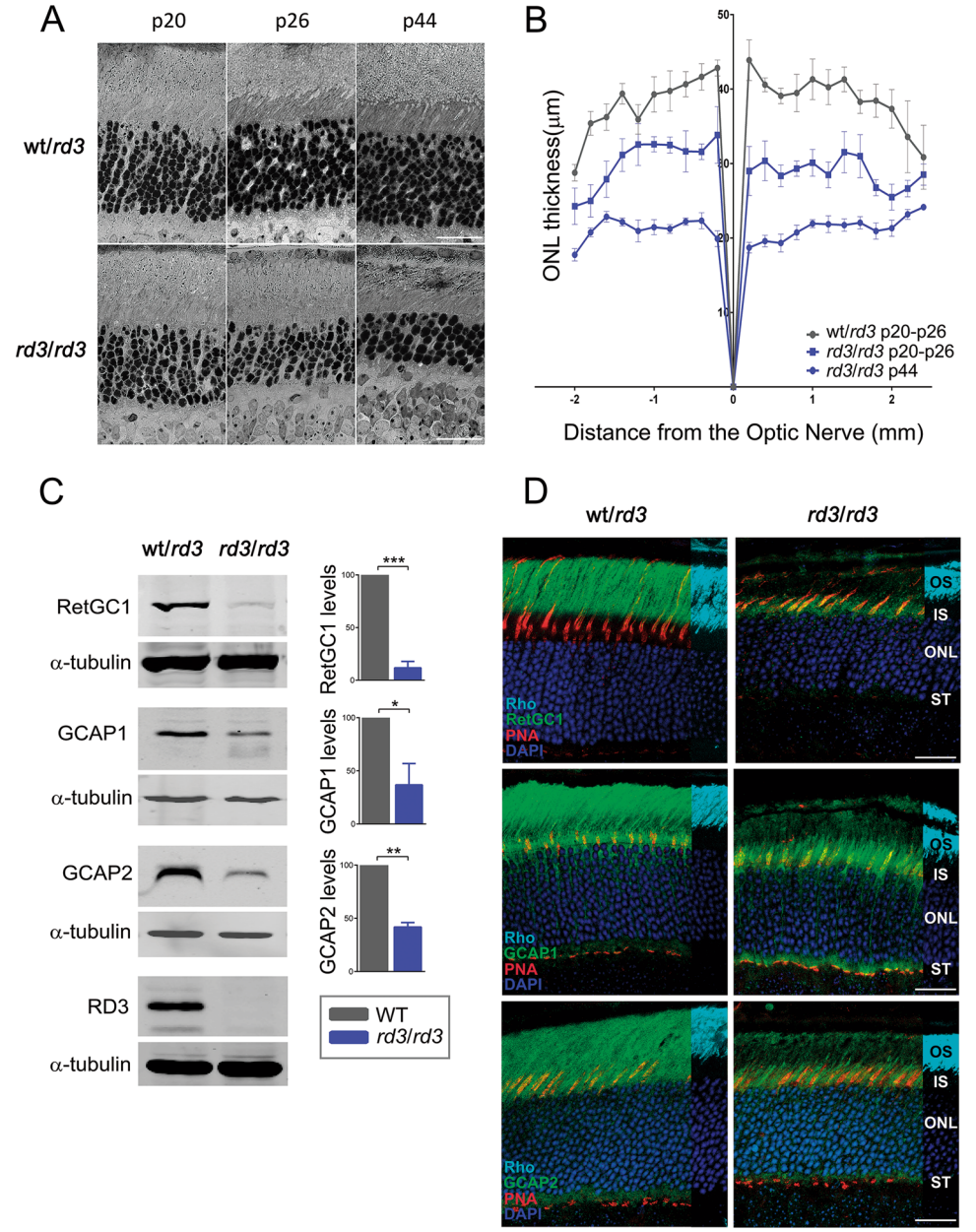

Fig. 1 Time course and molecular alterations that characterize the retinal degeneration in *rd3* mice strain B6.Cg-Rd3rd3/Boc. a Retinal micrographs of wild type and *rd3/rd3* mice at p20, p26, and p44 show the progressive retinal degeneration in *rd3/rd3* mice, that halves the number of photoreceptor cells at p44. Scale bar 20 μm. **b** Retinal morphometric analysis of wt/*rd3* and *rd3/rd3* mice at the indicated ages, showing outer nuclear layer (ONL) length (μm) at 200 μm intervals from the optic nerve in the vertical meridian of the eye, superior retina to the right. Each trace represents the average measurements of four mice analyzed, with error bars indicating the standard error of the mean (SEM). ($n = 2$ biological replicas at p20, and $n = 2$ biological replicas at p26 for wt/*rd3* and *rd3/rd3*; $n = 4$ biological replicas at p44 for *rd3/rd3*). **c** Expression levels of RetGC1, GCAP1, and GCAP2 in *rd3/rd3* mice compared to wt/*rd3* mice at p30. Histograms indicate the percentage of expression of each protein in *rd3/rd3* mice versus wt/*rd3* mice, after normalization with α-tubulin. No RD3 protein is detected in *rd3/rd3* mice with an antibody generated against the RD3 C-terminus. For the determination of protein levels, three independent experiments were performed: RetGC1 (wt/*rd3* versus *rd3*; $P < 0.0001$***); GCAP1 (wt/*rd3* versus *rd3*; $P < 0.032$*); and GCAP2 (wt/rd3 versus *rd3*; $P = 0.0017$**). **d** Immunofluorescence localization of RetGC1, GCAP1, and GCAP2 in wt/*rd3* and *rd3/rd3* mice at p24. RetGC1, GCAP1, and GCAP2 signals are greatly reduced in *rd3/rd3* mice, and mostly restricted to the photoreceptor inner layer. Cones are labeled with peanut agglutinin (PNA) in red; the rod outer segment layer with anti-Rhodopsin mAb 1D4 (1 cm overlay in cyan), and nuclei are labeled with DAPI (blue). Scale bar 20 μm. OS, outer segment; IS, inner segment; ONL, outer nuclear layer; ST, synaptic terminals.

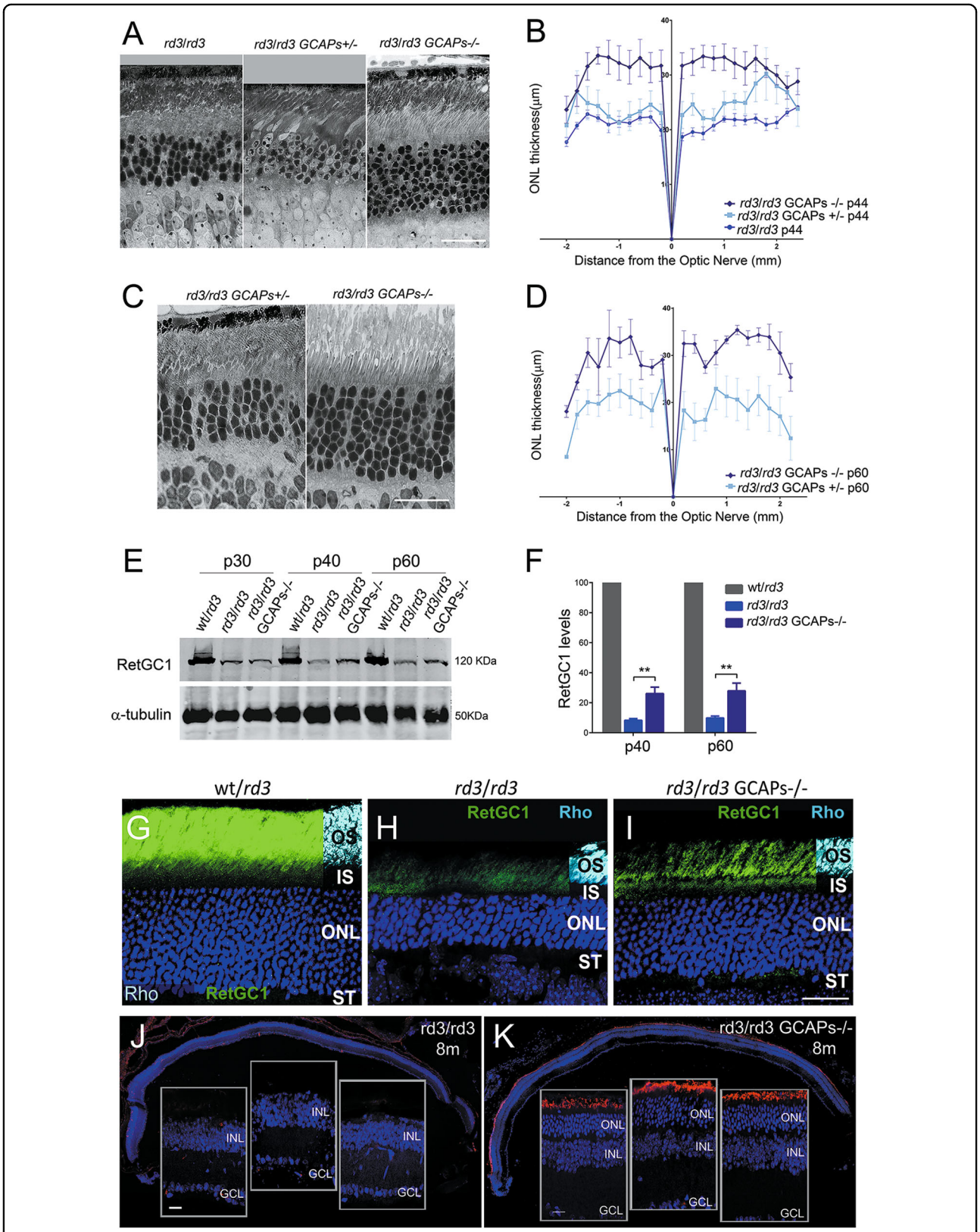

Fig. 2 (See legend on next page.)

(see figure on previous page)

Fig. 2 Retinal degeneration in *rd3* mice is substantially prevented by GCAPs ablation. a Retinal morphology of *rd3/rd3*; *rd3/rd3* GCAPs$^{+/-}$ and *rd3/rd3* GCAPs$^{-/-}$ mice at p44. Photoreceptor cell loss is substantially prevented in the GCAPs$^{-/-}$ background. Scale bar 20 µm. **b** Retinal morphometry analysis of the indicated genotypes at p44 showing ONL length (µm) along the vertical meridian of the eye. Each trace shows the average from measurements taken from four mice, with error bars showing the standard error of the mean (SEM). GCAPs removal results in preservation of 25% more photoreceptors at p44. **c** Morphology of the retina in *rd3/rd3* GCAPs$^{+/-}$ and *rd3/rd3* GCAPs$^{-/-}$ at p60. The protective effect of GCAPs ablation persists at this age. Scale bar 20 µm. **d** Statistical analysis of ONL length in *rd3/rd3* GCAPs$^{+/-}$ and *rd3/rd3* GCAPs$^{-/-}$ retinas at p60. Results are mean ± SEM of four biological replicas. **e** Level of expression of RetGC1 in *rd3/rd3* GCAPs$^{+/-}$ and *rd3/rd3* GCAPs$^{-/-}$ retinas at p30, p40, and p60. RetGC1 expression levels correlate with the fraction of photoreceptors preserved. **f** Statistical analysis of RetGC1 expression levels, mean ± SEM of three biological replicas per genotype. RetGC1 levels are not altered by the presence or absence of GCAPs at p30, consistent with *rd3/rd3* and *rd3/rd3* GCAPs$^{-/-}$ mice having a similar ONL thickness at this age. RetGC1 levels are significantly increased in the GCAPs$^{-/-}$ background at p40 and p60, reflecting the extent to which photoreceptor cells are preserved at these ages. Unpaired *t*-test (*rd3/rd3* versus *rd3/rd3* GCAPs$^{-/-}$ at p40, $P = 0{,}0023$**); (*rd3/rd3* versus *rd3/rd3* GCAPs$^{-/-}$ at p60, $P = 0{,}0043$**). **g**–**i** In the absence of GCAPs, more RetGC1 distributes to the rod outer segment (ROS) layer in *rd3* mice **i**, than in the presence of GCAPs **h**. Scale bar 20 µm. OS, outer segment; IS, inner segment; ONL, outer nuclear layer; ST, synaptic terminals. **j**, **k** The protective effect of GCAPs ablation persists at 8 months. A representative retinal section of *rd3/rd3* mice at 8 months, with nuclei stained with DAPI (blue), shows a complete loss of the photoreceptor cell layer **j**. A retinal section of *rd3/rd3* GCAPs$^{-/-}$ mice at 8 months shows an outer nuclear layer with five rows of nuclei that preserve their outer segments (note the ROS layer stained with anti-rhodopsin antibody). Retinal sections are representative of three mice per genotype. Scale bar 20 µm.

nuclei, $n = 4$), Fig. 2a, b. This substantial rescue effect of GCAPs ablation was preserved at p60 (Fig. 2c, d), when four biological replicas per genotype were analyzed. In the absence of GCAPs, the *rd3* mice preserved 75% of their photoreceptors at p60; while in the presence of GCAPs they preserved <50%.

This substantial preservation of photoreceptors in the absence of GCAPs correlated with an increase in RetGC1 levels in *rd3/rd3* GCAPs$^{-/-}$ retinas (Fig. 2e, f). Quite surprisingly, RetGC1 in *rd3/rd3* GCAPs$^{-/-}$ mice was distributed to rod outer segments (ROSs) to a higher extent than in *rd3/rd3* mice (Fig. 2g, i).

At 8 months of age, *rd3/rd3* mice did not retain any photoreceptor cells, while *rd3/rd3* GCAPs$^{-/-}$ mice preserved five rows of photoreceptors with visible outer segments, Fig. 2j, k.

We conclude that GCAPs ablation markedly slows down photoreceptor cell death in the *rd3* mice, implying that GCAP proteins are involved in the physiopathology of LCA12.

Morphological rescue of rd3 retinas by GCAPs ablation does not correlate with an amelioration of visual function

To test whether the substantial morphological rescue of *rd3* mice that resulted from GCAPs ablation correlated with an amelioration of visual function, light-elicited electroretinogram (ERG) responses were recorded from wt, *rd3/rd3*, GCAPs$^{-/-}$, and *rd3/rd3* GCAPs$^{-/-}$ mice at p40.

Rd3 mice showed substantially reduced scotopic and photopic responses (Fig. 3), as expected based on the drastically reduced RetGC levels in these mice, as previously reported[28]. Despite this substantially reduced sensitivity to light, *rd3* mice elicited diminished but reliable responses to flashes in the scotopic and photopic range (Fig. 3), indicating that at p40 they retained some rod and cone visual function.

GCAPs$^{-/-}$ mice presented reduced visual responses in the scotopic and photopic range due to the lack of GCAPs stimulation of guanylate cyclase activity, but they largely retained visual function (Fig. 3).

Strikingly, *rd3/rd3* GCAPs$^{-/-}$ mice at p40 yielded barely noticeable responses to flashes at either the scotopic or photopic range, despite maintaining 25% more photoreceptor cells than *rd3/rd3* mice and higher levels of RetGC at their retinas. A possible explanation for these results is that *rd3/rd3* GCAPs$^{-/-}$ responses reflect the lack of stimulation of RetGC activity by the GCAP proteins; whereas *rd3/rd3* mice retain GCAP stimulation of the remaining RetGC proteins.

Taken together our results show that GCAPs ablation in the *rd3* mice substantially prevented retinal degeneration but at the cost of impairing rather than ameliorating visual function.

Subcellular localization of RD3 in retinal sections

RD3 was described as a potent inhibitor of RetGC activity in vitro, and was predicted to localize to the inner segment layer where it could silence the cyclase during its transport to the cilium[25]. However, RD3 was immunolocalized to the outer segment layer of the retina in wt mice by specific antibodies against the COOH-terminus of the protein[15].

To determine RD3 subcellular localization by avoiding the use of anti-RD3 antibodies, we generated transient transgenic mice that expressed RD3 fused to a short tag (RD3.V5) in rod photoreceptors. To express RD3.V5 in rods, we made use of in vivo DNA electroporation after subretinal injection in newborn *rd3/rd3* mice with the construct pRho-RD3.V5-dsRed. RD3 was then immunolocalized at p20 using well-established anti-V5 antibodies (Methods section).

RD3.V5 showed the mosaic pattern of expression that characterizes in vivo DNA electroporation transgenesis, in

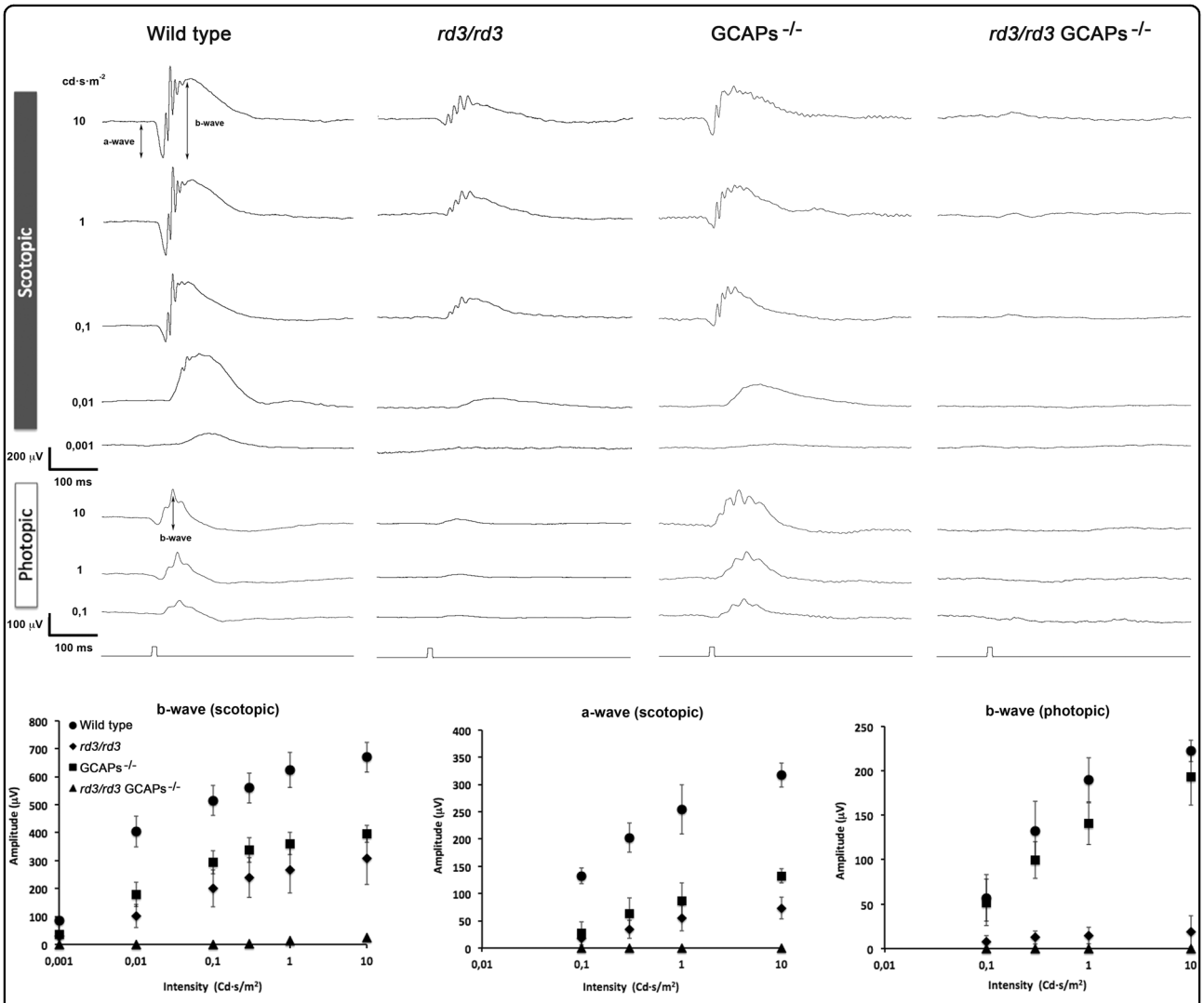

Fig. 3 Light responses are drastically reduced in *rd3/rd3* GCAPs$^{-/-}$ mice. Electroretinographic recordings from 40-d-old wt, *rd3/rd3*, GCAPs$^{-/-}$, and *rd3/rd3* GCAPs$^{-/-}$ mice in response to light stimuli of increasing intensity at scotopic or photopic conditions. Representative recordings are shown from one mouse of each genotype, evoked by light pulses of increasing intensity (indicated in cd/s/m^2). Scotopic a-wave and b-wave amplitudes (mean ± SD) and photopic b-wave amplitudes are plotted at different light intensities from a total of four wt mice, seven *rd3/rd3* mice, five GCAPs$^{-/-}$, and five *rd3/rd3* GCAPs$^{-/-}$ mice. Both GCAPs$^{-/-}$ and *rd3/rd3* mice showed substantially reduced responses when compared to wild-type responses. GCAPs ablation in *rd3/rd3* mice resulted in nearly abolished responses at the scotopic or photopic range.

which only transfected cells express the transgene. The expression of RD3.V5 in *rd3/rd3*-transfected rods restored RetGC1 expression and its localization to the outer segment, which indicated that the RD3.V5 protein was active (Fig. 4). RD3.V5 localized to the inner and outer segments of transfected cells, giving a much stronger signal at the inner segments. Particularly, there appears to be a membrane domain, probably at the connecting cilium, where the RetGC1 and RD3.V5 signals strongly colocalize (see the white signal from the merged green and magenta channels with "staple" shape, Fig. 4).

Therefore our results are in line with the results obtained by Dizhoor et al.[29] that localize RD3 mainly at the inner segment, although we observe some signal at the outer segment as well. The mosaic expression excludes that this signal is unspecific, as electroporated cells are surrounded by negative control cells. Anti-V5 antibodies unspecifically stain synaptic ribbons. This signal is clearly unspecific because it is detected in transfected and untransfected cells (Fig. 4).

GCAP2 in *rd3* mice is mostly in its phosphorylated Ca^{2+}-free form, a target for 14-3-3 binding

We have previously reported that an accumulation of Ca^{2+}-free GCAP2 at the inner segment is highly deleterious for rod cells[26]. In *rd3* photoreceptor cells, GCAP2

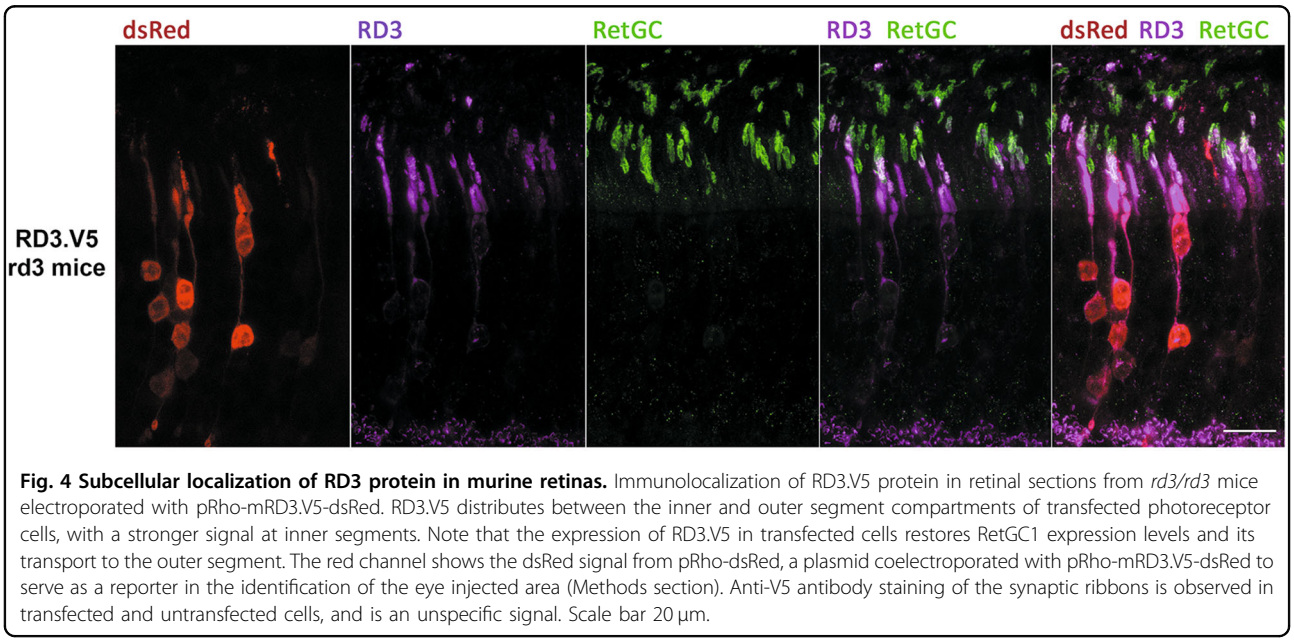

Fig. 4 Subcellular localization of RD3 protein in murine retinas. Immunolocalization of RD3.V5 protein in retinal sections from *rd3/rd3* mice electroporated with pRho-mRD3.V5-dsRed. RD3.V5 distributes between the inner and outer segment compartments of transfected photoreceptor cells, with a stronger signal at inner segments. Note that the expression of RD3.V5 in transfected cells restores RetGC1 expression levels and its transport to the outer segment. The red channel shows the dsRed signal from pRho-dsRed, a plasmid coelectroporated with pRho-mRD3.V5-dsRed to serve as a reporter in the identification of the eye injected area (Methods section). Anti-V5 antibody staining of the synaptic ribbons is observed in transfected and untransfected cells, and is an unspecific signal. Scale bar 20 µm.

is retained at the inner segment (Fig. 1d). To test whether GCAP2 is in its Ca^{2+}-free "deleterious" conformation in *rd3* mice, we analyzed GCAP2 levels of phosphorylation.

In vitro and in vivo studies have shown that GCAP2 is phosphorylated at Ser201 preferentially in its Ca^{2+}-free form[26,30]. In wt mice, ~50% of GCAP2 is phosphorylated when mice are reared under standard cyclic light, independently of their sacrifice in the dark or light period[26]. However, a GCAP2 mutant locked in its Ca^{2+}-free form (EF^{-}GCAP2) transgenically expressed in rods showed a much higher extent of GCAP2 phosphorylation. This indicates that the extent of GCAP2 phosphorylation in vivo reflects the fraction of GCAP2 molecules in the Ca^{2+}-free conformation[26].

The extent of GCAP2 phosphorylation in *rd3/rd3* versus wt mice was analyzed by resolving retinal homogenates at p21 in isoelectrofocusing gel strips that covered a linear pH gradient of 3–10 (Fig. 5a). Threefold more *rd3/rd3* protein sample (100 µg) than wt sample (25 µg) was loaded, in order to equilibrate the GCAP2 signal. Unphosphorylated GCAP2 presented an isoelectric point (IP) of 4.92, whereas phosphorylated GCAP2 an IP of 4.85. In wt mice, GCAP2 and GCAP2-P were present at a 1:1 ratio as originally reported. In contrast, GCAP2 and GCAP2-P were observed at a 1:3 ratio in *rd3* mice (Fig. 5b). This ratio of GCAP2 to GCAP2-P was very similar to the ratio reported for EF^{-}GCAP2 mice[26], and indicates that GCAP2 in *rd3* mice is mostly in its phosphorylated Ca^{2+}-free state.

To gain insight into the mechanism by which Ca^{2+}-free GCAP2 could contribute to the physiopathology of *rd3* mice, we searched for molecular targets of Ca^{2+}-free GCAP2 in the retina. We performed pull-down assays with purified myristoylated recombinant bGCAP2 that was in vitro phosphorylated—or with its mock control—on Triton-X100 solubilized bovine retinas, under EGTA conditions (Methods section). Experiments were performed in triplicate. Bound proteins were identified by liquid chromatography and mass spectrometry (LC-MS/MS) and subjected to label-free quantitative statistical analysis. For each identified protein (776 total proteins, Supplementary Table 1), the equation detailed in Methods section was used to determine its normalized spectral abundance factor (NSAF) in the GCAP2-P and the GCAP2 sample. The scatter plot in Fig. 5c presents the Log_2 (Mean $NSAF_{GCAP2\text{-}P}$/Mean $NSAF_{GCAP2}$) on the *x*-axis, versus the $-10Log(P\ value)$ in the *y*-axis, considering threshold values of 1,35 and 5 for the *x*- and *y*-axis, respectively. Proteins that showed an statistically significant preference for GCAP2-P are shown as red dots, while those with preference for unphosphorylated GCAP2 as blue dots (Fig. 5c).

The 14-3-3 proteins, known to interact with GCAP2-P[26], were identified with robust statistics as GCAP2-P binding proteins; as were proteins NDUFS5 (NADH dehydrogenase(ubiquinone) iron-sulfur protein 5), Ndel1 (nuclear distribution protein nude-like1), and RPL31 (60S ribosomal protein L31). On the other side, among the proteins with preference for unphosphorylated Ca^{2+}-free GCAP2, were HSP90(α,β) and HspB8, chaperones that may be required to stabilize this unstable form of the protein, and superoxide dismutase 1 and peroxiredoxin-6, involved in maintaining the redox state of the cell.

RetGC1 was only identified in two out of three experiments, with ≤6 spectral counts, and showed a slight preference for the unphosphorylated form of GCAP2

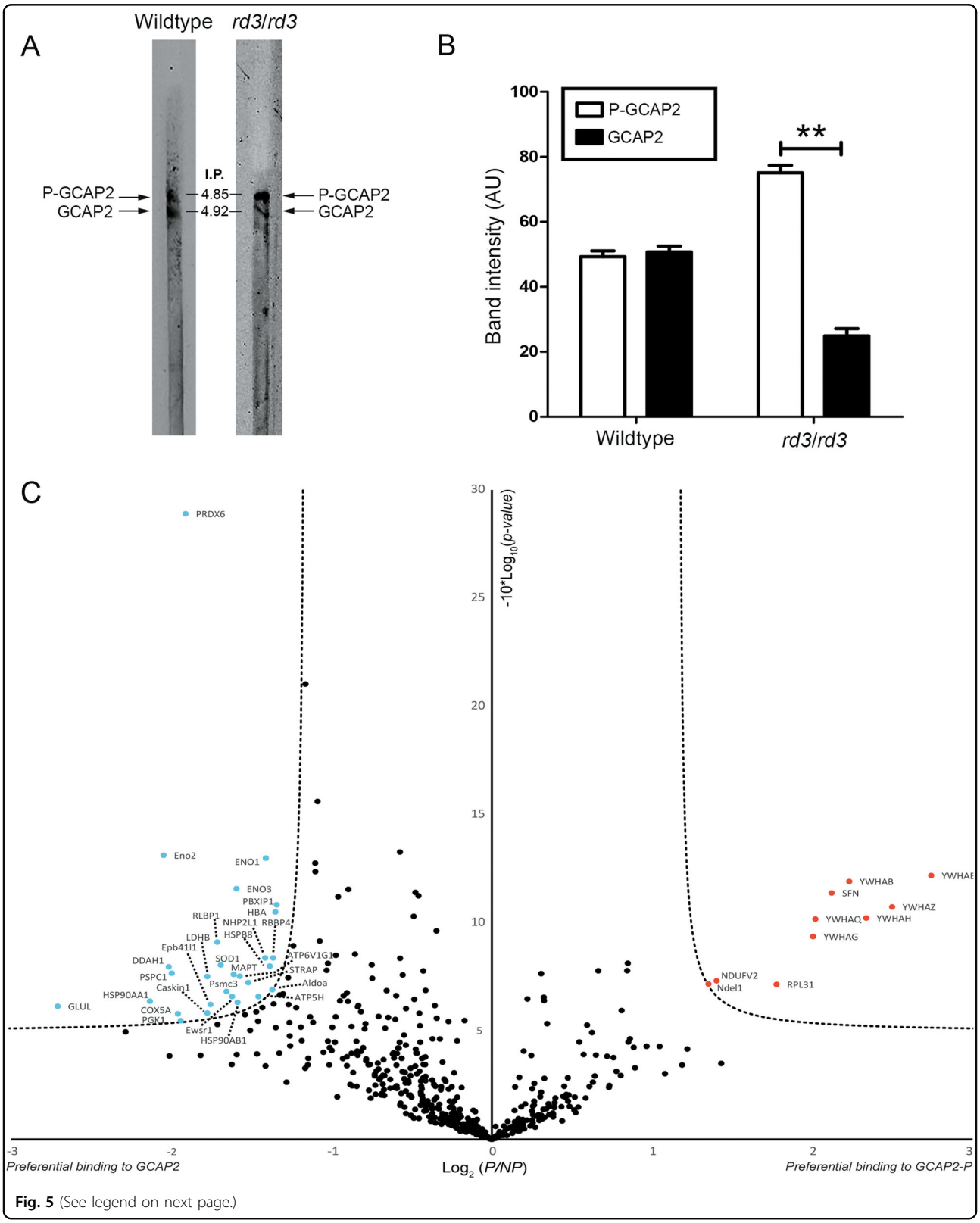

Fig. 5 (See legend on next page.)

(see figure on previous page)

Fig. 5 GCAP2 in *rd3/rd3* retinas is largely in its Ca^{2+}-free-phosphorylated state, which is a target for 14-3-3 binding. a Isoelectric focusing (IEF) separation of retinal homogenates from wt and *rd3/rd3* mice at p30 in linear pH 3–10 gradient gel strips. Following IEF, proteins were transferred to a nitrocellulose membrane and immunoblotted with anti-GCAP2 pAb. **b** The GCAP2-P to GCAP2 ratio was determined by densitometric analysis (mean ± SEM) of three independent isoelectrofocusing experiments. Unpaired *t*-test (GCAP2 versus GCAP2-P in wt mice, $P = 0.72$) and (GCAP2 versus GCAP2-P in *rd3* mice, $P = 0.0082$**). **c** Label-free quantitative proteomic analysis to identify putative protein interactions of Ca^{2+}-free GCAP2-P and GCAP2. Pull-down assays were performed on bovine retinal homogenates with purified myristoylated GCAP2 that was phosphorylated in vitro or a MOCK-phosphorylation control, under EGTA conditions. The volcano plot represents the statistical analysis of three independent pull-down assays. Log2 (*P/NP*) refers to Log2 (Mean $NSAF_{GCAP2\text{-}P}$/Mean $NSAF_{GCAP2}$), with NSAF being the normalized spectral abundance factor, see Methods section. The already reported 14-3-3 phosphobinding proteins (different isoforms) were clearly revealed as Ca^{2+}-free GCAP2-P interactors, validating the assay. Other putative interactors identified with statistical significance are marked in red (GCAP2-P) and blue (GCAP2). The whole list of identified proteins is provided in Supplementary Table 1.

(Supplementary Table 1). However, it is well established that the RetGC–GCAPs interaction is very sensitive to detergents, and virtually impossible to detect in pull-down assays.

ER stress and mitochondrial swelling are prominent early signs of retinal degeneration in the *rd3* mice that are substantially rescued by GCAPs ablation

One early alteration that we observed in *rd3* retinas at p20 was rhodopsin mislocalization. Although rhodopsin transport is not affected by the lack of RD3 and rhodopsin antibodies largely stain the outer segment layer in *rd3* mice (e.g., Fig. 1), a number of photoreceptor cells showed rhodopsin perinuclear staining in any taken frame of the *rd3* outer retina at p20 (Fig. 6a). This was not observed in age-matching wt or *rd3/rd3* $GCAPs^{-/-}$ mice (Fig. 6a). The number of cells per unit area that showed mislocalized rhodopsin in *rd3* mice was highest at p20 and diminished with age (Fig. 6b, c).

Because this signal could be reflecting rhodopsin retention at the ER due to ER dysfunction, we assessed ER stress by comparing the levels of ER stress marker C/EBP homologous protein (CHOP) in wt, *rd3/rd3* and *rd3/rd3* $GCAPs^{-/-}$ mice. CHOP is a transcription factor that links severe ER impairment with the induction of apoptosis[31]. We observed a clear induction of CHOP expression in *rd3* mice at p20 (Fig. 6d, e), that was substantially prevented by GCAPs ablation (Fig. 6d, e).

Apoptotic cell death was assessed by evaluating caspase 3 activation (detection of the p17 large fragment from caspase 3 cleavage) and the cleavage of poly (ADP-ribose) polymerase PARP, a main target of caspases. Figure 6d, e shows activated p17 fragment of caspase 3 at a much higher level in *rd3* mice than in wt or *rd3/rd3* $GCAPs^{-/-}$ mice, with statistical significance (experiment performed in triplicate). The extent of PARP1 cleavage in *rd3* mice versus wt and *rd3/rd3* $GCAPs^{-/-}$ mice confirms the induction of apoptotic cell death in *rd3* mice at p20, that is partially rescued by GCAPs ablation.

Actually, one of the most prominent alterations in *rd3* mice at p20–p26 revealed by ultrastructural analysis was mitochondrial swelling, indicative of apoptosis. Figure 7 shows representative electron micrographs of *rd3/rd3* mice at p20–p26 (Fig. 7b, d), opposed to *rd3*/wt heterozygous littermate controls (Fig. 7a, c). Retinas from *rd3/rd3* mice showed distinctive features like emerging vertical outer segment membrane discs (black arrows in Fig. 7b, d, and enlarged area in Fig. 7e); as well as disc structures that have been internalized at the inner segment (black arrowheads in Fig. 7f, g, h, k). The most prominent morphological alteration in *rd3/rd3* mice was mitochondrial swelling at the inner segment, noticeable at p20 at a fraction of cells (Fig. 7f, magnified at Fig. 7g), and at p26 at the majority of cells (Fig. 7i, j). This mitochondrial swelling preceded cell death.

Interestingly, the striking mitochondrial swelling in *rd3* photoreceptor cells (Fig. 7l) was greatly diminished in *rd3/rd3* $GCAPs^{-/-}$ mice (Fig. 7m) when four animals of each genotype were compared (Fig. 7n).

Taken together, our results show that GCAPs induce the ER stress response in *rd3* mice, inducing CHOP expression and triggering apoptosis at a very early stage of the disease, and that GCAPs ablation substantially suppresses this induction and prevents photoreceptor cell death.

Discussion

We here show that the GCAP proteins play a central role in the physiopathology of blinding diseases associated to loss of functional RD3 (LCA12), by showing that GCAPs ablation substantially delays retinal degeneration in the *rd3* mouse model. While preservation of the retinal morphology is not accompanied by restoration of visual function, it is very revealing of the molecular mechanisms that link the lack of functional RD3 with photoreceptor cell death, and may assist at designing therapies to expand the window for gene therapy intervention in LCA12 patients.

We first confirmed all the previously reported manifestations of the phenotype of the *rd3* mice[15], with further attention to meaningful details. RetGC1 levels are drastically reduced in *rd3* retinas as reported, but can still be detected, and are estimated at ~12% of the wild-type levels in *rd3* mice at p20 (Fig. 1). RetGC1 is retained at

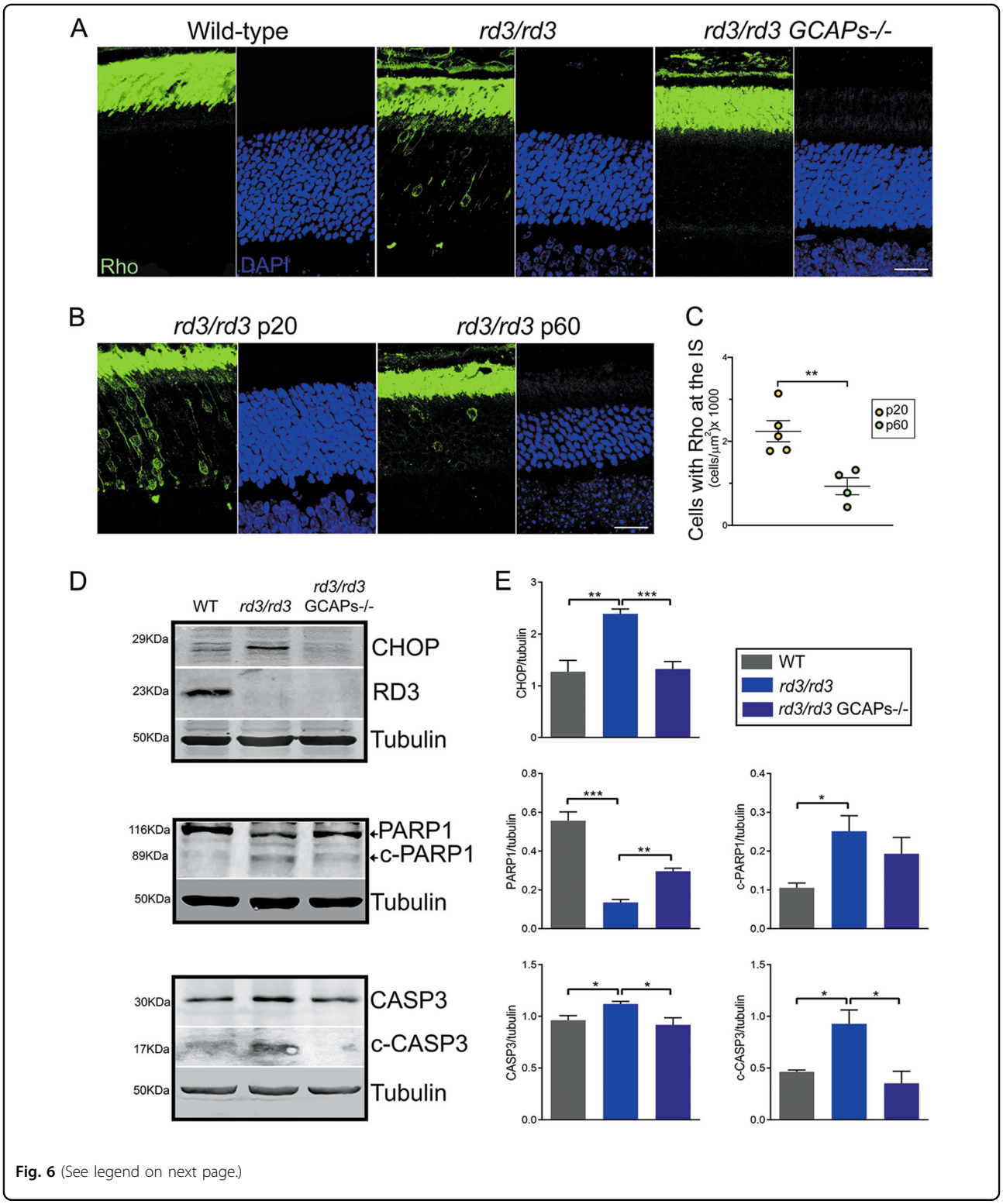

Fig. 6 (See legend on next page.)

proximal cell compartments, mostly at the inner segment and perinuclear regions (Figs. 1d and 4). GCAP1 and GCAP2 levels are reduced in *rd3* mice to ~37 and ~42% of wild-type levels. Although mostly retained at the inner segment as previously reported[15], traces of RetGC1, GCAP1, and GCAP2 are also observed at the outer

(see figure on previous page)

Fig. 6 Rhodopsin mislocalization, ER stress, and apoptosis are early signs of retinal degeneration in *rd3* mice that are palliated by GCAPs ablation. a Retinal sections from wt, *rd3/rd3*, and *rd3/rd3* GCAPs$^{-/-}$ mice at p20 stained with anti-rhodopsin antibody (green) and DAPI (blue). Rhodopsin mislocalization at the perinuclear region and proximal compartments is observed in a number of photoreceptor cells at any given frame of the outer retina in *rd3/rd3* mice at p20, but not in wt or *rd3/rd3* GCAPs$^{-/-}$ mice this age. Scale bar 20 µm. **b**, **c** Representative images and quantification of cells that present rhodopsin mislocalization at p20 versus p60 in *rd3* mice, expressed per unit area ($n = 5$ *rd3/rd3* mice at p20; $n = 4$ *rd3/rd3* mice at p60]. Unpaired *t*-test p20 versus p60, $P = 0.0058$**). **d** Levels of CHOP; full length and p17 kDa fragment of cleaved caspase 3; and full length and 89 kDa fragment of cleaved PARP1 proteins in retinal extracts from wt, *rd3/rd3*, and *rd3/rd3* GCAPs$^{-/-}$ at p20. Note that the full-length casp3 and c-casp3 signals were obtained from different exposure conditions of the same membrane, given that c-casp3 represents a small percentage of full-length casp3. No RD3 protein was observed in *rd3/rd3* or *rd3/rd3* GCAPs$^{-/-}$ extracts. **e** Six independent experiments were performed to determine CHOP expression levels (wt versus *rd3/rd3*, $P = 0.0012$**; and *rd3/rd3* versus *rd3/rd3* GCAPs$^{-/-}$, $P = 0.0001$***). Three independent experiments were performed to determine PARP1 and c-PARP1 levels (PARP1: wt versus *rd3*, $P = 0.001$***; and *rd3/rd3* versus *rd3/rd3* GCAPs$^{-/-}$, $P = 0.0018$**); (c-PARP1: wt versus *rd3*, $P = 0.026$*; and *rd3/rd3* versus *rd3/rd3* GCAPs$^{-/-}$, $P = 0.37$ NS). Three independent experiments were performed to determine casp3 and c-casp3 levels (casp3: wt versus *rd3*, $P = 0.035$*; and *rd3/rd3* versus *rd3/rd3* GCAPs$^{-/-}$, $P = 0.05$*); (c-casp3: wt versus *rd3*, $P = 0.026$*; and *rd3/rd3* versus *rd3/rd3* GCAPs$^{-/-}$, $P = 0.031$*).

segment layer (Fig. 1d), explaining why *rd3* mice elicit bigger ERG responses than *rd3/rd3* GCAPs$^{-/-}$ mice (Fig. 3).

The *rd3* strain of mice showed a fast rate of retinal degeneration, going from approximately ten rows of photoreceptor nuclei at p20 to approximately five rows at p44. GCAPs ablation substantially slowed down retinal degeneration, so that at 8 months of age *rd3/rd3* GCAPs$^{-/-}$ mice still retained five rows of photoreceptor nuclei. Therefore, the loss of RD3 still caused cell death in the absence of GCAPs, but at a substantially slower rate. We infer that: (i) the loss of RD3 causes an initial insult, with its origin in the closure of CNG-channels and the ensuing chronic decrease in $[Ca^{2+}]_i$; and (ii) the GCAP proteins mediate/amplify the response to this initial insult.

At a molecular level we show that >75% of GCAP2 in *rd3* mice is phosphorylated and therefore in its Ca^{2+}-free state, which is indicative of low $[Ca^{2+}]_i$ at *rd3* photoreceptor cell somas. Both GCAPs would therefore be in their Ca^{2+}-free, guanylate cyclase activator state at photoreceptor cell somas of *rd3* mice, where they result in cellular damage. How would GCAPs induce damage in this context?

We envision two possible pathways, sketched in our proposed model in Fig. 8.

First, as proposed by Dizhoor et al.[29] Ca^{2+}-free GCAPs could, in the absence of RD3, stimulate RetGCs and promote constitutive cGMP synthesis at the inner segment, where it would result in toxicity. Dizhoor's demonstration that RD3.GFP expressed as a transgene in rods localizes to the inner segment compartment[29] supports RD3 proposed role of silencing RetGCs while at the inner segment[25]. Dizhoor et al. also bred the *rd3* mice to GCAPs$^{-/-}$ mice and reported the retinal morphological rescue, interpreting the outcome as a demonstration of the importance of cyclase silencing at the inner segment for photoreceptor viability. While we believe that other scenarios cannot be discarded at this point, we consider our data to be consistent with Dizhoor's interpretation. We here show that the levels of RetGC in *rd3* mice are ~12% of the wild-type levels, that are present at the inner segment layer. By showing that GCAP2 is mostly phosphorylated, we can infer that GCAPs are in their Ca^{2+}-free form. Although 75% of the GCAP2 present in *rd3* mice (reduced to 42% of GCAP2 wild-type levels) is phosphorylated and bound to 14-3-3 and therefore not free to bind the cyclase, there is still ~10% of GCAP2 (referred to wild-type GCAP2 levels) that could bind the cyclase and activate it in a constitutive manner. Constitutive synthesis of cGMP would therefore rely on ~12% of the wild type levels of RetGC and ~10% of GCAP2, which is apparently low. However, constitutive synthesis of cGMP at the inner segment compartment of cones has been shown to be very toxic and the basis of the physiopathology in mouse models of achromatopsia caused by null mutations in cone CNG-channel subunits CNGA3 and CNGB3. In these models, activation of cGMP-dependent protein kinase (PKG) alters ER ionic homeostasis causing ER stress[32–34]. Actually, we here show that GCAPs mediate damage by activating ER stress-mediated apoptosis, by demonstrating CHOP induction as well as caspase 3 and PARP1 cleavage in *rd3* mice that are prevented in *rd3/rd3* GCAPs$^{-/-}$ mice (Fig. 6). Nevertheless, evidence of cGMP synthesis specifically at the inner segment compartment and/or PKG involvement is still missing in the *rd3* model and will require further investigation. An intriguing thought, assuming that preventing RetGC activity at the inner segment is critical for photoreceptor's viability, is that GCAP2 phosphorylation and 14-3-3 binding might serve as an additional mechanism to prevent cyclase activation in this compartment. Whether GCAP1 is phosphorylated is not known, and will require further investigation. However, it is GUCA1B gene encoding GCAP2 that was identified as a modifier gene of the *rd3* mouse phenotype[27], and GCAP2 expression that was downregulated in *rd3* mice[35].

A second putative pathway of damage involves the conformational instability of Ca^{2+}-free GCAP2,

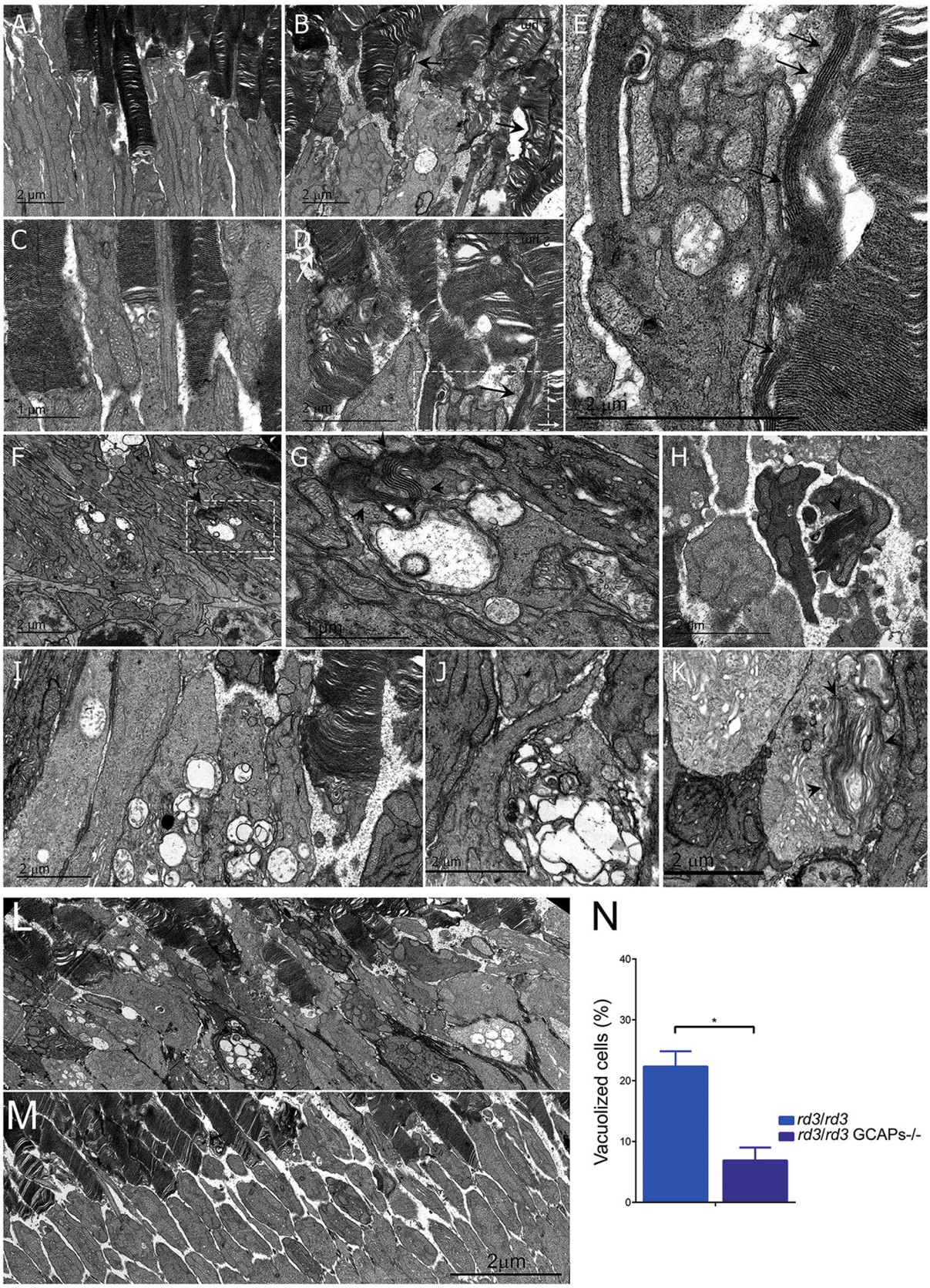

Fig. 7 (See legend on next page.)

(see figure on previous page)

Fig. 7 Mitochondrial swelling is an early sign of retinal degeneration in *rd3/rd3* mice that is substantially prevented by GCAPs ablation. **a**–**e** Comparison of *rd3/rd3* retinas at p20 (**b**, **d**) versus *rd3*/wt littermate controls (**a**, **c**). Retinas from *rd3/rd3* mice present distinctive features like emerging vertical outer segment membrane discs (black arrows in **b** and **d**, and in the enlarged area in **e**); as well as swelling mitochondria (arrowheads, **b** and **e**). **f**, **g**, **i**, **j** Mitochondrial swelling is a landmark ultrastructural alteration in *rd3/rd3* mice at early stages of retinal degeneration, as observed dramatically at a high number of photoreceptor cells at p26. **h**, **k** Other striking alterations are the internalization at the inner segment of what appears to be stacks of outer segment disc membranes (black arrowheads). **l**, **m**, **n** Mitochondrial swelling is substantially prevented by GCAPs ablation in the *rd3* mice, as observed by comparing a representative electron micrograph of retinal sections from *rd3/rd3* **l** and *rd3/rd3* GCAPs−/− mice **m** at p26. Images are the result of fusing four transmission electron microscopy fields obtained at 10,000× magnification. The number of photoreceptor cells that present mitochondrial swelling is substantially reduced in *rd3/rd3* GCAPs$^{-/-}$ mice versus *rd3/rd3* mice. **n** Four independent regions were analyzed per retina; and retinas were obtained from four mice of each genotype. Histograms represent the percentage of cells with presence of vacuoles, from the total number of cells. Unpaired *t*-test (*rd3/rd3* versus *rd3/rd3* GCAPs$^{-/-}$, $P = 0.019$*).

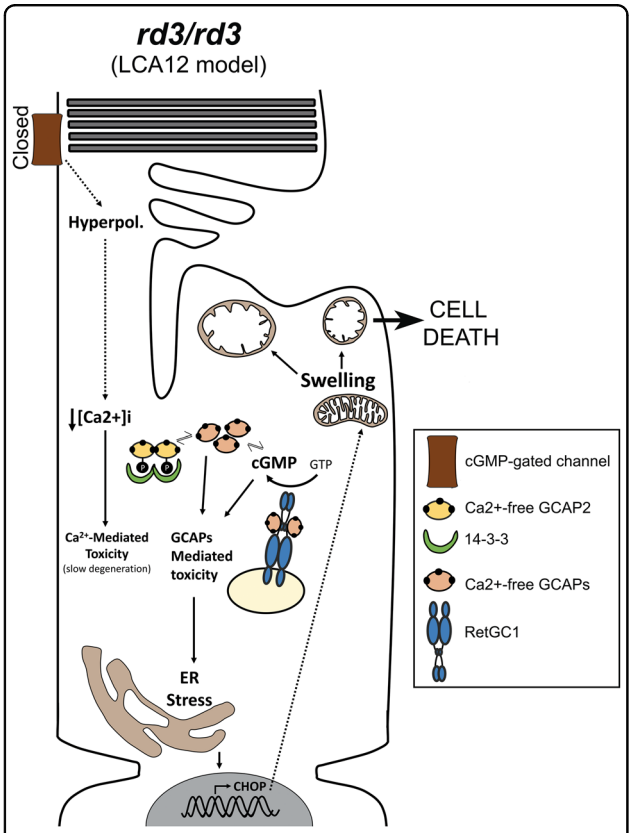

Fig. 8 Sketch summarizing the mechanisms that likely contribute to the physiopathology of *rd3* mice and LCA12 patients. The lack of RD3 represents an immediate insult for photoreceptor cells by causing chronic hyperpolarization and chronic low $[Ca^{2+}]_i$ due to the closure of CNG-channels by the severe drop in cGMP synthesis. This chronic low $[Ca^{2+}]_i$ likely represents the original insult causing damage to the cell. Chronic low Ca^{2+} cause the GCAP proteins to remain permanently in their Ca^{2+}-free conformation. GCAPs in their Ca^{2+}-free guanylate cyclase activator state in the absence of RD3 may stimulate cGMP synthesis at the inner segment, ultimately causing ER stress and ER stress-mediated apoptosis. Ca^{2+}-free GCAP2 conformational instability may also ultimately induce ER stress. GCAP2 phosphorylation and 14-3-3 binding might serve a protective role from both pathways of damage.

manifested by its high tendency to aggregate when expressed in bacteria[26]. We have previously shown that a form of GCAP2 locked in its Ca^{2+}-free form expressed as a transgene in rods is retained at the inner segment compartment by phosphorylation and 14-3-3 chaperone binding, leading to a fast retinal degeneration[26]. EF^{-}GCAP2 toxicity occurs in the presence of RD3 silencing the cyclase. One possibility would be that the Ca^{2+}-free form of GCAP2 formed toxic protein oligomers, with 14-3-3 binding serving a protective role by preventing this formation. In this manner, GCAP2 could cause damage in a similar way as how α-synuclein contributes to Parkinson's disease[36,37]. The instability of Ca^{2+}-free GCAP2 is also reflected in its high affinity for the HSP90 dimer observed in pull-down assays (Fig. 5), that raises the possibility that Ca^{2+}-free GCAP2 under chronic low $[Ca^{2+}]_i$ may trigger the heat shock response.

A few other proteins were selectively identified as putative interactors of GCAP2-P, like the cytoskeletal regulator Ndel1, nuclear-distribution gene E homolog like-1 protein, a modulator of dynein that has been involved in securing the selectivity of cargo delivered to axons[38], and at inhibiting primary cilia assembly in proliferating cells[39]. Ndel1 would be a putative candidate to mediate the morphological disc alterations observed in *rd3* mice. Future experiments will test this hypothesis, and aim at confirming other putative interactions.

Finally, by expressing RD3.V5 as a transgene in the rods of *rd3* mice, we report that RD3 localizes mainly to photoreceptor inner segments, although it also distributes to some extent to the outer segments (Fig. 4). The outer segment RD3 signal might not have been so apparent in the recent study of RD3.GFP localization in rods[29] due to the protein modification by the much bigger tag. RD3 main localization to the inner segment provides some insight into the mechanisms underlying trafficking of the cyclase to the cilium. The cyclase is probably transported in two stages: a first stage, in which it is escorted and silenced by RD3 to the base of the connecting cilium; and a second, in which the GCAPs displace RD3 to bind the cyclase, previous to RetGC/GCAPs complex entry into

the outer segment compartment. Future studies will be addressed at elucidating the mechanistic steps of this trafficking.

Materials and methods

Ethics statement

Pertaining to animal research, this study was conducted in accordance with the Association for Research in Vision and Ophthalmology (ARVO) statement for the use of animals in ophthalmic and vision research and in compliance with acts 5/1995 and 214/1997 for the welfare of experimental animals of the autonomous community (Generalitat) of Catalonia; ref. #9906, and approved by the ethics committee on animal experiments of the University of Barcelona, Bell 216/17, 217/17, and 218/17.

Mice

The B6.Cg-Rd3rd3/Boc strain of *rd3* mice used in this study were obtained from the Jackson's Laboratories (JAX Stock #8627 Maine, USA) as heterozygous wt/*rd3* mice[13]. These mice present a point mutation after residue 106 (C→T) that results in a premature stop codon after residue 106. The *rd3* mutation results in expression of a truncated form of the RD3 protein that is rapidly degraded[14]. Heterozygous animals were bred in order to obtain homozygous *rd3*/*rd3* mice. Mice were genotyped by real-time polymerase chain reaction (RT-PCR) by making use of the TaqMan® SNP genotyping assay (Life Technologies, Carlsbad, USA). For that purpose, forward and reverse primers were designed to amplify a fragment of 68 bp from the *Rd3* locus of genomic DNA that encompasses the *rd3* mutation (Fw: 5′-CTGGAGACGC TCATGATGGA-3′; and Rv: 5′-CGACGCTCCCTCTG TTGT-3′) and primer probes were designed to hybridize with either the amplified wild-type allele (VIC-5′-CT CTCTCATCTGCCCAGCC-3′) or knock-out allele (FAM-5′-CTCTCTCATCTACCCAGCC-3′). RT-PCR was performed in 25 µl reactions containing 12.5 µl TaqMan universal master Mix (Life Technologies); 300 nM each forward/reverse primer; 250 nM of each primer probe, and 20 ng of genomic DNA obtained from digested mouse tails (Nucleospin® Tissue, Macherey-Nagel, Düren, Germany). After 10 min incubation at 95 °C, thermal cycling was performed on the StepOne Real-time PCR System (Thermo Fisher Scientific, Waltham, Massachusetts) and consisted of 40 cycles (95 °C for 15 s; 60 °C for 1 min). End-point allelic discrimination genotyping was assessed by inspecting the fluorescence plots for the wild type versus mutated probe.

To obtain mice expressing the *rd3* mutation to homozygosis in the GCAPs$^{-/-}$ background, *rd3*/*rd3* mice were bred to GCAPs$^{-/-}$ mice. GCAPs$^{-/-}$ mice lack GCAP1 and GCAP2 expression, and their phenotype has been described[40].

Antibodies

Anti-GCAP1 and anti-GCAP2 polyclonal antibodies have been previously described[22]. The polyclonal antibodies against RetGC1 and RD3 were generated in rabbit against C-terminal peptides corresponding to the last 21aa of murine RetGC1 and the last 16aa of murine RD3. Peptides were conjugated to keyhole limpet hemocyanin carrier protein (Imject maleimide activated carrier protein spin kit, Thermo Fisher Scientific) for inoculation in rabbits. A 90-day, three antigen-injection protocol was followed. Serum from immunized rabbits was purified by affinity chromatography by using the immunizing peptide covalently coupled to an agarose column by –SH chemistry (Sulfolink immobilization kit for peptides, Thermo Fisher Scientific). The specificity of the antibodies is shown by Western blot analysis of whole retinal extracts in Supplementary Fig. 1.

Specimen preparation for light and electron microscopy

Mice of the indicated genotypes were reared under standard cyclic light (12 h dark:12 h light) and sacrificed by cervical dislocation. The vertical meridian of the eye was marked at the top for orientation purposes. The eye was enucleated, punctured, and immediately submerged in 2% paraformaldehyde, and 2.5% glutaraldehyde in 0.1 M cacodylate buffer pH 7.2 for 5 min. The cornea was excised and fixation was allowed to proceed for 1 h, before removal of the lense and further fixation of the eye cup for 12 h at 4 °C. Eye cups were washed with 0.1 M cacodylate buffer and fixed with 1% osmium tetroxide in 0.1 M cacodylate buffer for 2 h at room temperature. Specimens were dehydrated in ethanol (30–100%) or acetone, infiltrated with propylene oxide, and embedded in Epoxi embedding medium (Fluka Analytical, Munich, Germany). Retinal sections for histological analysis by light microscopy morphometry measurements were obtained with a Reichert Ultracut S ultramicrotome (Leica, Wetzlar, Germany) at 1-µm thickness and contrasted with Richardson's stain (0.5% methylene blue, 0.5% Azine II, and 0.5% borax in dH_2O). For transmission electron microscopy analysis, ultrathin sections were obtained (see below).

Retinal morphometry analysis

For morphometrical analysis, measurements of ONL thickness were taken on 1-µm sections at the vertical meridian of the eye that encompassed the optic nerve. Overlapping frames at 20× magnification were acquired covering the whole section with a Zeiss Axio Zoom. V16 stereo microscope (Zeiss, Oberkochen, Germany). An integrated image of the whole retinal section was assembled with the HUGIN fusion software. Measurements of ONL thickness were taken at 200-µm intervals from the optic nerve (12 divisions in the superior retina, and 10 divisions in the inferior retina). For each

morphometry analysis a minimum of four mice per genotype were used at indicated ages. Error bars represent the standard error of the mean (SEM).

Ultrathin sectioning and image acquisition at the transmission electron microscope

Ultrathin sections (70–90 nm) were obtained with a Reichert Ultracut S ultramicrotome (Leica), collected on 200 mesh copper grids, counterstained by heavy metal staining (2% uranyl acetate in 50% ethanol for 30 min), and contrasted with 2% lead citrate for 10 min. Ultrathin sections were analyzed in a JEOL 1010 transmission electron microscope and images acquired with a Bioscan Gatan wide angle slow scan CCD camera.

Immunofluorescence analysis in fixed tissue

For immunofluorescence analysis, eye cups were fixed in 4% paraformaldehyde, 0.02% glutaraldehyde in phosphate-buffered saline (PBS), pH = 7.4 for 2 h at room temperature. Eye cups were infiltrated in acrylamide (8.4% acrylamide, 0.014% bisacrylamide in PBS pH 7.4) overnight at 4 °C. Acrylamide polymerization was induced and eye cup acrylamide blocks immediately frozen in O.C.T. compound (Tissue-Tek, Electron microscopy Sciences, Hatfield, PA) using liquid nitrogen. Cryosections were obtained at 18-µm thickness with a CM15105 Leica Cryostat (Leica Microsystems, Wetzlar, Germany). Immunolocalization of GCAP1 and GCAP2 required an antigen retrieval protocol, consistent on incubation with proteinase K (0.05 mg/ml in PBS) for 2 min, followed by a 10 s heating shock at 70 °C. Sections were incubated with blocking solution (3% normal goat serum, 1% bovine serum albumin (BSA), 0.3% Triton-X100 in PBS pH7.4) for 1 h; first antibody in dilution buffer (3% normal goat serum, 0.4% BSA, 0.1% Triton-X100 in PBS pH 7.4) for 16 h at 4 °C; and secondary antibody (1.5 h at room temperature), and fixed with 4% paraformaldehyde prior to being mounted with Mowiol (Calbiochem #475904, San Diego, CA, USA). Antibodies used were anti-RetGC1 pAb; anti-GCAP1 pAb; anti-GCAP2 pAb; anti-rhodopsin mAb 1D4; anti-PNA-647 (# L32460, Thermo Fisher Scientific); anti-rabbit Alexa Fluor 488 (Thermo Fisher Scientific A-11034, Walthman, MA, USA); and anti-mouse Alexa Fluor 555 (Thermo Fisher Scientific #A-32727). Samples were mounted on 0.13–0.16 mm thick cover glasses.

Confocal microscopy and data analysis

Confocal microscopy images were acquired at a confocal laser scanning microscope Zeiss LSM 880 equipped with one GaAsP detector, with a 63×/1.4 NA oil objective. For localization of RetGC and GCAPs in Figs. 1 and 2, spectral bands were set to 493–550 nm for the 488 channel, 566–638 nm for the 555 channel, and to 638–755 nm for the 647 channel. The *Z*-stacks covered 16 µm of tissue with a 368 nm step size (~40 planes/stack). The image acquisition settings provided a pixel size of about 0.132 × 0.132 µm in 1024 × 1024 images.

Western blot

Retinas (at least $n = 3$ per condition) were homogenized in Laemmli sodium dodecyl sulfate (SDS) buffer with 1 mM phenylmethylsulfonyl fluoride (PMSF), and protease cocktail inhibitor (Complete mini EDTA-free, Roche). Samples were boiled for 10 min at 95 °C, and fractions corresponding to one tenth of a retina were resolved by 12 or 16% SDS–polyacrylamide gel electrophoresis. Proteins were transferred to nitrocellulose membranes (0.2 µm nitrocellulose, Bio-Rad, Hercules, CA, USA). Membranes were blocked for 1 h at room temperature with 5% non-fat dry milk in TBST and then were incubated overnight at 4 °C with custom polyclonal antibodies to RetGC1, RD3, GCAP1, and GCAP2, and antibodies anti-CHOP (Cell Signaling L63F7); anti-Caspase 3 (Cell Signaling 9662); anti-PARP1 (Cell Signaling 9542); goat anti-rabbit IgG (Heavy and Light chains) antibody Dylight™ 800 conjugated (Rockland #611-145-002, Pottstown, PA, USA); goat anti-mouse IgG (H&L) antibody Dylight™ 680 conjugated (Rockland #610-144-002-0.5); and donkey anti-goat conjugated to Horseradish Peroxidase (HRP) was from Thermo Fisher (86326). Detection was performed in an Odyssey Scanner (LI-COR Biosciences, Lincoln, Nebraska) or ImageQuant™ LAS500 (Ge Healthcare, Chicago, Illinois) image acquisition system. Band densitometric analysis was performed using the Fiji (Image J) software, and band intensity analysis presented in histograms always reflect band intensity of the protein of interest normalized by the intensity of tubulin in the loading control.

Isoelectric focusing separation of murine retinal homogenates

Retinas from wt and *rd3/rd3* mice were dissected at p21, at an early onset of retinal degeneration of *rd3* mice. Retinas were homogenized in homogenization buffer with phosphatase inhibitors [20 mM Hepes, 115 mM KCl, 10 mM NaCl, 10 mM $MgCl_2$, 50 mM NaF, 5 mM β-glycerophosphate, 1 mM PMSF, and a protease cocktail inhibitor (Complete mini EDTA-free, Roche, Basel, Switzerland); pH 7.4]. Samples were centrifuged at 13,200 rpm, 4 °C for 30 min, and supernatant fractions were kept. An aliquot was taken at this point for protein determination (BCA kit, Thermo Fisher Scientific). Protein material in supernatant fractions was precipitated by addition of three volumes of ice-chilled trichloroacetic acid (TCA)-acetone (13.3% w/v trichloroacetic acid in acetone, with dithiothreitol (DTT) to 20 mM final concentration); equilibration of samples to −20 °C for 72 h;

and centrifugation at 13,000×*g* for 1 h at 4 °C. Protein pellets were washed twice with cold 20 mM DTT in acetone; and allowed to air-dry for 10 min. Samples were dissolved in urea/thiourea/CHAPS/DTT (7 M urea, 2 M thiourea, 40 mM DTT, 4% CHAPS, and 2% IPG buffer pH 3–10) to ensure complete reduction, denaturing, and solubilization of proteins in the samples.

Samples were kept at −80 °C until use. For isoelectric focusing (IEF) separation, gel strips with a preformed linear pH gradient of pH 3–10 (prehydrated IPG Immobiline (TM) DryStrips pH 3–10, 18 cm, GE Healthcare) were used. Threefold more sample was loaded for *rd3/rd3* retinas than wt retinas in order to equilibrate the GCAP2 signal. IEF separation was conducted on an Ettan IPGphor3 system (GE Healthcare), following a 500 V step for 1 h, a gradient to 1000 V for 1 h, a gradient to 10,000 V for 3 h, and a 10,000 V step for 3 h. Gel strips were incubated in transfer buffer for 15 min, and proteins were transferred to nitrocellulose membranes by capillary action. GCAP2 was immunoblotted with anti-GCAP2 pAb and goat anti-rabbit IgG (Heavy and Light chains) antibody Dylight™ 800. Bands were visualized at an Odyssey scanner (LI-COR), and densitometry analysis was performed with the Fiji (ImageJ) software.

Expression, purification, and in vitro phosphorylation of myristoylated GCAP2 for pull-down assays

Myristoylated GCAP2 expression was induced in *Escherichia coli* BL21(DE3) cells transformed with pET-15b-bGCAP2 and the pBB131 plasmid encoding N-myristoyl transferase (a gift from Dr. J. Gordon, Washington University School of Medicine, Missouri, USA). Free myristic acid was added to 50 µg/ml to the cell culture and expression was induced for 4 h at 37 °C. bGCAP2 protein, was recovered from solubilized inclusion bodies and purified by on-column refolding using immobilized metal affinity chromatography (IMAC) on a Nickel-NTA [Nickel bound to agarose beads by chelation using nitrilotriacetic acid] as previously described[26].

To obtain phosphorylated bGCAP2 for pull-down assays, in vitro phosphorylation reactions were performed with protein kinase G (PKGIα, Calbiochem, Billerica, MA, USA). Each 50 µl reaction contained 30 mM Tris-HCl pH 7.5, 5 mM $MgCl_2$, 5 mM sodium phosphate buffer pH 7.5, 6 mM DTT, 2 mM EGTA, 10 µM ATP, and 500 µM cGMP, with 10 µg of bGCAP2 in the presence or absence of purified PKGIα (100 units) to obtain phosphorylated GCAP2 (GCAP2-P) and the mock-control (GCAP2). Phosphorylation reactions were allowed to proceed for 2 h at 30 °C, and GCAP2 and GCAP2-P were covalently linked to Epoxi-magnetic beads (Life Technologies, Carlsbad, CA, USA). GCAP2- or GCAP2-P-beads were then incubated with bovine retinal homogenates obtained by homogenization of fresh bovine retinas in binding buffer (10 mM HEPES, 135 mM NaCl, 5 mM KCl, 1 mM PMSF, 1 mM NaF, 1 mM β-mercaptoethanol, 1% Triton X-100, 4 mM EGTA, 2 mM EDTA, and Complete Mini protease inhibitors, pH 7.4). After 1 h incubation at room temperature, beads were washed and bound proteins were eluted under acidic conditions. Magnetic beads were extensively washed, and bound material was eluted in 0.2 M glycine pH 2.5 and immediately neutralized. Proteins in the bound fraction were identified by LC-MS/MS. The experiment included three biological replicates.

LC-MS/MS

Samples were reduced with 10 mM DTT at 60 °C for 30 min, and alkylated with 55 mM iodoacetamide for 30 min at room temperature. Samples were precipitated with 10% TCA. Pellets were dissolved in 2 µl of 8 M urea and brought to a final volume of 10 µl with 25 mM ammonium bicarbonate. Samples were digested with sequencing grade trypsin in 25 mM ammonium bicarbonate for 12 h. For LC-MS/MS, samples were resuspended in 0.1% formic acid and injected into a series Proxeon LC nanoEASY system (Thermo Fisher Scientific) coupled to a LTQ-Velos Orbitrap (Thermo Fisher Scientific). The resulting mass spectral peak lists were searched with the Sequest search engine (v.2.1.04, Matrix Sciences, London, UK) against the merged BOVIN-MOUSE UP SP r 2011-1.fasta sequence library. For database searching, raw mass spectrometry files were submitted to the in-house MOUSE-BOVIN_UP_SP_r_2014-5.fasta Swiss-Prot database (released February 2014; 22460 protein entries) using SEQUEST version 28.0 (Thermo Fisher Scientific). The criteria used to accept identification included a minimum of two peptides matched per protein, with a false discovery rate of 1%. All proteins were treated as ungrouped.

Characterizing differential protein interactions of GCAP2-P and GCAP2

For label-free quantitative proteomic analysis of proteins identified with GCAP2-P versus GCAP2, we first filtered the protein lists to remove any duplications resulting from the use of bovine and mouse fasta sequence libraries. Only those proteins unequivocally assigned by at least a unique peptide were retained. For each protein identified the NSAF was calculated with the following equation:

$$\mathrm{NSAF}_k = \frac{(\mathrm{SpC}_k + 1)/L_k}{\sum_{i=0}^{n}(\mathrm{SpC}_i + 1)/L_i} \quad (1)$$

where NSAF_k is the Normalized Spectral Abundance Factor[41] for a given protein k; SpC_k is the Spectral Count for protein k, L_k is the length of the protein in number of amino acids; and the denominator is the summation of

the NSAFs of all identified proteins in that sample. This expression corrects for differences in sampling depth between both conditions assayed, and avoids the discontinuity seen in simple count ratios when a protein shows spectral count = 0 in one of the samples.

Mean NSAF values were then calculated from triplicate biological samples, followed by a *t*-test comparison (two tails, unequal variance). To obtain the volcano plot, the $\log_2 \frac{\text{Mean}_P}{\text{Mean}_{NP}}$ was plotted in the *x*-axis; and the $-10\log(p\,value)$ from the *t*-test was plotted in the *y*-axis, with Mean_P referring to Mean $\text{NSAF}_{\text{GCAP2-P}}$, and Mean_{NP} referring to Mean $\text{NSAF}_{\text{GCAP2.}}$ Threshold curves for the volcano plot were obtained by fitting values to

$$f(x) = \frac{1}{x^2 - n} + m \quad (2)$$

were *n* is the value of the $\log_2 \frac{\text{Mean}_P}{\text{Mean}_{NP}}$ ratio threshold and *m* is the $-10\log(p$ value) threshold. *m* and *n* values were fixed to 5 and 1.35 respectively. (Notes: taking $a \equiv \log_2\left(\frac{P}{NP}\right)$ and $b \equiv -10\log(p - value)$, the proteins passing the thresholds are those proteins that: $a < -\sqrt{n}$ and $b > f(x)$ for the negative side; and $a > \sqrt{n}$ and $b > f(x)$, for the positive side.

Electroretinography

A total of 4–7 mice were tested for each animal group. Dark-adapted (>12 h) animals were anesthetized with an intraperitoneal injection of ketamine (70 mg/kg; Ketalar, Parke-Davis, Wellington, New Zealand) and xylazine (7 mg/kg; Rompun, Bayer, Leverkusen, Germany) in saline solution (NaCl 0.9%) and pupils were dilated with one drop of 1% tropicamide. A corneal electrode was used to record ERGs from right eyes (Burian-Allen, Hansen Ophthalmic Development Lab, Coralville, IA). Electrode was placed in the visual axis 1–2 mm from the cornea and a drop of 2% methyl-cellulose (Methocel, Ciba Vision, Hetlingen, Switzerland) was dropped between cornea and electrode. Mice were maintained for >5 min in absolute darkness before the recordings. Mouse temperature during the recording was maintained at 37 °C with a liquid heating pad. Full-field flash ERG responses were recorded with the retina illuminated with a LED-driven Ganzfeld dome. A series of light flashes of increasing intensity (from 0.001 to 10 cd/s/m^2) were averaged both in scotopic and photopic conditions. Photopic cone responses were recorded following 5 min of light adaptation with a background white light (50 cd/m^2). Light intensity was controlled for each animal group (Mavo-Monitor USB, Gossen, Germany). Recorded electrophysiological responses were amplified, filtered (CP511 AC amplifier; Grass Instruments, Quincy, MA), and digitalized (ADInstruments Ltd, Oxfordshire, UK). The recording process was controlled with Scope version 3.8.1 software (Power Lab, ADInstruments Ltd). The stimulation protocols were designed according to the International Society for Clinical Electrophysiology of Vision.

Generation of pRho-mRd3.V5-dsRed expression vector and in vivo DNA electroporation

The expression vector used for in vivo DNA electroporation was based on the plasmid pRho-DsRed. pRho-DsRed was a gift from Connie Cepko (Addgene plasmid#11156; http://n2t.net/addgene:11156;RRID:Addgene_11156)[42]. This plasmid contains the 2.2 kb-version of the rod opsin promoter from Bos taurus[43]; a multicloning site; a Kozak sequence; the DsRed2 reporter gene; and the β-globin poly(A) signal[42]. To make pRho-mRD3.V5-DsRed, murine *rd3* cDNA was amplified by PCR with a forward primer that introduced an XbaI restriction site and the reverse primer introducing the V5 epitope in frame with RD3 COOH-terminal sequence, followed by an EcoRI restriction site. The mRD3.V5 DNA was inserted in the XbaI and EcoRI sites of pRho-DsRed, and the resulting expression vector was verified by sequencing. For in vivo electroporation, pRho-mRd3.V5-dsRed vector was amplified with the pureLinkTM Expi Endotoxin-Free Mega Plasmid Purification Kit (Invitrogen, Carlsbad, California).

In vivo DNA electroporation in the retina following DNA injection in the subretinal space was performed as originally described[42] with minor modifications. A DNA solution (6 µg/µl) was prepared by mixing pRho-DsRed and pRho-mRD3.V5-DsRed at a molar ratio of 1:4 in phosphate saline buffer with 0.1% v-v fast green. Even though pRho-mRD3.V5-DsRed expressed dsRed, we found the levels of expression too low for detection of the eye injected area at the fluorescence dissection scope. Therefore pRho-DsRed was coinjected with pRho-mRD3.V5-DsRed. Pups were injected the day they were born at the subretinal space, with 0.2–0.5 µl of DNA by using a Hamilton syringe with a blunt 30-gauge needle under a dissecting microscope (Zeiss KL1500LCD. Stemi2000, Germany). Tweezer-type electrodes were placed softly holding the head of the pup, and five 80 V square pulses of 50 ms duration with 950 ms intervals were applied using a CUY21 electroporator (Nepagene, Chiba, Japan). Electroporated eyes were processed at p20–p25 for immunofluorescence localization analysis as described above. Antibodies were anti-RetGC1 pAb and the anti-V5 mAb (2F11F7, Invitrogen) by secondary antibodies α-rabbit Alexa Fluor 488 (Life Technologies) and α-mouse Alexa Fluor 647 (Life Technologies) both at 1:500 for 1.5 h at room temperature. The image has been acquired with a LEICA SP5 microscope using a 63 × 1.4 NA oil objective. The pixel and step sizes are 100 nm and 198 nm

respectively providing an effective image volume of 131 µm × 131 µm × 9.5 µm. Two Hybrid detectors in photon counting mode and a photomultiplier tube (PMT) have been used to acquire the different channels. The spectral configuration for the channel 1 used a 488 nm laser line and an emission window from 498 to 535 nm. The channel 2 used the 633 nm laser line and an emission window between 642 and 722 nm. Finally, the channel 3 used the 543 nm laser line with the emission window set between 551 and 616 nm.

Acknowledgements
We acknowledge the assistance of Dr. A. Gimeno and L. Gómez-Segura at the Vivarium facility with antibody generation in rabbits and with animal procedures. We kindly acknowledge the excellent technical assistance of Dr. Benjamín Torrejón with image acquisition at the Leica TCS-SL at the CCiT-UB. We thank Dr. Cristina Muñoz for her advice on ER stress analysis. J.A. and P.L. acknowledge financial support from the Spanish Ministry of Economy and Competitiveness through the "Severo Ochoa" program for Centres of Excellence in R&D (SEV-2015-0522), from Fundació Privada Cellex, Fundación Mig-Puig, from Generalitat de Catalunya through the CERCA program, and Laser lab Europe (No. 654148). Pdl.V. was supported by a grant from the Spanish Instituto de Salud Carlos III [ISCIII] (PI18/00754). A.M. acknowledges funding from the Spanish Ministry of Economy and Competitiveness (MINECO): BFU2016-80583-R; from the Ramón Areces Foundation: XVII Edition on Rare Diseases; and from Generalitat de Catalunya through the CERCA program. J.A., P.L., and A.M. acknowledge funding from the Foundation La Marató de TV3: ref. 20141730.

Author details
[1]Department of Physiological Sciences, University of Barcelona School of Medicine - Health Science Campus of Bellvitge, L´Hospitalet de Llobregat, 08907 Barcelona, Spain. [2]Institute of Neurosciences, University of Barcelona, Castelldefels, 08035 Barcelona, Spain. [3]Institut d'Investigació Biomèdica de Bellvitge - IDIBELL, L´Hospitalet de Llobregat, Castelldefels, 08908 Barcelona, Spain. [4]ICFO-Institut de Ciències Fotoniques, The Barcelona Institute of Science and Technology, Castelldefels, 08860 Barcelona, Spain. [5]Centres Cientifics i Tecnològics (CCiTUB), University of Barcelona, Castelldefels, 08036 Barcelona, Spain. [6]Physiology Unit, Dept of Systems Biology, School of Medicine, University of Alcalá, Alcalá de Henares, 28805 Madrid, Spain. [7]Visual Neurophysiology Group-IRYCIS, Madrid, Spain

Author contributions
Conceived and designed the experiments: A.P.B., S.L.B., Pdl.V., and A.M. Performed the experiments: A.P.B., S.L.B., Pdl.V., J.A., P.L., M.J.F., J.M.E., and A.M. Analyzed the data: S.L.B., A.P.B., Pdl.V., and A.M. Wrote the paper: A.M.

Conflict of interest
The authors declare that they have no conflict of interest.

Publisher's note
Springer Nature remains neutral with regard to jurisdictional claims in published maps and institutional affiliations.

Supplementary Information accompanies this paper at (https://doi.org/10.1038/s41419-020-2255-0).

Received: 5 November 2019 Revised: 9 January 2020 Accepted: 10 January 2020
Published online: 24 January 2020

References

1. Burns, M. E. & Arshavsky, V. Y. Beyond counting photons: trials and trends in vertebrate visual transduction. *Neuron* **48**, 387–401 (2005).
2. Arshavsky, V. Y. & Burns, M. E. Photoreceptor signaling: supporting vision across a wide range of light intensities. *J. Biol. Chem.* **287**, 1620–1626 (2012).
3. Perrault, I. et al. Retinal–specific guanylate cyclase gene mutations in Leber's congenital amaurosis. *Nat. Genet.* **14**, 461–464 (1996).
4. Payne, A. et al. A mutation in guanylate cyclase activator 1A (GUCA1A) in an autosomal dominant cone dystrophy pedigree mapping to a new locus on chromosome 6p21.1. *Hum. Mol. Genet.* **7**, 273–277 (1998).
5. Kelsell, R. E. et al. Mutations in the retinal Guanylate Cyclase (RetGC-1) gene in dominant cone-rod dystrophy. *Hum. Mol. Genet.* **7**, 1179–1184 (1998).
6. Marino, V. et al. A novel p.(Glu111Val) missense mutation in GUCA1A associated with cone-rod dystrophy leads to impaired calcium sensing and perturbed second messenger homeostasis in photoreceptors. *Hum. Mol. Genet.* **27**, 4204–4217 (2018).
7. Kitiratschky, V. B. D. et al. Mutations in the *GUCA1A* gene involved in hereditary cone dystrophies impair calcium-mediated regulation of guanylate cyclase. *Hum. Mutat.* **30**, E782–E796 (2009).
8. Michaelides, M. et al. Mutation in the gene GUCA1A, encoding Guanylate Cyclase-Activating Protein 1, causes cone, cone-rod, and macular dystrophy. *Ophthalmology* **112**, 1442–1447 (2005).
9. Wilkie, S. E. et al. Identification and functional consequences of a new mutation (E155G) in the gene for GCAP1 that causes autosomal dominant cone dystrophy. *Am. J. Hum. Genet.* **69**, 471–480 (2001).
10. Vocke, F. et al. Dysfunction of cGMP signalling in photoreceptors by a macular dystrophy-related mutation in the calcium sensor GCAP1. *Hum. Mol. Genet.* **26**, ddw374 (2016).
11. Peshenko, I. V. et al. A G86R mutation in the calcium-sensor protein GCAP1 alters regulation of retinal guanylyl cyclase and causes dominant cone-rod degeneration. *J. Biol. Chem.* **294**, 3476–3488 (2019).
12. Jiang, L. et al. A novel GCAP1(N104K) mutation in EF-hand 3 (EF3) linked to autosomal dominant cone dystrophy. *Vis. Res.* **48**, 2425–2432 (2008).
13. Chang, B., Heckenlively, J. R., Hawes, N. L. & Roderick, T. H. New mouse primary retinal degeneration (rd-3). *Genomics* **16**, 45–49 (1993).
14. Friedman, J. S. et al. Premature truncation of a novel protein, RD3, exhibiting subnuclear localization is associated with retinal degeneration. *Am. J. Hum. Genet.* **79**, 1059–1070 (2006).
15. Azadi, S., Molday, L. L. & Molday, R. S. RD3, the protein associated with Leber congenital amaurosis type 12, is required for guanylate cyclase trafficking in photoreceptor cells. *Proc. Natl Acad. Sci. USA* **107**, 21158–21163 (2010).
16. Dizhoor, A. M., Olshevskaya, E. V. & Peshenko, I. V. Mg2+/Ca2+ cation binding cycle of guanylyl cyclase activating proteins (GCAPs): role in regulation of photoreceptor guanylyl cyclase. *Mol. Cell. Biochem.* **334**, 117–124 (2010).
17. Peshenko, I. V. et al. Enzymatic properties and regulation of the native isozymes of retinal membrane guanylyl cyclase (RetGC) from mouse photoreceptors. *Biochemistry* **50**, 5590–5600 (2011).
18. Makino, C. L. et al. Enzymatic relay mechanism stimulates cyclic GMP synthesis in rod photoresponse: biochemical and physiological study in Guanylyl Cyclase Activating Protein 1 knockout mice. *PLoS ONE* **7**, e47637 (2012).
19. Méndez, A. et al. Role of guanylate cyclase-activating proteins (GCAPs) in setting the flash sensitivity of rod photoreceptors. *Proc. Natl. Acad. Sci. USA* **98**, 9948–9953 (2001).
20. Burns, M. E., Méndez, A., Chen, J. & Baylor, D. A. Dynamics of cyclic GMP synthesis in retinal rods. *Neuron* **36**, 81–91 (2002).
21. Baehr, W. et al. The function of Guanylate Cyclase 1 and Guanylate Cyclase 2 in rod and cone photoreceptors. *J. Biol. Chem.* **282**, 8837–8847 (2007).
22. López-Begines, S., Plana-Bonamaisó, A. & Méndez, A. Molecular determinants of Guanylate Cyclase Activating Protein subcellular distribution in photoreceptor cells of the retina. *Sci. Rep.* **8**, 2903 (2018).
23. Jacobson, S. G. et al. Determining consequences of retinal membrane guanylyl cyclase (RetGC1) deficiency in human Leber congenital amaurosis en route to therapy: residual cone-photoreceptor vision correlates with biochemical properties of the mutants. *Hum. Mol. Genet.* **22**, 168–183 (2013).
24. Linberg, K. A., Fariss, R. N., Heckenlively, J. R., Farber, D. B. & Fisher, S. K. Morphological characterization of the retinal degeneration in three strains of mice carrying the *rd-3* mutation. *Vis. Neurosci.* **22**, 721–734 (2005).
25. Peshenko, I. V. et al. Retinal Degeneration 3 (RD3) protein inhibits catalytic activity of retinal membrane Guanylyl Cyclase (RetGC) and its stimulation by activating proteins. *Biochemistry* **50**, 9511–9519 (2011).
26. López del Hoyo, N., López-Begines, S., Rosa, J. L., Chen, J. & Méndez, A. Functional EF-hands in neuronal calcium sensor GCAP2 determine its phosphorylation state and subcellular distribution in vivo, and are essential for photoreceptor cell integrity. *PLoS Genet.* **10**, e1004480 (2014).

27. Danciger, M. et al. Genetic modifiers of retinal degeneration in the *rd3* Mouse. *Investig. Opthalmology Vis. Sci.* **49**, 2863–2869 (2008).
28. Molday, L. L. et al. RD3 gene delivery restores guanylate cyclase localization and rescues photoreceptors in the Rd3 mouse model of Leber congenital amaurosis 12. *Hum. Mol. Genet.* **22**, 3894–3905 (2013).
29. Dizhoor, A. M., Olshevskaya, E. V. & Peshenko, I. V. Retinal guanylyl cyclase activation by calcium sensor proteins mediates photoreceptor degeneration in an *rd3* mouse model of congenital human blindness. *J. Biol. Chem.* **294**, 13729–13739 (2019).
30. Peshenko, I. V., Olshevskaya, E. V. & Dizhoor, A. M. Ca^{2+}-dependent conformational changes in guanylyl cyclase-activating protein 2 (GCAP-2) revealed by site-specific phosphorylation and partial proteolysis. *J. Biol. Chem.* **279**, 50342–50349 (2004).
31. Oyadomari, S. & Mori, M. Roles of CHOP/GADD153 in endoplasmic reticulum stress. *Cell Death Differ.* **11**, 381–389 (2004).
32. Ma, H. et al. cGMP/Protein Kinase G signaling suppresses inositol 1,4,5-trisphosphate receptor phosphorylation and promotes endoplasmic reticulum stress in photoreceptors of cyclic nucleotide-gated channel-deficient mice. *J. Biol. Chem.* **290**, 20880–20892 (2015).
33. Thapa, A. et al. Endoplasmic reticulum stress-associated cone photoreceptor degeneration in cyclic nucleotide-gated channel deficiency. *J. Biol. Chem.* **287**, 18018–18029 (2012).
34. Butler, M. R. et al. Endoplasmic reticulum (ER) Ca^{2+} -channel activity contributes to ER stress and cone death in cyclic nucleotide-gated channel deficiency. *J. Biol. Chem.* **292**, 11189–11205 (2017).
35. Cheng, C. L. & Molday, R. S. Changes in gene expression associated with retinal degeneration in the rd3 mouse. *Mol. Vis.* **19**, 955–969 (2013).
36. Plotegher, N. et al. The chaperone-like protein 14-3-3η interacts with human α-synuclein aggregation intermediates rerouting the amyloidogenic pathway and reducing α-synuclein cellular toxicity. *Hum. Mol. Genet.* **23**, 5615–5629 (2014).
37. Yacoubian, T. A. et al. Differential neuroprotective effects of 14-3-3 proteins in models of Parkinson's disease. *Cell Death Dis.* **1**, e2–e2 (2010).
38. Kuijpers, M. et al. Dynein regulator NDEL1 controls polarized cargo transport at the axon initial segment. *Neuron* **89**, 461–471 (2016).
39. Inaba, H. et al. Ndel1 suppresses ciliogenesis in proliferating cells by regulating the trichoplein–Aurora A pathway. *J. Cell Biol.* **212**, 409–423 (2016).
40. Méndez, A. et al. Role of guanylate cyclase-activating proteins (GCAPs) in setting the flash sensitivity of rod photoreceptors. *Proc. Natl. Acad. Sci. USA* **98**, 9948–9953 (2001).
41. Zybailov, B. et al. Statistical analysis of membrane proteome expression changes in Saccharomyces cerevisiae research articles. *J. Proteome Res.* **5**, 2339–2347 (2006).
42. Matsuda, T. & Cepko, C. L. Electroporation and RNA interference in the rodent retina in vivo and in vitro. *Proc. Natl Acad. Sci. USA* https://doi.org/10.1073/pnas.2235688100 (2004).
43. Zack, D. J. et al. Unusual topography of bovine rhodopsin promoter-lacZ fusion gene expression in transgenic mouse retinas. *Neuron* **6**, 187–199 (1991).